Doctoral Thesis

THE LOAD-BEARING BEHAVIOUR OF THE STEEL-CONCRETE-STEEL COMPOSITE (SCSC) PLATE

submitted in satisfaction of the requirements for the degree of
Doctor of Science in Civil Engineering
of the TU Wien, Faculty of Civil Engineering

Dipl.-Ing. Bálint Palotás
Student number 11730881
[redacted]

Doctoral advisor: Univ.-Prof. Dipl.-Ing. Dr.techn. Josef Fink
Institute of Structural Engineering,
Research Unit Steel Structures, TU Wien
Karlsplatz 13/212, 1040 Vienna, Austria

Thesis reviewer: O.Univ.Prof. Dipl.-Ing. Dr.-Ing. M.Eng. Johann Kollegger
Institute of Structural Engineering,
Research Unit Structural Concrete, TU Wien
Karlsplatz 13/212, 1040 Vienna, Austria

Thesis reviewer: Univ.-Prof. Dipl.-Ing. Dr.techn. Harald Unterweger
Institute of Steel Structures, TU Graz
Lessingstraße 25/III, 8010 Graz, Austria

Vienna, October 2021 .....

Preface

This doctoral thesis was carried out at TU Wien, Institute of Structural Engineering, Research Unit Steel Structures, from January 2017 to October 2021.

First of all, I would like to thank my doctoral advisor Professor Josef Fink for his valuable guidance and support. I would also like to thank my colleagues at the Institute of Structural Engineering for the pleasant and constructive working atmosphere.

Furthermore, I would like to send my gratitude to my family for their support during the years I spent as an university assistant.

Abstract

The analysed innovative steel-concrete-steel composite (SCSC) plate has been researched at TU Wien, Institute of Structural Engineering, Research Unit Steel Structures. The aim of the investigations performed in the last years is to construct a load-bearing structure for single-track short-span railway bridges. The trough bridge system is developed for the Austrian Federal Rail Company (ÖBB) because numerous old railway bridges have to be replaced in Austria. The innovative SCSC plate is a special composite structure that is fabricated by connecting two 15 mm thick outer steel plates to a 170 mm thick concrete core. The steel and the concrete parts of the SCSC plate are connected by means of shear connectors. These composite dowels are welded alternately onto the bottom and top steel plates. Thus, the shear force resistant connection of the steel plates is reached through the concrete core, and the amount of welding work is minimalized.

The presented doctoral thesis is divided into three blocks. In the first block the load-carrying mechanisms of the SCSC plate is presented comprehensively based on the results of finite element analyses. The load level used for fatigue limit state (FLS) is examined. The second block introduces an engineering model of the SCSC plate which is appropriate to substitute the time-consuming numerical methods. Here, the structure of the developed two-dimensional spring framework model is explained, and the validation of the model is performed in the case of static loads. In the third block the effects from the cyclic loading is examined. In the case of high dowel forces, permanent displacement appears between the surfaces of the steel circular hole of the shear connector and the concrete part inside the hole. This permanent displacement in the composite connection is called inelastic slip. It is presented through the spring framework model calculation how the increasing inelastic slip due to the cyclic loading leads to a redistribution of forces as well as to the increase of deflection.

Summing up, it is shown in this doctoral thesis that the SCSC plate can be analysed with a two-dimensional spring framework model which is also appropriate to model the cyclic behaviour of concrete. Thus, the presented dissertation is a preliminary step to derive the design models for the SCSC plate in the fatigue limit state.

Contents

Notations

Abbreviations

CDP	Concrete Damage Plasticity (material model for concrete)
FEA	Finite-Element-Analysis
FLS	Fatigue Limit State
LM71	Load Model 71
ÖBB	Austrian Federal Rail Company (Österreichische Bundesbahnen)
ÖNORM B	Eurocode, National specifications, Austrian Standards
ÖNORM EN	Eurocode, Austrian Standards
SCSC	Steel-Concrete-Steel-Composite
ULS	Ultimate Limit State

Roman lower-case letters

[d]	Member displacement vector
f_{b0}	Initial equibiaxial compressive yield stress of concrete
f_{b0}	Initial uniaxial compressive yield stress of concrete
$q_{d.LM71}$	Design value of the traffic effects, distributed load
$q_{d.LM71,ABAQUS}$	Design value of the traffic effects considered in ABAQUS, distributed load
q_k	Characteristic value of the traffic effects, line load
$q_{k.LM71}$	Characteristic value of the traffic effects, distributed load
u, w	Local coordinates
w	Vertical displacement
x, y, z	Global coordinates
z	Moment arm

Roman upper-case letters

C	Spring stiffness
C_{hys}	Spring stiffness after the first loading cycle
C_M	Rotational spring stiffness
C_x	Horizontal spring stiffness
C_z	Vertical spring stiffness
[D]	Joint displacement vector
E	Young's modulus
F	Force
F_h	Horizontal force in the shear connector
[F]	Joint force vector
I_y	Area moment of inertia around the axis "y"

K_c	The ratio of the second stress invariant on the tensile meridian to that on the compressive meridian at initial yield
[K]	Global stiffness matrix
$[K_m]$	Member stiffness matrix
L	Length
L_Φ	Determinant length
M	Bending moment
N	Number of load cycles
N	Normal force
[P]	Member force vector
S_y	First moment of area about the axis "y"
T	Shear flow
V	Shear force
V	Volume
W	Weight

Greek letters

α	Factor for classified vertical loads
Υ_{Ff}	Partial factor for fatigue loads
ϵ	Eccentricity
λ	Damage equivalent factor
μ	Viscosity parameter
ν	Poisson's ratio
ρ	Material's mass density
Φ	Dynamic factor
φ	Dilation angle
φ	Rotation angle

1. Introduction

1.1 Background

Lit.: [7], [8]

The Austrian Federal Rail Company, ÖBB, has to replace old single-track short-span (up to 25 m) railway bridges at the end of their technical service life. One design type is already in use, where a massive steel deck slab with a thickness of 120 mm is the load bearing structure in the transverse direction and transfers the loads to the main steel girders of the cross section (see figure 1.1(a)). As this steel deck system has some disadvantages (complicated welded connections, high self-weight, limited availability of thick plates), an innovative steel-concrete-steel composite (SCSC) plate (see figure 1.1(b)) is being researched at TU Wien to offer an alternative structure. The SCSC plate is a special composite element that is fabricated by connecting two 15 mm thick steel plates to a 170 mm thick concrete core. The steel and the concrete material are connected structurally by means of shear connectors which are welded alternately onto the bottom and top steel plates are used. The construction will be introduced comprehensively in chapter 2.1.

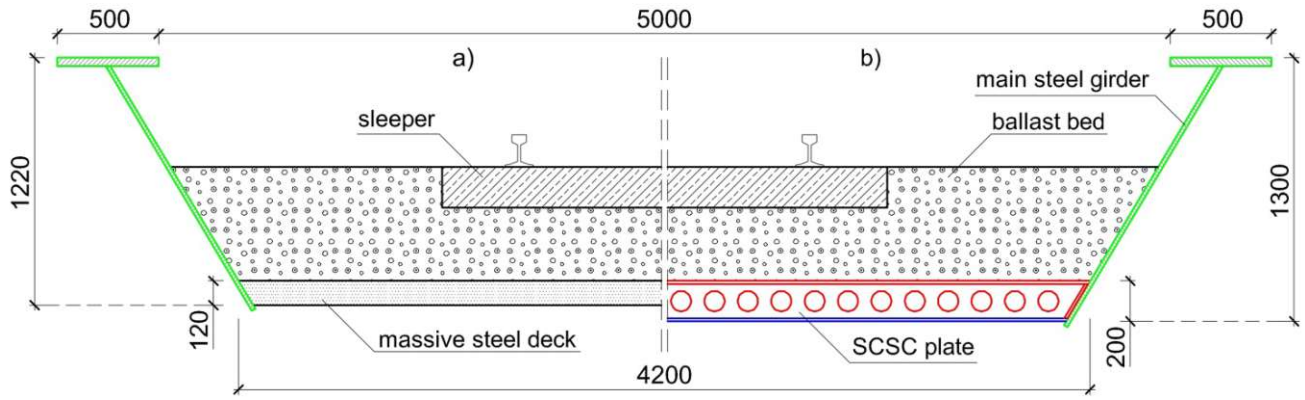

Figure 1.1: Regular trough bridge section for a structure with a span of 16 m, comparison of two deck systems: a) massive steel deck slab; b) SCSC plate. Dimensions in [mm]

At the Research Unit Steel Structures, numerical analyses using the ABAQUS finite element program [1] and laboratory studies have already been completed.

Herrmann [2] has taken the first important steps to prove the applicability of the SCSC plate for bridge constructions. He described the production, the load-bearing mechanisms and the production costs of the innovative structure in the case of different types of shear connectors. Moreover, Herrmann investigated the static load-bearing capacity of the SCSC plate with ABAQUS as well as through experimental static strength tests.

Steurer [3] tested the shear carrying capacity of only one composite connection of the SCSC plate. The laboratory tests with nine test specimens were performed in 2015. Based on the experimental test results, Steurer described the load-deformation behaviour of the composite connection through diagrams. Additionally, Steurer carried out large-scale laboratory tests in 2016 to determine the static load-bearing capacity of the SCSC plate. The span of the specimens was 4080 mm, which corresponds to the dimension of the examined trough bridge deck slab. The length of the specimens was set at 3,0 m. The test facility is illustrated in figure 1.2(a). The SCSC plate section was supported by bearing pedestals that were pre-stressed against the floor of the laboratory by threaded rods. The loading was created by water-filled pressure pads, which covered a load area of 3x3 m. Figure 1.2(b) demonstrates the deflected specimen at the maximum test load. In this case the vertical displacement in the middle of the span was 170 mm, which is very noticeable in the figure.

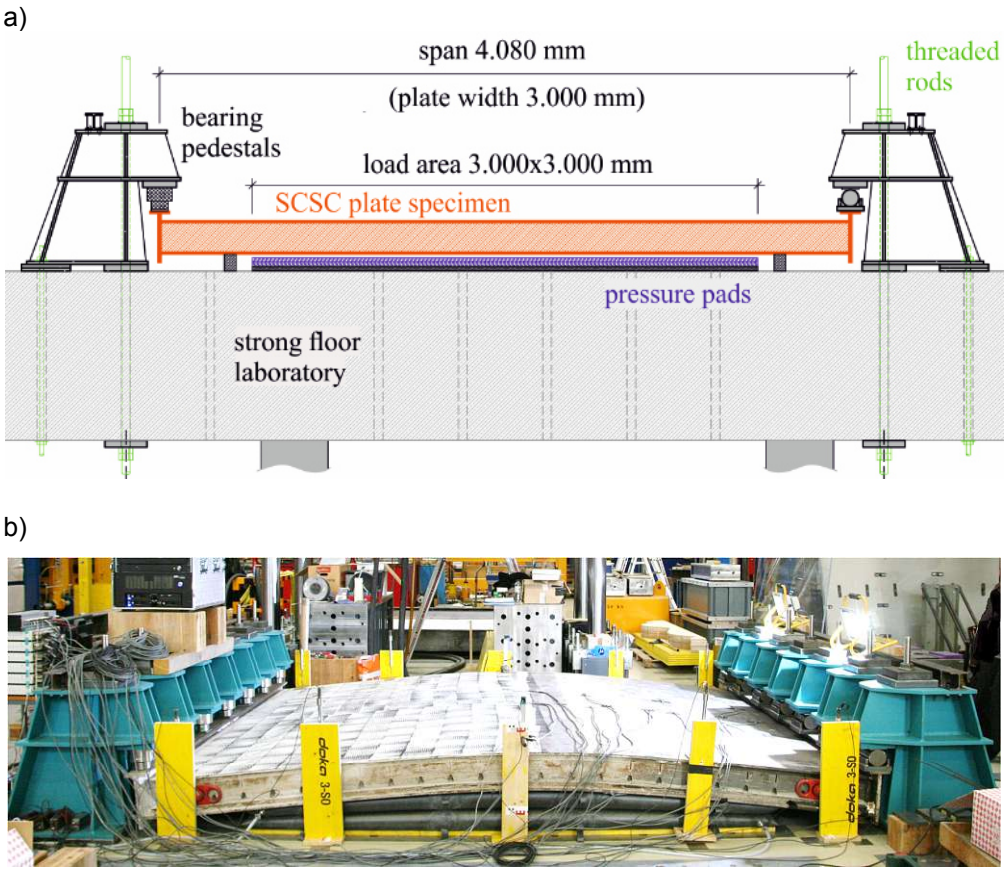

Figure 1.2: Large-scale laboratory test of the SCSC plate: a) cross section of the test facility for the static load-carrying investigations; b) deflection of the SCSC plate specimen due to the maximum test load [3]

Takács [4] evaluated the fatigue behaviour of the SCSC plate, focusing on the shear connectors. Three-dimensional finite element models constructed with ABAQUS served the basis values of stresses for the lifetime calculations using the local strain-life method. Actually, Takács evaluated the number of load cycles at the point when the first crack in the steel occurs in the case of traffic Load Model 71 (see chapter 2.2). Moreover, parameter studies were carried out in his thesis to examine the influences of the steel grade, concrete grade and the ballast bed height.

In the mentioned three investigations the behaviour of the SCSC plate was examined only in the transverse direction of the bridge. The reason of this fact is that the innovative plate is designed to transfer the loads to the main steel girders of the bridge cross-section (see figure 1.1). Actually, the SCSC plate is a load-bearing structure in transverse direction. However, it is neglected in the previous investigations that the plate is also stressed in the longitudinal direction. Logically, the whole SCSC plate is under tension in the case of bending from vertical loading. This means that it is necessary to examine if the concrete core of the plate was damaged due to the longitudinal tension. Obviously, the SCSC plate with a cracked concrete has a reduced load-carrying capacity compared to the plate with undamaged concrete. In order to clarify the effects from the longitudinal tension, numerical analyses and experimental tests are currently done at TU Wien, Research Unit Steel Structures.

Lorenz [5] researched the application of the SCSC plate for slab railway bridges with short spans (up to 8 m). In this case the SCSC plate is the solo load-bearing element in the longitudinal direction. Logically, the shear connectors lie parallel to the length of the slab bridge. Thus, in contrast with the three investigations introduced above, in the case of this simple structure there is not significant additional tension perpendicular to the direction of the shear connectors.

1.2 Objectives

The thesis includes three main objectives:

The first aim is to present comprehensively the complex load-bearing behaviour of the SCSC plate based on the contact stresses at the composite connections calculated with ABAQUS. The load level used for fatigue limit state (FLS) is only examined in this thesis. To prove the introduced load-carrying mechanisms, simple models are also analysed which reproduce properly the results of ABAQUS. The substitution of the complex ABAQUS calculation is not expected from these simple models as the considered external loadings are based on the results of the Finite-Element-Analysis software.

The second objective is to develop an engineering model of the SCSC plate which is appropriate for the engineering practice to analyse the innovative composite structure and substitute the time-consuming ABAQUS calculation. Thus, the structure of a two-dimensional spring framework model will be explained which reproduces properly the values of the displacements and internal forces calculated with ABAQUS. The complex ABAQUS model is not applicable for the calculation of the cyclic loading as the time taken for the calculation is huge. Therefore, the validation of the spring framework model is performed in the case of static loads.

The third objective is to analyse the effects from the cyclic loading on the SCSC plate. Due to the external loading of the plate, permanent displacement appears between the surfaces of the steel circular hole and the concrete part inside this hole in the case of high dowel forces. This permanent displacement in the composite connection is called inelastic slip, too. The effects from the inelastic slip need to be considered through the evaluation of cyclic loading which is possible through the further developed version of the spring framework model.

It is important to note that the verifications of the ultimate limit state (ULS) and serviceability limit state (SLS) do not belong to the tasks of the doctoral thesis. Moreover, the additional stresses in the longitudinal direction from the bending of the trough bridge are not considered through the following analyses. This means that only the main mechanisms of the SCSC plate in the transverse direction will be examined. Logically, in the case of the slab railway bridges investigated by Lorenz [5] the engineering models, which will be introduced in this thesis, are applicable to describe properly the load-bearing behaviour of the composite construction without neglecting additional stresses perpendicular to the direction of the shear connectors.

As the effects from tensile cracking and compressive crushing of the concrete material is negligible at the load level used for fatigue limit state according to the ABAQUS results, these failure mechanisms are not modelled with the spring framework model.

1.3 Outline and content

In chapter 2, the construction design is presented involving the demonstration of the ABAQUS model of the SCSC plate. Here, the load model for fatigue limit state is also described. Moreover, the chapter explains comprehensively the load-carrying mechanisms of the SCSC plate based on the contact stresses in the composite connections detected with ABAQUS. Finally, this chapter includes four simple engineering models which describe approximately the behaviour of the examined construction part of the SCSC plate.

In chapter 3, the structure of various framework models are presented. The chapter explains how the most complex two-dimensional spring framework model reproduces the values of the displacements and internal forces calculated with ABAQUS. Here, the evaluation of the spring stiffness values for the spring framework model is also demonstrated.

Chapter 4 presents the results and consequences from cyclic loading which is calculated with the further developed two-dimensional spring framework model. The chapter describes how the increasing inelastic slips in the composite connections, which means actually the cyclic creep of the concrete, are considered in the spring framework model.

Chapter 5 includes conclusions and suggestions for further research.

2. The load-bearing behaviour of the SCSC plate based on finite element analysis

2.1 Construction design

Lit.: [7], [8]

One aspect of the SCSC plate is a special sandwich-structured composite element that is fabricated by connecting two 15 mm thick steel plates to a 170 mm thick concrete core. The composite plate is illustrated in figure 2.1, where, as approximation, the main steel girders of the trough bridge are modelled as the supports and the small vertical steel plates pointed out in green. Typically, the core of sandwich elements is rather light. In our case, however, the plate needs to carry significant loads. Therefore the role of the concrete core is complex: On the one hand it maintains the positioning of the outer steel plates, ensuring the load transfer between the components, on the other hand it has a distinct load-carrying function.

Another feature of the SCSC plate is a special steel-concrete composite slab construction without reinforcement in the concrete. Generally, reinforced concrete is used in composite slabs, which is cast on a profiled steel decking, but in our case we use a 15 mm thick steel plate instead of a traditional decking sheet. Additionally, a top steel layer is installed, which is unusual in common composite slabs. The steel and the concrete material must be connected structurally by means of shear connectors to ensure the transmission of forces. In the SCSC plate, shear connectors welded alternately onto the bottom and top steel plates are used (see figure 2.1(c)). The shear connectors are 20 mm thin and 170 mm high steel stripes with circular holes (diameter 100 mm), embedded into the concrete core. The bottom and the top steel section are assembled with 480 mm clearance between the shear connectors. Both of the steel plates are welded to small portions of the main steel girder web plates, which is pointed out in green in figure 2.1(a). Finally, this steel construction is filled with concrete.

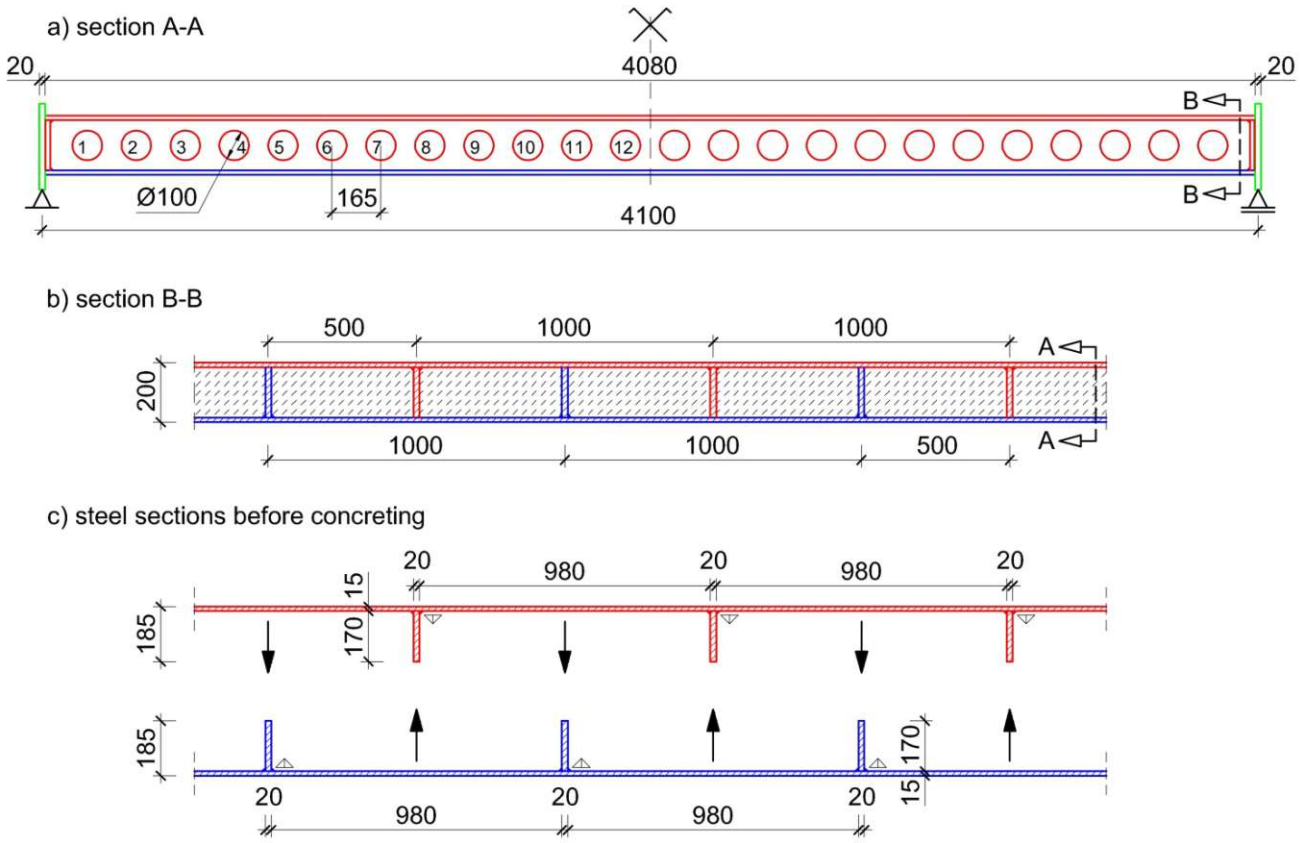

Figure 2.1: The design of the SCSC plate: a) the load-bearing structure in cross direction; b) shear connectors at a 500 mm central distance; c) the top steel section and the bottom steel section before concreting. Dimensions in [mm]

All of the shear connectors are welded to one stiffener at each end. These stiffeners feature a width of 110 mm, a height of 170 mm and a thickness of 15 mm. Their function is to transfer the shear forces from the shear connectors to the main steel girders. In the model (see figure 2.1) the stiffeners lie parallel to the main steel girder webs and these elements are close to each other, so the shear forces are transmitted easily through the very short parts on the ends of the horizontal steel plates. Figure 2.2 shows the ABAQUS [1] model (see chapter 2.3) comprising portions of three shear connectors with one stiffener at each of the ends.

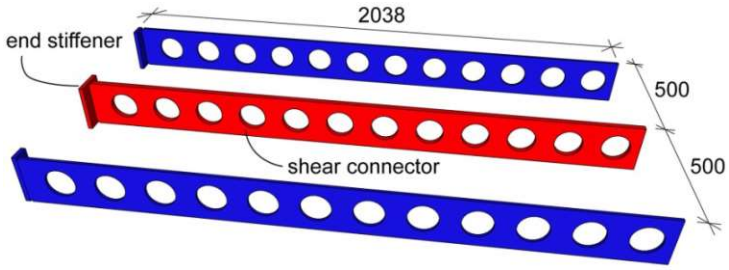

Figure 2.2: The three shear connectors of the ABAQUS model with the end stiffeners. Dimensions in [mm]

As illustrated in figure 2.3, only half of the plate is modelled in cross direction. Therefore, the shear connectors feature 12 circular holes as shown in figure 2.2, too. 1 m length means that the two outside shear connectors of the figure have a thickness of 10 mm, furthermore their end stiffeners have a width of 55 mm. In the real SCSC plate all of the shear connectors are 20 mm thick and all of the end stiffeners are 110 mm wide. In the ABAQUS model (see chapter 2.3), the central shear connector (pointed out in red in figure 2.2) is welded to the upper steel plate, while the outside shear connectors (pointed out in blue in figure 2.2) are welded to the bottom steel plate.

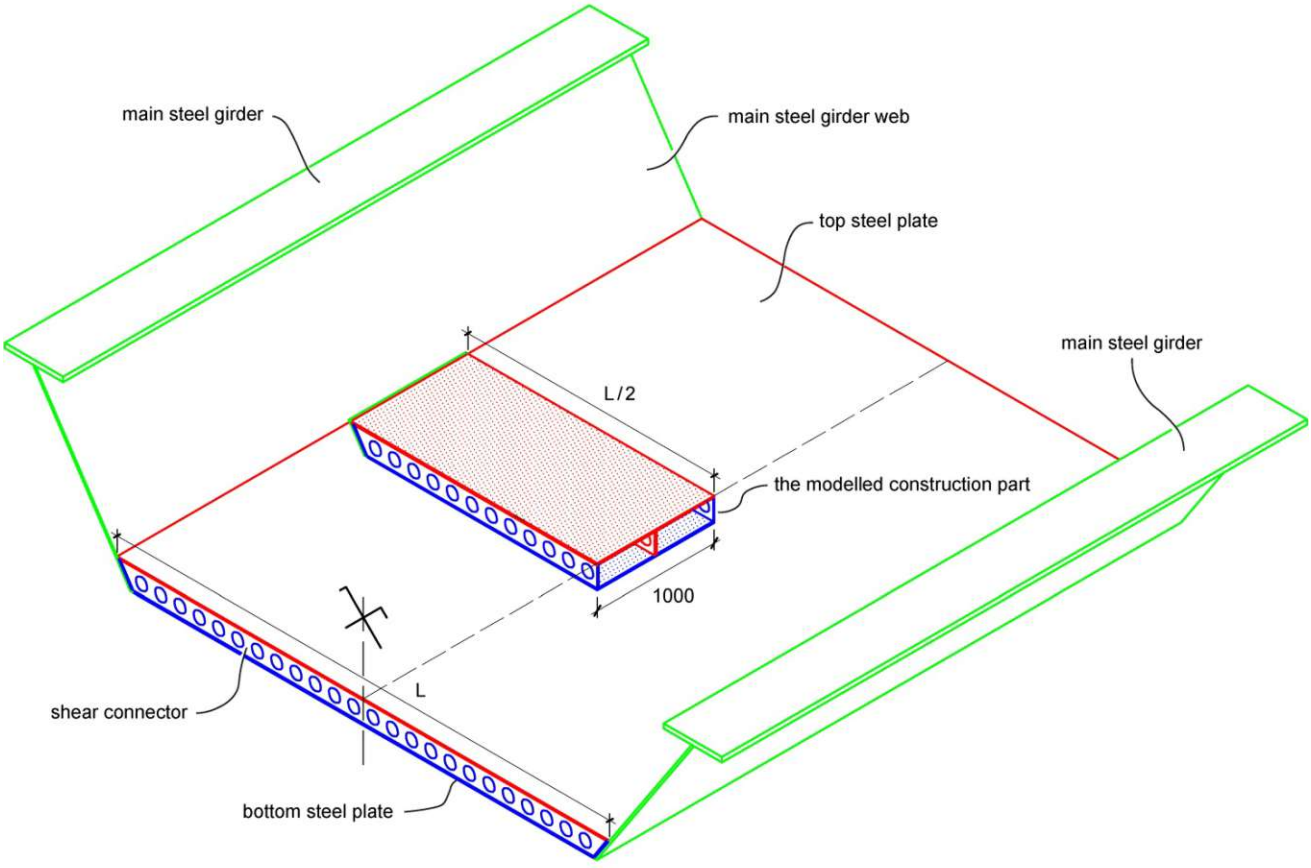

Figure 2.3: The modelled part of the construction is shown in the middle of the illustrated part of the trough bridge

2.2 Load model for fatigue limit state

Through the finite element analysis only the fatigue limit state is examined in chapter 2. Takács analysed the fatigue life of shear connectors of the SCSC plate in his dissertation [4] based on the local strain-life method. For this approach the permanent actions shall be also considered beside the traffic effects. To analyse the same situation in this thesis, the load model and the ABAQUS model correspond to the output data in [4]. Thus, a load model for the ABAQUS calculation is presented in this chapter which consists of the dead load of the structure and the traffic Load Model 71. In this way, additional loads (for instance nosing force, actions due to traction and braking, wind actions and derailment actions) are not taken into account in this thesis.

The dead load consists of the load of the SCSC plate (both the steel and the concrete parts without end stiffeners), the ballast bed with a height of 550 mm, the insulation, the reinforced concrete sleepers, the rails and the rail fastening system. Figure 2.4(a) shows a regular trough bridge section for a structure with a span length of 16 m. As an approximation, the dead load of the illustrated parts in figure 2.4(a) (except the main steel girders and the end stiffeners) means a line load of 19,87 kN/m for the ABAQUS model designed with 1 m length (see figure 2.4(b)). The detailed calculation of the loadings is demonstrated in appendix A.

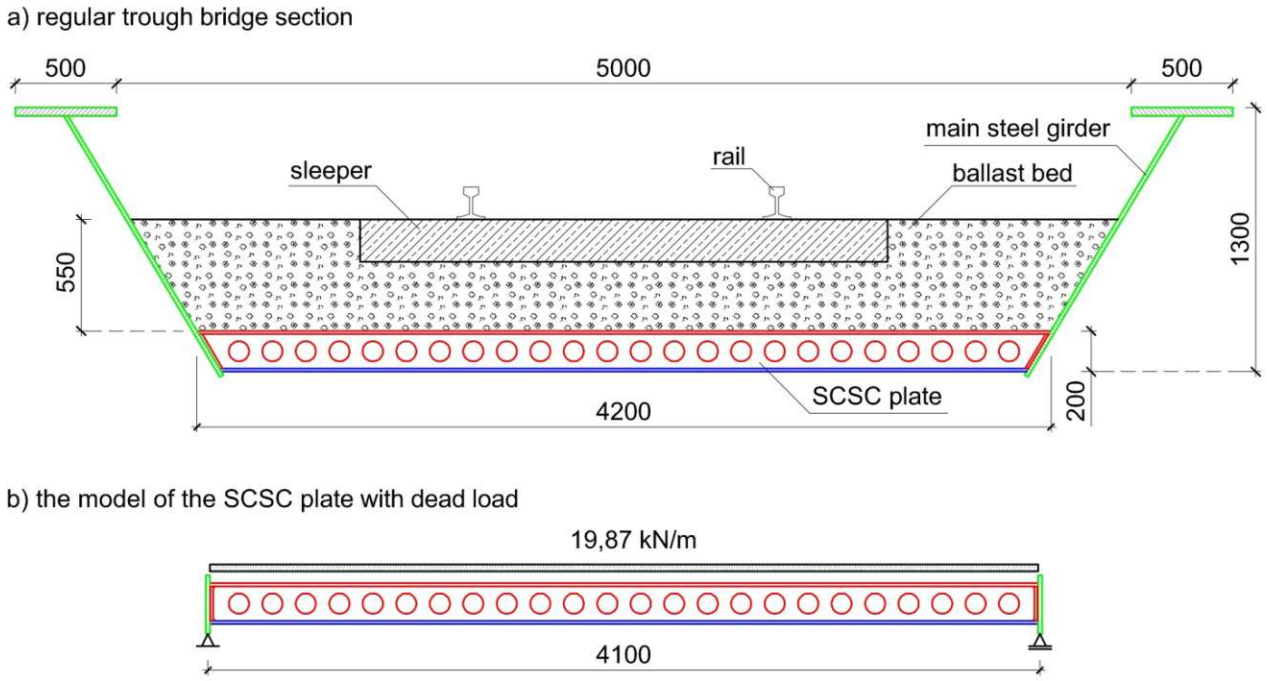

Figure 2.4: The dead load of the SCSC plate: a) trough bridge section for the load calculation (the rail fastening system is not illustrated); b) the model of the SCSC plate with the line load representing all the dead loads. Dimensions in [mm]

The static effect due to normal traffic is also considered in ABAQUS. This vertical railway loading is represented with Load Model 71 according to ÖNORM EN 1991-2 [9]. The characteristic values for vertical loads are shown in figure 2.5.

For the ABAQUS calculation the concentrated loads of the Load Model 71 are converted into a line load (q_k) as an approximation. Logically, q_k represents the traffic loading in longitudinal direction:

$$q_k = \frac{4 \cdot 250\ kN}{6{,}4\ m} = 156{,}25\ kN/m \tag{2.1}$$

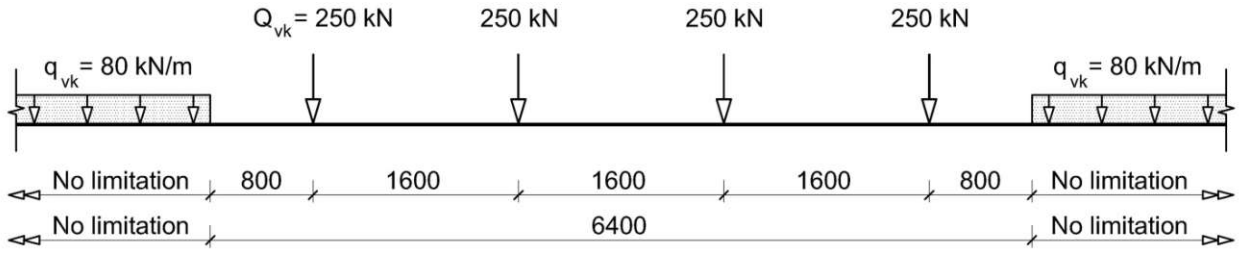

Figure 2.5: Load Model 71. Dimensions in [mm]

The distribution of the load q_k in transverse direction results from the dimensions of the reinforced concrete sleeper, the high of the ballast bed and the load spread beneath sleepers (4:1). Figure 2.6 illustrates this distribution to the reference plane which is actually the upper edge of the SCSC plate. The dimensions of sleeper are chosen from ÖNORM B 1991-2 [10].

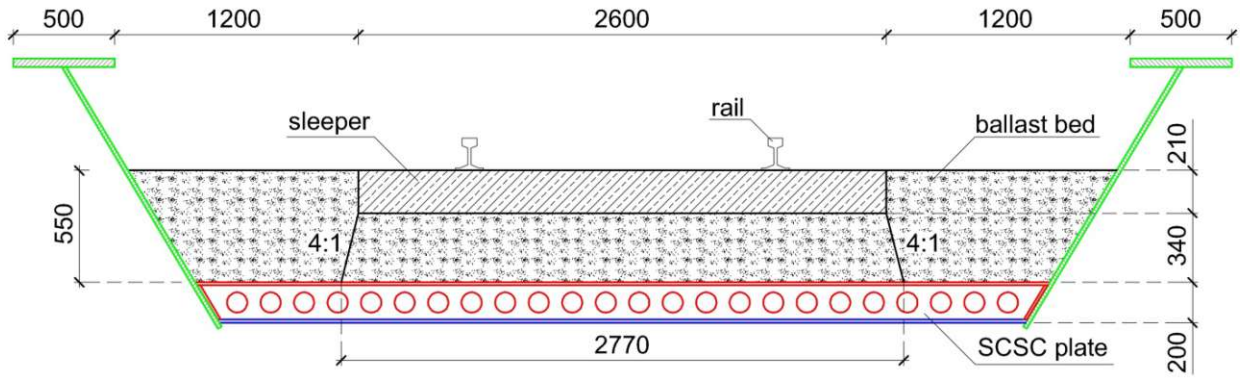

Figure 2.6: Transverse distribution of loads by the sleepers and ballast. Dimensions in [mm]

So, the line load (q_k) can be considered as distributed load ($q_{k,LM71}$) acting on the SCSC plate:

$$q_{k.LM71} = \frac{q_k}{L_{transverse}} = \frac{156{,}25\ kN/m}{2{,}77\ m} = 56{,}41\ kN/m^2 \tag{2.2}$$

As the length of the ABAQUS model is even 1 m, the distributed load ($q_{k,LM71}$) can be represented with a line load of 56,41 kN/m in transverse direction (see figure 2.7). Logically, in the three-dimensional ABAQUS model the surface of the top steel plate is loaded with the distributed load.

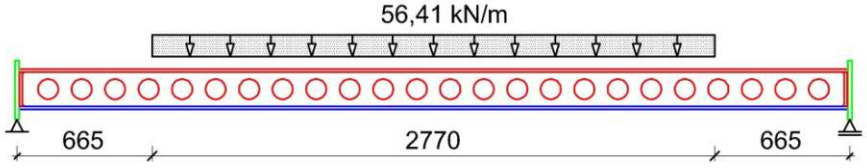

Figure 2.7: The model of the plate with the line load representing the static effect due to normal traffic. Dimensions in [mm]

To get the design value of the distributed load, the result above ($q_{k,LM71}$) shall be multiplied by the partial safety factor γ_{Ff}, the dynamic factor Φ, and the damage equivalent factor λ. Moreover, to consider rail traffic which is heavier or lighter

than normal rail traffic, a factor α shall be used due to Load Model 71 according to ÖNORM EN 1991-2, chapter 6.3.2 [9]. However, in the case of the fatigue assessment the safety verification is carried out excluding factor α (see ÖNORM EN 1991-2, Annex D.2 [9]).

According to ÖNORM EN 1993-2 [12] the partial factor for fatigue loads (γ_{Ff}) shall be taken as 1,0. To consider the dynamic magnification of stresses, the dynamic factor Φ is defined in ÖNORM EN 1991-2 [9]. The factor depends on the quality of track maintenance and the determinant length L_Φ. According to ÖNORM B 1991-2 [10] the case "carefully maintained track" can be applied in Austria ($\Phi = \Phi_2$). For the calculation of the determinant length the Table 6.2 in ÖNORM EN 1991-2 [9] is used, where the case 4.3 (Deck slab for trough bridges: spanning perpendicular to the main girders) is chosen. In this case the determinant length is:

$$L_\Phi = Twice\ span\ of\ deck\ slab + 3\ m = 2 \cdot 4{,}08 + 3 = 11{,}16\ m \tag{2.3}$$

Thus, the dynamic factor for carefully maintained track:

$$\Phi_2 = \frac{1{,}44}{\sqrt{L_\Phi} - 0{,}2} + 0{,}82 = \frac{1{,}44}{\sqrt{11{,}16} - 0{,}2} + 0{,}82 = 1{,}279 \tag{2.4}$$

Moreover, according to ÖNORM EN 1993-1-9 [11] the stress range caused by the fatigue loads should be multiplied by the damage equivalent factors λ_i. Due to the multiplication with these factors, the equivalent constant amplitude stress range for N = $2 \cdot 10^6$ cycles can be calculated. The equivalence factors are determined in ÖNORM EN 1993-2, chapter 9.5.3 [12], and take into account the damage effect of traffic, the length of the influence line of the detail under analysis, the traffic volume, the design life of the bridge and the number of tracks. The determination is shown in equation (2.5):

$$\lambda = \lambda_1 \cdot \lambda_2 \cdot \lambda_3 \cdot \lambda_4 \qquad but\ \lambda \leq \lambda_{max} \tag{2.5}$$

According to ÖNORM B 1993-2 [13], in the area of the Austrian Federal Rail Company (ÖBB) the factor λ_1 need to be used from the ÖNORM EN 1993-2, Table 9.4 (for rail traffic with 25 t axles) [12]. The length of the influence line of the SCSC plate is 4,0 m according to the approximation of Herrmann [2]. In this case, the factor λ_1 has a value of 1,16.

The damage equivalent factor for the traffic volume (λ_2) is 1,0 according to ÖNORM EN 1993-2, Table 9.5 [12] in the case of an annual traffic tonnage of $25 \cdot 10^6$ tonnes passing over the bridge on each track. The traffic volume of $25 \cdot 10^6$ t/track for fatigue is given in ÖNORM EN 1991-2 [9]. The damage equivalent factor for the design life (λ_3) is also 1,0 as the indicative design working life is 100 years for bridges from ÖNORM EN 1990, Table 2.1 [14]. The trough bridge examined in this dissertation has only one track. In this case the factor λ_4 is 1,0 according to ÖNORM EN 1993-2, Table 9.7 [12].

Thus, the factor λ means a value of 1,16 (see equation 2.6), which is smaller than the maximal value (λ_{max} = 1,4) defined in ÖNORM EN 1993-2 [12].

$$\lambda = 1{,}16 \cdot 1{,}0 \cdot 1{,}0 \cdot 1{,}0 = 1{,}16 \tag{2.6}$$

Finally, the design value of the traffic effects is calculated according to ÖNORM EN 1991-2 [9]:

$$q_{d.LM71} = \gamma_{Ff} \cdot \Phi_2 \cdot \lambda \cdot q_{k.LM71} = 1{,}0 \cdot 1{,}279 \cdot 1{,}16 \cdot q_{k.LM71} = 1{,}484 \cdot 56{,}41 = 83{,}71\ kN/m^2 \tag{2.7}$$

The combination of actions for fatigue verification is illustrated in figure 2.8, where both the dead load and the rail traffic load are shown. The partial safety factor for the dead load is 1,0 for the fatigue assessment, thus the characteristic value of the load from figure 2.4(b) is shown in figure 2.8, too.

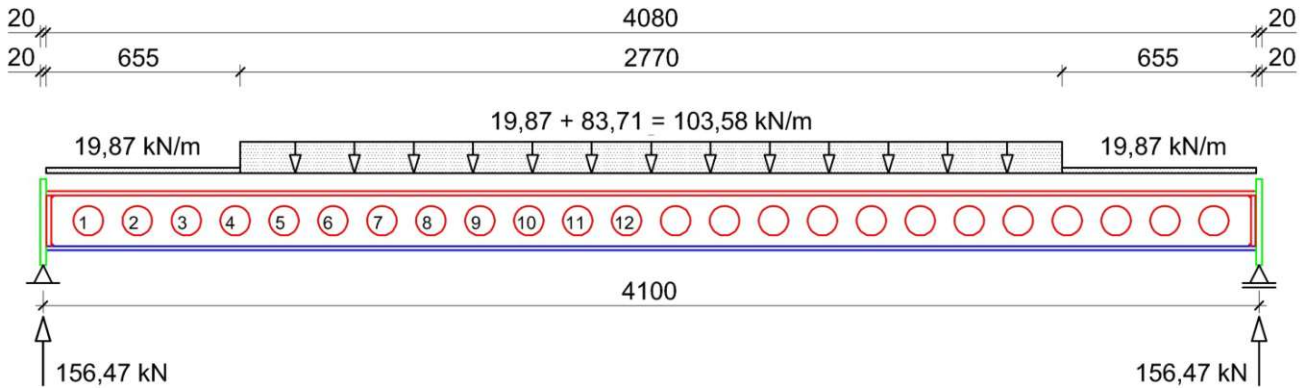

Figure 2.8: The design values of the dead load and the traffic effects for a model with 1 m length. Dimensions in [mm]

The complete load history of the simulation is divided into two STEPS in ABAQUS. In the first STEP the dead load of the SCSC plate is considered, and in the second STEP the traffic load is represented. However, the total dead load acts in the second STEP, too. Both of the loads in these two STEPS are stepwise applied. Actually, the analysis results have been saved in ABAQUS at the predetermined FRAMES. The dead load is separated into five FRAMES. At the fifth FRAME acts the total dead load of the structure. The load increase is consistent. The analysis results of the second STEP are available at 50 FRAMES. For instance at the first FRAME of the second STEP act the total dead load from the first STEP and 2 % of the predetermined traffic load. At the last FRAME of the second STEP acts the total traffic load beside the self-weight of structural elements. A total traffic load of 290 kN/m^2 was used for the model by Takács in [4], which is approximately $5 \cdot q_{k,LM71}$. Due to this modelling in ABAQUS, it is possible to investigate the results in the case of higher loadings, too (for instance in chapter 3.7.2 of this thesis). Thus, the load level used for fatigue limit state (see figure 2.8) belongs to the FRAME 15 in ABAQUS as an approximation. However, the traffic loads at the FRAME 15 is:

$$q_{d.LM71,ABAQUS} = (15/50) \cdot 290\ kN/m^2 = 87{,}00\ kN/m^2 \tag{2.8}$$

The small difference compared to the calculated value ($q_{d,LM71}$ = 83,71 kN/m^2) can be neglected. Actually, in the figure 2.9 illustrated external vertical loading of the ABAQUS model used for fatigue limit state is on the side of safety.

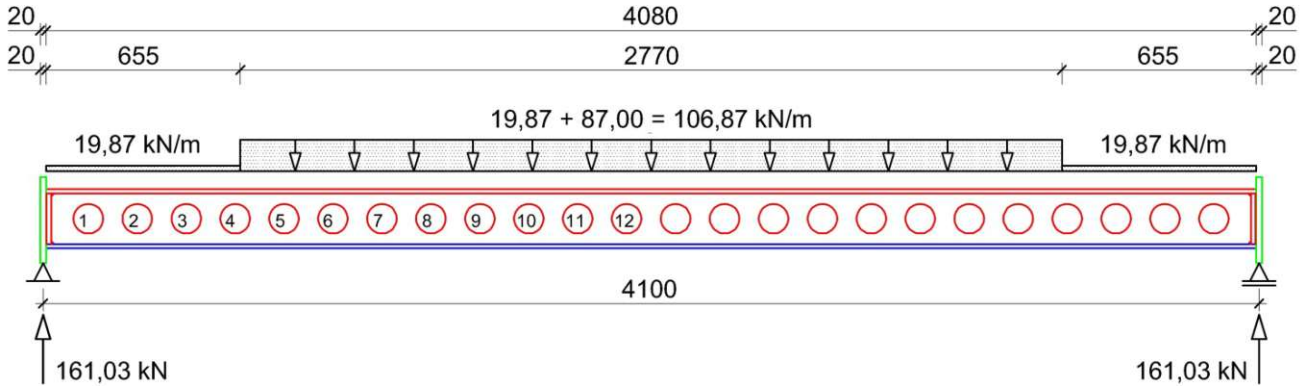

Figure 2.9: The external vertical loading for the ABAQUS model with 1 m length. Dimensions in [mm]

2.3 Numerical simulation with ABAQUS

2.3.1 Construction parts of the model

As mentioned in chapter 2.1, only half of the plate is modelled in cross direction in ABAQUS (see figure 2.3). Moreover, the length of the model is 1 m, so the two outside shear connectors in figure 2.10 (shear connectors 1 and 3) have a thickness of 10 mm. Their end stiffeners (end stiffeners 1 and 3) have a width of 55 mm. The central shear connector (shear connector 2) is 20 mm thick, and their end stiffener (end stiffener 2) features a width of 110 mm. The main steel girder web (see figure 2.3) is modelled with the vertical end plate pointed out in green in figure 2.10. The thickness of this steel end plate is 20 mm. The end stiffeners cannot push the end plate as a gap of 2 mm is designed between them.

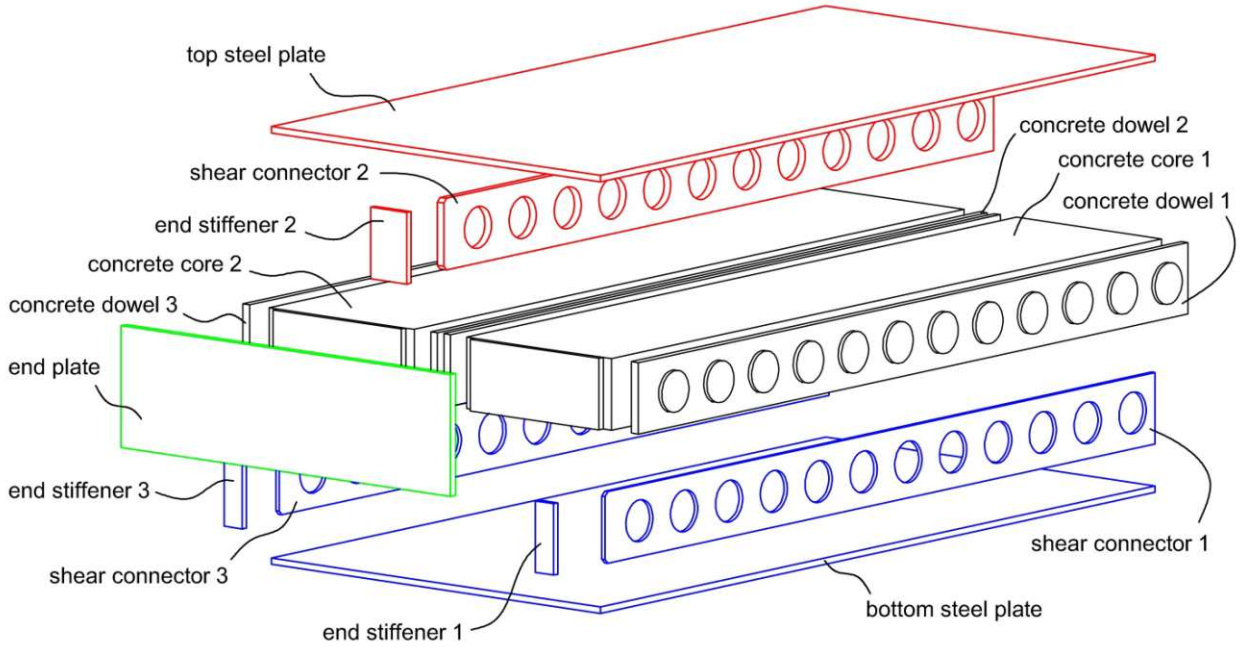

Figure 2.10: The construction parts of the ABAQUS model. The structural elements are shifted from each other for ease of view.

A three-dimensional modelling space is specified in the PART module for the three-dimensional solid elements. Moreover, all the three-dimensional parts of the model are defined as deformable part. This type of parts can deform under load. The material properties of the parts are specified in the PROPERTY module. The material definition for steel and concrete is presented in chapter 2.3.2.

The model consists of four main parts: the bottom steel section, the top steel section, the end plate and the concrete. For the bottom steel section five construction parts (see figure 2.11) are created in the PART module of ABAQUS: the bottom steel plate, the shear connector 1, the end stiffener 1, the shear connector 3 and the end stiffener 3. However, the two shear connectors as well as the two end stiffeners are congruent.

Figure 2.11(a) illustrates the surfaces with magenta colour, where the construction parts are fused together. In the INTERACTION module of ABAQUS tie constraints are defined to model the welded connections. This type of constraint ties two separate surfaces together so that relative motion is not allowed. As fillet weld is designed on both sides of the shear connectors in the case of the real SCSC plate, the whole contact surfaces of the shear connectors are chosen for the constraint in the ABAQUS model as an approximation. In this case, logically, the welding seam is not modelled as an individual part in ABAQUS.

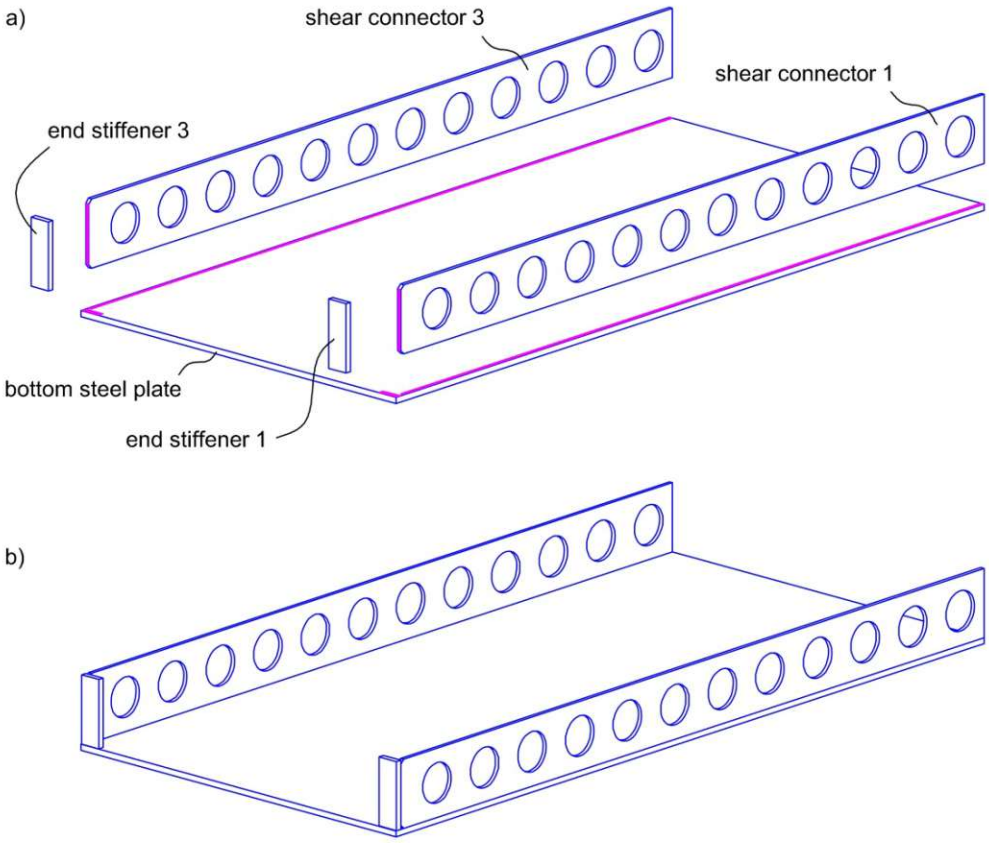

Figure 2.11: The bottom steel section of the ABAQUS model: a) the construction parts are shifted from each other for ease of view. The elements are fused together at the magenta coloured surfaces. b) The bottom steel section after assembly.

For the top steel section three construction parts (see figure 2.12) are created in the PART module: the top steel plate, the shear connector 2 and the end stiffener 2. The top steel plate and the bottom steel plate are congruent. They feature a width of 1000 mm, a length of 2040 mm and a thickness of 15 mm. Figure 2.12(a) illustrates the surfaces with magenta colour, where the three construction parts are fused together. As in the case of the bottom steel section, the whole contact surfaces of the shear connector is chosen for the constraint in the ABAQUS model.

Figure 2.13(a) represents the five construction parts for the concrete inside the SCSC plate. The three concrete dowels represent the concrete around the steel shear connectors. Obviously, the concrete parts inside the holes of the shear connectors belong to the concrete dowels, too. These parts of the concrete (see figure 2.13(a): concrete dowels 1, 2 and 3) play an important role in the load-bearing behaviour of the SCSC plate, because high local forces are transferred through them. Thus, compared to the concrete cores, a finer mesh is required at the concrete dowels to ensure that the results from ABAQUS are adequate. The hexahedral meshing of the solid parts of the model is created according to the conclusions of the parameter studies of Takács [4]. Actually, eight-node brick elements with reduced integration (element type of ABAQUS: C3D8R) are used for the model. The structured meshing technique is applied to simple three-dimensional regions as the concrete cores 1 and 2. In this case the mesh topology is simple. The swept meshing technique is used to mesh complex solid regions, such as the concrete dowels 1, 2 and 3. The mesh density is determined using the SEED menu in the MESH module of ABAQUS. The edge length of a finite element is approximately 5 mm for the steel construction parts and for the concrete dowels. A mesh density with 10 mm edge length is applied for the concrete cores.

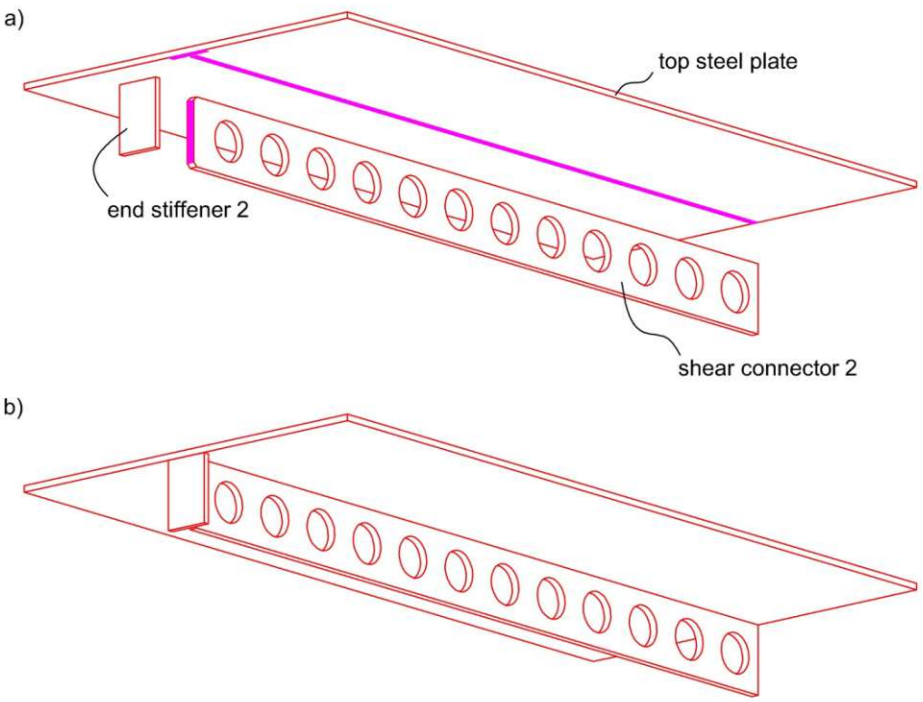

Figure 2.12: The top steel section of the ABAQUS model: a) the construction parts are shifted from each other for ease of view. The elements are fused together at the magenta coloured surfaces. b) The top steel section after assembly.

Figure 2.13(a) illustrates the surfaces with magenta colour, where the construction parts of concrete are fused together. Logically, the whole contact surfaces of the concrete cores and concrete dowels are chosen for the constraint in the ABAQUS model, because of the material continuity of concrete.

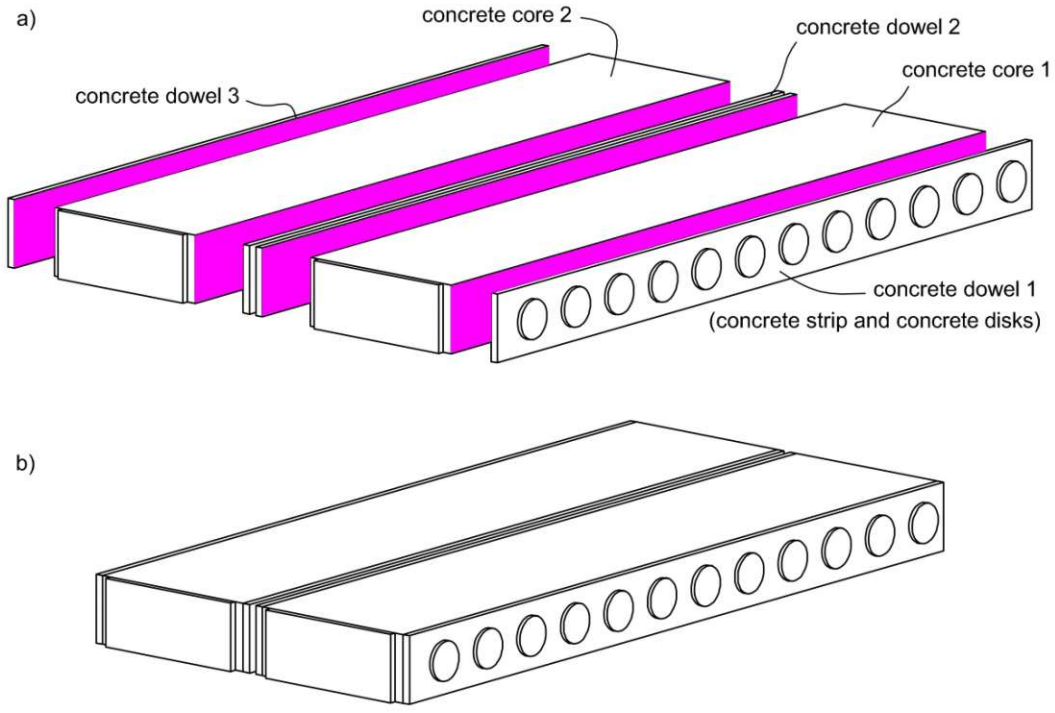

Figure 2.13: The concrete parts of the ABAQUS model: a) the construction parts are shifted from each other for ease of view. The elements are fused together at the magenta coloured surfaces. b) The concrete after assembly.

The end plate (see figure 2.14) features a width of 1000 mm, a high of 290 mm and a thickness of 20 mm. Figure 2.14 illustrates the surfaces with magenta colour, where the end plate and the steel sections are fused together. As fillet weld is designed on one side of the bottom and the top steel plates in the case of the real SCSC plate, only half of the contact surfaces of the steel plates are chosen for the constraint in the ABAQUS model as an approximation. Logically, there is not any tie constraint between the bottom and top steel sections.

Figure 2.14 illustrates the four main parts. Beside the tie constraints for the end plate described above, additional contact conditions are defined between the four main parts in the INTERACTION module of ABAQUS. The HARD CONTACT relationship is used for the surfaces which are in contact. Contact pressure can be transmitted between them, and the transfer of tensile stress across the interface is not allowed. Friction is used only between the shear connectors and the concrete dowels. Namely, only at the inside surface of the holes of the shear connectors act friction through a friction coefficient of 0,3. The other contact surfaces are frictionless. Figure 2.15 illustrates the ABAQUS model after assembly.

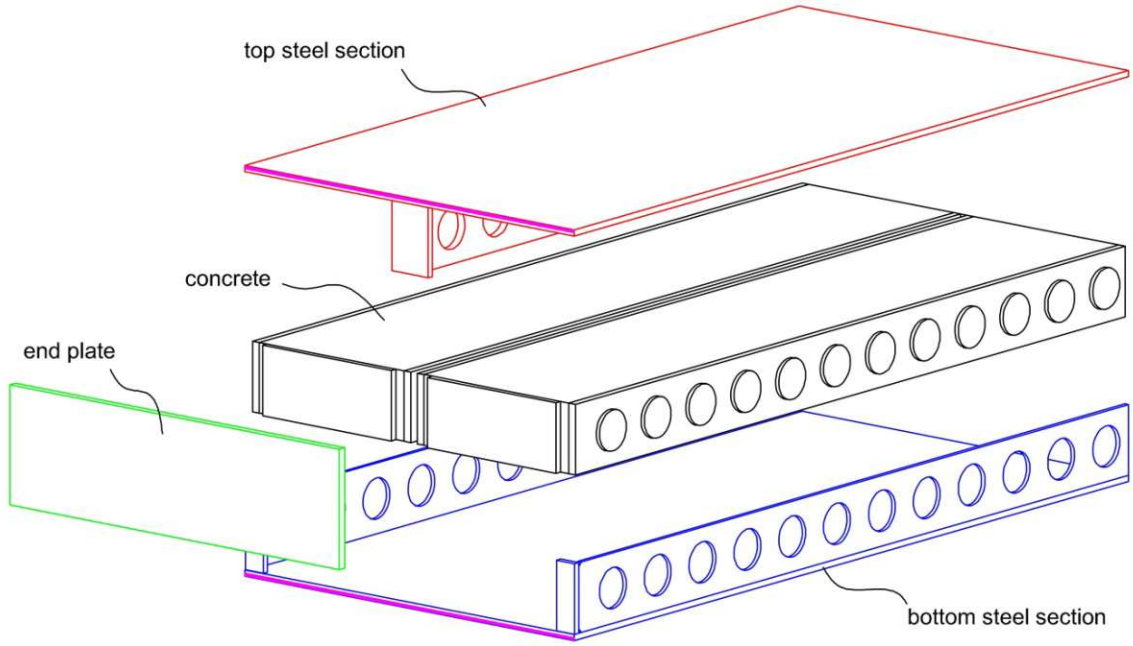

Figure 2.14: The four main parts of the ABAQUS model. The parts are shifted from each other for ease of view. The end plate is fused together with the top and the bottom steel section at the magenta coloured surfaces.

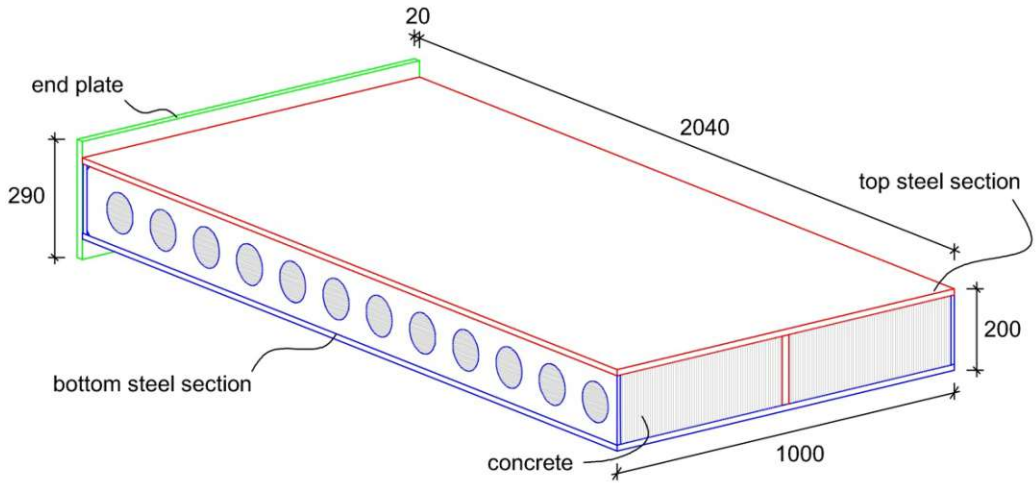

Figure 2.15: The ABAQUS model of the SCSC plate after assembly of the four main parts

2.3.2 Boundary conditions

In the analyses with ABAQUS, boundary conditions are applied to those surfaces of the construction parts where the displacements and rotations are known. These surfaces of the model are usually constrained to remain fixed during the calculation. For example the regions of a support have zero vertical displacements.

For the simulation of the vertical support at the end plate, an analytical rigid part is defined which is a rigid planar surface in this case. Figure 2.16 illustrates with magenta colour that the end plate and the analytical rigid surface are fused together. In the INTERACTION module of ABAQUS tie constraints are defined to model this connection. The analytical rigid surface is associated with a rigid body reference node in the middle of the surface (see figure 2.16). The motions of the rigid surface are controlled by the motions of the reference node. Actually, the boundary conditions are defined for the reference node of the rigid surface. The translational degrees of freedom in the y and z directions and the rotational degrees of freedom about the x and z directions are constrained. This means that only the displacements in the x direction and the rotations about the y direction are possible.

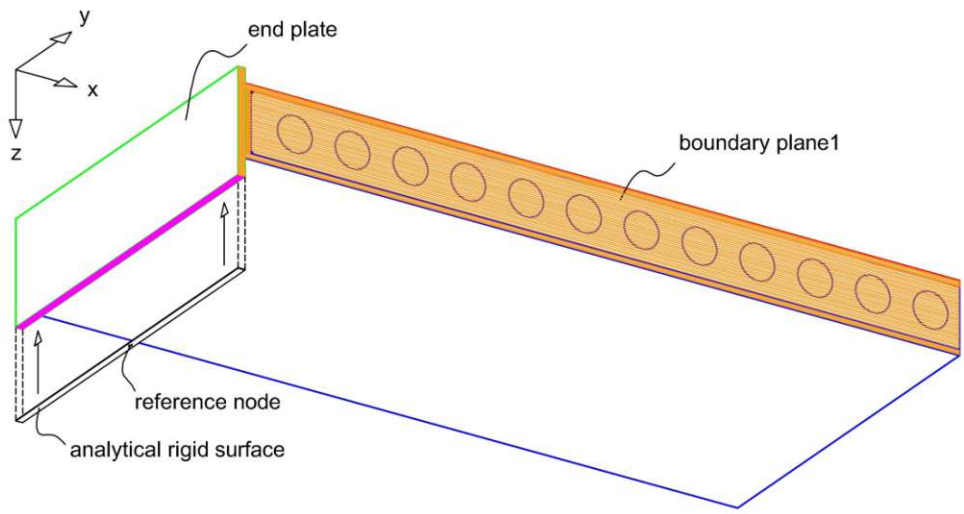

Figure 2.16: Boundary conditions of the ABAQUS model. The analytical rigid surface is shifted for ease of view. Bottom view

The orange-coloured surface illustrated in figure 2.16 is a boundary plane for the ABAQUS model. Actually, the total length of a trough bridge is much more than the 1 m length of the modelled part in ABAQUS (see figures 2.3 and 2.15). Thus, the boundary conditions at the boundary 1 represent the effects from the following construction parts. In this case, all the nodes on the plane are fixed in the y direction as an approximation. This means that the boundary plane 1 remains a vertical plane after loading, too.

The ABAQUS model has two additional boundary surfaces shown in figure 2.17. However, the boundary plane 3 has the same meaning as the boundary plane 1. Thus, the nodes of this plane have also zero horizontal displacement in the y direction.

The boundary plane 2 demonstrates that only half of the SCSC plate is modelled in cross direction (x direction). Logically, in the case of loading, this plane has to remain a vertical plan. Actually, the motions of the nodes on the surface are constrained to remain fixed in x direction. Therefore, the rotations of this surface about the y and z directions are also not possible.

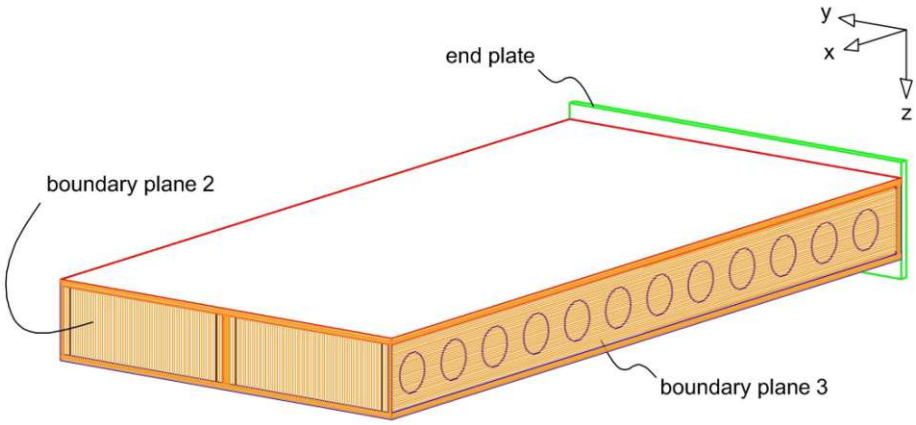

Figure 2.17: Boundary conditions of the ABAQUS model. Top view (3D)

2.3.3 Material models

The CLASSIC METAL PLASTICITY model of ABAQUS is used with each steel elements of the model in conjunction with the LINEAR ELASTIC material model. Actually, isotropic elasto-plasticity is considered with an isotropic hardening model in ABAQUS. The elastic properties are completely given by the Young's modulus (E = 210 000 N/mm^2) and the Poisson's ratio (ν = 0,3). Moreover, the material's mass density (structural steel S355: $\rho = 7{,}85 \cdot 10^{-9}$ tonne/mm^3) must be defined for the explicit dynamic analysis. However, in the case of quasi static loading of the model, the mass density does not influence the results.

For the plasticity calculations, the yield stress is given as a tabular function of plastic strain. The stress at a given state is interpolated from this table of data (see table 2.1) which is based on the calculations of Takács [4]. Actually, Takács described the nonlinear relationship between stress and strain through the Ramberg-Osgood equation [15]. Moreover, material data for cyclic loading are used for this calculation.

Plastic strain	Stress
[-]	N/mm^2
0,000000	139,35
0,000034	170,25
0,000131	208,02
0,000497	254,15
0,001889	310,35
0,007182	379,40
0,027306	463,55
0,039528	490,00

Table 2.1: ABAQUS settings for structural steel S355

In table 2.1 defined material data is illustrated in figure 2.18. When the stress in the steel material reaches 490 MPa, the material will deform continuously. However, this feature is not shown in the figure.

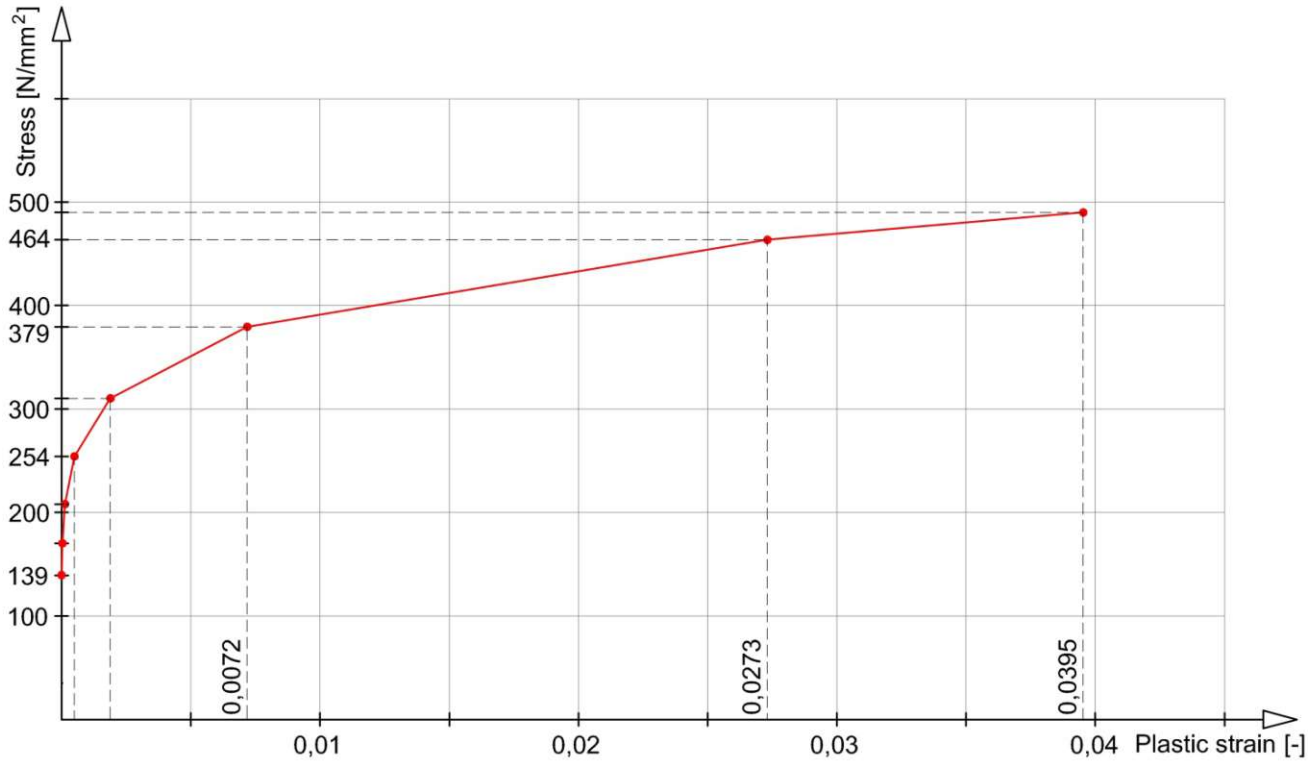

Figure 2.18: The stress-strain curve to define the plastic behaviour of steel used during the ABAQUS analysis

The CONCRETE DAMAGED PLASTICITY model of ABAQUS is used with each concrete elements of the model. The inelastic behaviour of concrete is represented with this model based on the concepts of isotropic damaged elasticity in combination with isotropic tensile and compressive plasticity. The model is appropriate for plain concrete and can describe the tensile cracking and compressive crushing of the concrete material. The evolution of failure surface is controlled by the compressive and tensile plastic strains.

Under uniaxial compression the stress-strain response follows a linear elastic relationship until the initial yield (19,20 N/mm^2, see table 2.2). Moreover, for concrete C40/50, stress hardening is defined until the ultimate stress of 48 N/mm^2. The last phase in the plastic regime is the strain softening. Table 2.2 illustrates the stress-inelastic strain relationship and the damage variables used in ABAQUS. The values are calculated by Takács in [4] based on the advices in [16] and [17]. The damage parameter with zero represents the undamaged material, while a variable with the value of one means the total loss of strength. However, these variables are used for the unloading response through the degradation of the elastic stiffness. As in this thesis, the evaluations with ABAQUS does not consist any unloading phase, the given damage variables in the tables 2.2 and 2.3 do not influence the results.

Figure 2.19 represents the inelastic material behaviour of concrete in the case of compression according to the data in table 2.2. The damage variables depending on the inelastic strain are illustrated in figure 2.20.

Additionally, the following basis parameters for concrete C40/50 are defined in ABAQUS:

$E = 35200\, N/mm^2$ (Young's modulus of the concrete)

$\nu = 0{,}2$ (Poisson's ratio)

$\rho = 2{,}4 \cdot 10^{-9}\ tonne/mm^3$ (Mass density)

Moreover, according to the default values in ABAQUS:

$\varphi = 36°$ (Dilation angle)

$\epsilon = 0{,}1$ (Eccentricity)

$f_{b0}/f_{c0} = 1{,}16$ (The ratio of initial equibiaxial compressive yield stress to initial uniaxial compressive yield stress)

$K_c = 0{,}67$ (The ratio of the second stress invariant on the tensile meridian to that on the compressive meridian at initial yield)

$\mu = 0\ N \cdot s/mm^2$ (Viscosity parameter)

Inelastic strain	Stress	Damage variable
[-]	N/mm^2	[-]
0,00000	19,20	0,00
0,00007	29,09	0,00
0,00020	37,15	0,00
0,00039	43,08	0,00
0,00064	46,74	0,00
0,00096	48,00	0,00
0,00128	47,11	0,02
0,00165	44,36	0,08
0,00208	39,66	0,17
0,00257	32,90	0,31
0,00294	29,02	0,40
0,00386	24,70	0,49
0,00531	20,36	0,58
0,00728	16,18	0,66
0,00977	12,34	0,74
0,01279	8,95	0,81
0,01631	6,16	0,87
0,02034	4,08	0,91
0,02489	2,80	0,94
0,02993	2,40	0,95
0,09999	0,40	0,99

Table 2.2: ABAQUS settings for compressive behaviour of concrete C40/50

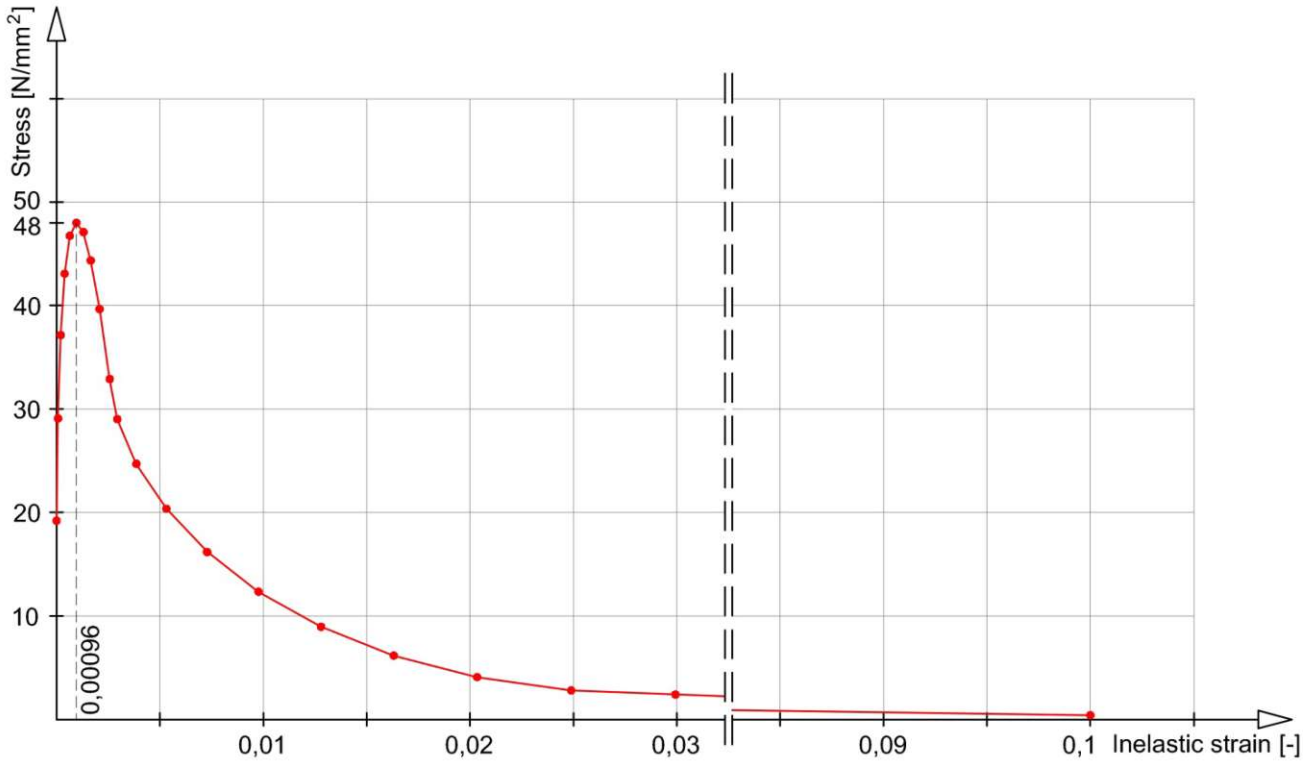

Figure 2.19: The stress-strain curve to define the plastic behaviour of compressed concrete used during the ABAQUS analysis

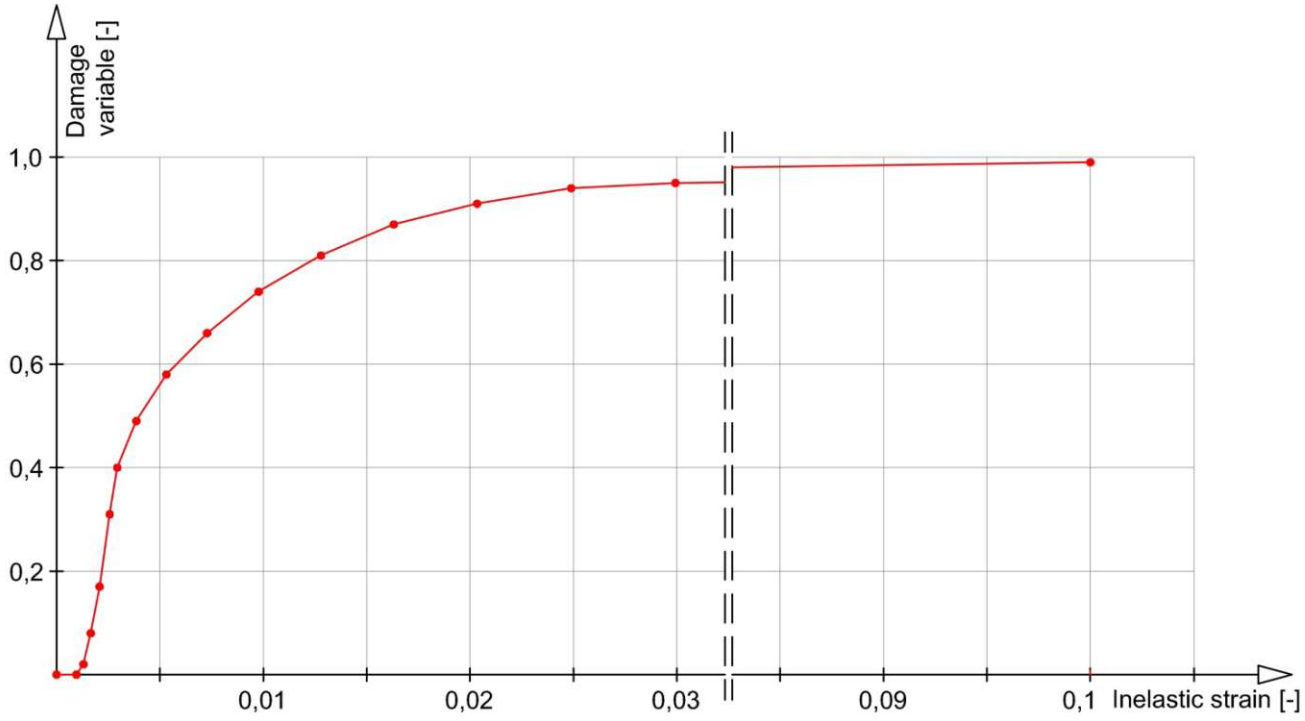

Figure 2.20: The damage-inelastic strain curve for the compressed concrete material used during the ABAQUS analysis

Under uniaxial tension the stress-strain response is linear until the failure stress (3,509 N/mm^2, see table 2.3) is reached. At this point micro-cracking occurs in the concrete. Beyond the failure stress a softening stress-inelastic strain response represents the behaviour of concrete (see table 2.3 and figure 2.21). Here, the strain is regarded as crack opening in

ABAQUS. The values are based on the calculations in [4]. As illustrated in the table, a crack of 0,209 mm means practically the total damage of the finite element. The data of table 2.3 are represented in the figures 2.21 and 2.22, too.

Crack opening	Stress	Damage variable
[mm]	N/mm^2	[-]
0,000	3,509	0,00
0,010	2,868	0,18
0,020	2,344	0,33
0,030	1,915	0,45
0,042	1,511	0,57
0,060	1,046	0,70
0,080	0,698	0,80
0,110	0,381	0,89
0,140	0,208	0,94
0,170	0,114	0,97
0,200	0,062	0,98
0,209	0,052	0,99

Table 2.3: ABAQUS settings for tensile behaviour of concrete C40/50

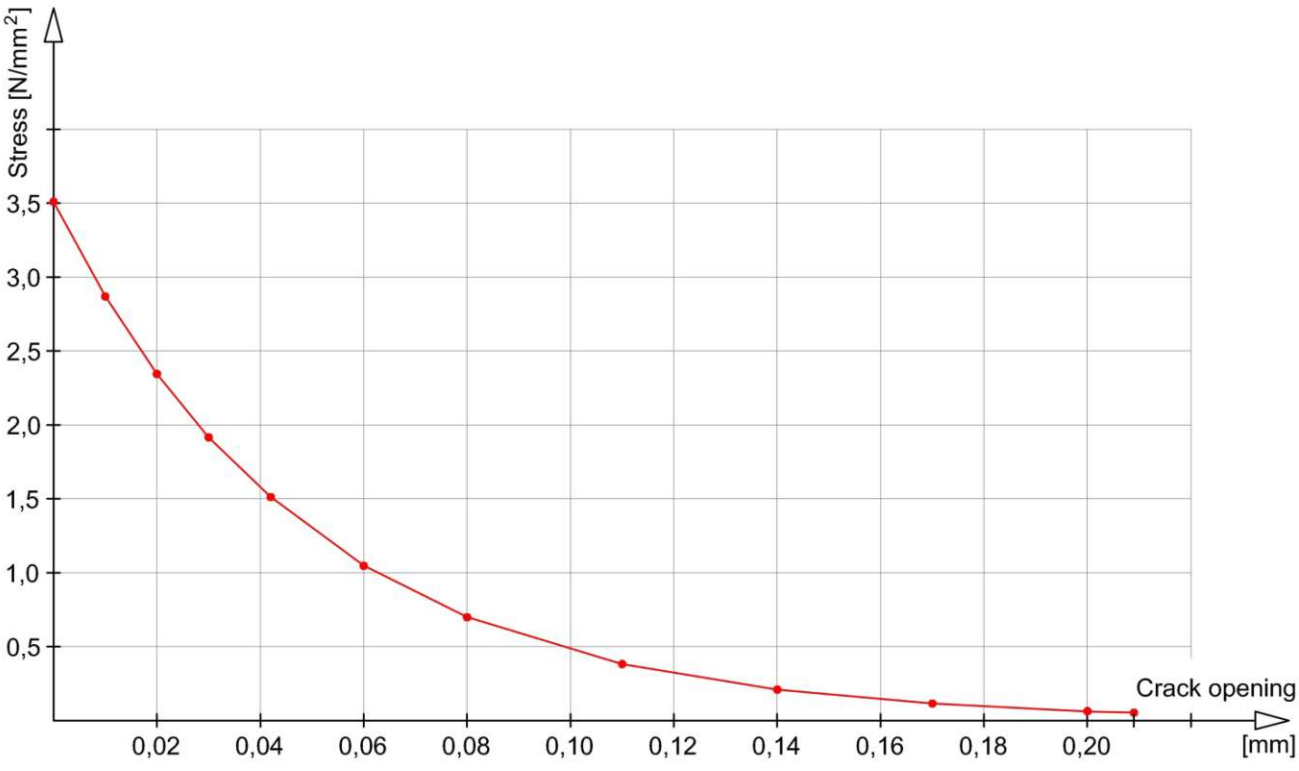

Figure 2.21: The stress-crack opening curve to define the behaviour of concrete under tension used in the ABAQUS analysis

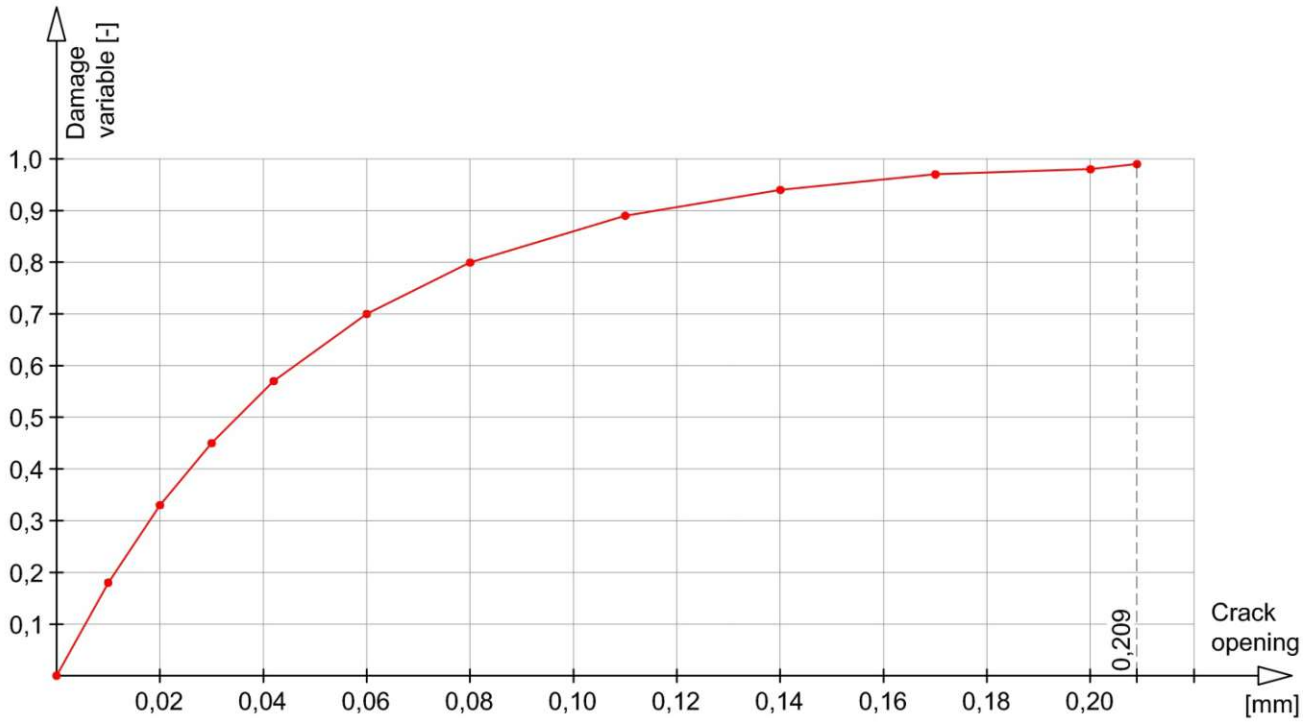

Figure 2.22: The damage variable-crack opening curve for the concrete material under tension used in the ABAQUS analysis

2.4 Load-carrying mechanism of the SCSC plate

2.4.1 Result analysis based on contact stresses calculated with ABAQUS

Lit.: [7], [8]

The complex load-bearing behaviour of the SCSC plate will be described in this chapter based on the contact stresses at the composite connections calculated with ABAQUS. Beside the presentation of the load-carrying mechanisms of the SCSC plate, the aim of chapter 2.4 is to define simple models which reproduce properly the results (maximal normal forces in the steel and concrete structure elements, the deflection of the composite plate, the dowel forces) of the complex ABAQUS calculation. The substitution of the complex ABAQUS calculation is not the expected from the simple models.

In chapter 2.4.1 the complex ABAQUS model will be analysed. As mentioned above, the analysis of the load-carrying mechanism uses the contact pressure and the contact traction values at the surface of the circular holes of the shear connectors. As described in chapter 2.2, the total vertical loading of the model at the examined loading in fatigue limit state is 322,06 kN, which is logically equal to the reaction forces at the support of the model (see figure 2.9). Figure 2.23 illustrates the shear forces transferred from the shear connectors to the end stiffeners according to the ABAQUS calculation. As the end stiffeners lie parallel to the main steel girder webs and the gap between them is only 2 mm, the forces are transmitted through the very short parts on the ends of the horizontal top and bottom steel plates. Thus, it is assumed that from the half of the total external loading (322,06/2 = 161,03 kN) the resultant of the three shear forces in figure 2.23 (16,00 + 32,00 + 16,00 = 64,00 kN) is transferred through the steel parts of the SCSC plate to the support. The rest part of the loading is transmitted through the concrete to the support:

$$F_{verical,concrete-support} = 161{,}03 - 64{,}00 = 97{,}03\ kN \tag{2.9}$$

Actually, as during modelling in ABAQUS friction was not taken into account between the steel web and the concrete core, the vertical components of forces from the concrete core press the bottom steel plate close to the support. However, this part of the external loading is considered as a loading which is transferred through the concrete.

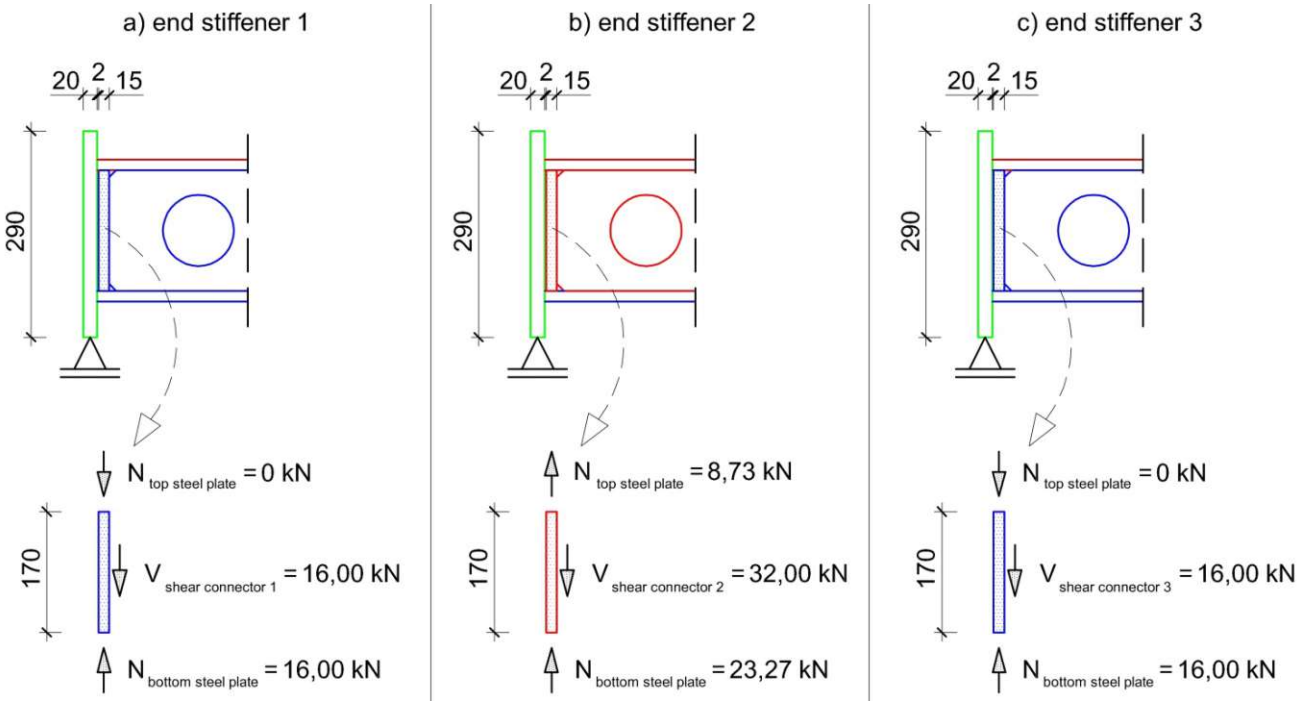

Figure 2.23: Static equilibriums of the three end stiffeners based on the ABAQUS calculation results

Without the concrete and the main steel girder webs, the bottom and the top steel sections would move relatively to each other due to bending from vertical loading. Figure 2.24 represents that compared to the bottom steel section, the top steel section would shift in the direction of the support, namely to the left in the figure.

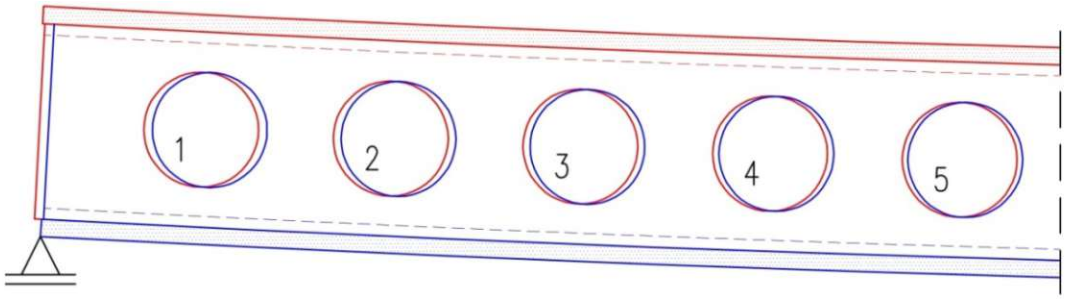

Figure 2.24: Slipping of the steel sections of the SCSC plate due to bending in case of missing concrete core. End stiffeners are not shown for the ease of view.

With a concrete filling between the shear connectors, they could not move unrestrictedly relative to each other. In accordance with figures 2.25 and 2.26, the concrete core would press the top steel section to the right, just as the bottom steel section to the left.

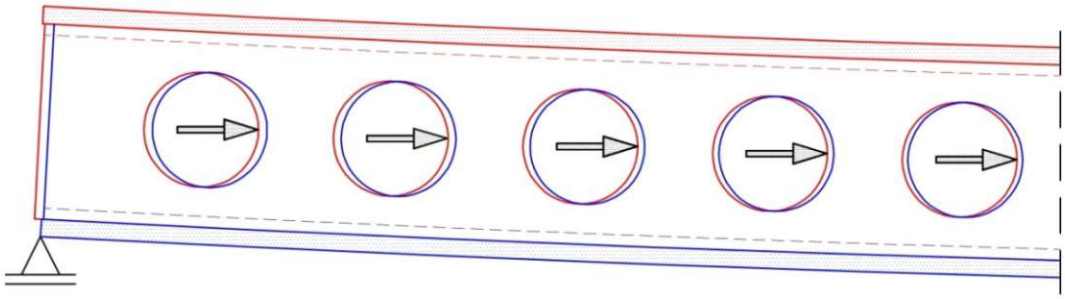

Figure 2.25: The effect of the concrete core on the top steel section

So, the directions of contact pressures on the surface of the circular holes are easily understandable. Logically, contact pressures calculated with ABAQUS reveal matching results which are illustrated in figures 2.27, 2.28, 2.31 and 2.32.

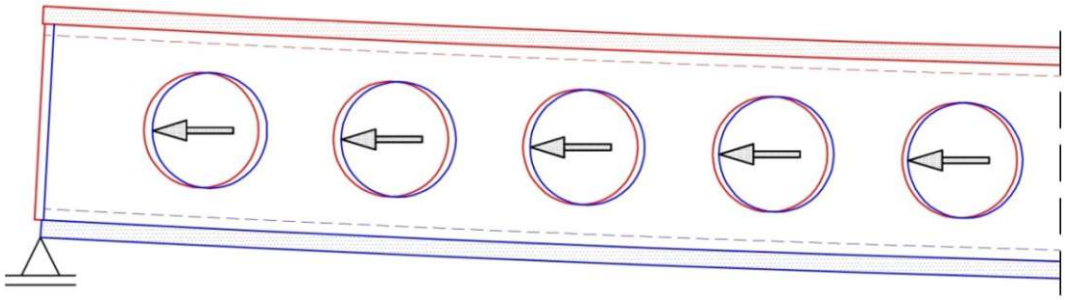

Figure 2.26: The effect of the concrete core on the bottom steel section

As friction between steel and concrete on the surface of the circular holes is taken into account in ABAQUS modelling, frictional shear stresses (see figures 2.29, 2.30, 2.33 and 2.34) control the resultant forces in the composite connections. The figures 2.27, 2.28, 2.29 and 2.30 illustrate the contact stresses at the shear connector of the top steel section, as the figures 2.31, 2.32, 2.33 and 2.34 show these stresses at the shear connector of the bottom steel section. Moreover, each of these figures represents the horizontal and vertical components of the resultant forces calculated from the illustrated stresses of the finite elements along the edge of the circular holes in the steel shear connectors.

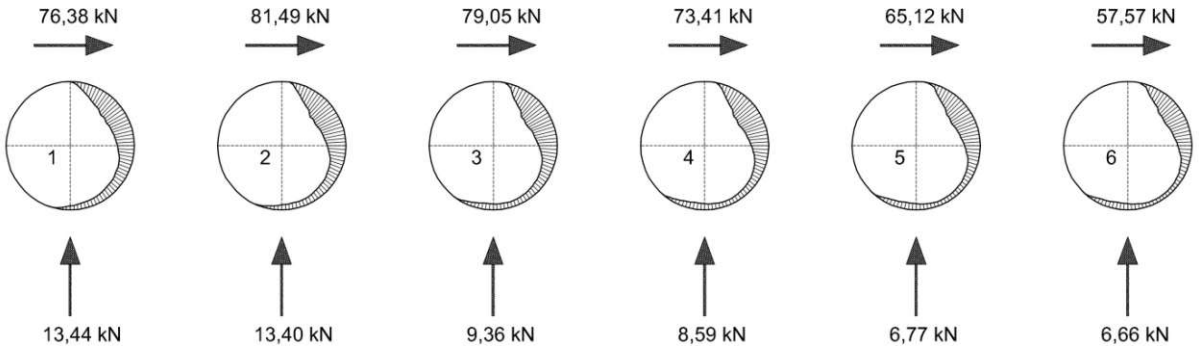

Figure 2.27: Contact pressures on the surface of the circular holes numbered 1 - 6 (top steel section) according to ABAQUS

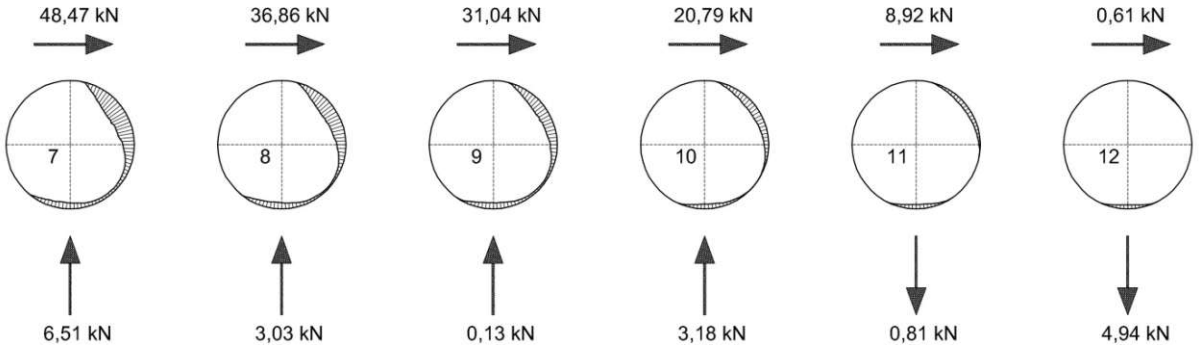

Figure 2.28: Contact pressures on the surface of the circular holes numbered 7 - 12 (top steel section) according to ABAQUS

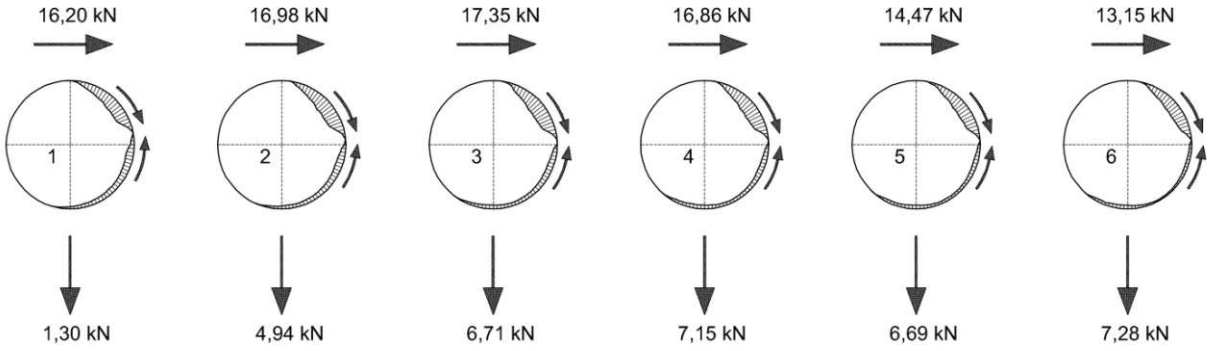

Figure 2.29: Frictional shear stresses on the surface of the circular holes num. 1 - 6 (top steel section) according to ABAQUS

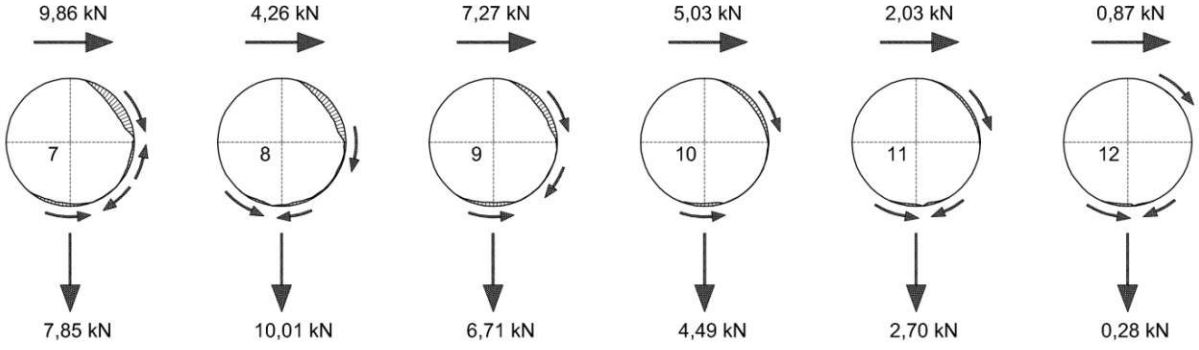

Figure 2.30: Frictional shear stresses on the surface of the circular holes num. 7 - 12 (top steel section) according to ABAQUS

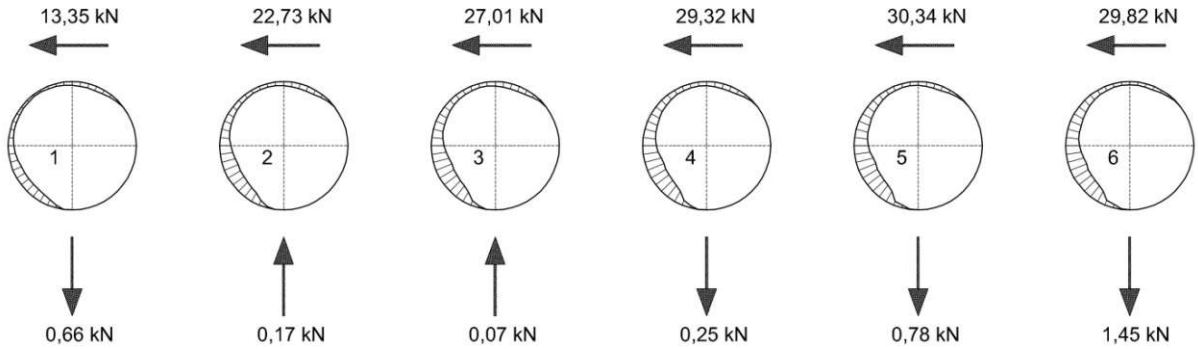

Figure 2.31: Contact pressures on the surface of the circular holes numbered 1 - 6 (bottom steel section) according to ABAQUS

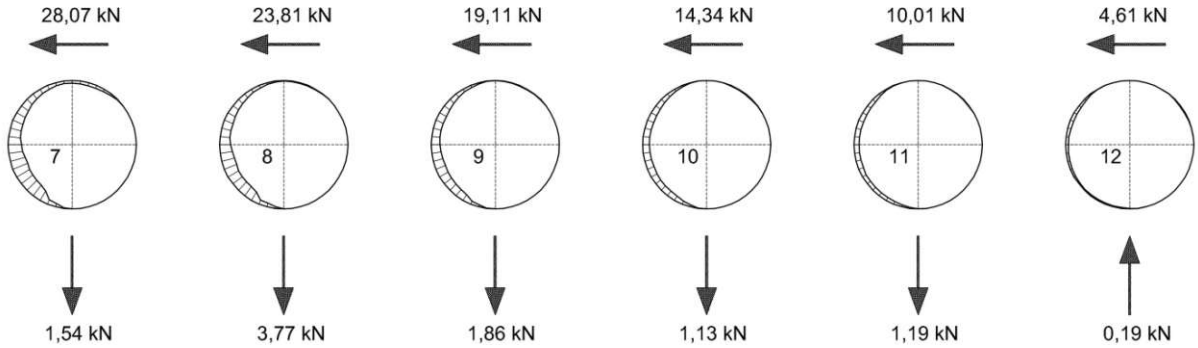

Figure 2.32: Contact pressures on the surface of the circular holes numbered 7 - 12 (bottom steel section) according to ABAQUS

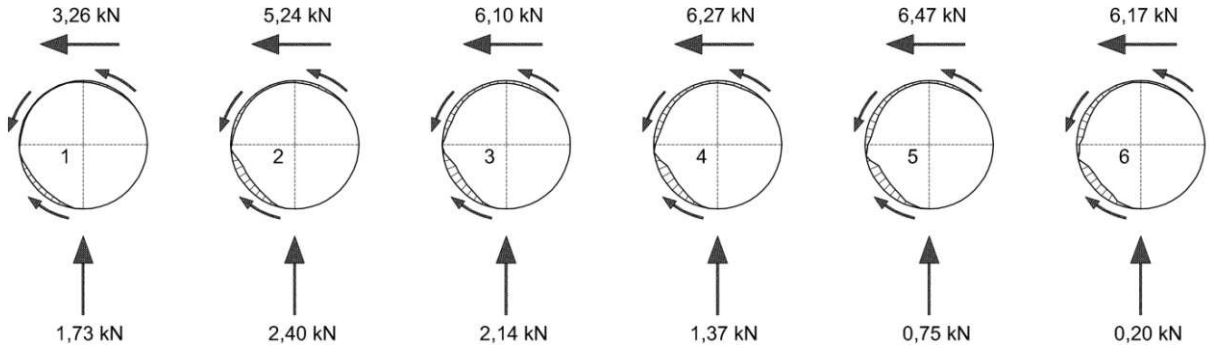

Figure 2.33: Frictional shear stresses on the surface of the circular holes num. 1 - 6 (bottom steel section) according to ABAQUS

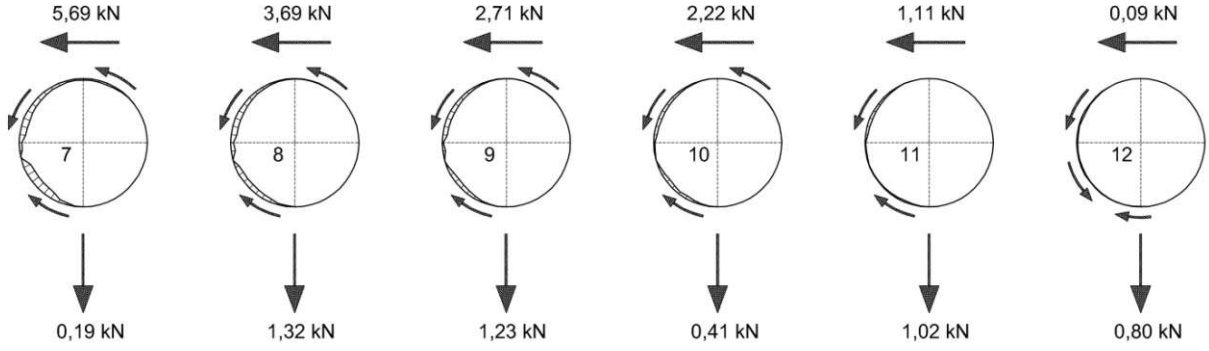

Figure 2.34: Frictional shear stresses on the surface of the circular holes num. 7 - 12 (bottom steel section) according to ABAQUS

Through the frictional shear stresses a small resultant moment acts also at each of the circular holes. However, this effect is not symbolised in the previous figures. Moreover, it is noticeable in the above illustrated figures that the shear connector of the top steel section has more stress results (stripes in radial direction) compared to the shear connector of the bottom steel section. The reason of this fact is that in the case of the shear connector of the top steel section a finer mesh is used in ABAQUS modelling. Another important point to mention is that the shear connector of the top steel section (shear connector 2 in figure 2.12) is 20 mm thick, as the shear connectors of the bottom steel section (shear connectors 1 and 3 in figure 2.11) have a thickness of 10 mm. The resultant forces in figures 2.31 – 2.34 represent the forces at one outside shear connector. Thus, it is clear that, for example, at the sixth hole of the shear connector of the top steel section the horizontal resultant force is approximately double of the horizontal resultant force at the sixth hole of the shear connector of the bottom steel section. However, the contact stresses are approximately the same (see the contact pressures in figures 2.27 and 2.31). The resultant of the contact stresses (contact pressures and frictional shear stresses) is derived simply through addition. Table 2.4 shows these resultant force components at each hole. Positive horizontal force means a direction to the right in figures 2.27 – 2.34, as positive vertical force represents a direction downwards. The positive directions are also given in figure 2.16 through the coordinate system.

Hole numb.	1	2	3	4	5	6	7	8	9	10	11	12	Σ
$F_{horizontal}$ (shear con. 2)	92,58	98,47	96,40	90,27	79,59	70,72	58,33	41,12	38,31	25,82	10,95	1,48	704,04
$F_{vertical}$ (shear con. 2)	-12,14	-8,46	-2,65	-1,44	-0,08	0,62	1,34	6,98	6,58	1,31	3,51	5,22	0,79
$F_{horizontal}$ (shear con. 1)	-16,61	-27,97	-33,11	-35,59	-36,81	-35,99	-33,76	-27,50	-21,82	-16,56	-11,12	-4,70	-301,54
$F_{vertical}$ (shear con. 1)	-1,07	-2,57	-2,21	-1,12	0,03	1,25	1,73	5,09	3,09	1,54	2,21	0,61	8,58

Table 2.4: Horizontal and vertical components of resultant forces in the composite connections. Forces in [kN]

In table 2.4 given horizontal and vertical components of resultant forces at the holes of the shear connectors can be calculated in ABAQUS directly with the so-called “Free Body Cuts” method, too. However, these values are not meaningful for the further analysis as different effects are included in one resultant. Actually, according to figure 2.27, 2.28, 2.31 and 2.32, two effects produce contact pressures between the steel and the concrete at the surface of a circular hole. Figures 2.35 and 2.36 illustrate the different type of pressures with green and red in the case of one single hole.

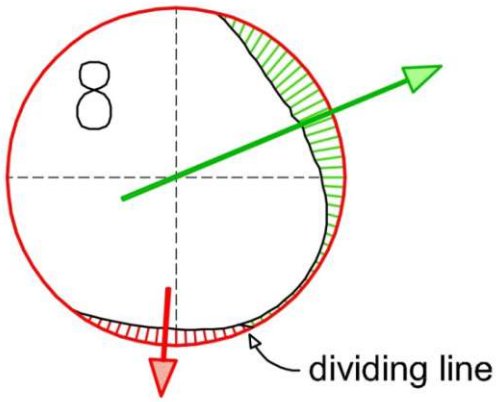

Figure 2.35: Contact pressures on the surface of the circular hole (hole number 8, shear connector 2) according to ABAQUS

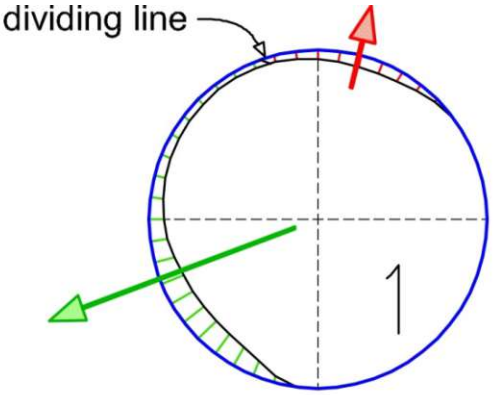

Figure 2.36: Contact pressures on the surface of the circular hole (hole number 1, shear connector 1) according to ABAQUS

Corresponding to the effect described above through the figures 2.24, 2.25 and 2.26, it is clear that the concrete core is compressed between the circular holes of the top and bottom steel sections to prevent the horizontal displacements between them. The green components of the contact pressures in figures 2.35 and 2.36 represent this effect (effect 1: shear load transfer). The red components of contact pressures symbolise the vertical load transfer between the steel structure and the concrete (effect 2). Considering effect 2, the top steel section gets vertical loads through the concrete from the external loading (see figures 2.35 and 2.37), and the bottom steel section transfers vertical forces to the support through it (see figures 2.36 and 2.38). In figures 2.37 and 2.38 illustrated truss frame models include concrete members which are loaded through the external loading (see figure 2.37) or through the shear connector of the bottom steel section (see figure 38).

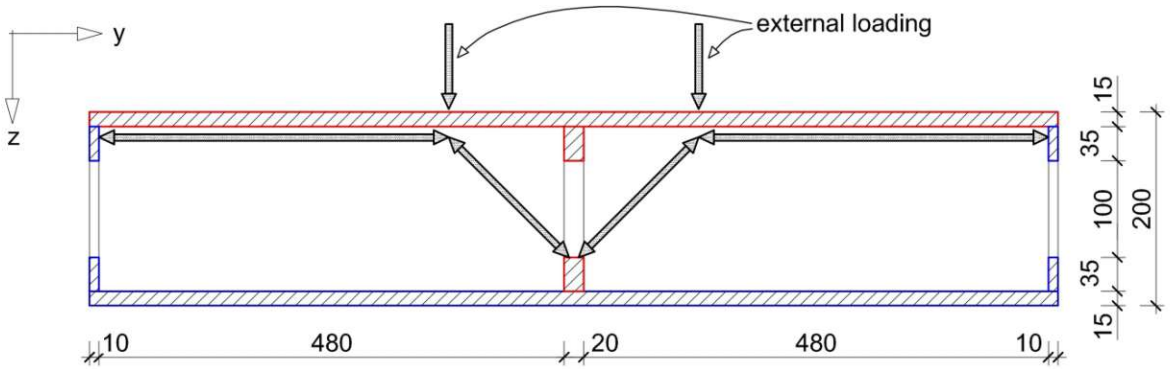

Figure 2.37: The planar truss frame model illustrates the load transfer to the central shear connector from the external loading

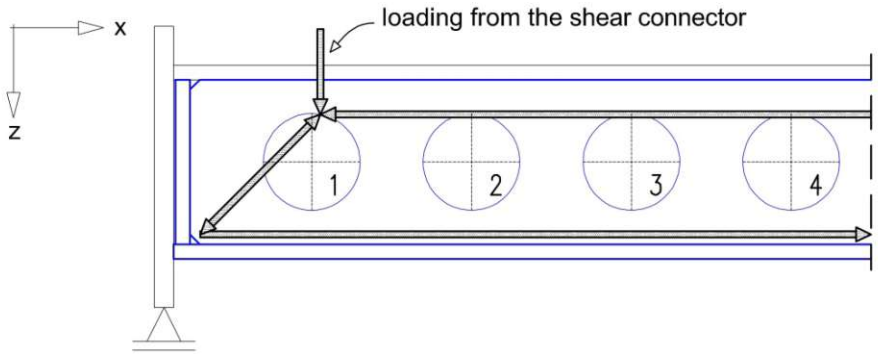

Figure 2.38: The planar truss frame model symbolises the force transfer to the support from the first circular hole of the shear connector of the bottom steel section

Figures 2.35, 2.36 and 2.39 illustrate the resultant forces of the two different effects, too. The lengths of the arrows symbolise the magnitude of the forces. However, in the case of these three figures, the arrows of the resultants at the top steel section denote just the half of the total forces in the composite connections. Thus, the forces are symbolised which act into the direction of one shear connector of the bottom steel section (for instance shear connector 1). Logically, figure 2.39(b) represents the forces at only one shear connector of the bottom steel section (shear connector 1). In this way, it is possible to compare the green arrows at the top and the bottom steel section (see figure 2.39).

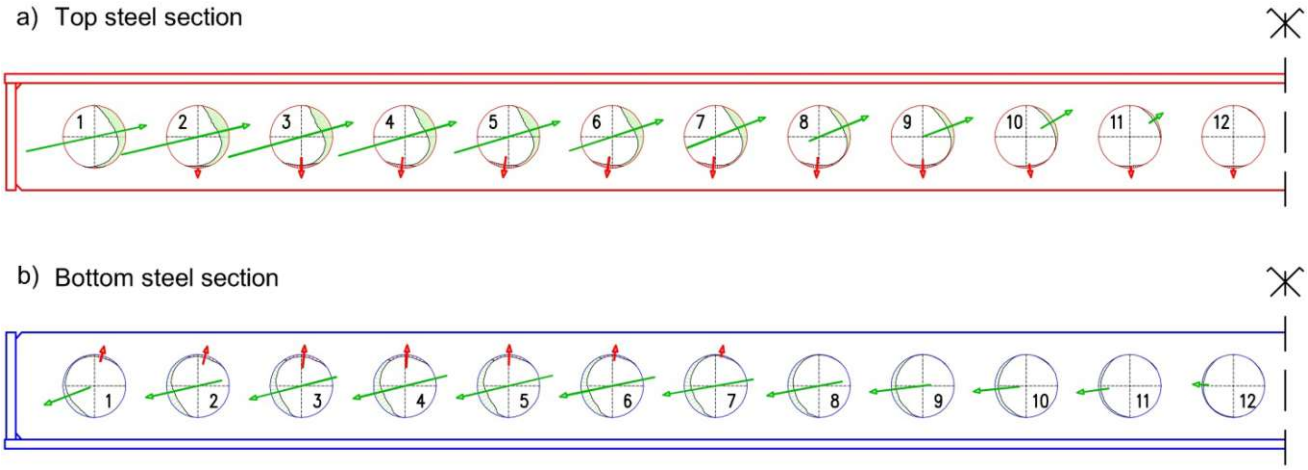

Figure 2.39: Contact pressures on the surface of the circular holes: a) top steel section; b) bottom steel section

The dividing line between the two parts of the contact pressures (effect 1 and 2) is located visually (for example: see figures 2.35 and 2.36). As frictional shear stresses control the resultant forces, these contact stresses are also divided into two parts. Here, the dividing line positions defined at the contact pressures are also used.

The values representing effect 2 (red arrows in figure 2.39) are given in tables 2.5 and 2.6. In the case of the shear connector 2, the horizontal and vertical resultant forces from the contact pressures and from the frictional shear stresses are represented separately in table 2.5. Moreover, the horizontal and vertical resultants of the two types of contact stresses are registered in the fifth and sixth row of the table. Table 2.6 presents the resultants for the shear connector 1 in kN.

Number of hole	1	2	3	4	5	6	7	8	9	10	11	12	Σ
Contact pressure $F_{horizontal}$ (shear con. 2)	0,00	0,00	0,00	-1,41	-1,68	-1,68	-1,02	-0,87	0,08	0,96	0,26	0,00	-5,36
Contact pressure $F_{vertical}$ (shear con. 2)	2,96	5,67	12,54	12,67	12,92	12,77	12,90	12,68	11,50	8,38	6,94	5,71	117,64
Frictional shear str. $F_{horizontal}$ (shear con. 2)	0,70	1,46	3,57	3,75	3,50	3,42	2,74	-0,61	3,02	1,76	0,28	0,75	24,34
Frictional shear str. $F_{vertical}$ (shear con. 2)	0,03	0,06	0,08	0,42	0,44	0,47	0,48	0,00	0,14	0,03	0,31	0,19	2,65
Resultant $F_{horizontal}$ (shear con. 2)	0,70	1,46	3,57	2,34	1,82	1,74	1,72	-1,48	3,10	2,72	0,54	0,75	18,98
Resultant $F_{vertical}$ (shear con. 2)	2,99	5,73	12,62	13,09	13,36	13,24	13,38	12,68	11,64	8,41	7,25	5,90	120,29

Table 2.5: Effect 2: horizontal and vertical components of forces in the composite connections of the top steel section

Number of hole	1	2	3	4	5	6	7	8	9	10	11	12	Σ
Contact pressure $F_{horizontal}$ (shear con.1)	1,21	1,35	0,57	0,39	0,13	0,42	0,65	0,15	0,23	0,32	0,14	0,42	5,98
Contact pressure $F_{vertical}$ (shear con. 1)	-4,82	-5,65	-7,15	-7,01	-6,36	-4,75	-3,44	-0,70	-0,45	-0,42	-0,14	-0,29	-41,18
Frictional shear str. $F_{horizontal}$ (shear con. 1)	-1,00	-1,46	-2,05	-2,00	-1,86	-1,34	-1,01	-0,19	-0,11	-0,06	0,02	0,05	-11,01
Frictional shear str. $F_{vertical}$ (shear con. 1)	-0,30	-0,35	-0,17	-0,11	-0,04	-0,13	-0,19	-0,04	-0,06	-0,05	0,01	0,07	-1,36
Resultant $F_{horizontal}$ (shear con. 1)	0,21	-0,11	-1,48	-1,61	-1,73	-0,92	-0,36	-0,04	0,12	0,26	0,16	0,47	-5,03
Resultant $F_{vertical}$ (shear con. 1)	-5,12	-6,00	-7,32	-7,12	-6,40	-4,88	-3,63	-0,74	-0,51	-0,47	-0,13	-0,22	-42,54

Table 2.6: Effect 2: horizontal and vertical components of forces in the composite connections of the bottom steel section

Logically, the differences between the resultant forces in figures 2.27 – 2.34 and the matching results in tables 2.5 and 2.6 delivers the values representing effect 1 (green arrows in figure 2.39). Only the horizontal and vertical resultants of these forces are illustrated in table 2.7.

Hole numb.	1	2	3	4	5	6	7	8	9	10	11	12	Σ
$F_{horizontal}$ (shear con. 2)	91,88	97,01	92,83	87,93	77,77	68,98	56,61	42,60	35,21	23,10	10,41	0,73	685,06
$F_{vertical}$ (shear con. 2)	-15,13	-14,19	-15,27	-14,53	-13,44	-12,62	-12,04	-5,70	-5,06	-7,01	-3,74	-0,68	-119,41
$F_{horizontal}$ (shear con. 1)	-16,82	-27,86	-31,63	-33,98	-35,08	-35,07	-33,40	-27,46	-21,94	-16,82	-11,28	-5,17	-296,51
$F_{vertical}$ (shear con. 1)	4,05	3,43	5,11	6,00	6,43	6,13	5,36	5,83	3,60	2,01	2,34	0,83	51,12

Table 2.7: Effect 1: horizontal and vertical components of forces in the composite connections. Forces in [kN]

Next, the horizontal force transferred between the shear connectors 1 and 2 will be evaluated. According to table 2.7, the total horizontal force at the 12 holes of the shear connector 2 is 685,06 kN. Here, only effect 1 is considered. In the case of the shear connector 1, this resultant is 296,51 kN. It is assumed that shear connector 3 delivers the same force because of the symmetry of the structure and loading. From the shear connector 2 horizontal forces are transmitted to the end plate and to the end stiffeners 1 and 3, too. Thus, necessarily, the total horizontal force of 685,06 kN is not transferred only to the outside shear connectors (shear connector 1 and 3) from the shear connector 2. Figure 2.40 illustrates the horizontal forces delivered through the concrete core to the support. The end stiffener of the top steel section does not receive any compression from the concrete. The outside end stiffeners have contact surfaces to the outside concrete dowels and to the concrete core, too. Thus, two different forces are marked at these construction parts in figures 2.40(b) and 2.40(c). It is also remarkable that the ABAQUS calculation results are not perfectly the same at the end stiffeners 1 and 3. However, logically, the differences are not significant. The resultant of the five horizontal forces in figure 2.40 is 298,55 kN.

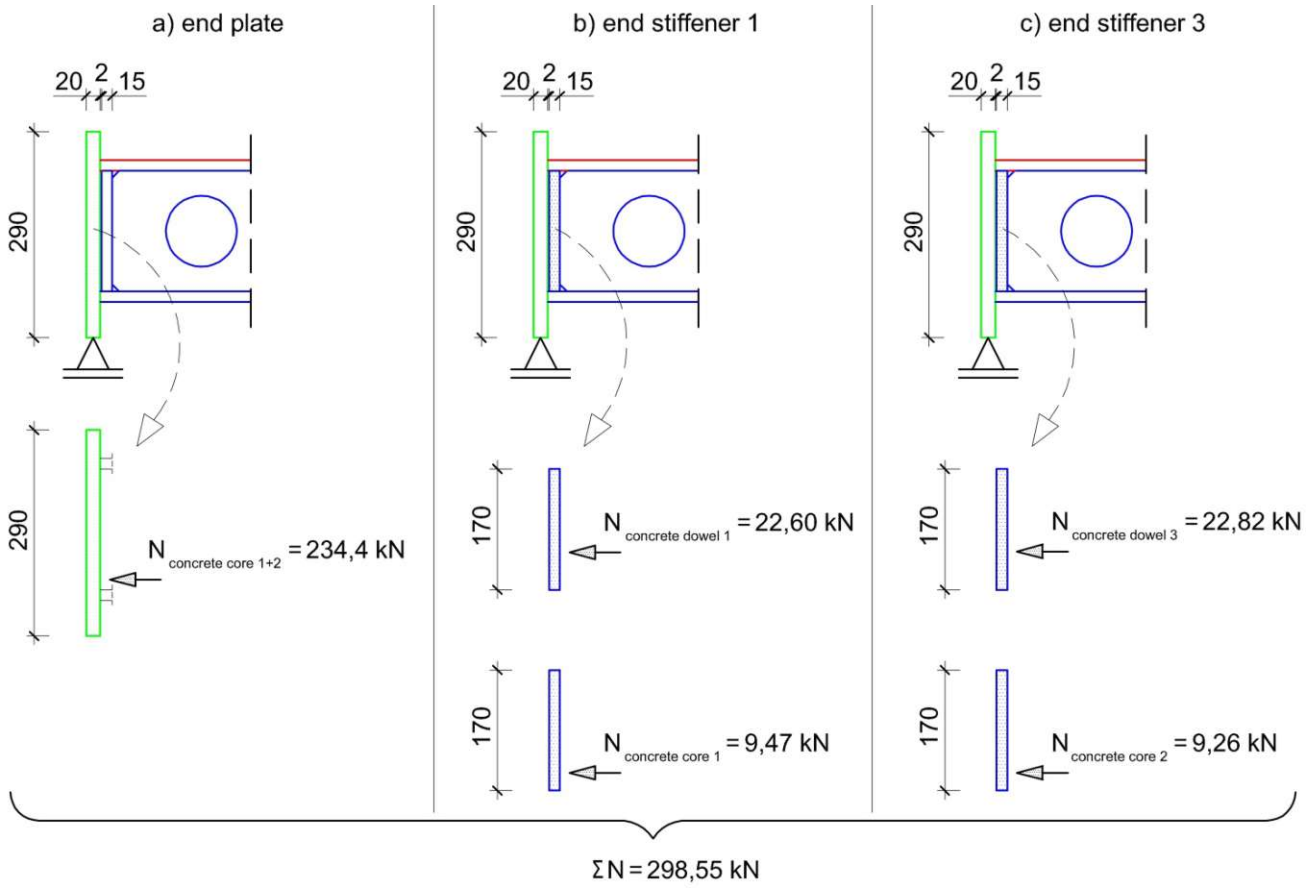

Figure 2.40: Horizontal compressions from the concrete parts at the support based on the ABAQUS calculation results

The horizontal tensile forces in the bottom steel plate and in the two outside shear connectors compensate the compressions illustrated in figure 2.40. Moreover, a small tensile force acts at the end of the top steel plate, too. However, logically, this force is negligible compared to the tension in the bottom steel plate. These forces are illustrated in figure 2.41. Through the figures 2.40 and 2.41 the static equilibriums of the end plate and the two outside end stiffeners regarding the horizontal forces are also shown. The marked forces in the bottom steel plate in figures 2.41(b) and 2.41(c) are transferred between the end stiffeners and the bottom steel plate as shear forces acting in the contact surface between them. However, these forces are illustrated in the steel plates close to the end stiffeners for ease of view. Obviously, the horizontal forces represented in figure 2.41(a) occur also close to the end plate.

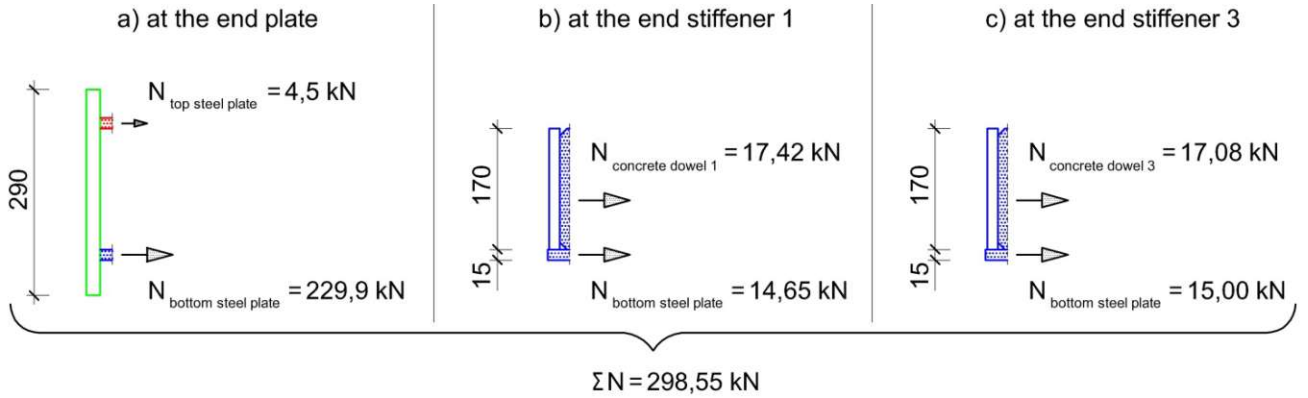

Figure 2.41: Horizontal tensile forces in the steel structures around the support as compensations of the compressive forces from the concrete parts. The values are based on the ABAQUS calculation results. Dimensions in [mm]

Additionally, it is assumed that the total horizontal compression force of 298,55 kN at the support arises due to the compressed concrete parts pressed from the shear connector of the top steel section (see effect 1 in figure 2.39(a)). This means that there is not any horizontal component of loads transferred only through the concrete core to the support. Thus, from the total horizontal force at the 12 holes of the shear connector 2 (685,06 kN) 298,55 kN is transmitted to the end steel plate and the end stiffeners 1 and 3. The residual force of 386,51 kN (685,06 kN – 298,55 kN) means the interaction between the central shear connector (shear connector 2) and the outside shear connectors (shear connector 1 and 3). Actually, half of the force of 386,51 kN acts between the shear connector 2 and shear connector 1. Logically, the other half of the force appears between the shear connectors 2 and 3.

As a control, the force between the shear connectors can be also calculated through the evaluation of the forces at the plane of symmetry. Here, each of the five concrete parts is considered. As illustrated in figure 2.42, at the plane of symmetry compressions occur at the top part of the concrete sections, while the bottom parts have tension. The resultant forces calculated from the compressive and tensile stresses from ABAQUS are shown in the figure. The total compression in the five concrete parts is 442,47 kN, while the total tension means a value of 237,05 kN. The difference between these two values (205,42 kN) is considered as the compression between the outside shear connectors and the plane of symmetry (boundary plane 2 in figure 2.17). Thus, the assumption mentioned above is valid here, too: there is not any horizontal component of loads transferred only through the concrete core to the support.

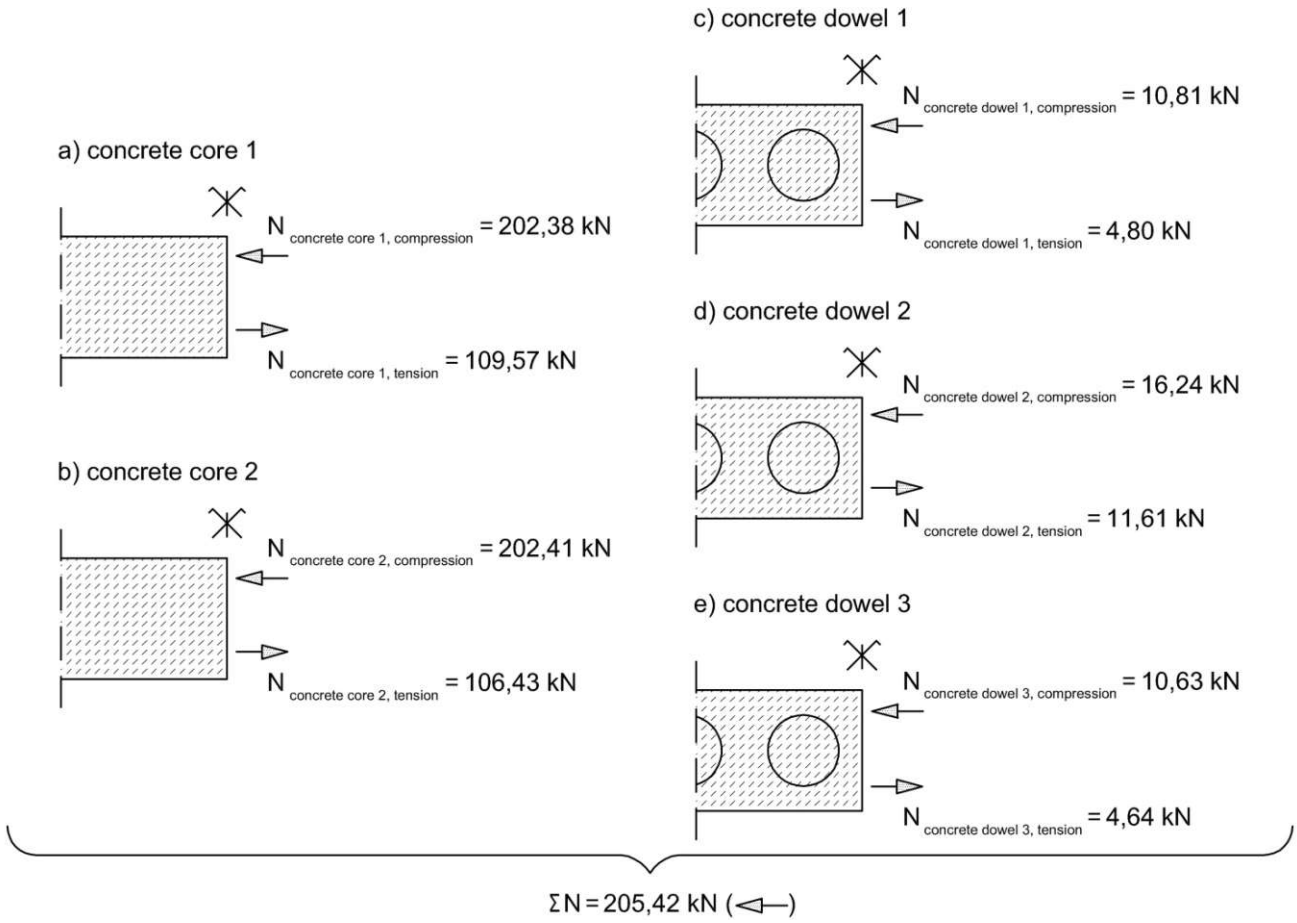

Figure 2.42: Horizontal compression and tension in the concrete parts at the plane of symmetry based on the ABAQUS results

Therefore, from the total horizontal force at the holes of the two outside shear connectors (2·296,51 = 593,02 kN) 205,42 kN is transmitted to the plane of symmetry (see figure 2.17: boundary plane 2) which is actually a support in the ABAQUS model. The residual force of 387,60 kN (593,02 kN – 205,42 kN) is the transmitted force between the central

and the two outside shear connectors. This result is practically equal to the value of 386,51 kN calculated above through the evaluation of horizontal forces at the support. For the further calculation the average of the two results (387,06 kN) is used. Thus, the transmitted forces are also modified a little bit. Namely, the transferred horizontal force between the shear connector 2 and the support (end plate and end stiffeners) is considered as:

$$F_{horizontal,top\ steel\ section-support} = 685{,}06 - 387{,}06 = 298{,}00\ kN \tag{2.10}$$

Moreover, the transferred horizontal force between the two outside shear connectors and the plane of symmetry is:

$$F_{horizontal,bottom\ steel\ section-plane\ of\ symmetry} = 593{,}02 - 387{,}06 = 205{,}96\ kN \tag{2.11}$$

Logically, these values are almost equal to the ABAQUS results presented above (298,55 kN, 205,42 kN). As a summary of the above described calculation, the static equilibrium of the concrete regarding the horizontal forces are illustrated in figure 2.43. The forces at the holes of the shear connectors are summarized into one resultant. To show the resultant horizontal force from the central shear connector, the concrete is divided in the middle of the model, and the two concrete sections are shifted from each other. It is notable to mention that the illustrated resultants of the horizontal forces in the composite connections (685,06 kN, 296,51 kN) represent only effect 1. These values are calculated in table 2.7. This means that the horizontal forces at the shear connectors due to effect 2 is neglected as an approximation.

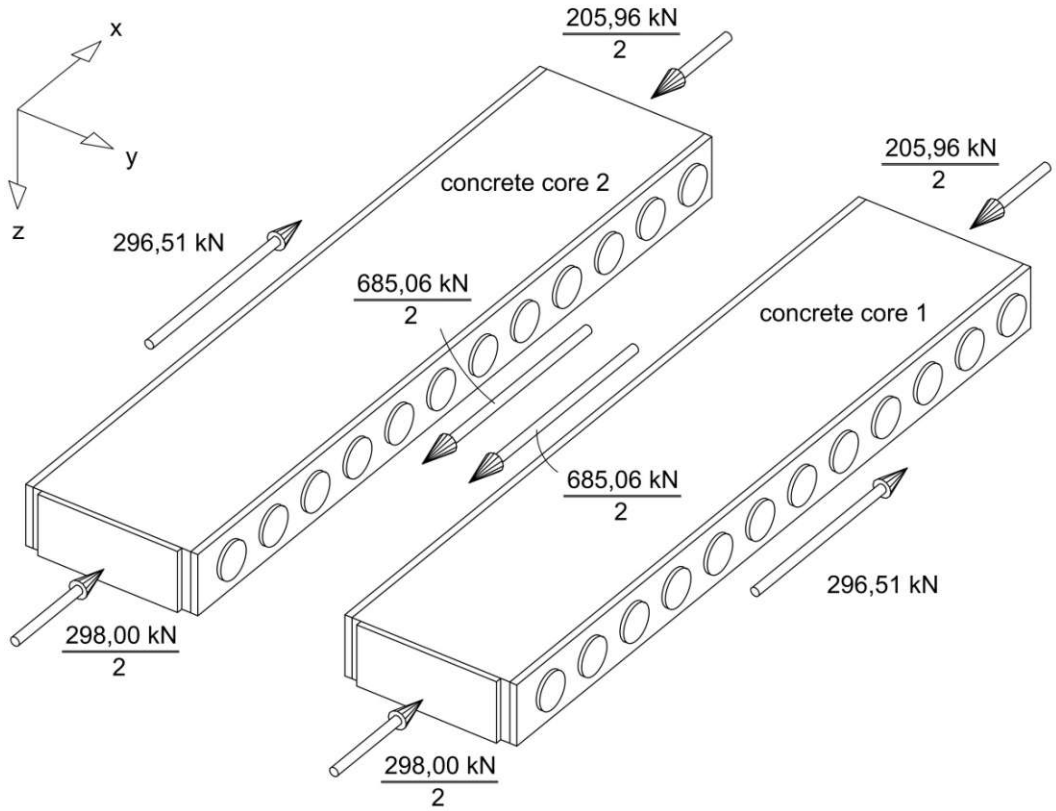

Figure 2.43: The static equilibrium of the concrete parts regarding the horizontal forces in x direction. The two concrete portions are shifted from each other to illustrate the resultant of the horizontal forces from the central shear connector (685,06 kN).

Next, the horizontal components of the forces from effect 1 (see table 2.7) will be distributed between the single circular holes. The compressed concrete parts of the ABAQUS model will be symbolised by concrete struts as an approximation. Moreover, at the following force distribution a minimal number of concrete struts are used. The transferred force of

298,00 kN between the shear connector of the top steel section and the support means that the concrete core can be symbolised with four concrete struts around the support at both side of the central shear connector (see figure 2.44). According to the results in table 2.7, the top steel section delivers 281,72 kN (91,88 kN + 97,01 kN + 92,83 kN) to the support from the first three holes. This means that additionally 16,28 kN (298,00 kN – 281,72 kN) is transferred from the fourth circular hole to the support. As mentioned above, support means the end plate and the two outside end stiffeners.

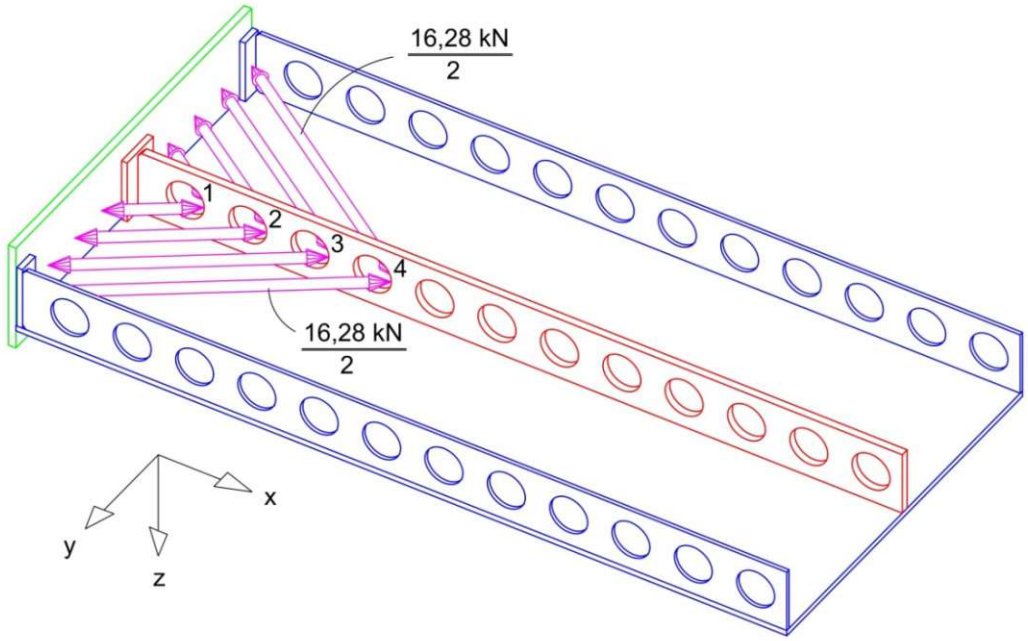

Figure 2.44: The violet-coloured struts symbolise the horizontal force transfer between the top steel section and the support

The transferred force of 205,96 kN between the shear connectors of the bottom steel section and the plane of symmetry means that the concrete core can be symbolised with six concrete struts around the plane of symmetry at both of the two outside shear connectors (see figure 2.45).

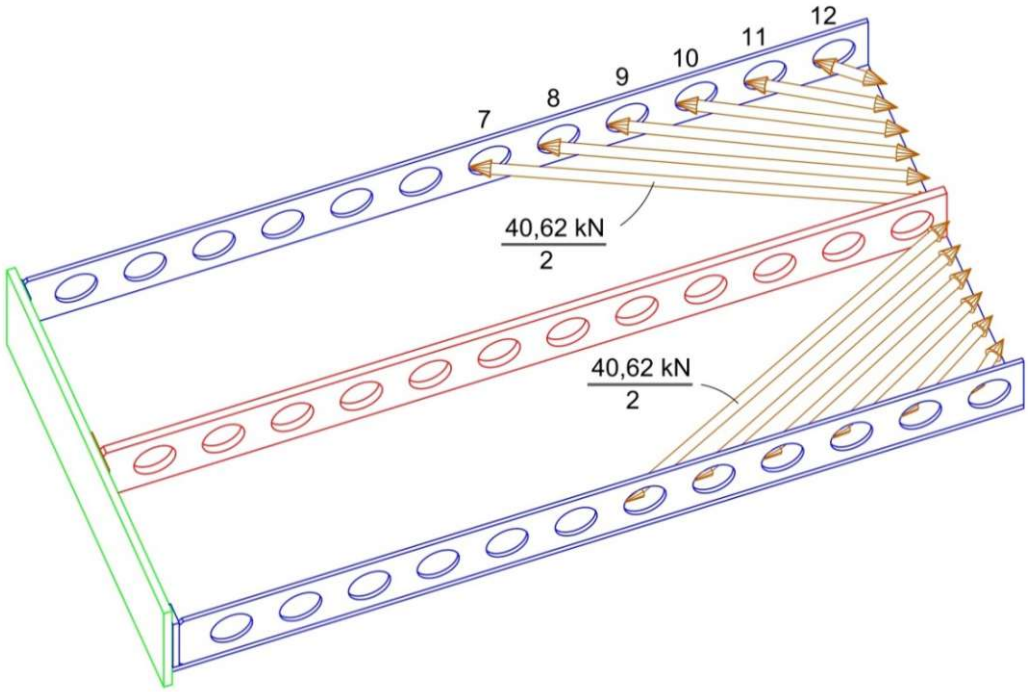

Figure 2.45: The brown struts show the horizontal force transfer between the bottom steel section and the plane of symmetry

According to the results in table 2.7, the bottom steel section delivers a horizontal force of 165,34 kN to the plane of symmetry from the last five holes (hole numbers 8, 9, 10, 11, 12). This means that additionally 40,62 kN (205,96 kN – 165,34 kN) is transferred from the two seventh hole of the outside shear connectors to the plane of symmetry.

Table 2.7 is modified, so that the above mentioned horizontal forces delivered to the support and to the plane of symmetry are deleted. In this way, in table 2.8 only the horizontal forces are summarized which are transmitted between the shear connectors. Logically, the total sum of the forces at the shear connector 2 is 387,06 kN in the table. Obviously, in the case of the shear connector 1, this resultant is half of the force of 387,06 kN, as both the shear connectors 1 and 3 are considered in the load-carrying mechanisms.

Number of hole	1	2	3	4	5	6	7	8	9	10	11	12	Σ
$F_{horizontal}$ (shear con. 2)	-	-	-	71,65	77,77	68,98	56,61	42,60	35,21	23,10	10,41	0,73	387,06
$F_{horizontal}$ (shear con. 1)	-16,82	-27,86	-31,63	-33,98	-35,08	-35,07	-13,09	-	-	-	-	-	-193,53

Table 2.8: Effect 1: horizontal components of forces in the composite connections acting between the shear connectors

At the first circular holes of the two outside shear connectors act 16,82 kN separately (see table 2.8). It is assumed that these forces are transferred to the fourth circular hole of the top steel section. Additionally, this fourth hole receives load from the second holes of the outside shear connectors, too. Namely, 38,01 kN (71,65 kN – 2 · 16,82 kN) need to be delivered there from the two outside shear connectors together. In this way, the total horizontal force at the fourth hole of the central shear connector (71,65 kN, see table 2.8) is reached. However, in the second holes of the outside shear connectors remains 8,855 kN (27,86 kN – 0,5 · 38,01 kN) to be transmitted to the other holes of the shear connector of the top steel section. Thus, the remaining forces to distribute are shown in the first and the second table row of table 2.9. The further steps of the load distribution are similar to the above described method. Thus, the remaining forces are illustrated step by step in the additional table rows without any explanation.

In this way, the horizontal forces due to the effect 1 are distributed between the top and the bottom steel sections. Thus, the interaction can be modelled with 15 concrete struts between the shear connectors 1 and 2 as well as between the shear connectors 2 and 3. Figure 2.46 illustrates these concrete struts with the green arrows. Moreover, the 15 force components are given in the table 2.10 where the transmitted forces between the shear connectors 1 and 2 are shown. Because of the symmetry of the structure and the loading, the same forces are transferred between the shear connectors 2 and 3. Obviously, the forces in the table mean only the components in the x direction (see the coordinate system in figure 2.44) of the force occurring in the concrete struts illustrated in figure 2.46. The numbering of struts is carried out from the end plate to the plane of symmetry (from left to right in figure 2.46). Logically, the total sum of the forces in table 2.10 is 193,53 kN. It is remarkable in table 2.10 that in the case of four concrete struts (number 5, 7, 12, 15) the forces do not exceed 4,1 kN. These forces are not significant compared to the forces in the other struts. Thus, figure 2.47 represents only 11 concrete struts to illustrate the main effects between the central shear connector and one of the outside shear connectors. The 11 struts illustrated in figure 2.47 deliver 96,3 % of the total loading represented in figure 2.46 with 15 concrete struts. Additionally, 7 concrete struts from 11 are pointed out in green in figure 2.47. These struts transmit forces in x direction higher than 10 kN. The grey arrows illustrate the concrete struts (number 3, 9, 13, 14) with a force component in x direction between 4,1 kN and 10 kN. The 7 green struts transfer 81,1 % of the total loading. Thus, the significant part of transmission can be symbolised through only these 7 struts between one outside shear connector and the central shear connector.

Number of hole	1	2	3	4	5	6	7	8	9	10	11	12
$F_{horizontal}$ (shear connector 2)	-	-	-	-	77,77	68,98	56,61	42,60	35,21	23,10	10,41	0,73
$F_{horizontal}$ (shear connector 1)	-	-8,855	-31,63	-33,98	-35,08	-35,07	-13,09	-	-	-	-	-
$F_{horizontal}$ (shear connector 2)	-	-	-	-	-	68,98	56,61	42,60	35,21	23,10	10,41	0,73
$F_{horizontal}$ (shear connector 1)	-	-	-1,60	-33,98	-35,08	-35,07	-12,62	-	-	-	-	-
$F_{horizontal}$ (shear connector 2)	-	-	-	-	-	-	56,61	42,60	35,21	23,10	10,41	0,73
$F_{horizontal}$ (shear connector 1)	-	-	-	-1,09	-35,08	-35,07	-13,09	-	-	-	-	-
$F_{horizontal}$ (shear connector 2)	-	-	-	-	-	-	-	42,60	35,21	23,10	10,41	0,73
$F_{horizontal}$ (shear connector 1)	-	-	-	-	-7,865	-35,07	-13,09	-	-	-	-	-
$F_{horizontal}$ (shear connector 2)	-	-	-	-	-	-	-	-	35,21	23,10	10,41	0,73
$F_{horizontal}$ (shear connector 1)	-	-	-	-	-	-21,635	-13,09	-	-	-	-	-
$F_{horizontal}$ (shear connector 2)	-	-	-	-	-	-	-	-	-	23,10	10,41	0,73
$F_{horizontal}$ (shear connector 1)	-	-	-	-	-	-4,03	-13,09	-	-	-	-	-
$F_{horizontal}$ (shear connector 2)	-	-	-	-	-	-	-	-	-	15,04	10,41	0,73
$F_{horizontal}$ (shear connector 1)	-	-	-	-	-	-	-13,09	-	-	-	-	-

Table 2.9: Effect 1: distribution of the horizontal forces in the composite connections between the shear connectors

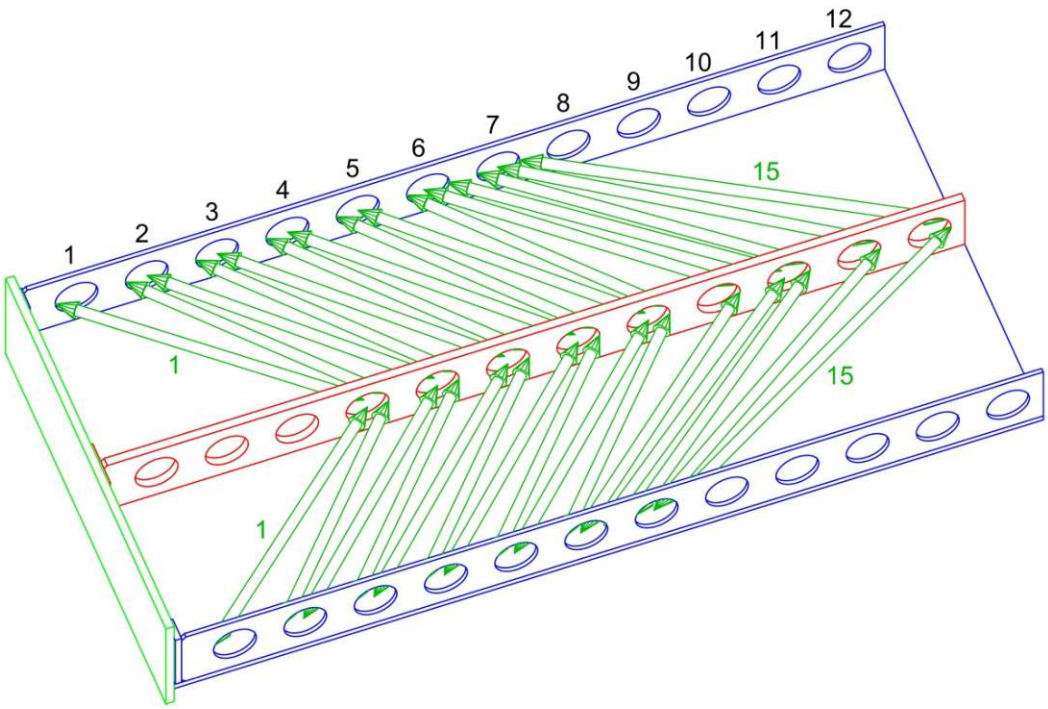

Figure 2.46: The green concrete struts symbolise the horizontal force transfer between the steel sections. For simplification, the top steel plate is not shown.

Number of the concrete strut	$F_{x,horizontal}$ [kN]	Number of the Involved circular hole at the outside shear connector	Number of the involved circular hole at the central shear connector
1	16,82	1	4
2	19,005	2	4
3	8,855	2	5
4	30,03	3	5
5	1,60	3	6
6	32,89	4	6
7	1,09	4	7
8	27,215	5	7
9	7,865	5	8
10	13,435	6	8
11	17,605	6	9
12	4,03	6	10
13	7,52	7	10
14	5,205	7	11
15	0,365	7	12
Σ	193,53	-	-

Table 2.10: Forces in the concrete struts. The components in the x direction (parallel with the shear connectors) are shown.

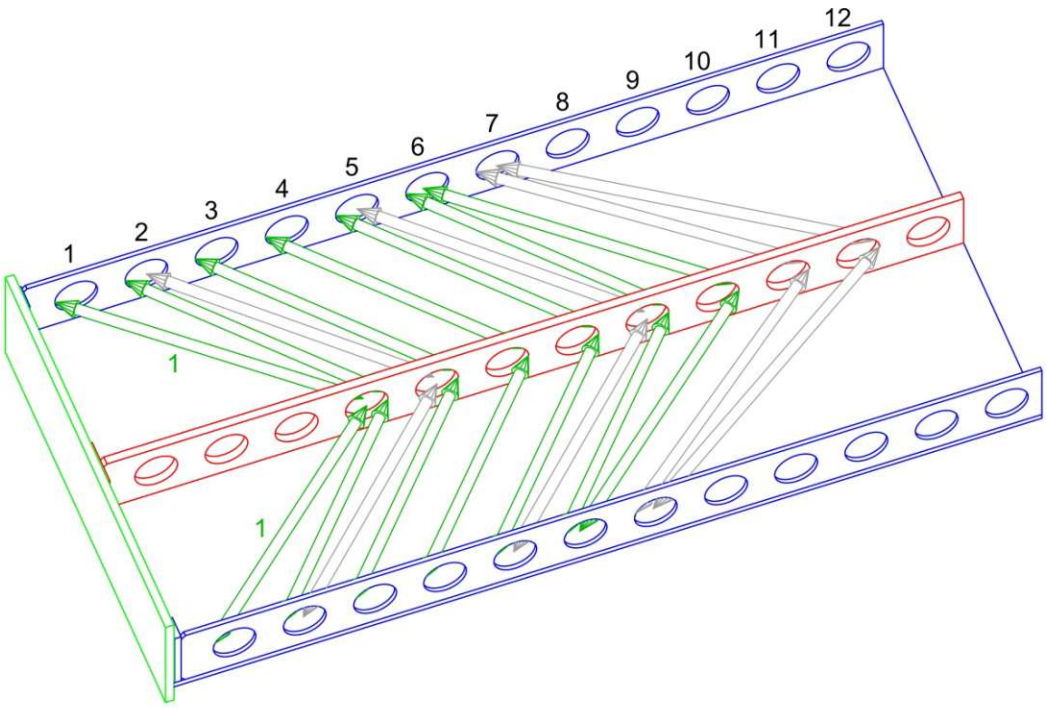

Figure 2.47: The green and grey concrete struts symbolise the horizontal force transfer between the steel sections. For simplification, struts with horizontal forces under 4,1 kN are not shown.

It is clear from the results in table 2.7, that the green concrete struts illustrated in figure 2.46 are not perfectly horizontal. The total sum of the forth table row (51,12 kN) represents all the vertical forces at the circular holes of the shear connector 1 occurring from the 15 green struts in figure 2.46 and the six brown struts in figure 2.45. Similarly, the total

sum of the second table row (-119,41 kN) illustrates the vertical forces at the circular holes of the shear connector 2 occurring from the 15 green struts and the four violet-coloured struts in figure 2.44.

In the following step, the vertical forces at the holes of the central shear connector occurring from the external loading through the concrete core are evaluated based on the contact stresses. Figure 2.48 illustrates a portion of figure 2.39, where the contact pressures are shown. As in the case of figure 2.39, the lengths of the arrows symbolise the magnitude of the forces, so that the arrows of the resultants at the top steel section denote just the half of the total forces in the composite connections. Moreover, the arrows of the resultants at the bottom section represent the forces at only one shear connector of the bottom shear section (for example at shear connector 1).

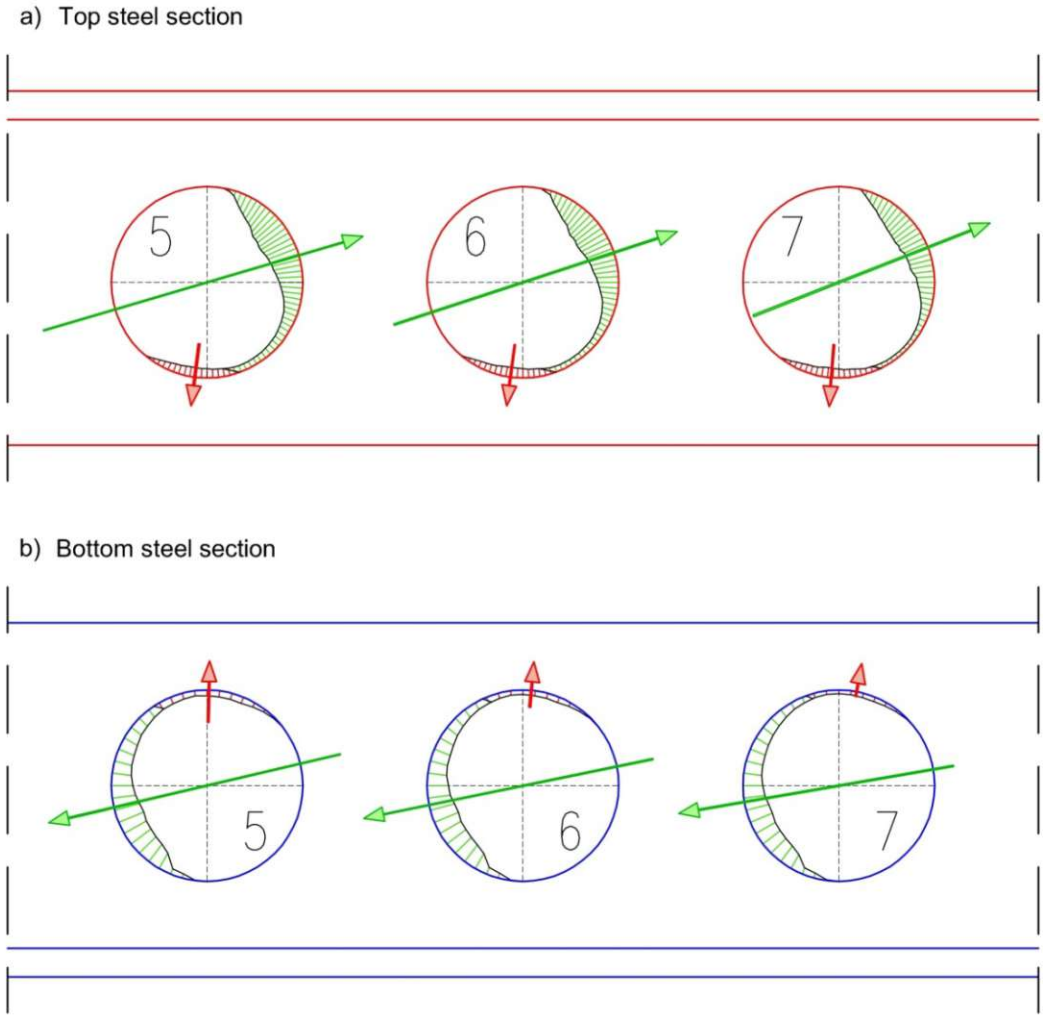

Figure 2.48: Contact pressures on the surface of the circular holes num. 5, 6 and 7: a) top steel section; b) bottom steel section

Next, the vertical components of the resultant forces pointed out in red in figure 2.48 are examined. As frictional shear stresses control the resultant forces in the composite connections, in the further calculation both the contact pressures and the contact tractions are considered. However, the frictional shear stresses modify the values from the contact pressures just a little bit (see tables 2.5 and 2.6). According to the last row in table 2.5, the vertical component of the resultant force from effect 2 at the fifth hole of the top steel section is 13,36 kN, which acts downwards. In the case of the fifth hole of the bottom steel section, this vertical force is 6,40 kN, which acts upwards (see table 2.6). The opposing forces (actually the forces from the steel shear connectors on the concrete) are illustrated in figure 2.49(a). It is assumed, that 6,40 kN

vertical force is transmitted between the fifth holes of shear connectors 1 and 2 (see figure 2.49(b)). As illustrated in figure 2.49(c), this effect is modelled through concrete struts, which are actually coupling members between the top and the bottom steel sections to prevent the differences between the deflections of the two steel sections (see figure 2.53). So, the top steel section at the fifth hole receives 12,80 kN vertical force from the two outside shear connectors together. The remaining part of the vertical component of the force at the fifth hole of the top steel section (13,36 kN – 12,80 kN = 0,56 kN = 2 · 0,28 kN) is considered as a load delivered directly from the external loading through the concrete (see figure 2.49(d)).

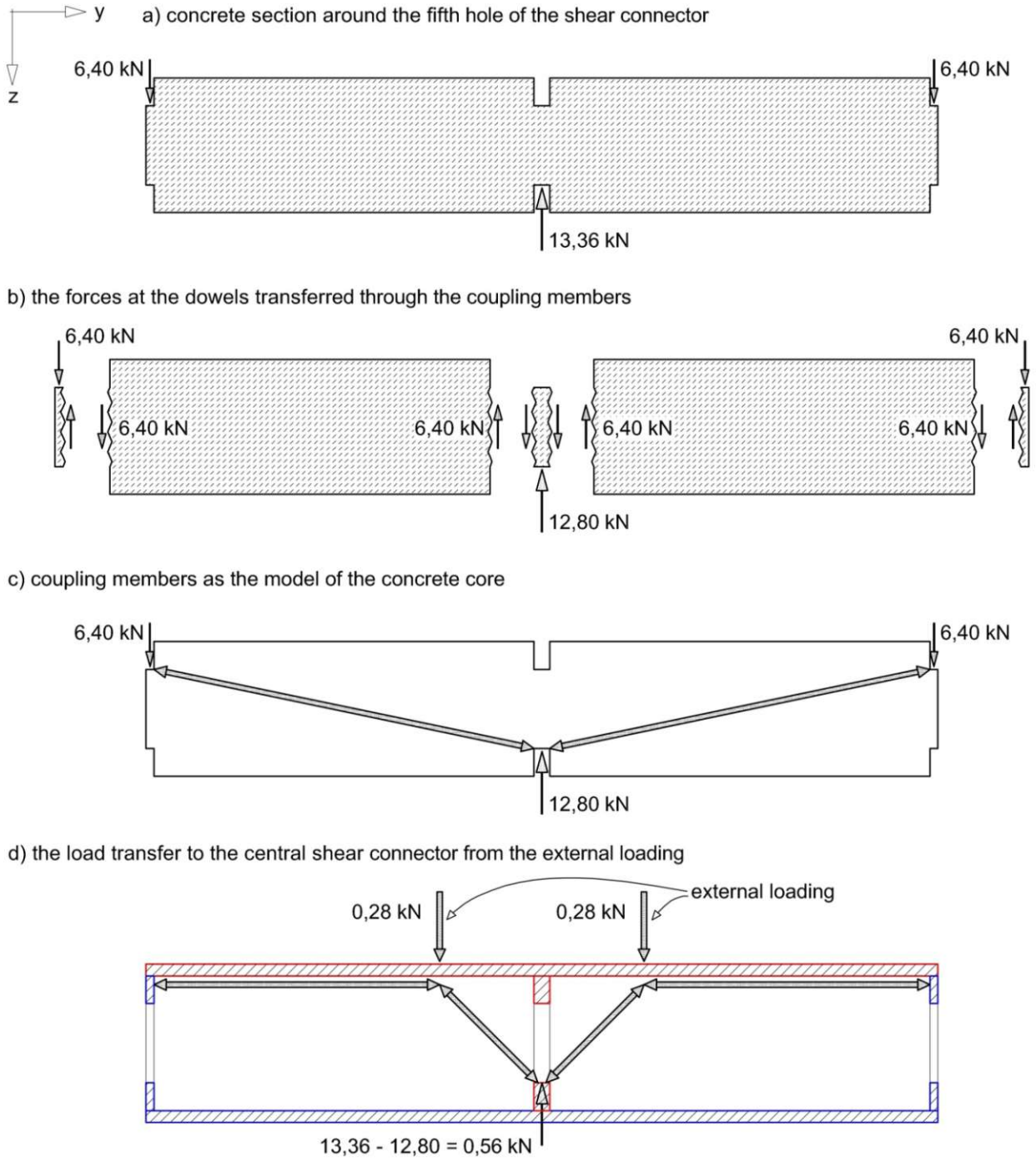

Figure 2.49: Analysis of the force transmission in the concrete at the fifth circular holes of the shear connectors: a) the concrete section with the loads at the composite connections; b) the concrete section with the forces transferred between the shear connectors (exploded view); c) concrete model with the coupling members; d) planar truss frame model to represent the load transfer to the central shear connector from the external loading

Next, the forces at the tenth holes of the shear connectors are also analysed. The vertical component of the resultant force from effect 2 at the tenth hole of the top steel section is 8,41 kN (downwards). At the tenth hole of the bottom steel section, this vertical force is 0,47 kN (upwards). Therefore, according to the above described assumption, the top steel section at the tenth hole receives 0,94 kN (2 · 0,47 kN) vertical force from the two outside shear connectors (see figure 2.50(b)). The remaining part of the vertical force component (8,41 kN – 0,94 kN = 7,47 kN = 2 · 3,735 kN) is considered as a load delivered directly from the external loading through the concrete according to the truss frame model in figure 2.50(d).

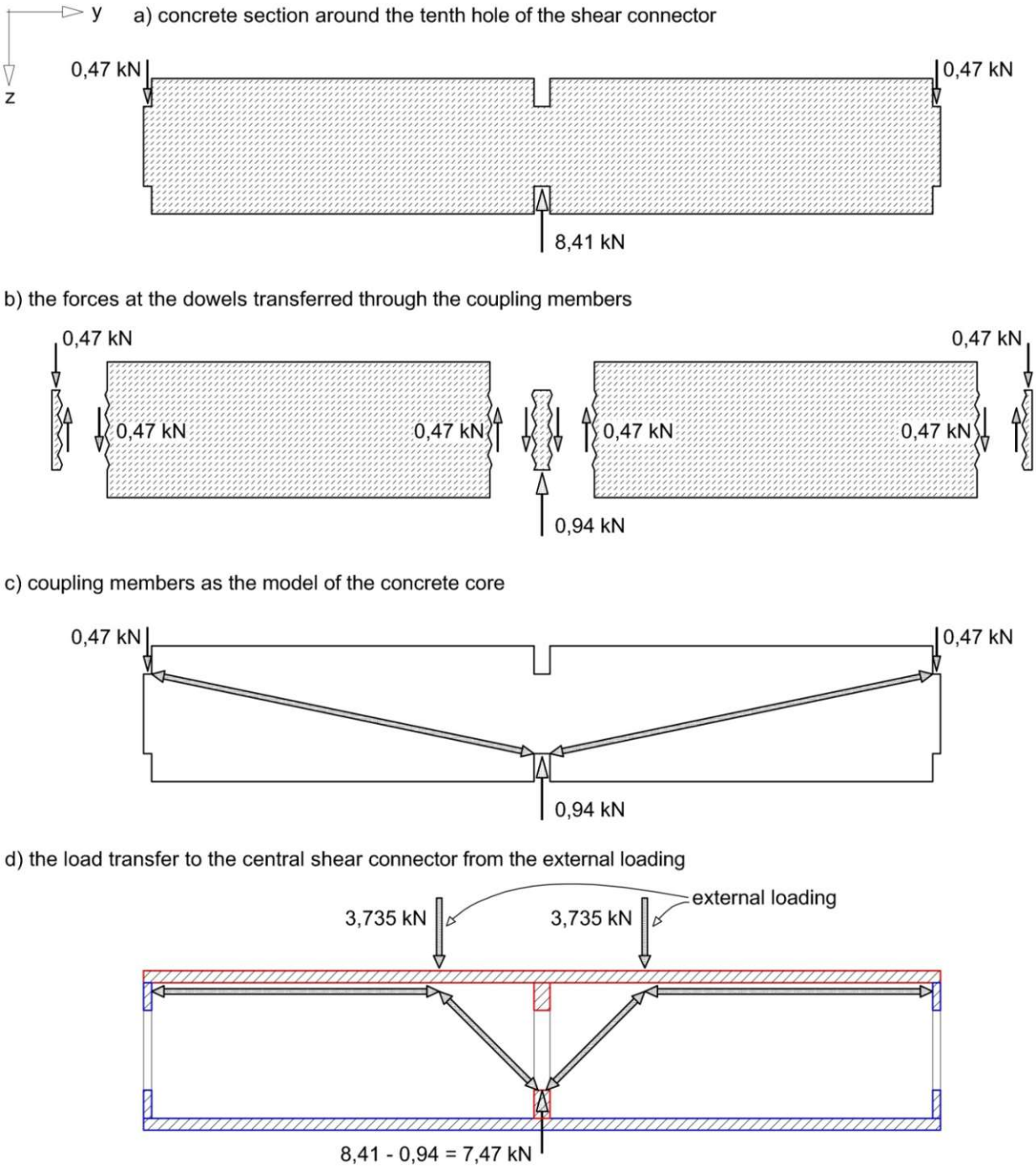

Figure 2.50: Analysis of the force transmission in the concrete at the tenth circular holes of the shear connectors: a) the concrete section with the loads at the composite connections; b) the concrete section with the forces transferred between the shear connectors (exploded view); c) concrete model with the coupling members; d) planar truss frame model to represent the load transfer to the central shear connector from the external loading

According to the calculation method described above, the forces can be evaluated at the holes numbered 5 - 12. To clarify the differences in force transmission at the first four circular holes, the forces in the concrete at the second holes of the shear connectors is analysed. The vertical component of the resultant force from effect 2 at the second hole of the top steel section is 5,73 kN (downwards). At the second hole of the bottom steel section, this vertical force is 6,00 kN (upwards). Therefore, the top steel section at the second hole receives 5,73 kN (2 · 2,865 kN) vertical force from the two outside shear connectors (see figure 2.51(b)). Thus, remaining vertical forces (6,00 kN – 2,865 kN = 3,135 kN) occur at the shear connectors of the bottom steel section. It is assumed that these forces are delivered from the holes of the outside shear connectors to the support through the concrete symbolised with the truss frame model in figure 2.51(d)).

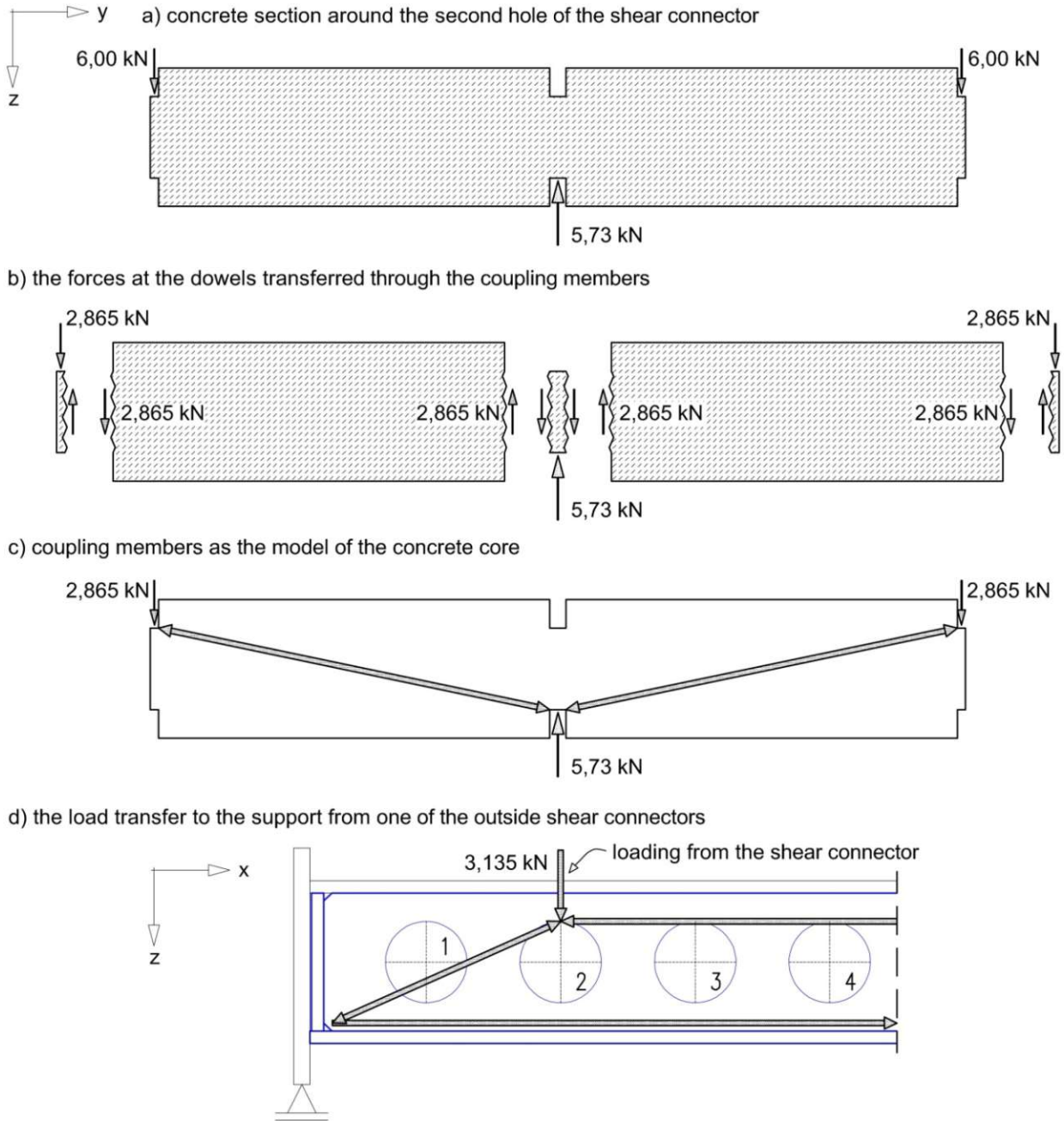

Figure 2.51: Analysis of the force transmission in the concrete at the second circular holes of the shear connectors: a) the concrete section with the loads at the composite connections; b) the concrete section with the forces transferred between the shear connectors (exploded view); c) concrete model with the coupling members; d) planar truss frame model to represent the load transfer to the support from the outside shear connector

The calculation results are shown in table 2.11. The above presented results are pointed out in red in the table. In the first table row the forces at the holes of the top steel section derived from the external loading through the concrete are given. In the second table row the vertical components of concrete struts acting between shear connectors 1 and 2 (coupling members) are represented. As was illustrated at the second circular hole, in the case of the first four circular holes the remaining part of the vertical force component occurs at the holes of the shear connectors of the bottom shear section. These forces are given in the third table row referring to one of the outside shear connectors (shear connector 1) and mean the force transmission from the outside shear connector to the support through the concrete. Thus, logically, the top steel section does not receive any vertical loads from the external loading at the first four circular holes of the shear connector. Therefore, the forces in the first table row are zero at these holes. The signs in table 2.11 mean the direction of the vertical contact forces on the steel circular holes. Thus, the positive values (force direction: downwards) in the second table row symbolise the forces at the central shear connector.

Hole numb.	1	**2**	3	4	**5**	6	7	8	9	**10**	11	12	Σ
Forces from the external loading $F_{vertical}$ (shear con.2)	0,00	**0,00**	0,00	0,00	**0,56**	3,48	6,12	11,12	10,62	**7,47**	6,99	5,46	51,82
Forces in the coupling member $F_{vertical}$ (shear con. 1, 2)	1,495	**2,865**	6,31	6,545	**6,40**	4,88	3,63	0,74	0,51	**0,47**	0,13	0,22	34,195
Force transfer to the support $F_{vertical}$ (shear con. 1)	-3,625	**-3,135**	-1,01	-0,575	**0,00**	0,00	0,00	0,00	0,00	**0,00**	0,00	0,00	-8,345

Table 2.11: Effect 2: Partition of the vertical components of forces in the composite connections. Forces in [kN]

The total sum of the forces in the first row of table 2.11 is 51,82 kN. This means that the shear connector of the top steel section receives 51,82 kN from the external loading of the ABAQUS model (161,03 kN). Here, the shear connector of the top steel section means only the construction part modelled in ABAQUS (see figure 2.12). Logically, the ABAQUS model is loaded with the half of the total external loading (322,06/2 = 161,03 kN). As illustrated in figures 2.49(d) and 2.50(d), it is assumed that this loading (the sum of the forces in the first row of table 2.11) is transferred through the concrete to the circular holes of the shear connector. This load transmission is shown in figure 2.52, too. The concrete struts are illustrated with black and grey struts. The arrows pointed out in grey symbolise the members which transfer vertical forces less than 1,0 kN. Thus, the main effect from this load transmission can be illustrated with the black arrows. It is remarkable in the figure that horizontal concrete struts act between the outside shear connectors and the external load input positions to ensure the static balance of the truss model. It is assumed, that the external vertical loads act at the meeting points of the horizontal and the diagonal struts in figure 2.40. However, the external loads are not shown in the figure for ease of view.

The total sum of the forces in the second row of table 2.11 is 34,195 kN. This means that the shear connector of the top steel section receives 68,39 kN (2 · 34,195 kN) from the two shear connectors of the bottom steel section through the concrete struts which are called as coupling members (see figures 2.49(c), 2.50(c) and 2.51(c)). These members are illustrated in figure 2.53 with black and grey struts. The grey arrows symbolise the coupling members which transfer vertical forces less than 1,0 kN. Therefore, the main effect from the coupling members can be illustrated with the black arrows.

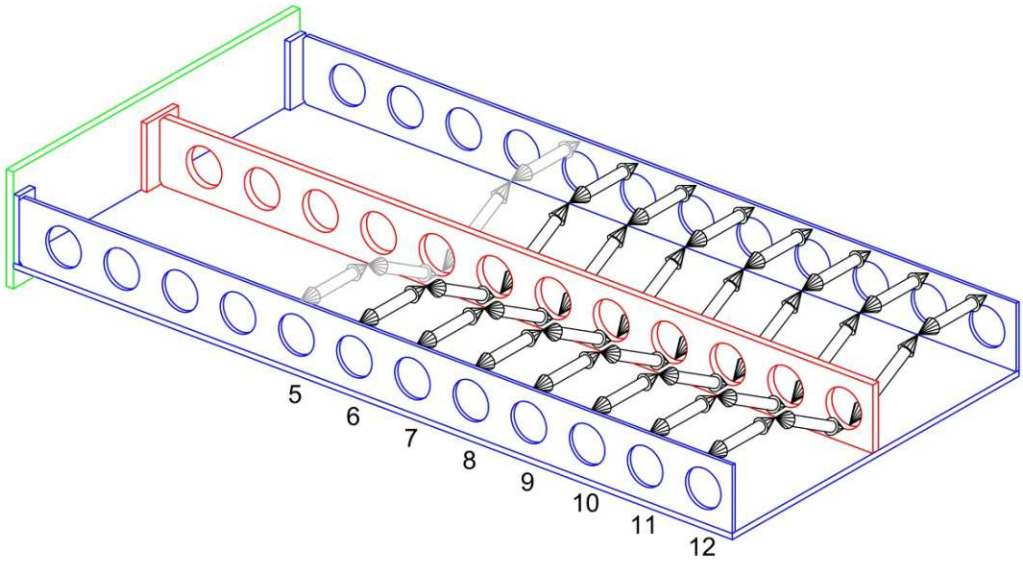

Figure 2.52: Truss frame model of the concrete core: the black and grey concrete struts symbolise the load transfer to the central shear connector. The external loads are not shown for ease of view.

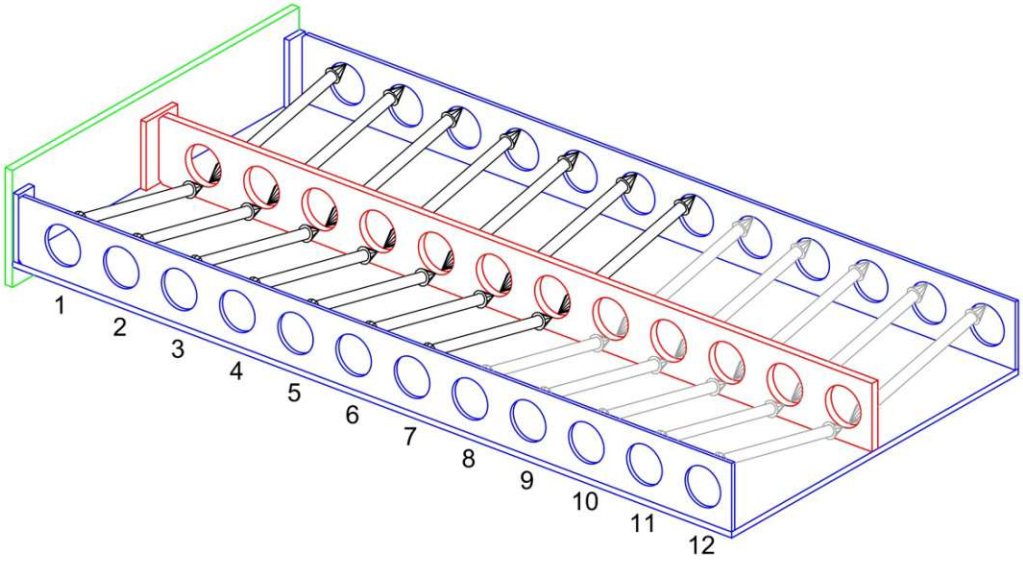

Figure 2.53: Concrete model with coupling members: the black and grey concrete struts symbolise the force transfer between the shear connectors to prevent the differences between the deflections of the steel sections

Moreover, it is clear from the third table row that one outside shear connector transfers 8,345 kN vertical load to the support through the concrete. The force transmission is illustrated with the truss frame model in figure 2.51(d) in the case of the loading at the second circular hole of shear connector 1. The two outside shear connectors together transmit 16,69 kN (2 · 8,345 kN). This load transmission is symbolised with two truss frame models for the concrete in figure 2.54, too. As shown in the figure, at the top part of the concrete a horizontal compression member acts between the load input position (the top of the circular hole) and the plane of symmetry. Moreover, at the bottom part of the concrete a horizontal tension member symbolises the concrete which compensates the horizontal forces from the diagonal concrete struts. In this way, the vertical loads from the outside shear connectors induce only vertical forces in the bottom steel plate next to the end plate (actually at the support). Thus, horizontal forces do not press the steel end plate and the end stiffeners. This

model corresponds to the above used assumption that the total horizontal compression force at the support arises due to the compressed concrete parts pressed from the shear connector of the top steel section.

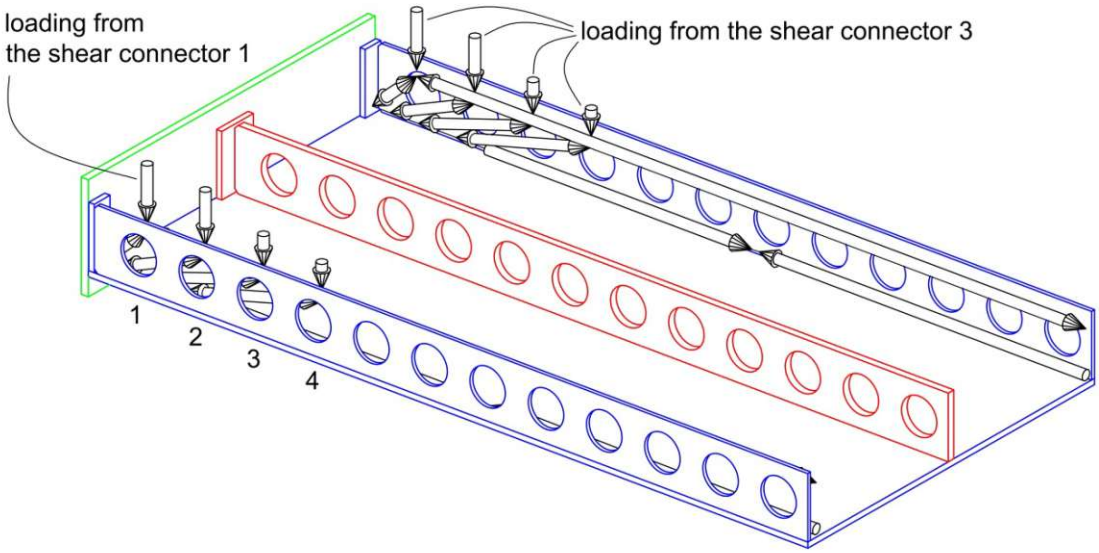

Figure 2.54: Truss frame model to symbolise the load transfer to the support from the outside shear connectors

Next, the static equilibrium of the shear connectors is examined only in the case of the vertical forces as a summary about the presented effects. According to the ABAQUS calculation results, the shear connector 1 receives directly from the external loading 7,42 kN through the top steel plate. Actually, as an approximation of the results of the FEA software, the outside shear connectors are loaded from the areas illustrated in figure 2.55(a).

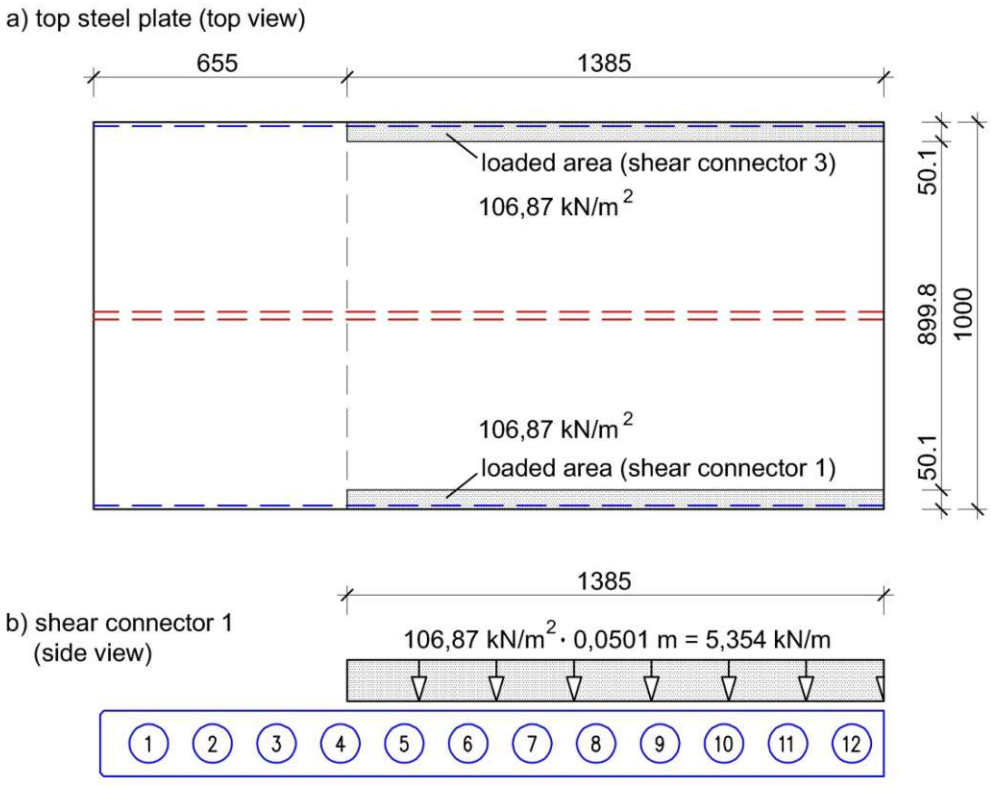

Figure 2.55: The external vertical loading on the outside shear connectors: a) top view of the top steel plate with the examined loading; b) side view with the loading acts on one outside shear connector

Thus, the external loading on the shear connector 1 is given in figure 2.55(b) and the total vertical load can be easily calculated:

$$\sum F_{\,external\ loading,shear\ connector\ 1} = 1{,}385\ \text{m} \cdot 5{,}354\ \text{kN/m} = 7{,}42\ kN \tag{2.12}$$

16,00 kN is delivered from one outside shear connector to the end stiffener (see the shear forces in figure 2.23(a)). Moreover, shear connector 1 gets 51,12 kN vertical load due to the effects symbolised with brown and green arrows above (see figures 2.45 and 2.46). This value is calculated in the last row of table 2.7. Additionally, this construction part transfers 34,195 kN to the central shear connector through the coupling members, and 8,345 kN to the support from the first four circular holes of the shear connector (see table 2.11). Thus, the static balance is given as:

$$\sum F_{\,vertical,shear\ connector\ 1} = 7{,}42\ - 16{,}00 + 51{,}12\ - 34{,}195 - 8{,}345 = 0{,}00\ kN \tag{2.13}$$

This equilibrium is valid for the shear connector 3, too.

Next, the static balance of the central shear connector is presented. The shear connector 2 receives directly from the external loading 31,20 kN through the top steel plate according to the ABAQUS calculation results. As an approximation of the results of the FEA software, shear connector 2 is directly loaded from the areas illustrated in figure 2.56(a).

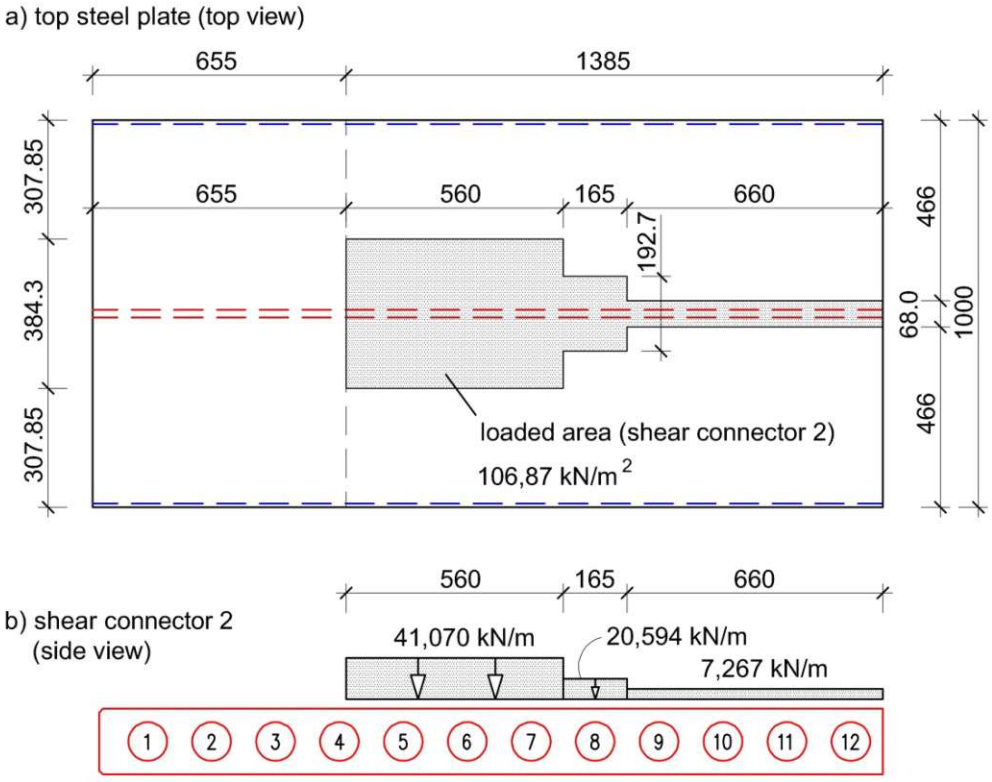

Figure 2.56: The external vertical loading on the outside shear connectors: a) top view of the top steel plate with the examined loading; b) side view with the loading acts on the central shear connector

Thus, the external loading on the shear connector 2 is given in figure 2.55(b). Therefore, the total vertical load is:

$$\sum F_{\,external\ loading,shear\ connector\ 2} = 0{,}56 \cdot 41{,}070 + 0{,}165 \cdot 20{,}594 + 0{,}660 \cdot 7{,}267 = 31{,}2\ kN \tag{2.14}$$

32,00 kN is delivered from the shear connector to the end stiffener (see figure 2.23(b)). Moreover, the shear connector 2 transfers 119,41 kN vertical load due to the effects symbolised with violet-coloured and green arrows (see figures 2.44 and 2.46). This value is calculated in the second row of table 2.7. Additionally, this construction part gets 68,39 kN from the two outside shear connectors through the coupling members, and 51,82 kN from the external loading transferred through the concrete to the circular holes of the shear connector (see table 2.11). Thus, the static balance is given as:

$$\sum F_{vertical,shear\ connector\ 2} = 31{,}20 - 32{,}00 - 119{,}41 + 68{,}39 + 51{,}82 = 0{,}00 \qquad (2.15)$$

It was shown in equation 2.9 that 97,03 kN from the total external loading of the ABAQUS model (161,03 kN) is transmitted through the concrete to the support. It is clear that vertical forces are transmitted from the central shear connector to the support through the concrete core which is symbolised with the violet-coloured concrete struts in figure 2.44. However, the struts in the figure are horizontal as an approximation. To evaluate the value of the transmitted vertical forces, the vertical component of the force in the fourth circular hole (14,53 kN, see the second row of table 2.7) need to be divided. It is assumed that a vertical force of 2,85 kN is transferred from this circular hole to the support roughly corresponding to the partition of the horizontal components. From the first three holes 44,59 kN (15,13 kN + 14,19 kN + 15,27 kN) is transmitted to the support according to the results in table 2.7. Thus, a vertical force of 47,44 kN (2,85 kN + 44,59 kN) is transferred from the central shear connector to the support through the concrete core. Moreover, as it was presented above in table 2.11, 16,69 kN ($2 \cdot 8{,}345$ kN) is delivered from the outside shear connectors to the support through the concrete part around the shear connectors. Therefore, from the three shear connectors of the ABAQUS model 64,13 kN (47,44 kN + 16,69 kN) is transferred to the support through the concrete. The remaining part of the external vertical load transmitted directly through the concrete to the support is 32,90 kN (97,03 kN – 64,13 kN). It is assumed, logically, that the external loads close to the support are transferred through the concrete to the support. Thus, as symbolised in figure 2.57, a truss frame model for both of the concrete cores at the two sides of the central shear connector is applicable to carry 32,90 kN from the external loads. At the top part of the concrete a compression member acts between the load input position and the plane of symmetry. Moreover, at the bottom part of the concrete a tension member symbolises the concrete which compensates the horizontal forces from the diagonal concrete struts in the figure.

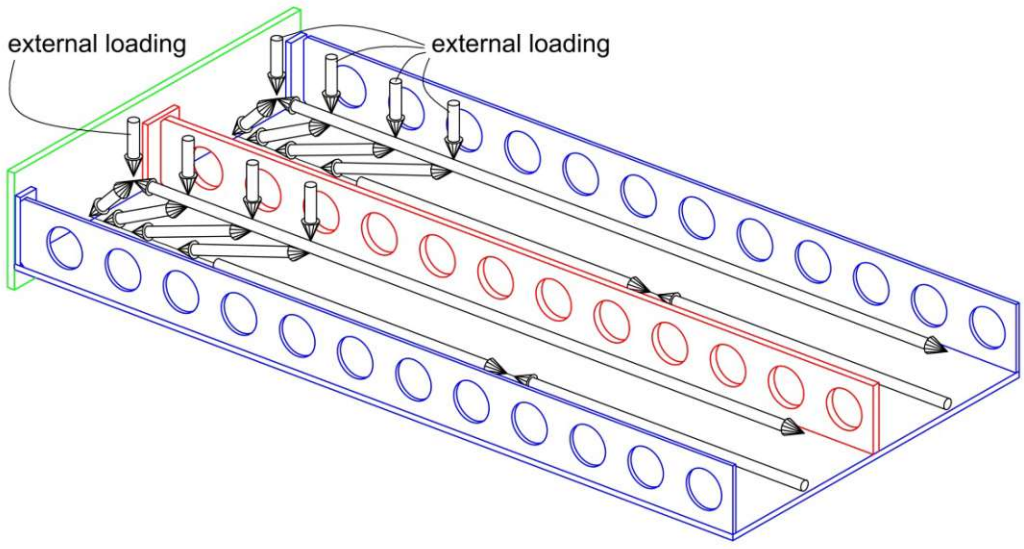

Figure 2.57: The truss frame model symbolise the force transfer from the external loads to the support through the concrete

Actually, this model is similar to the system in figure 2.54. Namely, horizontal forces do not press the steel end plate and the end stiffeners from the loads transmitted through the concrete. One frame truss in figure 2.57 symbolises the whole concrete between two shear connectors. The external vertical loads are illustrated in the figure, too. However, the exact loaded areas and the values of the external loads will be presented in chapter 2.4.2.

Finally, the static equilibrium of the concrete is examined only in the case of the vertical forces as a control of results. From the total external loading the shear connectors and the concrete parts of the model receive forces through the top steel plate which is directly loaded. Equation 2.16 demonstrates the load part which acts on the top of the concrete:

$$\sum F_{vertical,external\ loading-concrete} = 161{,}03 - 31{,}20 - 7{,}42 - 7{,}42 = 114{,}99\ kN \tag{2.16}$$

Here, 161,03 kN is the total external loading of the ABAQUS model, 31,20 kN means the external loading which acts on the shear connector 2 (see equation 2.14), while 7,42 kN is the external loading delivered to one outside shear connector (see equation 2.12). In accordance with the ABAQUS results, it is considered in equation 2.16 that the top steel plate does not deliver external load directly to the steel end plate. Actually, only the vertical force from end stiffener 2 (8,73 kN, see figure 2.23(b)) is transferred through the top steel plate to the end plate. The loaded area is illustrated in figure 2.58. Actually, from the total loaded area, which is the surface of the top steel plate, the loaded areas in figures 2.55(a) and 2.56(a) are extracted.

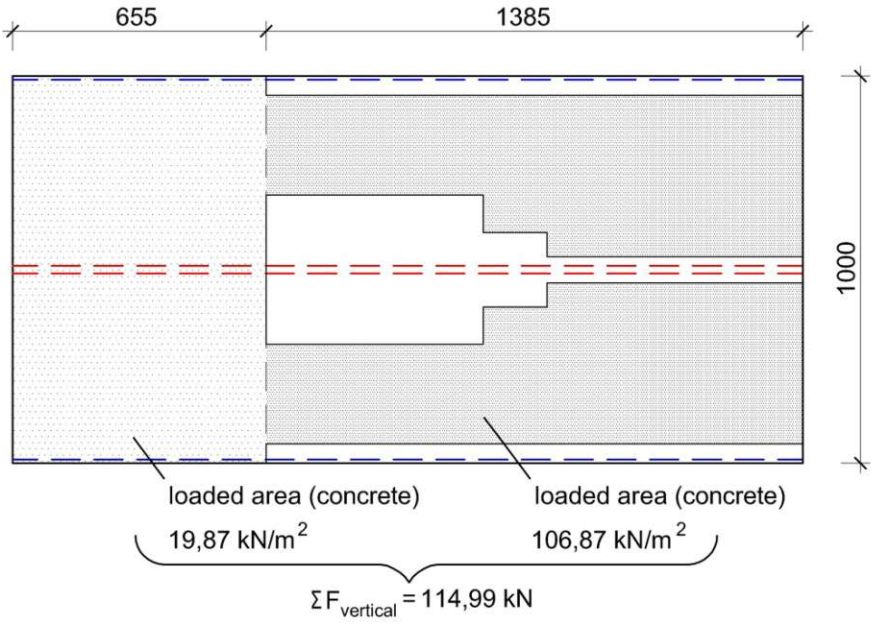

Figure 2.58: The external vertical loading on the concrete. Top view

The vertical load of 114,99 kN can be partitioned into two parts. According to the above presented calculations based on the ABAQUS results, 32,90 kN is transmitted through the concrete directly to the support (see figure 2.57). This means that the remaining part of the load needs to be delivered to the steel structures of the model. Equation 2.17 shows the simple calculation of this part of the vertical loading:

$$\sum F_{vertical,concrete-\ steel\ structures} = 114{,}99 - 32{,}90 = 82{,}09\ kN \tag{2.17}$$

The forces occurring between the concrete and the steel parts (shear connectors) were evaluated in this chapter. It was detected that the shear connector of the top steel section receives 51,82 kN from the external vertical loading from the

concrete core (see the first row of table 2.11). Moreover, the shear connectors of the bottom steel section get vertical loads due to the effect symbolised with brown arrows in figure 2.45. However, these arrows are horizontal in the figure as an approximation. As a modification of this model, figure 2.59 illustrates a simple truss model which symbolises the vertical load transfer, too. Here, the diagonal concrete struts transfer the vertical external loads to the circle holes of the outside shear connectors. Moreover, horizontal concrete struts act between the load input positions of the external loads and the plane of symmetry to compensate the horizontal components of the diagonal struts.

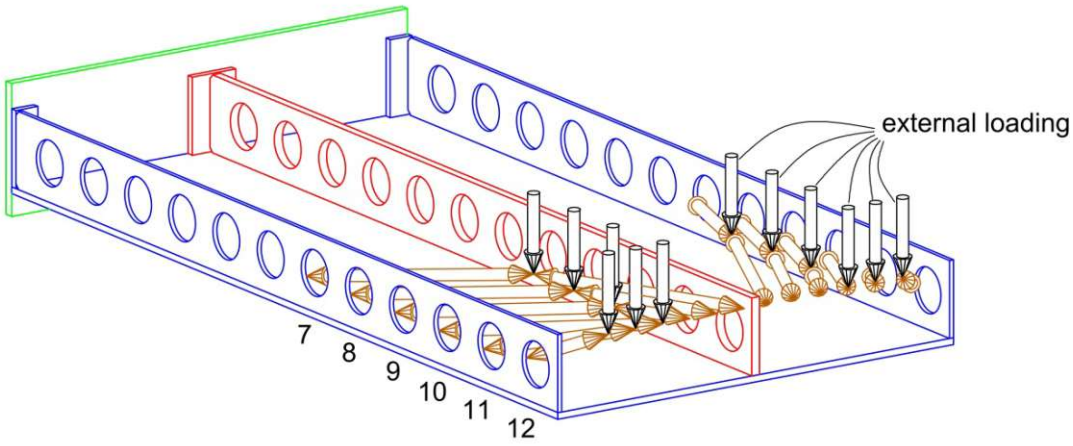

Figure 2.59: The brown concrete struts represent the force transfer from the external loading to the outside shear connector through the concrete

The total sum of the vertical components of the diagonal concrete struts in figure 2.59 need to be calculated. It was presented above that the total sum of the vertical forces at the circular holes of the shear connector 1 occurring from the 15 green struts (see figure 2.46) and the six brown struts (see figure 2.45) is 51,12 kN (see the last row in table 2.7). Moreover, it was assumed that a vertical force of 2,85 kN is transferred from the fourth circular hole of the central shear connector to the support. Thus, the vertical component of the 15 green struts in figure 2.46 can be easily calculated from the second row in table 2.7:

$$\sum F_{vertical,shear\ connector\ 2\ -\ shear\ connector\ 1} = 0{,}5 \cdot [(14{,}53 - 2{,}85) + 13{,}44 + 12{,}62 + 12{,}04 + 5{,}70 + 5{,}06 + 7{,}01 + 3{,}74 + 0{,}68] = 0{,}5 \cdot 71{,}97 = 35{,}985\ kN \quad (2.18)$$

Thus, the vertical component of the six brown struts in figure 2.36 is:

$$\sum F_{vertical,shear\ connector\ 1\ -external\ loading} = 51{,}12 - 35{,}985 = 15{,}135\ kN \quad (2.19)$$

According to this result, the reaction forces (effects on the concrete from the outside shear connectors) are illustrated in figure 2.60 with the vertical brown arrows. Next, the vertical load from the concrete acting on the three shear connector of the model can be easily calculated:

$$\sum F_{vertical,concrete-\ steel\ structures} = 51{,}82 + 2 \cdot 15{,}135 = 82{,}09\ kN \quad (2.20)$$

As the results in equations 2.17 and 2.20 are equal, the concrete core is in static equilibrium considering the vertical forces. As a summary of the results, figure 2.60 represents the concrete parts of the ABAQUS model with the vertical forces. The external loading is illustrated schematically with two concentrated loads (114,99/2 kN). The total sum of the reaction forces in the figure is 114,99 kN. Logically, this value is equal to the external loading part on the concrete structures calculated in equation 2.16.

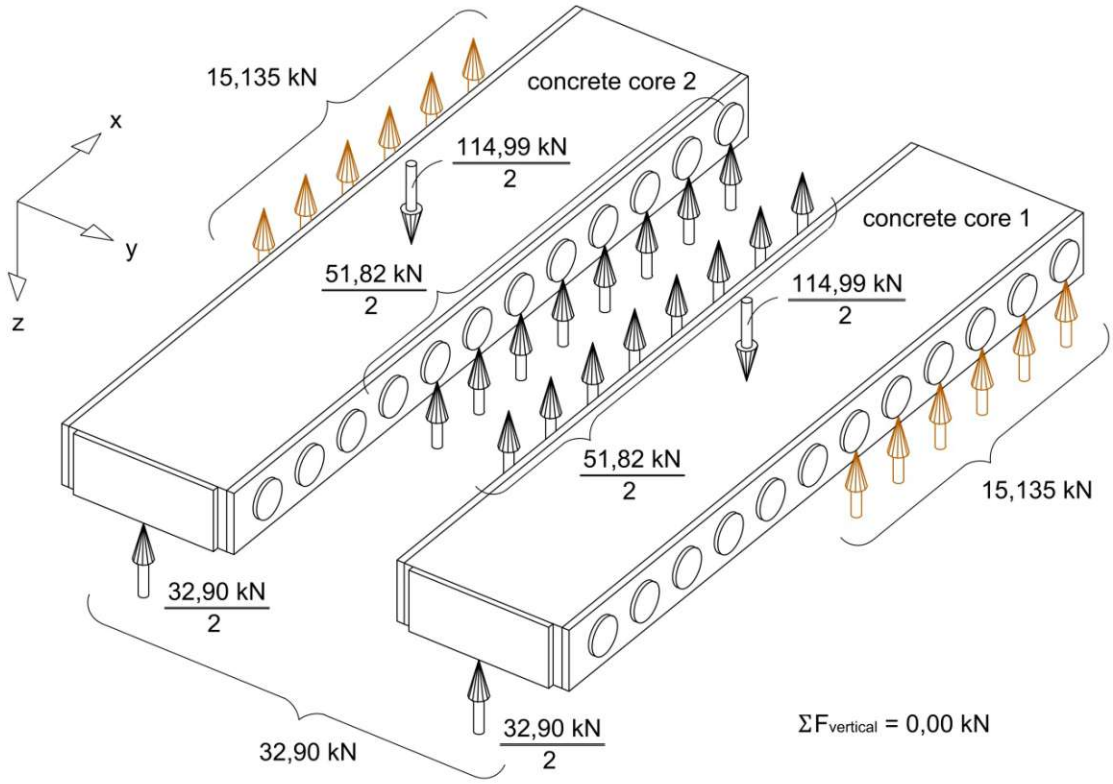

Figure 2.60: The vertical forces acting on the concrete model. The two concrete portions are shifted from each other to illustrate the vertical dowel forces at the central shear connector.

2.4.2 The model of the load-bearing structure

Based on the results of the ABAQUS calculation presented in chapter 2.4.1, simple engineering models will be defined in this chapter to describe approximately the behaviour of the examined construction part of the SCSC plate. Firstly, the external loading of the ABAQUS model (see figures 2.61(a) and (b)) is divided into 12 parts. Namely, the loaded area (the top steel plate) is partitioned according to figure 2.61(c). It will be presented at each of the 12 parts that the external loading can be transferred through the steel structures and the concrete struts specified in chapter 2.4.1.

Table 2.12 summarizes the above mentioned load distribution. The first table row illustrates the external vertical loading for fatigue limit state distributed according to the geometry of the 12 loaded areas. To avoid rounding errors, the loads of 17,633 kN and 17,634 kN are used in the table for the same magnitude of force. Thus, the total value of external loading given in the table is equivalent to the loading illustrated in figure 2.61(b).

The second table row shows the loading which acts directly on the central shear connector (see figure 2.56). Actually, this part of the external loading is transferred through the top steel plate to the shear connector of the top steel section. The total sum of this loading (31,20 kN) was calculated in equation 2.14. It is remarkable that the load distribution is not uniform. The unstressed surface between the concrete and the top steel plate detected with ABAQUS around the central shear connector is considered as the area from which the external loads are delivered to the central shear connector. The approximate shape of this area (load area 1) is illustrated in the middle of figure 2.62(a). Thus, the values in the second table row can be easily calculated according to the demonstrated load area. The third table row shows the loading which acts directly on the two outside shear connectors together (see figure 2.55). Logically, this part of the external loading is also transferred through the top steel plate. Corresponding to the results of ABAQUS, the load distribution is considered

uniform as an approximation. The two loaded areas (loaded area 2) are illustrated in figure 2.62(a) with the two rectangles at the edges of the model. In the fourth row of table 2.12 the loads of the central shear connector derived from the external loading through the concrete (see figures 2.49(d), 2.50(d) and 2.52) are given. Thus, these values are equal to the results shown in the first row of table 2.11. The shaded area in figure 2.62(b) (load area 3) represents the loaded area which belongs to this force transmission. The fifth table row shows the load part (load area 4) transmitted to the outside shear connectors through the concrete (see the brown arrows in figure 2.59). Figure 2.62(c) illustrates the location of the external loads which are delivered here.

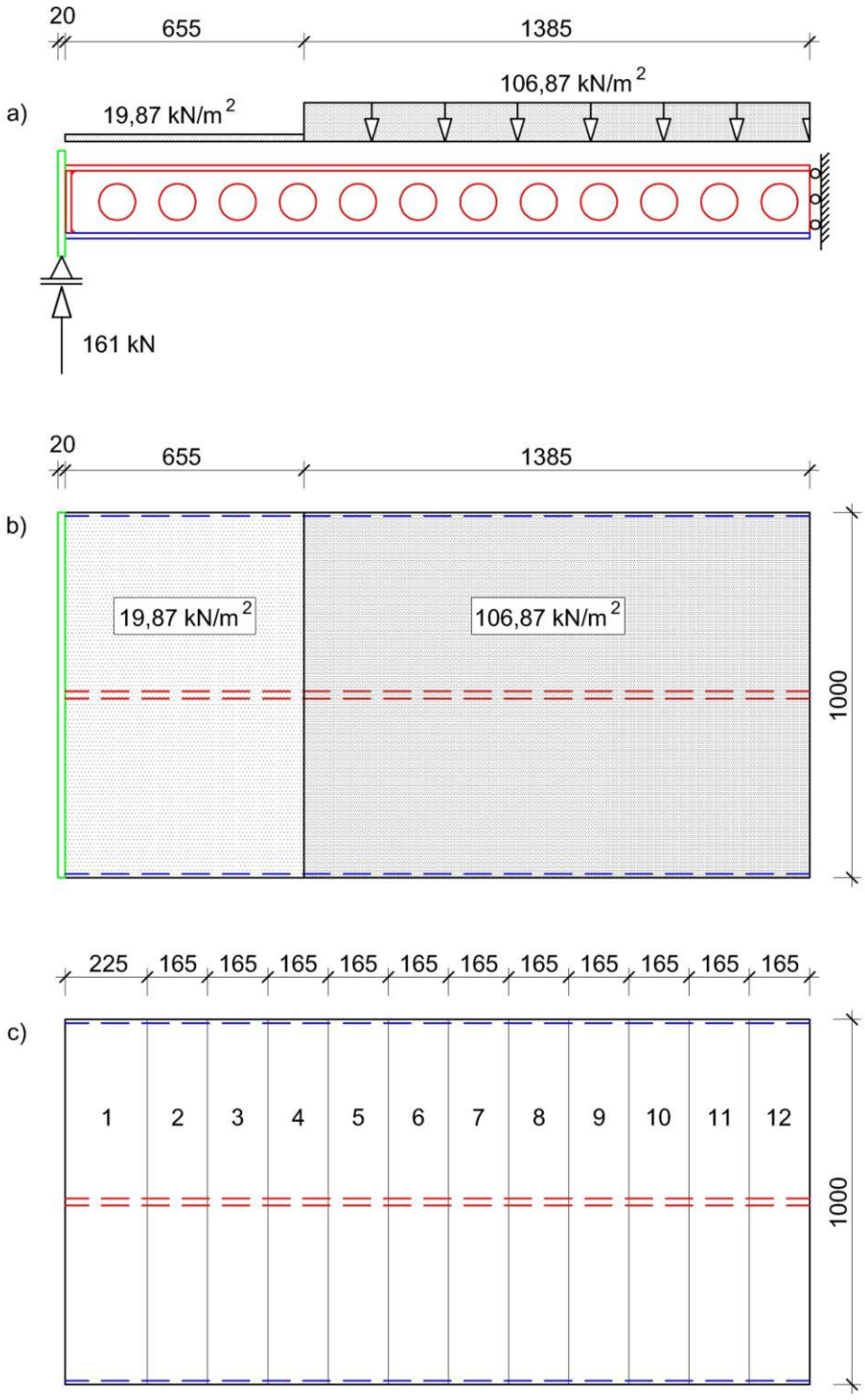

Figure 2.61: The external vertical loading for fatigue limit state: a) side view; b) top view; c) the partition of the loaded area

Number of the loaded area	1	2	3	4	5	6	7	8	9	10	11	12	Σ
External loading	4,471	3,279	3,279	8,933	17,633	17,633	17,633	17,634	17,634	17,634	17,634	17,634	161,03
Loading of the central shear connector through the top steel plate	0,000	0,000	0,000	2,670	6,777	6,777	6,777	3,398	1,200	1,200	1,200	1,200	31,20
Loading of the outside shear connectors through the top steel plate	0,000	0,000	0,000	0,696	1,768	1,768	1,768	1,768	1,768	1,768	1,768	1,768	14,84
Loading of the central shear connector through the concrete	0,00	0,00	0,00	0,00	0,56	3,48	6,12	11,12	10,62	7,47	6,99	5,46	51,82
Loading of the outside shear connectors through the concrete	0,00	0,00	0,00	0,00	0,00	0,00	0,800	1,348	4,046	7,196	7,676	9,206	30,27
Loading of the concrete	4,471	3,279	3,279	5,567	8,528	5,608	2,168	0,000	0,000	0,000	0,000	0,000	32,90

Table 2.12: Division of the external vertical loading between the construction parts. Forces in [kN]

Finally, in the last row of table 2.12 the loads transmitted through the concrete to the support (see the model in figure 2.57) are shown. These external loads act on the shaded areas (load area 5 and 6) in figure 2.62(d). It is remarkable in the figure that the total loading of 19,87 kN/m^2 close to the support (loaded area 5: see figure 2.62(d)) is delivered through the concrete. The loaded areas 5 and 6 are shaded differently to demonstrate the different load intensities. Obviously, the sum of the five force components in table 2.12 (see table rows 2 – 6) is equal to the external loading (table row 1) at each of the 12 areas specified in figure 2.61(c).

Necessarily, the partition of the loaded area in figure 2.62 is only an approximation of the ABAQUS results. For instance, the load parts in the figures 2.62(b) and 2.62(c) cannot be separated by a clear border. However, figure 2.62 represents properly the magnitude of forces at each of the 12 load areas.

Next, based on the presented load distribution between the construction parts, two simple models can be introduced and analysed. One model examines only the concrete part of the SCSC plate. The other one includes all of the steel structures of the composite plate. Thus, because of the high complexity of the SCSC plate, the interaction between the concrete and steel structures is not modelled with the presented engineering models. However, to take into account the positive effects of this interaction, it is assumed that the top and the bottom steel sections are connected. This means that in contrast with figure 2.24, they cannot move relative to each other. The simple models fit only to the given plate geometry and loading.

Figure 2.63 illustrates the bending moments in the middle of the span. It is shown in the figure that the modelling with concentrated loads in the case of the engineering model does not influence appreciably the bending moment. To verify the ABAQUS results in the middle of the span (see figure 2.64) the bending moment is calculated from the compressive and tensile forces of the construction components, too. According to the results in figure 2.64, the total sum of the nine compressive forces is 1267,44 kN and the total sum of the nine tensile forces is 1269,53 kN. The calculation of these two resultants is demonstrated in appendix B.

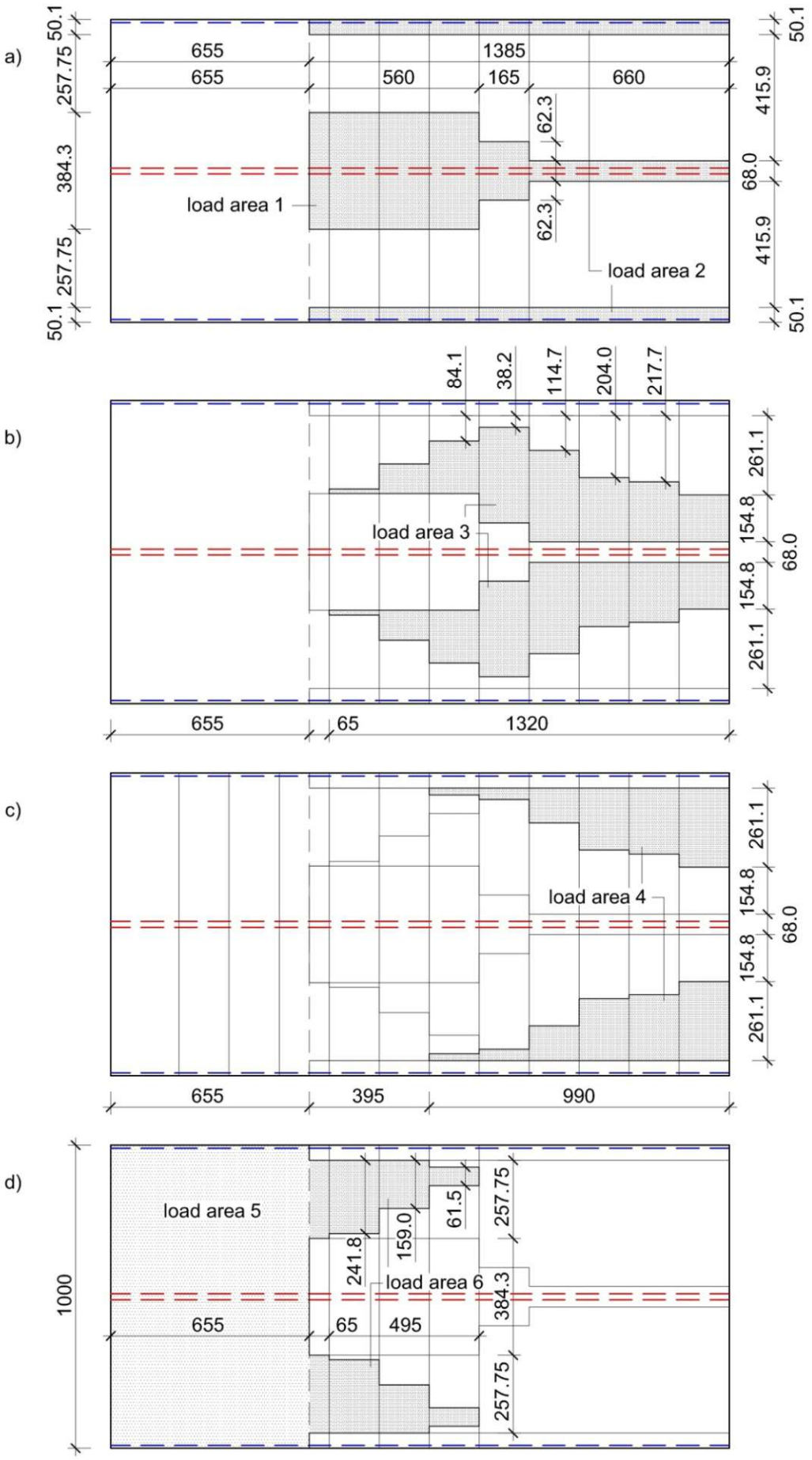

Figure 2.62: Partition of the loaded area to show the load transmission to the different construction parts

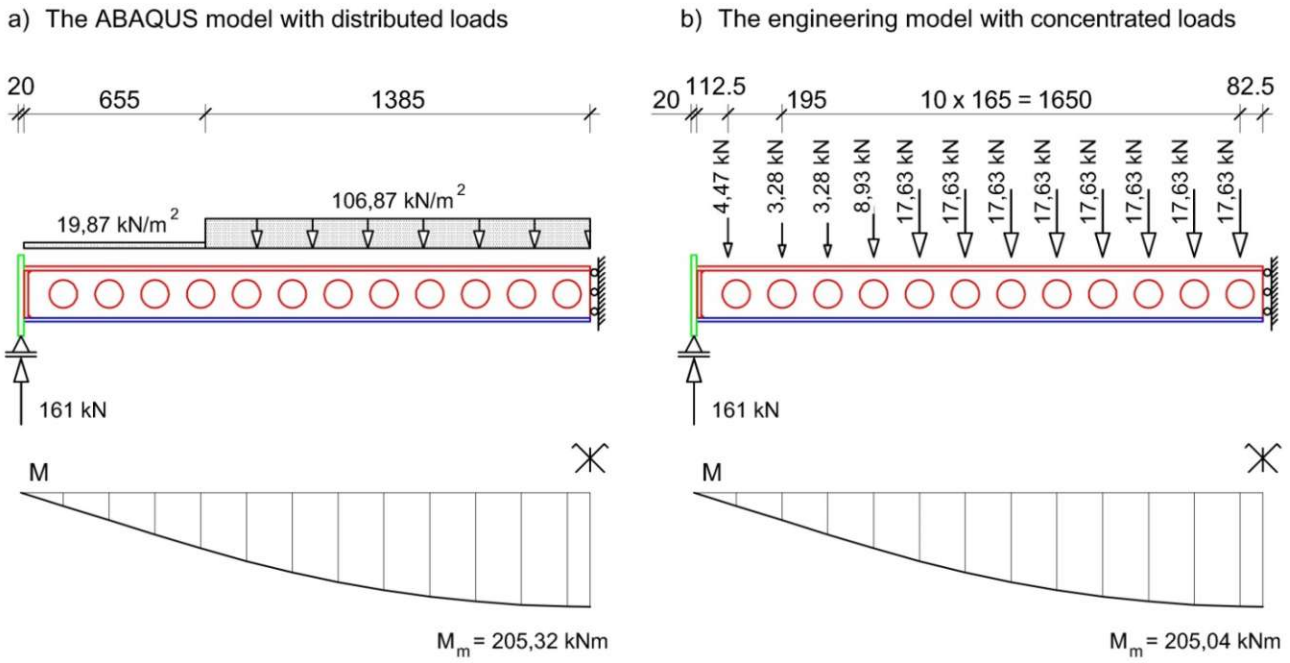

Figure 2.63: The loaded model of the SCSC plate and the bending moment diagram: a) ABAQUS model with line loads; b) engineering model with concentrated loads. Dimensions in [mm]

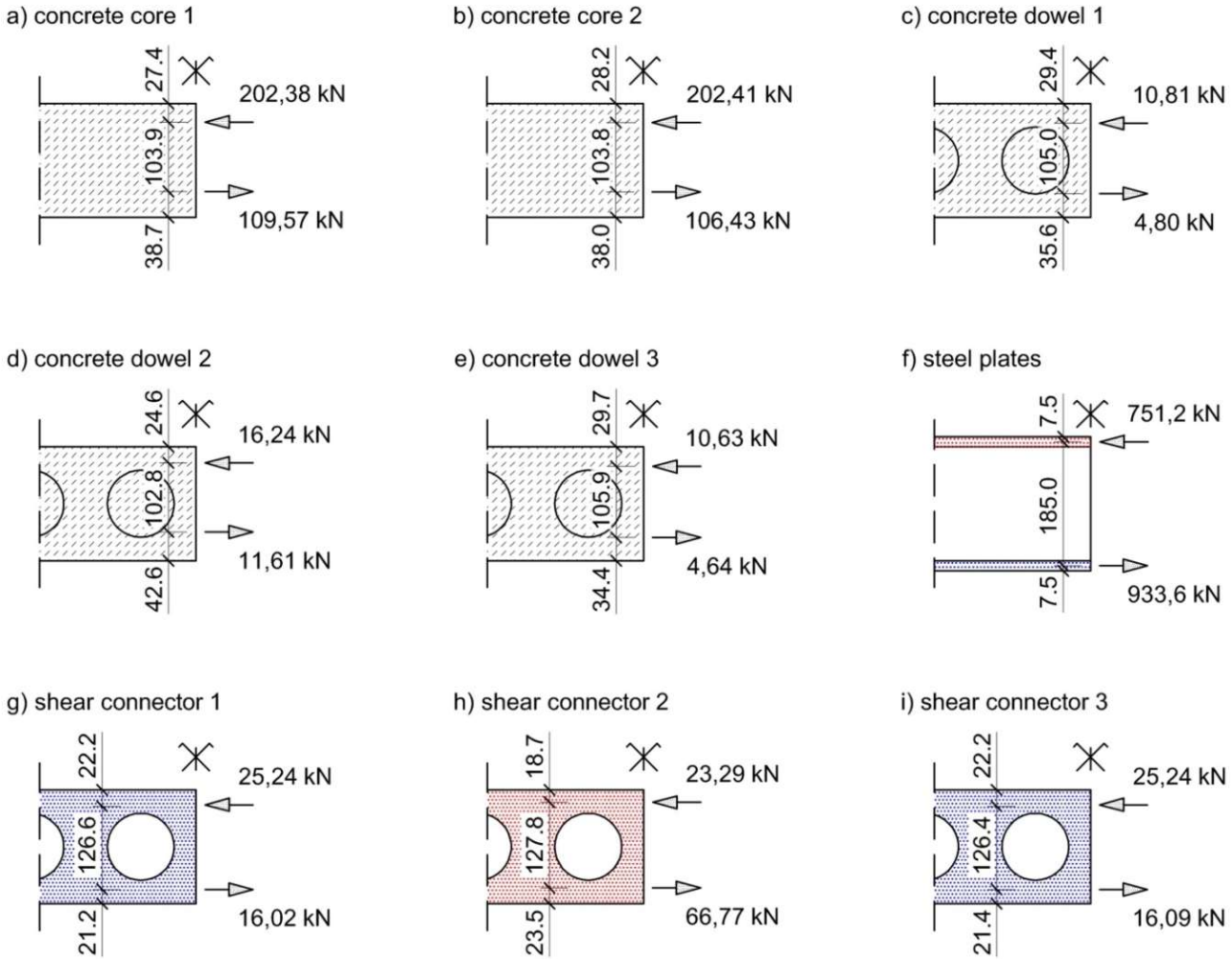

Figure 2.64: Horizontal compression and tension in the concrete and steel structure parts at the plane of symmetry based on the ABAQUS calculation results. Dimensions in [mm]

Obviously, the resultant compressive and tensile forces should be the same because of the pure bending of the structure. However, the difference between the results (2,09 kN) is negligible compared to the acting forces (1267,44 kN, 1269,53 kN). Additionally, the results in figure 2.64 indicate a bending moment of 203,07 kNm in the middle of the span The detailed calculation of this value is presented in appendix B. The difference from the desired value (205,32 kNm, see figure 2.63(a)) is not significant. The reason for this difference is partly that the positions of the high forces in the steel plates are assumed in the middle of the plates (see figure 2.64(f)) as an approximation. Through the addition of compressive and tensile forces in figure 2.64, the forces in the concrete and steel structure parts can be detected separately. Thus, in the concrete parts of the construction the total sum of the compressive forces is 442,47 kN. Furthermore, a resultant tensile force of 237,05 kN act in the concrete.

In the top steel plate and in the three shear connectors together acts a compressive force of 824,97 kN. The bottom steel plate and the shear connectors carry a tensile force of 1032,48 kN according to the ABAQUS results (see figure 2.64). Logically, the compression in the concrete is higher than the tension because the compressive strength of the concrete (48 N/mm^2) is greater than the tensile strength (3,509 N/mm^2). Actually, in the case of the loading used for fatigue limit state, the tensile stress reaches the ultimate tensile strength of the concrete in the lower parts of the concrete core. Obviously, the resultant tensile force in the steel structure is higher than the resultant compressive force to compensate the above mentioned force difference in the concrete.

It is important to note that the following models cannot detect the tensile cracking and compressive crushing of the concrete material. Actually, it is assumed that failure mechanisms of concrete do not occur in the case of the examined load level used for fatigue limit state. This assumption bases on the ABAQUS calculation. In the case of higher loads, an expansion of the presented models is necessary to evaluate the effects from failure of concrete.

Next, a simple two-dimensional truss frame model will be defined which illustrates the concrete core. Logically, the loading of the concrete model is specified according to figure 2.62(d). The loaded area is also shown in figure 2.65(a) where the involved areas from the above described partition are also numbered. Thus, the line loads can be approximated with seven concentrated loads acting on the examined structure (see figures 2.65(b) and (c)). The bending moment diagram calculated from the concentrated loads is shown in figure 2.65(d). The positions of the horizontal resultant forces in the middle of the span are detected with ABAQUS (see figure 2.64). Based on the force positions at the two concrete cores (see figures 2.64(a) and (b)), the thickness of the two horizontal truss members (27,4 + 28,2 = 55,6 mm and 38,7 + 38,0 = 76,7 mm, see figure 2.66(a)) of the truss frame model are calculated. The model illustrated in figure 2.66(b) consists of seven simple truss models, one for each of the external vertical concentrated loads. The horizontal forces in the truss members (205,49 kN, see figure 2.66(b)) can be easily calculated from the bending moment in the middle of the span (21,34 kNm, see figure 2.65(d)) and the moment arm (z = 170 – 55,6/2 – 76,7/2 = 103,85 mm, see figure 2.66(b)):

$$N = M/z = 21{,}34\ kNm\ /\ 0{,}10385\ m = 205{,}49\ kN \tag{2.21}$$

Corresponding to chapter 2.4.1, the two outside shear connectors transmit loads to the support through the concrete with a truss frame model (see figure 2.54). Thus, additional horizontal forces occur in the concrete in the middle of span. To calculate these forces, the bending moments are calculated from the matching loads (see figure 2.67) in the case of one outside shear connector. The length of the examined concrete beam (2023 mm) is a little bit shorter than the length of the model in figure 2.66 (2040 mm) because of the thickness of the end stiffener (15 mm) and the gap between the end plate and the end stiffener (2 mm). Additionally, is it remarkable in figure 2.67(b) that the load input positions are at the top of the circular holes of the outside steel shear connector. However, this fact does not influence the bending moments illustrated in figure 2.67(c).

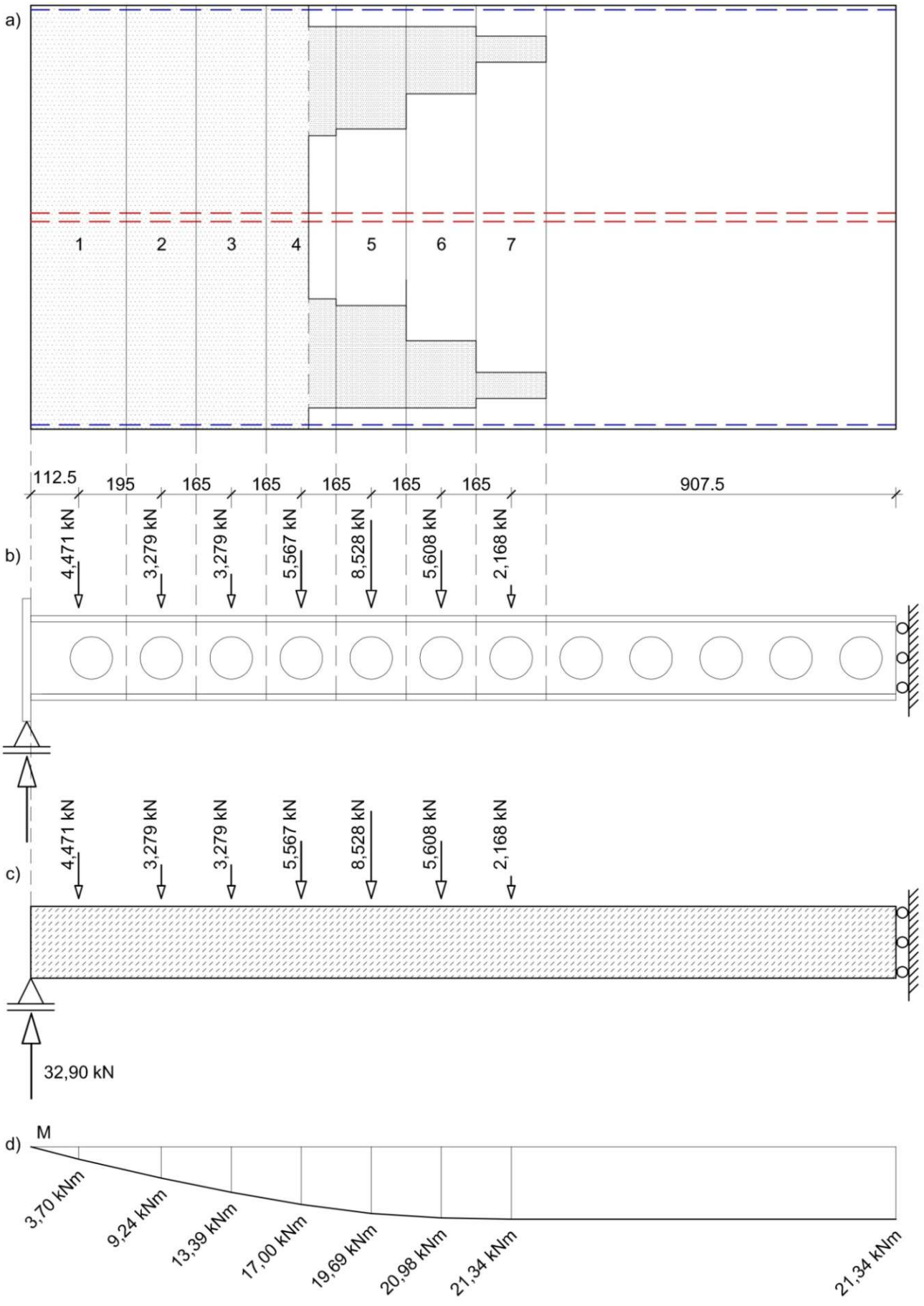

Figure 2.65: Model design for concrete: a) loaded area, top view; b) side view; c) the loaded concrete beam; d) bending moments

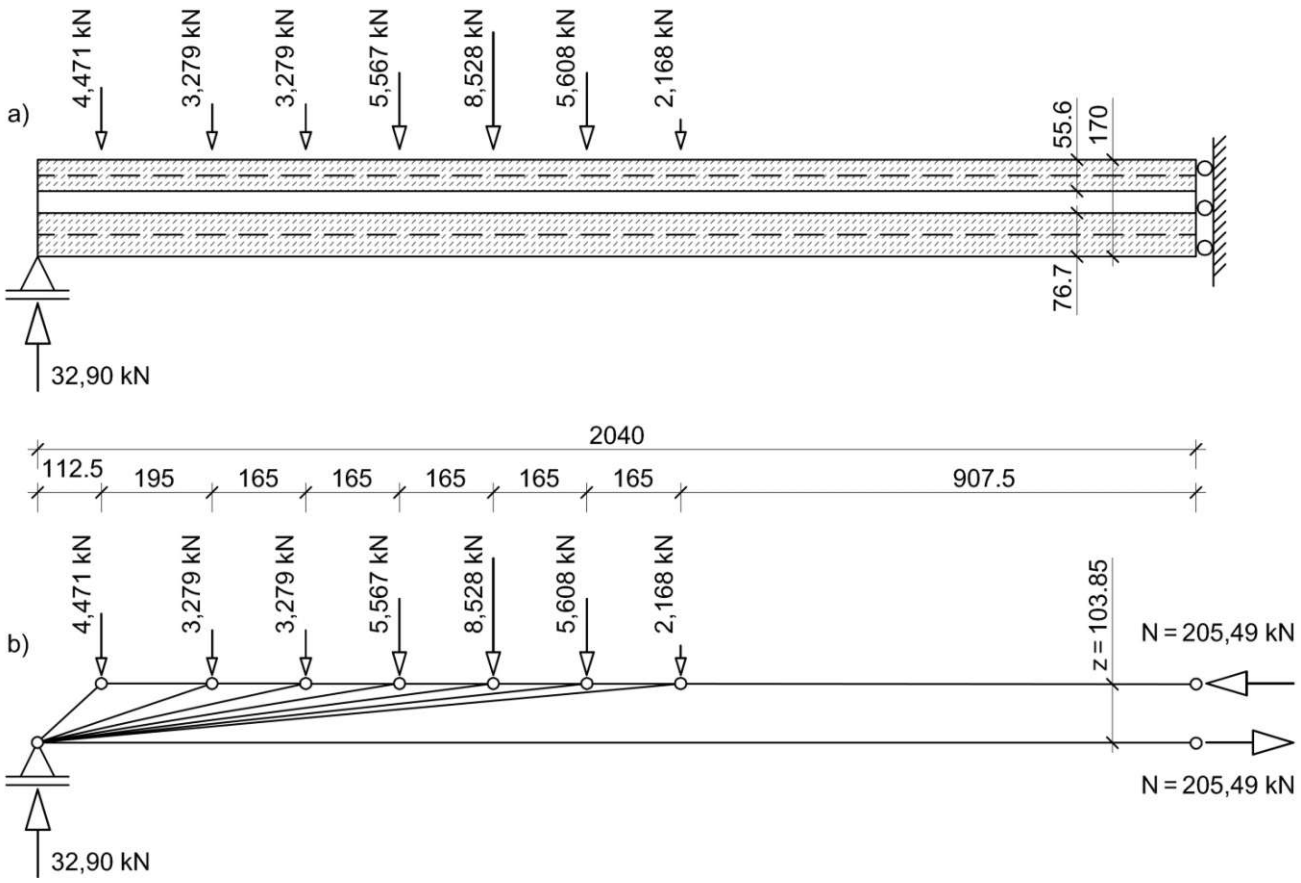

Figure 2.66: Model design for concrete: a) the horizontal truss members with the external loading; b) the truss frame model

The positions of the horizontal resultant forces in the middle of the span are detected also with ABAQUS (see figure 2.64). However, the force positions from the two outside concrete dowels (see figures 2.64(c) and (e)) are used here to calculate the thickness of the horizontal truss members. Thus, the thickness of the compression member is 59,10 mm (29,4 + 29,7), while the tension member is 70,00 mm (35,6 + 34,4) thick. Therefore, the distance between the midlines of the horizontal truss members of the model is 105,45 mm (170 – 59,10/2 – 70,00/2) as illustrated in figure 2.68. This model consists of four simple truss models, one for each of the loads from the shear connector. These four truss models are represented in the same figure to show the forces in the horizontal truss members from the total loading illustrated in figure 2.67(b). The horizontal forces in the truss members (20,67 kN) in figure 2.68 are calculated from the bending moment in the middle of the span (2,18 kNm, see figure 2.67(c)) and the moment arm (z = 105,45 mm, see figure 2.68):

$$N = M/z = 2{,}18\ kNm\ /\ 0{,}10545\ m = 20{,}67\ kN \tag{2.22}$$

At this point, the forces through the truss frame models can be compared with the ABAQUS results in the middle of the span. The five concrete parts of the ABAQUS model (see figures 2.64(a), (b), (c), (d) and (e)) detect a total compressive force of 442,47 kN and a resultant tensile force of 237,05 kN. These resultants are illustrated in figure 2.69(a). As explained above, there is not force equilibrium at the concrete part of the ABAQUS model because of the steel - concrete interaction in the composite structure. Namely, it is assumed that the resultants arise from two effects. Firstly, the separate load-bearing behaviour of the concrete induces a pure bending moment in the middle of the span. Thus, a tensile force of 237,05 kN and a compressive force of 237,05 kN occur in the concrete. Secondly, the additional compressive force of 205,42 kN (442,47 – 237,05) arises at the top part of the cross section from the composite effect illustrated in figure 2.59.

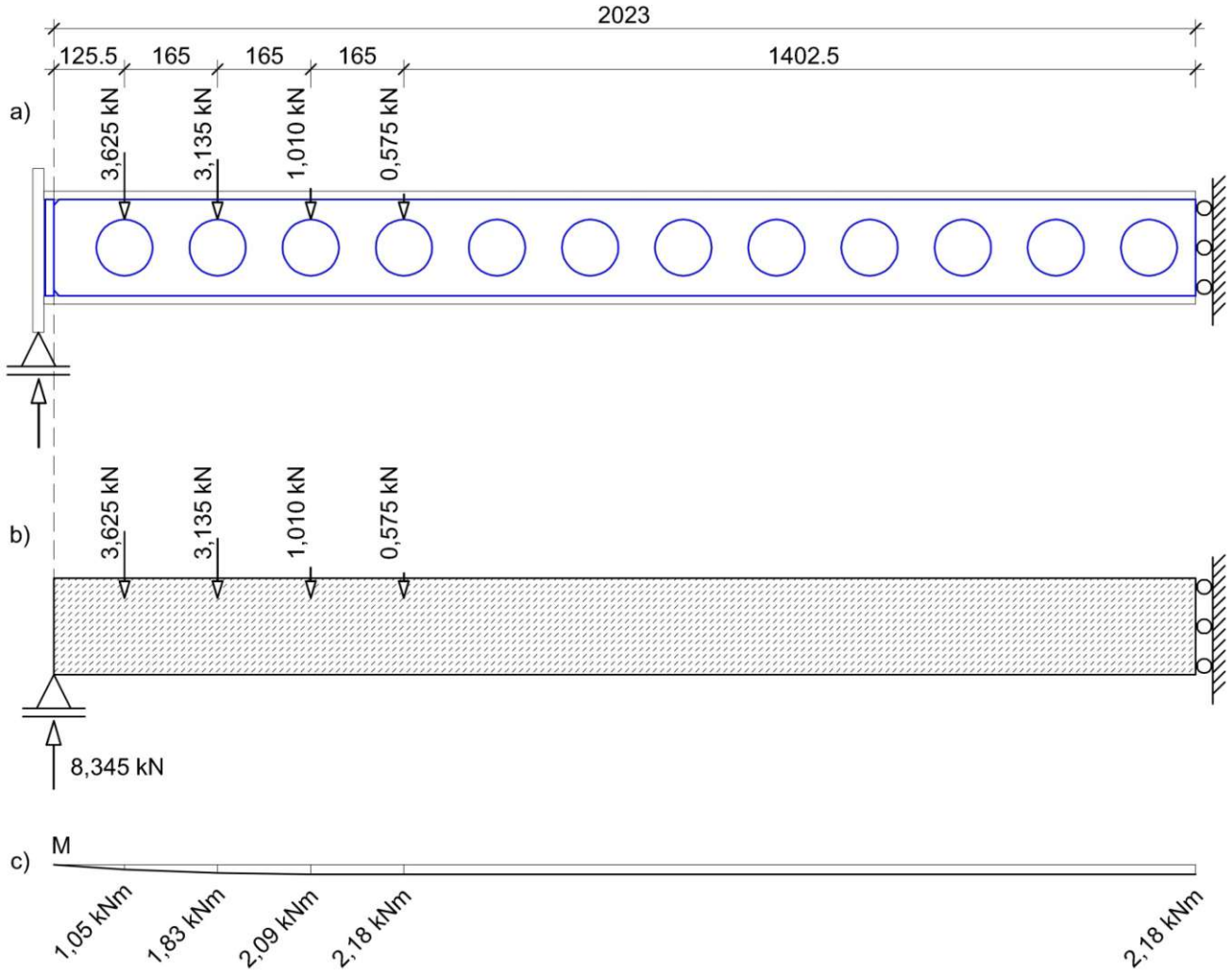

Figure 2.67: Model design for concrete next to the outside shear connector: a) concentrated vertical loads at the holes of the shear connector of the bottom steel section; b) the loaded concrete beam; c) bending moment diagram. Dimensions in [mm]

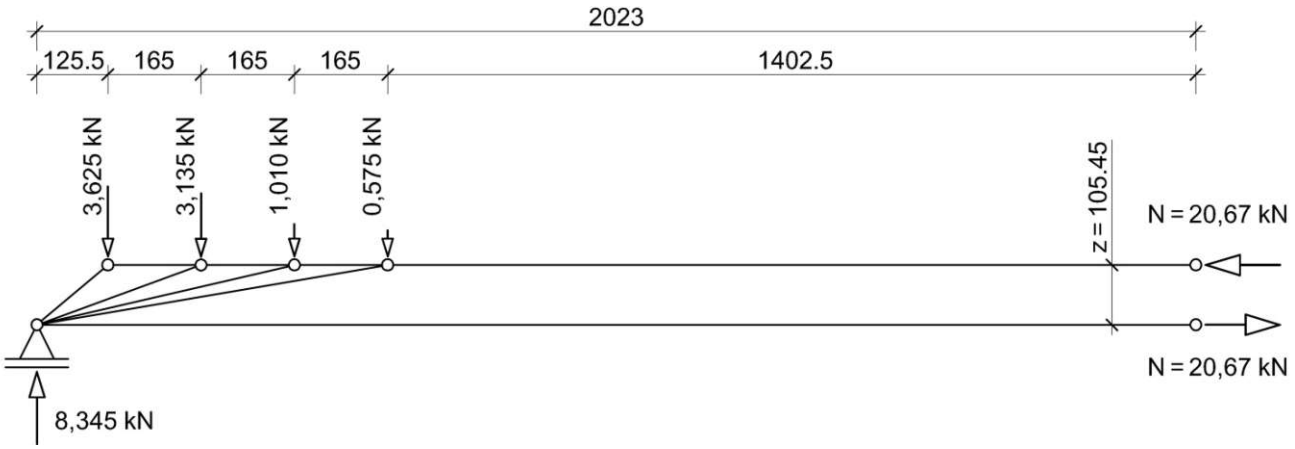

Figure 2.68: Truss frame model for the concrete next to the outside shear connector. Dimensions in [mm]

The results from the truss frame models illustrated in figures 2.66(b) and 2.68 give a resultant tensile and compressive force of 246,83 kN (205,49 + 2 · 20,67) in the concrete (see figure 2.69 (b)). Logically, these forces occur from the separate load-carrying capacity of the concrete. Thus, the tensile forces from the two calculations (ABAQUS and truss

model) are comparable. Namely, the simple truss models through the described load distribution reproduce properly the result of the ABAQUS calculation. Actually, the simple engineering model delivers 246,83 kN which is 104,1 % of the ABAQUS result. Obviously, the compressions in the concrete cannot be analysed through the introduced truss model.

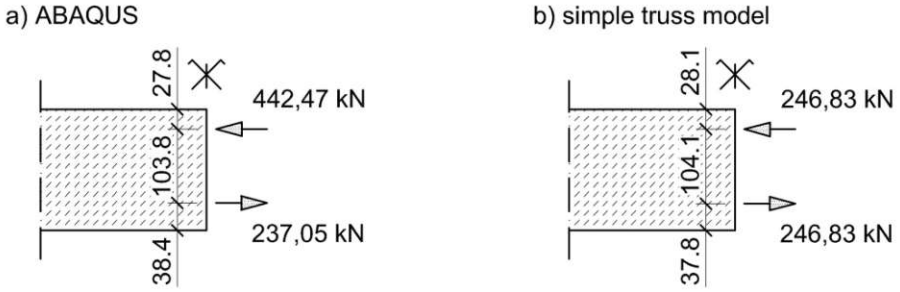

Figure 2.69: Horizontal compression and tension in the concrete at the plane of symmetry: a) ABAQUS calculation results; b) results from the simple truss model. Dimensions in [mm]

Next, the steel structures of the SCSC plate are examined through a simple model. The model consists of the bottom and top steel sections. However, they are structurally connected here to symbolise the shear transfer through the concrete. As in the case of the concrete model, the partition of the loaded area (see figure 2.62) is the basis of the following calculations. Figure 2.70(a) shows the concentrated loads which represent the external loading from the loaded areas illustrated in figures 2.62(a), (b) and (c). However, two additional effects modify the bending moments in the steel structure. Figure 2.70 (b) illustrates that a small bending occur from the fact that the forces transferred through the concrete (see figure 2.66) act at the end of the bottom steel plate. Moreover, as shown in figure 2.70(c), the distinct load-carrying function of the concrete represented in figure 2.68 reduces the bending of the steel structure. The bending moment diagram from the marked forces is given in figure 2.70(d). However, the forces in figure 2.70(c) are doubled for the bending moment calculation as there are two outside shear connectors in the presented model. Thus, the maximal bending moment in the middle of the span is 179,34 kNm. Obviously, this result is equal to the difference between the bending moment of the whole structure (205,04 kNm, see figure 2.63(b)) and the bending moment acts on the concrete model (21,34 kNm + 2 · 2,18 kNm = 25,70 kNm, see figures 2.65(d) and 2.67(c)).

The cross section of the model is illustrated in figure 2.71. The profile of the shear connector is considered with a continuous cutting in the middle with 100 mm as an approximation. In this way, the used steel profile consists of two parts according to figure 2.71. However, these two parts together mean the cross section of the steel structure model.

The area moment of inertia of the cross section around the axis “y”:

$$I_y = \frac{1000 \cdot 200^3}{12} - \frac{2 \cdot 480 \cdot 170^3}{12} - \frac{40 \cdot 100^3}{12} = 270\,293\,333\ mm^4 \tag{2.23}$$

The three shear connectors of the ABAQUS model (see figures 2.64(g), (h) and (i)) detect together a total compressive force of 73,77 kN and a resultant tensile force of 98,88 kN as illustrated in figure 2.72(a). The resultant forces in the steel plates are also shown in the figure. The bending stress in the beam element used for the engineering model can be easily calculated in the middle of the span with the Euler-Bernoulli’s Beam Equation. The bending moment illustrated in figure 2.70(d) and the area moment of inertia of the cross section according to the equation 2.23 are used for this calculation. The stress diagram is given in figure 2.72(b). Based on these bending stresses, the resultant compressive and tensile forces are evaluated in the steel plates and the shear connectors. However, the three shear connectors are considered together. The results are also shown in figure 2.72(c).

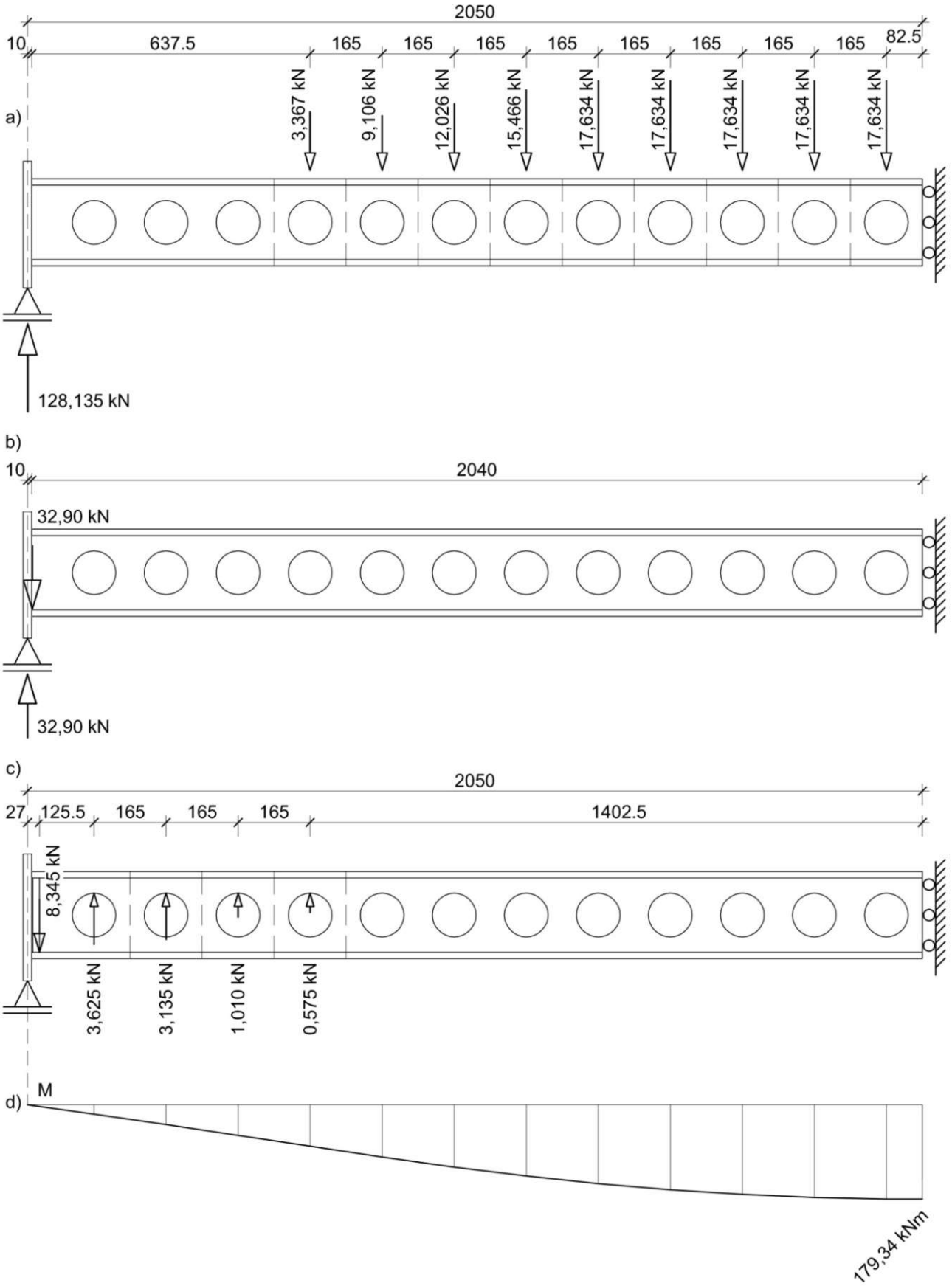

Figure 2.70: Model design for the steel structures of the SCSC plate: a) the external loading on the model; b) loading from the concrete pressures next to the end plate; c) effects from the load transfer between one outside shear connector and the support on the steel structure; d) bending moment diagram due to the loads illustrated in figures (a), (b) and (c). The forces in figure (c) are doubled for the bending moment calculation as two outside shear connectors are designed in the model.

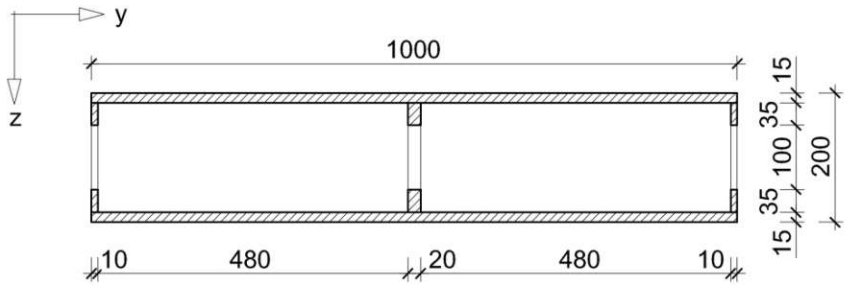

Figure 2.71: The cross section for the model of the steel construction parts. Dimensions in [mm]

Only the tensile forces from the two calculations (ABAQUS and simple beam model) are comparable because the compressive forces in the steel elements are influenced through the concrete of the SCSC plate in the case of the ABAQUS model. Thus, referring to the tensions in the bottom steel plate, the simple beam model of the steel structures reproduces properly the result calculated with ABAQUS (933,6 kN). Namely, the engineering model delivers 920,6 kN which is 98,6 % of the ABAQUS result.

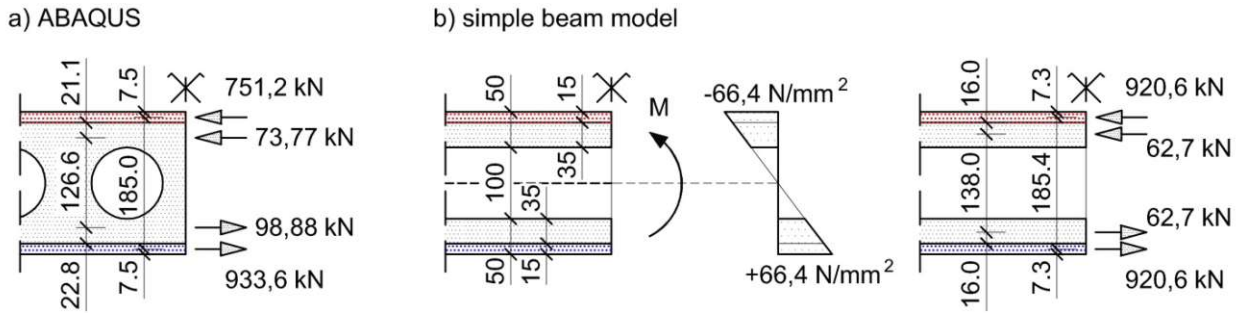

Figure 2.72: Horizontal compressive and tensile forces in the steel construction parts at the plane of symmetry: a) ABAQUS calculation results; b) results from the simple beam model. Dimensions in [mm]

Next, the maximal deflections are compared. The maximal vertical displacement is 7,01 mm according to the ABAQUS calculation. As an engineering model for the calculation of the displacements, the steel elements of the SCSC plate are modelled with the structural analysis program RFEM [18] to take into account the shear deformations of the steel sections due to the circular holes in the shear connectors. The mesh refinements are defined here as 1 cm. The top and the bottom steel sections are structurally connected. Obviously, the loading is identical with the loading of the simple steel beam (see figure 2.70). So, the maximal vertical deflection in the middle of the span is 6,88 mm from RFEM, which is practically equal to the ABAQUS result.

Finally, the fourth model is created to detect the horizontal dowel forces in the shear connector of the top steel section. The dowel forces of the bottom steel section are not examined because these forces are smaller as the dowel forces in the central shear connector. Both of the two simple models (model 4(a) and model 4(b)) presented below are based on the longitudinal shear flow (T [N/mm]) at the top horizontal plane of the central shear connector. The ABAQUS calculation result of the shear flow distribution is illustrated in figure 2.73. However, the shear stresses in the examined horizontal plane were evaluated with ABAQUS. Thus, in figure 2.73(b) represented shear flow is found as the shear stress multiplied by the thickness of the shear connector. It is important to mention that the figure illustrates the whole shear connector to show the symmetric distribution of the shear stresses. However, the ABAQUS model consists of just the half of the element as it was presented in chapter 2.3.1.

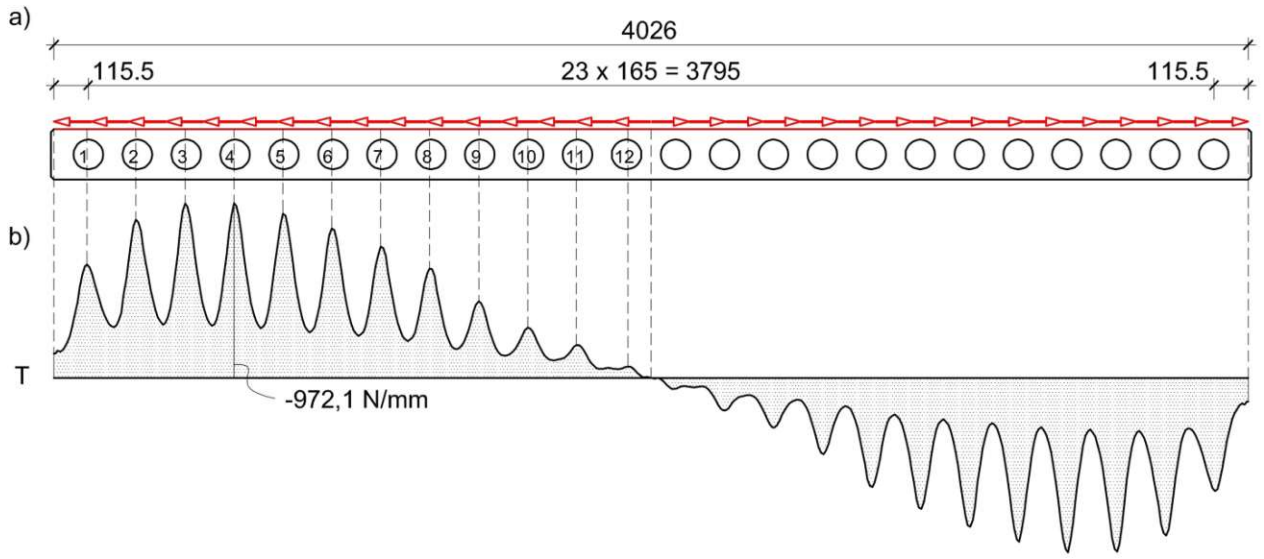

Figure 2.73: Shear flow at the top horizontal plane of the central shear connector according to the ABAQUS calculation results: a) side view of the shear connector; b) shear flow along the steel member. Dimensions in [mm]

As a good estimate, the horizontal dowel forces can be calculated from the presented horizontal shear flow. It is assumed that the horizontal dowel force compensates the horizontal shear force which acts above the examined hole. Actually, the shear flow distribution is divided according to figure 2.74(b). The area of a marked sector in the figure gives the resultant horizontal shear force belonging to the matching hole of the shear connector. Logically, the direction of the horizontal dowel force at a hole of the shear connector is opposite the direction of the marked shear forces in figure 2.73(a) (see the red arrows). Logically, the dowel force means the effect from the concrete core of the SCSC plate on the steel shear connector. The calculated forces are represented in figure 2.74(c). The black line illustrates the results in a graph format for ease of view. Moreover, the exact ABAQUS results (according to the first row in table 2.4) are also demonstrated in figure 2.74(c) with the green line. Thus, it is clear to see that the approximate calculation is applicable.

The simple model 4(a) consists of the steel parts of the SCSC plate. Actually, the cross section in figure 2.71 is used. The area moment of inertia of this cross section around the axis "y" is given in equation 2.23. As illustrated in figure 2.75(a), the total external loading of the SCSC plate acts on this model. Figure 2.75(b) shows the shear force diagram, while figure 2.75(c) represents the longitudinal shear flow distribution at the top horizontal plane of the central shear connector. The shear flow values are calculated according to equation 2.24 based on the shear formula in solid mechanics. In the development of this formula the Euler-Bernoulli assumptions are used.

$$T = -\frac{V \cdot S_y}{I_y} \tag{2.24}$$

where:

$T\ [N/mm]$	Shear flow
$V\ [N]$	Shear force carried by the section (see the shear force diagram in figure 2.75(b))
$S_y\ [mm^3]$	First moment of area about the neutral axis "y" for the top steel plate of the cross section
$I_y\ [mm^4]$	Area moment of inertia of the whole cross section around the axis "y"

The first moment of area (S_y) considers the area above the point where the shear stresses are calculated.

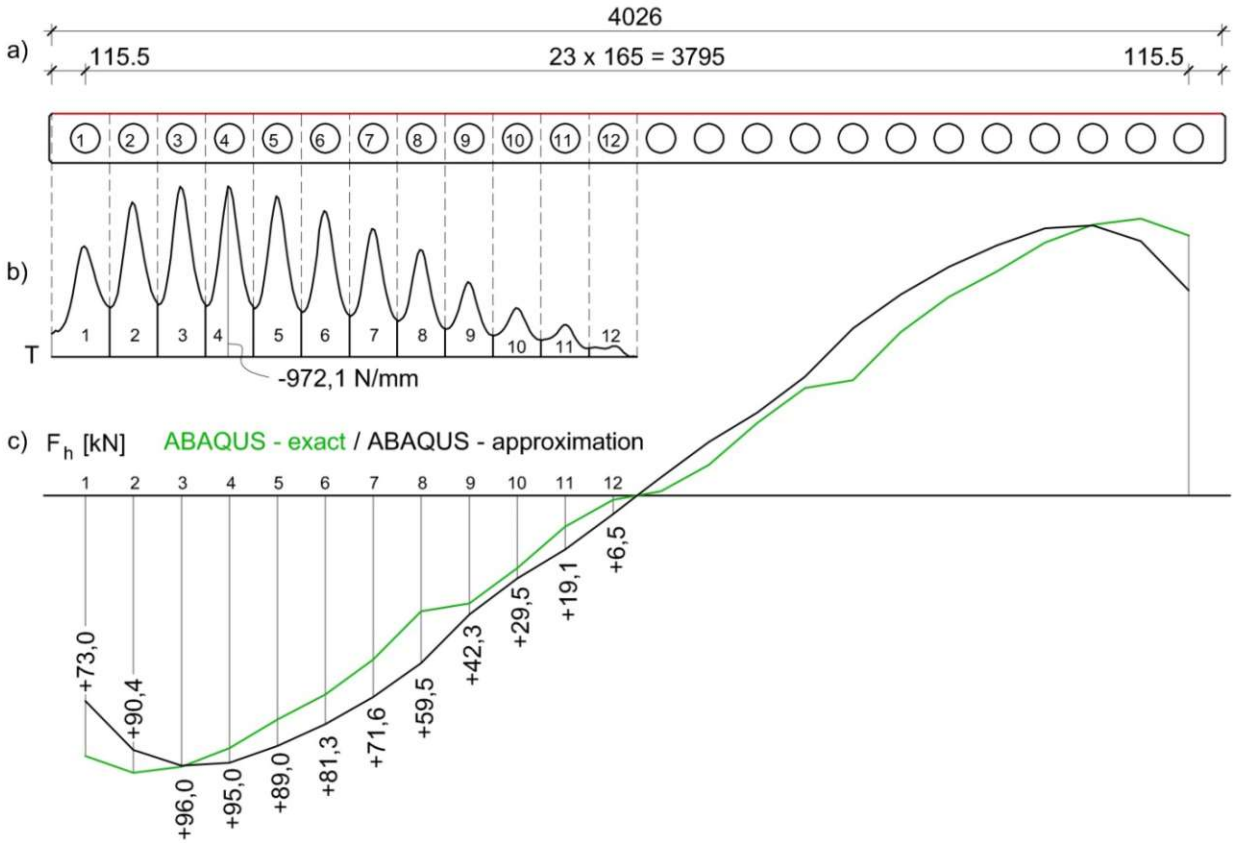

Figure 2.74: The evaluation of the horizontal dowel forces in the shear connector of the top steel section based on the ABAQUS results: a) side view of the shear connector; b) the partition of the shear flow diagram; c) horizontal forces at the holes of the shear connector 2. Dimensions in [mm]

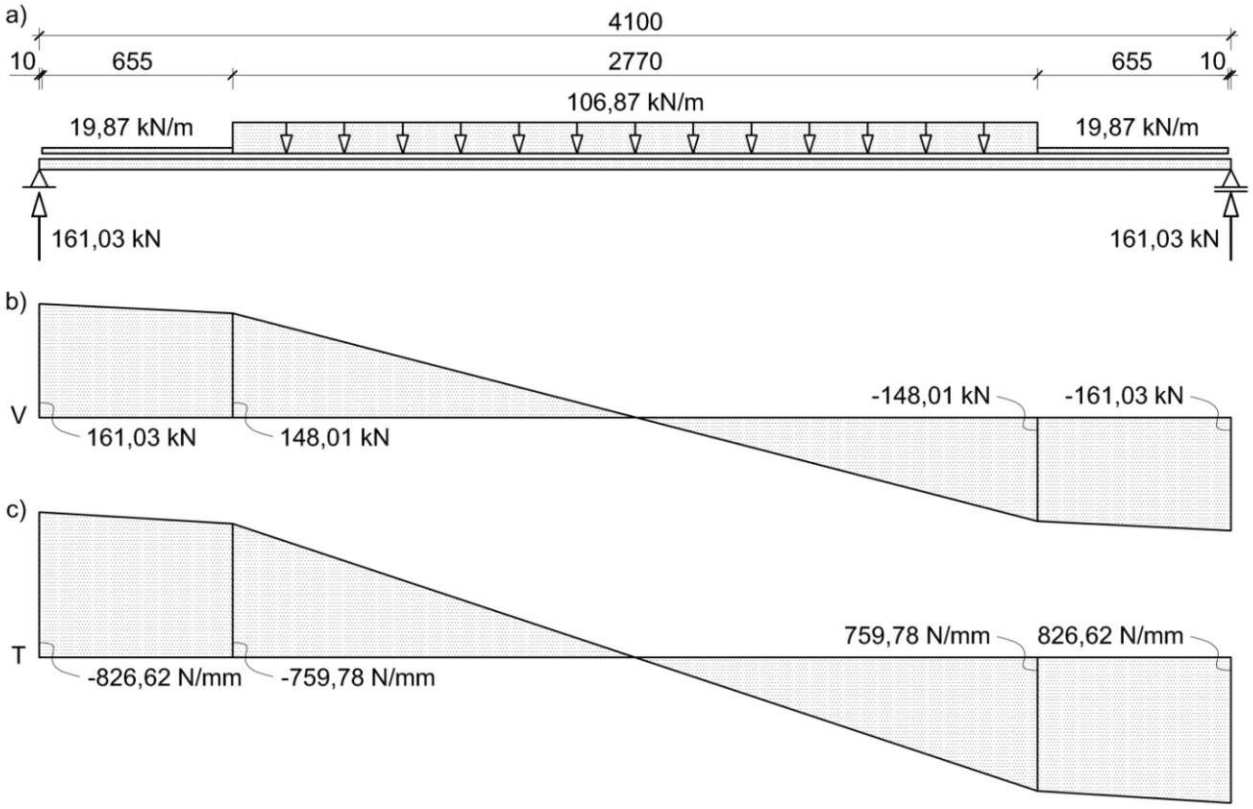

Figure 2.75: Simple model 4(a): a) external loading on the model; b) shear force diagram; c) shear flow distribution

As the shear stresses need to be evaluated at the top horizontal surface of the shear connector, the first moment of area considers only the top steel plate of the cross section (see equation 2.25).

$$S_y = A \cdot z = 15000 \cdot 92{,}5 = 1\,387\,500\ mm^3 \tag{2.25}$$

where:

$A\ [mm^3]$	Area of the top steel plate
$z\ [mm]$	Distance from neutral axis to centroid of the top steel plate

It is assumed that the total shear flow calculated above acts on the central shear connector. The shear flow diagram in figure 2.75(c) is partitioned according to figure 2.76(b). As shown in figures 2.75(a) and 2.75(b), the width of the sector 1 is 165 mm as an approximation. The marked areas of the shear flow diagram (see figure 2.76(b)) denotes the resultant longitudinal shear forces which effect on the 165 mm wide parts of the shear connector. The absolute values of these forces give the horizontal dowel forces illustrated in figure 2.76(c).

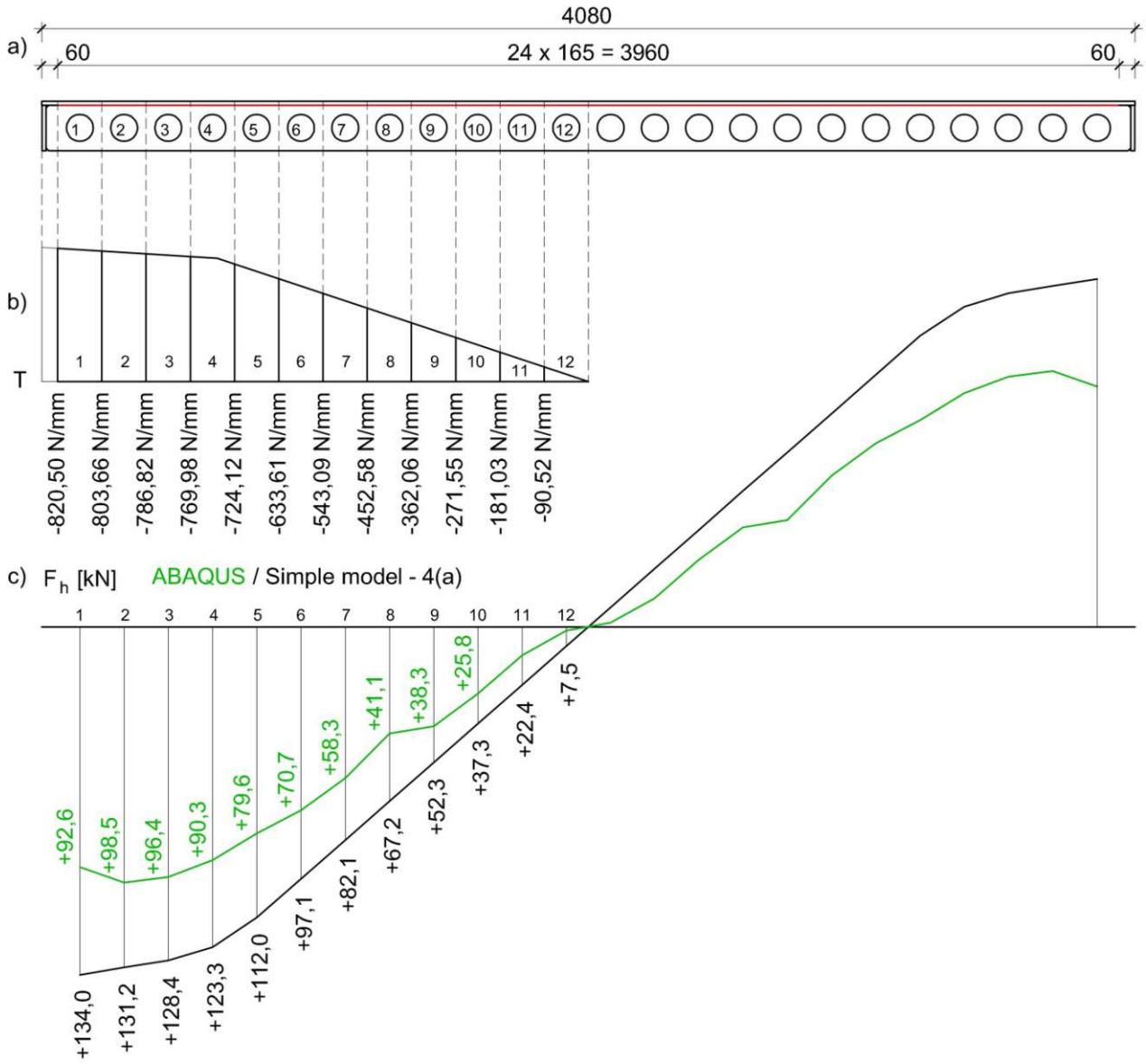

Figure 2.76: The evaluation of the horizontal dowel forces in the shear connector of the top steel section based on model 4(a): a) side view of the shear connector; b) the partition of the shear flow diagram; c) horizontal forces at the holes of the shear connector 2. Dimensions in [mm]

It is clear through the figure that the calculation with model 4(a) overestimates significantly the ABAQUS results. Thus, an additional simple model (model 4(b)) is examined, too. Only the cross section of the top steel plate is considered here. However, the cross section has a cutting in the middle of the shear connector to represent approximately the holes (see figure 2.77). The area moment of inertia of the cross section around the axis "y" is given in equation 2.26 without a detailed calculation:

$$I_y = 17\,616\,174\ mm^4 \tag{2.26}$$

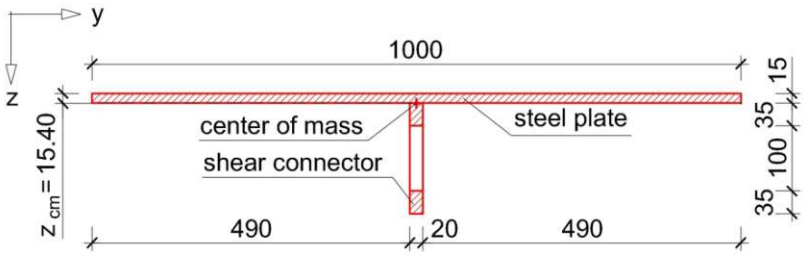

Figure 2.77: The cross section for the model 4(b). Dimensions in [mm]

The external loading on the load areas 1 and 3 (see figures 2.62(a) and 2.62(b)) are used as the loading of model 4(b). So, the values in figure 2.78(a) are calculated through the addition of the values in the second and fourth rows of table 2.12.

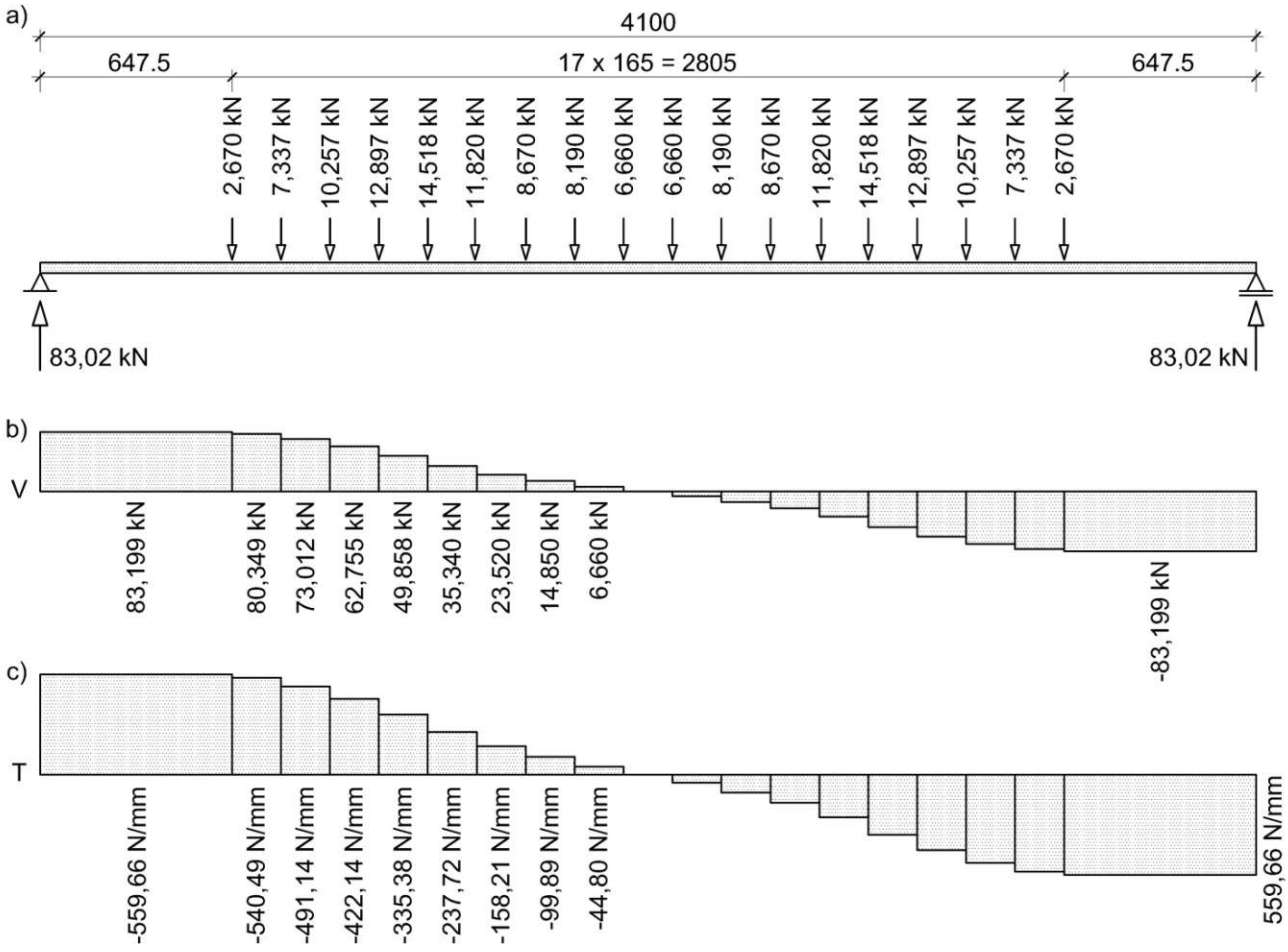

Figure 2.78: Simple model 4(b): a) external loading on the model; b) shear force diagram; c) shear flow distribution

Logically, the loadings of the central shear connector detected with ABAQUS are used in the case of model 4(b). Figure 2.78(b) shows the shear force diagram, while figure 2.78(c) represents the longitudinal shear flow distribution at the top horizontal surface of the shear connector. As in the case of model 4(a), the shear flow values are calculated according to equation 2.24. Obviously, the shear stresses are evaluated at the top plane of the shear connector, thus the first moment of area (Q) considers the top steel plate of the cross section which is calculated in equation 2.27:

$$S_y = A \cdot z = 15000 \cdot 7{,}9 = 118\,500\, mm^3 \tag{2.27}$$

where:

$A\ [mm^3]$	Area of the top steel plate
$z\ [mm]$	Distance from neutral axis to centroid of the top steel plate

The shear flow diagram in figure 2.78(c) is partitioned according to figure 2.79(b). By analogy with the approximation at the model 4(a), the width of the sector 1 is 165 mm (see figures 2.79(a) and 2.79(b)).

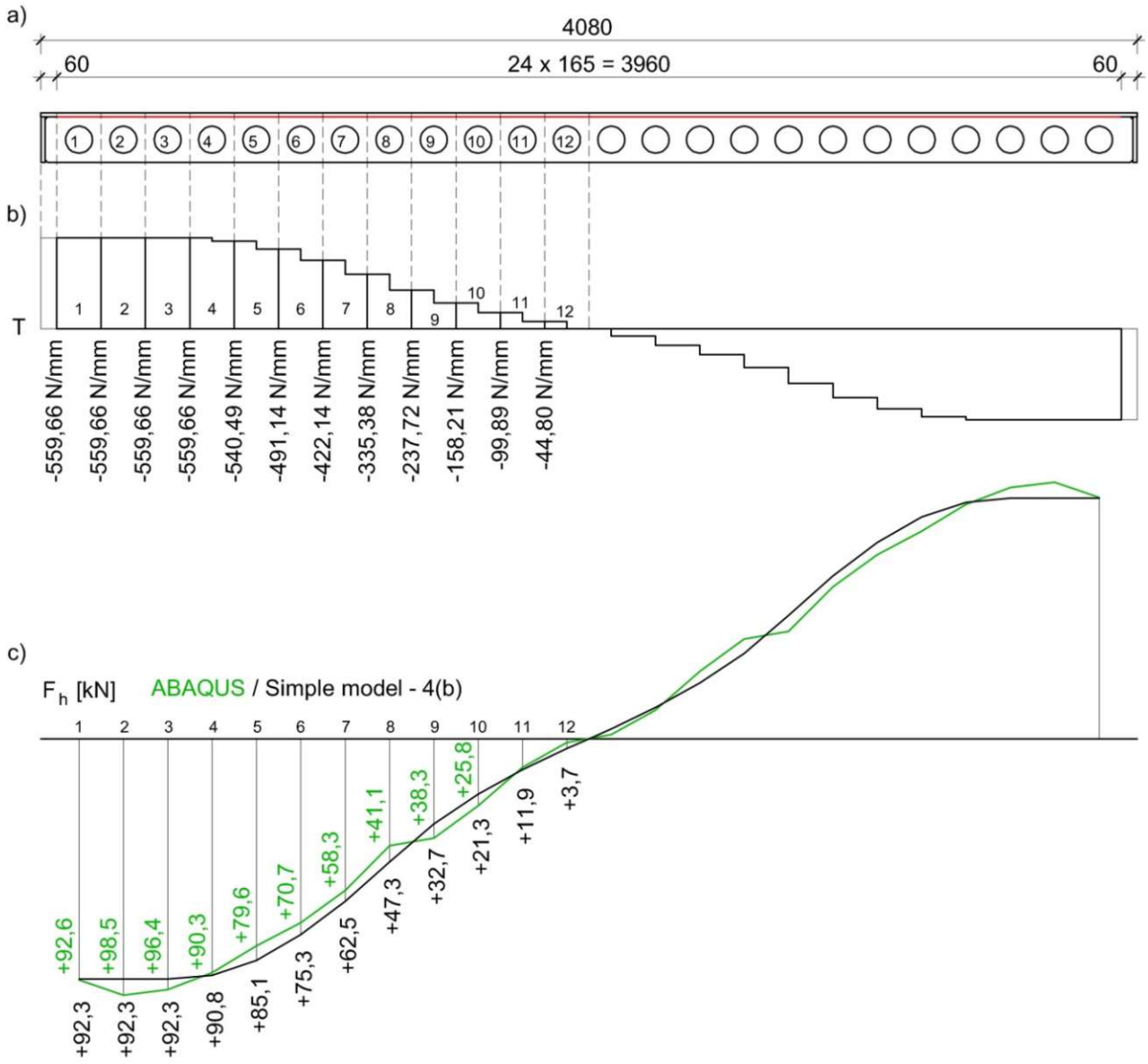

Figure 2.79: The evaluation of the horizontal dowel forces in the shear connector of the top steel section based on model 4(b): a) side view of the shear connector; b) the partition of the shear flow diagram; c) horizontal forces at the holes of the shear connector 2. Dimensions in [mm]

The marked areas of the shear flow diagram in figure 2.79(b) denotes the resultant longitudinal shear forces which effect on the 165 mm wide parts of the shear connector. The absolute values of these forces give the horizontal dowel forces illustrated in figure 2.79(c). This figure also illustrates that through the calculation with model 4(b) the horizontal dowel forces are almost the same as the ABAQUS results.

As shown in chapter 2.4.2, the ABAQUS calculation results can be approximately reproduced with four different engineering models. Two truss frame models describe the concrete and the steel structures of the SCSC plate separately. As the composite connection is not modelled with these simple models, the forces in the shear connectors detected with ABAQUS are not calculated with these two models. The third engineering model is constructed in RFEM to show the maximal deflection of the complex SCSC plate. Finally, the fourth model delivers the horizontal dowel forces in the central shear connector. It is important to mention that the presented models use the divided external loading detected with ABAQUS. Obviously, the aim of the simple models was not the substitution of the complex ABAQUS calculation. In the following chapters (see chapter 3.6.1 and 3.6.2) two-dimensional spring framework models will be introduced which operates without any results from ABAQUS. These more complex framework models are only appropriate for the engineering practice to analyse the composite structure and substitute the time-consuming ABAQUS calculation.

3. The spring framework model

3.1 Introduction of the chapter

The aim of chapter 3 is to explain the structure of the spring framework model and its parameters, to present the principles of the calculation method (Direct Stiffness Method) and to demonstrate how the framework model calculation reproduces the values of the displacements and internal forces calculated in ABAQUS.

Firstly, in chapter 3.2, the experimental tests performed in February 2020 at the laboratory of TU Wien, Institute of Structural Engineering will be described. Due to the test results, it is possible to evaluate the spring stiffness values for the spring framework model. Secondly, in chapter 3.3, a short overview will be given about the Direct Stiffness Method. Following that, in chapter 3.4, the validation of the framework model calculation takes place through modelling the steel structure elements of the SCSC plate. Various types of models will be introduced in chapters 3.5, 3.6 and 3.7 to show the parity of results to the ABAQUS calculation results. These complex two-dimensional framework models include the concrete members too, and the ABAQUS analysis designed model (1 m long and 2,06 m wide) is represented.

3.2 Experimental test results to evaluate the spring stiffness values

Six experimental tests were performed in February 2020 at the laboratory of TU Wien, Institute of Structural Engineering in order to evaluate the spring stiffness values referring to the composite connection. Actually, the flexible composite joints between the concrete and steel members at the shear connectors are modelled through the springs. As the stiffness of these springs depend on the elasticity of the materials, on the geometrical feature of the joint and on the forces occurring in the shear connectors: The real shape of a shear connector was built to execute the laboratory tests. Therefore, a piece of the steel shear connector was constructed with a thickness of 20 mm. As illustrated in figure 3.1, the circular hole of the product was logically designed with a 100 mm diameter.

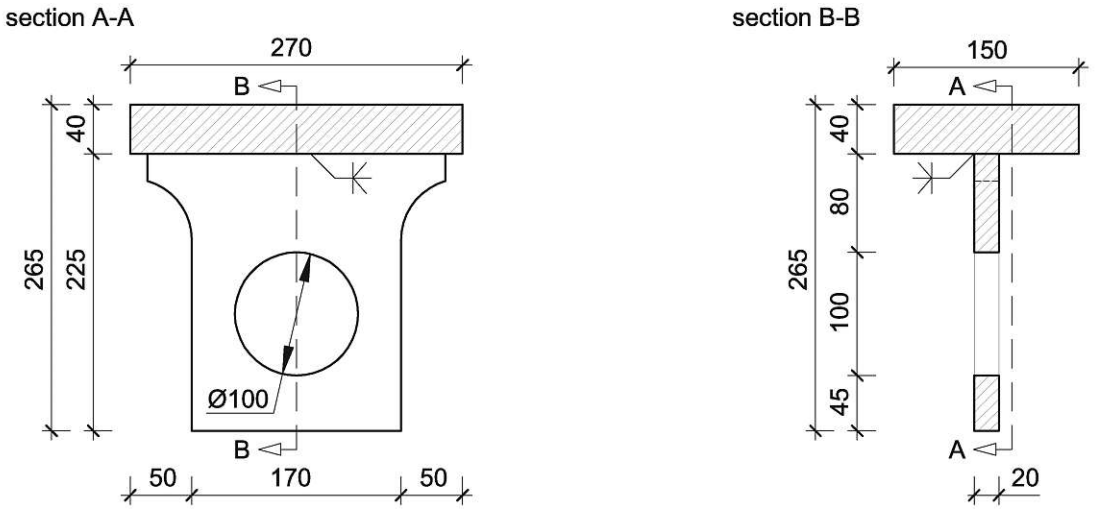

Figure 3.1: The steel part of the specimen to execute the laboratory tests

This steel part is partly embedded into a concrete block which has a size of 38x38x25 cm, where the 25 cm dimension is the height. The formwork of the concrete is a steel hollow section, which also belongs to the specimen. Directly under the steel shear connector part in the specimen, polystyrene is installed instead of concrete. Due to this, the load transfer is possible between the steel and concrete parts only at the hole of the shear connector, which is actually the composite connection of the SCSC plate. The complex specimen is illustrated in figure 3.2.

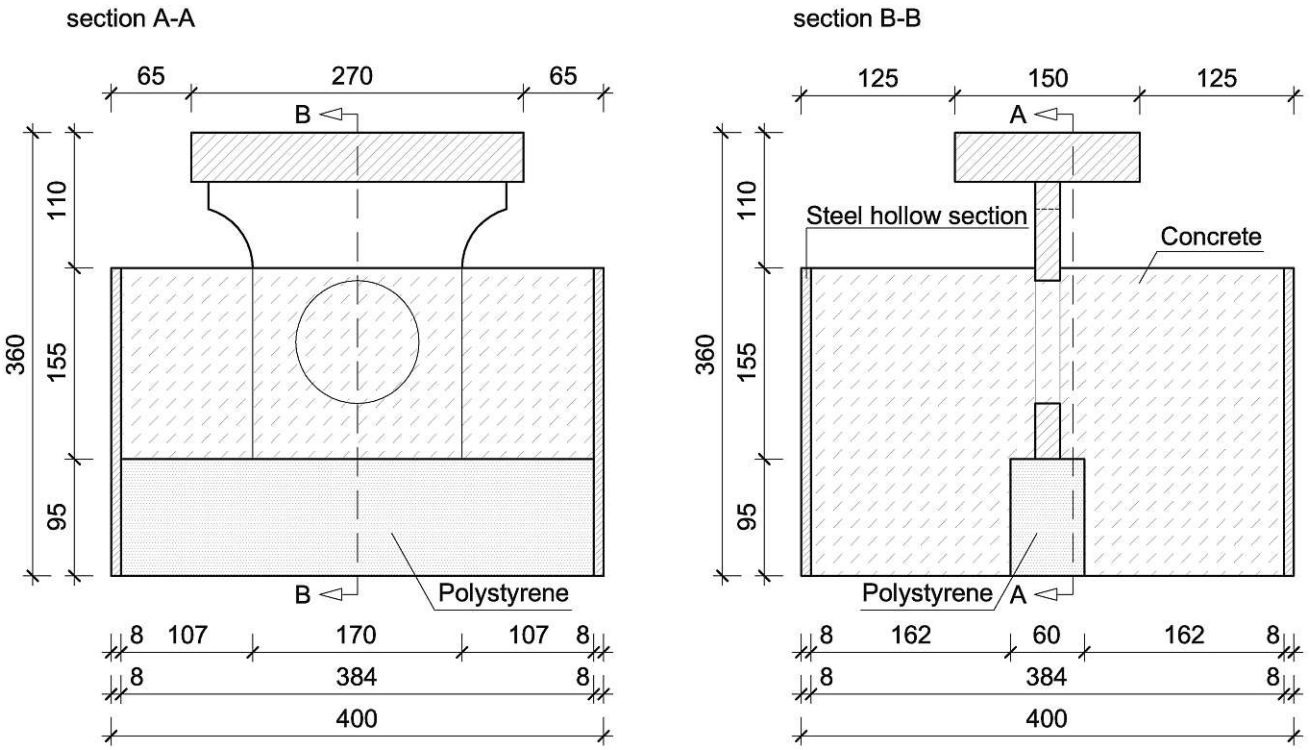

Figure 3.2: The complex specimen to execute the laboratory tests. Dimensions in [mm]

Moreover, the steel part of the specimen, the steel hollow section and the used polystyrene are shown in figure 3.3 before concreting. The wooden beams are installed temporarily because of the positioning of the steel part during concreting. C40/50 concrete and S355 structural steel is used according to the ABAQUS model.

Figure 3.3: The steel part of the specimen, the steel hollow section as the formwork and the polystyrene

During the laboratory tests, the loading of the specimen occurs on the upper part of the steel piece which is outside the concrete. Figure 3.4 illustrates the experimental setup. Simultaneously two specimens were loaded with a dynamic and fatigue testing system developed by *Schenck*. With this servohydraulic system high force tests up to 1600 kN can be performed at the laboratory of TU Wien, Institute of Structural Engineering.

Figure 3.4: The experimental setup at the laboratory of TU Wien

The load transfer takes place through the shear connector in the concrete block. Thereafter, the concrete transfers the forces into the massive steel plate of the test instrument. To get the force-slip diagrams describing the composite connection, the first loading takes place relatively slowly, growing by 20 kN/s. Three different load levels (maximal forces: 91 kN, 78 kN, 67 kN) were used to achieve the results. With one load level always two specimens were tested. So, a total number of six experimental tests were fulfilled. After the first loading, the specimens were unloaded down to a minimum force of 18 kN. This minimum force represents the force in the shear connector due to the static loading (dead load) of the SCSC plate. The difference between the maximal and minimal forces expresses the force in the shear connector through the traffic loading of the bridge. After the first unloading phase, the following load cycles (until the 2 millionth loading cycle) were completed with a loading-velocity of 5 Hz frequency. Thus, 5 loading-unloading cycles were completed per second. From the average of the results of the six tests, a slip-force diagram (see figure 3.5) was constructed, with which the spring stiffness values for the spring framework model can be received. For the curve of the static loading in figure 3.5, the average slips at 10 force values (10 kN, 20 kN, 30 kN, 40 kN, 50 kN, 54,5 kN, 60 kN, 70 kN, 80 kN, 91 kN) were calculated. Logically, up to the load level of 60 kN each of the six tests delivers slips to calculate an average. For example at the load level of 91 kN only two experimental tests are available.

In the chapter 3.5 the horizontal and vertical spring stiffness used for the framework model are constant as an approximation. This means, that the same spring stiffness value ($C_{first,1}$ = 325,0 kN/mm in figure 3.5) is used at each hole of the shear connectors and at each load level of the SCSC plate. This spring stiffness belongs to the maximal force in the shear connectors (91 kN). However, the maximal force is 98,5 kN in ABAQUS. Moreover, as a second model, a horizontal spring stiffness (527,4 kN/mm) belonging to the average force in the shear connectors (54,5 kN) is used. As at this point there are not results from the framework model available, the average force is chosen from the ABAQUS results as an approximation. The aim of these two calculations in chapter 3.5 is to keep on the safe side while analysing.

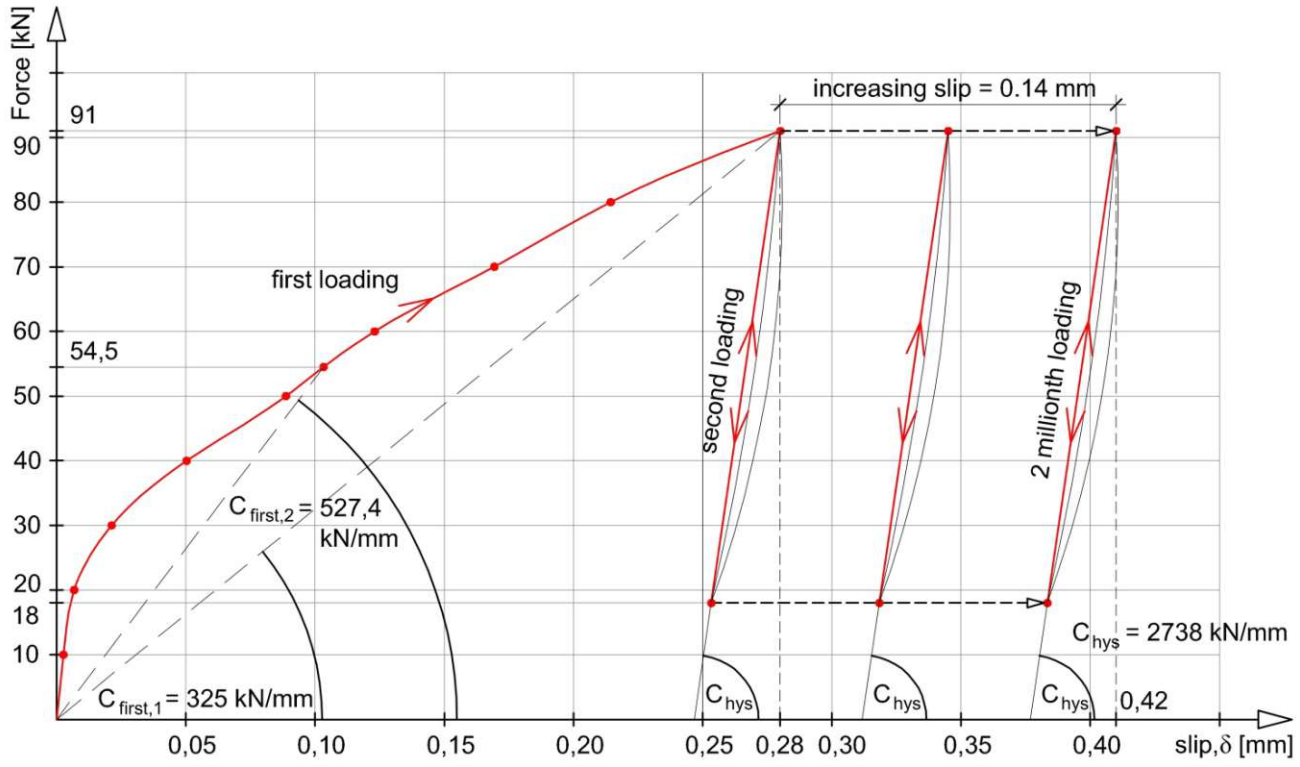

Figure 3.5: The force-slip diagram of the shear connector through the laboratory tests

In the chapter 3.6 the spring model is more complex as the spring stiffness value depends on the force in the shear connector. Here, the exact force-slip curve for the first loading (see figure 3.5: red curve for the first loading) is considered. In order to this precise calculation method, 100 calculation steps are used to represent the static loading (first loading). Namely, the external vertical load of the spring framework model is divided into 100 parts. At each calculation step, the used spring stiffness values are different as they are chosen according to the actual forces in the shear connector and the force-slip diagram illustrated in figure 3.5. This complex calculation is performed with a self-developed program in MATLAB [6]. However, structural frame analysis programs (e.g. RSTAB [19]) can also implement load increments and nonlinear spring properties.

It is also shown that permanent displacements (inelastic slips) in the composite connection already occur due to the first loading. Another effect is that the stiffness of the concrete increases after the first loading, as the concrete at the composite connection (in the holes of the shear connectors) becomes more compressed. Therefore, the spring stiffness will be greater at the second loading. Figure 3.5 illustrates that from the second loading this spring stiffness (C_{hys} = 2738 kN/mm), which is calculated on the basis of the hysteresis loops, is constant. Further increase of the inelastic slip occurs due to the additional loading cycles (see figure 3.5: increasing slip). The average of the increasing slip values of the six specimens is 0,14 mm.

The results of the six experimental tests and the calculations of the average values used for figure 3.5 are presented in appendix C.

3.3 Direct Stiffness Method

The Direct Stiffness Method is a common implementation of the Finite Element Method, where the structure is idealised through members connected at joints. With the well-known Hooke's-law and the elementary concepts of equilibrium, the member stiffness equations can be derived and written in matrix form. In the case of a beam member shown in figure 3.6, the force-displacement relationships are illustrated below (see equation 3.1). The member properties of the beam are the length L, the elastic modulus E, the cross-section area A, and the area moment of inertia I_v. The coordinate system {u,w} is called the local coordinate system, which is identical in figure 3.6 with the global coordinate system {x,z}. Moreover, the two end joints (i and j) are illustrated in the figure. Significant is that the external forces and the reactions can act only at the joints.

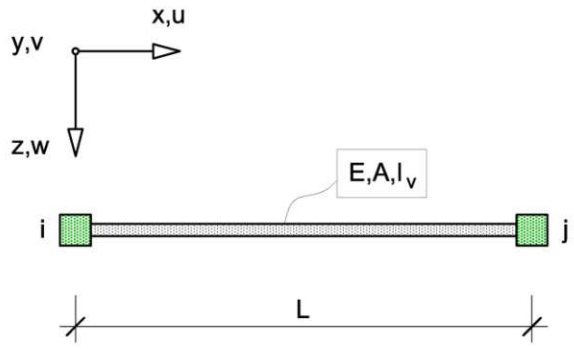

Figure 3.6: Beam member referred to the local coordinate system {u,w}

$$\begin{bmatrix} N_i \\ V_i \\ M_i \\ N_j \\ V_j \\ M_j \end{bmatrix} = \begin{bmatrix} \frac{EA}{L} & 0 & 0 & -\frac{EA}{L} & 0 & 0 \\ 0 & \frac{12EI}{L^3} & -\frac{6EI}{L^2} & 0 & -\frac{12EI}{L^3} & -\frac{6EI}{L^2} \\ 0 & -\frac{6EI}{L^2} & \frac{4EI}{L} & 0 & \frac{6EI}{L^2} & \frac{2EI}{L} \\ -\frac{EA}{L} & 0 & 0 & \frac{EA}{L} & 0 & 0 \\ 0 & -\frac{12EI}{L^3} & \frac{6EI}{L^2} & 0 & \frac{12EI}{L^3} & \frac{6EI}{L^2} \\ 0 & -\frac{6EI}{L^2} & \frac{2EI}{L} & 0 & \frac{6EI}{L^2} & \frac{4EI}{L} \end{bmatrix} \cdot \begin{bmatrix} u_i \\ w_i \\ \varphi_i \\ u_j \\ w_j \\ \varphi_j \end{bmatrix} \tag{3.1}$$

The relationship shown above, actually the equilibrium matrix equation of a member is often demonstrated in a short form (see equation 3.2).

$$[P] = [K_m] \cdot [d] \tag{3.2}$$

The member force vector [P], the member stiffness matrix $[K_m]$, and the member displacement vector [d] have to be considered in the member's local coordinate system.

As a complex plane structure consists of several members, the member stiffness equations have to be assembled into the global stiffness equations. Actually, a global stiffness matrix (structure stiffness matrix) is edited on the basis of the local stiffness matrices. Here, two simple statements regard to the complex structure need to be used. Firstly, it is considered, that the displacements of the end joints of the members are the same in the case of meeting members. Obviously, connected joints move together. Secondly, there is force equilibrium at every joint of the structure. This means practically that the sum of the member forces at a joint is balanced with the external force which acts at the examined joint. With the consideration of these conditions, the global stiffness matrix can be assembled through simple matrix additions. For this assembly process, the member equations must be considered in a common coordinate system, for instance in the global coordinate system {x,z} illustrated in figure 3.6. Therefore, displacement and force transformations have to be done, which is generally necessary, as in a complex structure not all the members lie parallel with the global x-axis. The global stiffness equations are shown in matrix notation in equation 3.3.

$$[F] = [K] \cdot [D] \tag{3.3}$$

The joint force vector [F] of the complete structure, the global stiffness matrix [K], and the joint displacement vector [D] of the complete structure have to be considered in the global coordinate system. The support conditions as displacement boundary conditions need to be applied in the global stiffness equations. Moreover, the known external forces must be considered in the joint force vector [F].

The last step of the Direct Stiffness Method is the solution for joint displacements, reaction forces and internal member forces. The equation 3.3 is solved by numerical methods such as Gauss elimination. Hand computations are possible only in the case of simple systems with a few members. From the complete displacement solution [D] the displacements of the members can be extracted. Next, the member displacement vector [d] in the member's local coordinate system can be calculated in the case of each member. Finally, the internal forces can be evaluated via the equilibrium matrix equations demonstrated above (see equation 3.1). However, these equations deliver the forces at the end joints, which mean the loading of the beam members.

The computer implementation of the Direct Stiffness Method is easily performable in MATLAB. However, the global stiffness equations need to be prepared for the MATLAB calculation. Actually, the known and unknown components of the joint force vector and of the joint displacement vector need to be separated.

3.4 Validation of the calculation method through simple models

3.4.1 Modelling with the top steel section of the SCSC plate

3.4.1.1 Introduction

The aim of this chapter is to demonstrate how the framework model calculation reproduces the real values of the displacements and internal forces. Essentially, the validation of the framework model calculation takes place through using a simple steel beam which is the top steel section of the SCSC plate. However, the simple framework model does not include end stiffeners and main steel girder webs. Moreover, the shear connector does not have any circular holes, which is not the case for the shear connector of the SCSC plate. The real values will be presented in chapter 3.4.1.2. These values are calculated using formulas based on the Euler-Bernoulli Beam Theory, which are in appendix D.1 of the dissertation. In chapter 3.4.1.3, the simple framework model will be illustrated and the calculation results will be shown using the Direct Stiffness Method. A span length of 4.1m is used, as with the SCSC plate model. The load is also applied

according to the load model for the SCSC plate model. However, the loaded area is 1cm longer at both supports so that a line load can be applied over the entire length. Due to this, it is easier to perform the calculations for the real values. This small difference between the loadings causes a small increase of the total vertical load at the support. In this case, the vertical load is 161.23 kN (see figure 3.7(a)) and in the case of the SCSC plate model it is 161.03 kN (see chapter 2.2). The line load for the SCSC plate is illustrated in figure 3.7(a). The framework model with the external vertical loads is shown in figure 3.7(b). With the Direct Stiffness Method just the nodes can be loaded. Therefore, figure 3.7(b) illustrates a loading scheme with nodal loads. These two patterns (see figures 3.7(a) and 3.7(b)) are equivalent and mean a total vertical load of 161.23 kN at each support. To avoid rounding errors during the calculation, the exact values of forces are used. However, rounded values are shown in figure 3.7 for ease of view. In chapter 3.4.1.3, it will also be demonstrated that the framework model reproduces the real values of the displacements and internal forces with a good approximation.

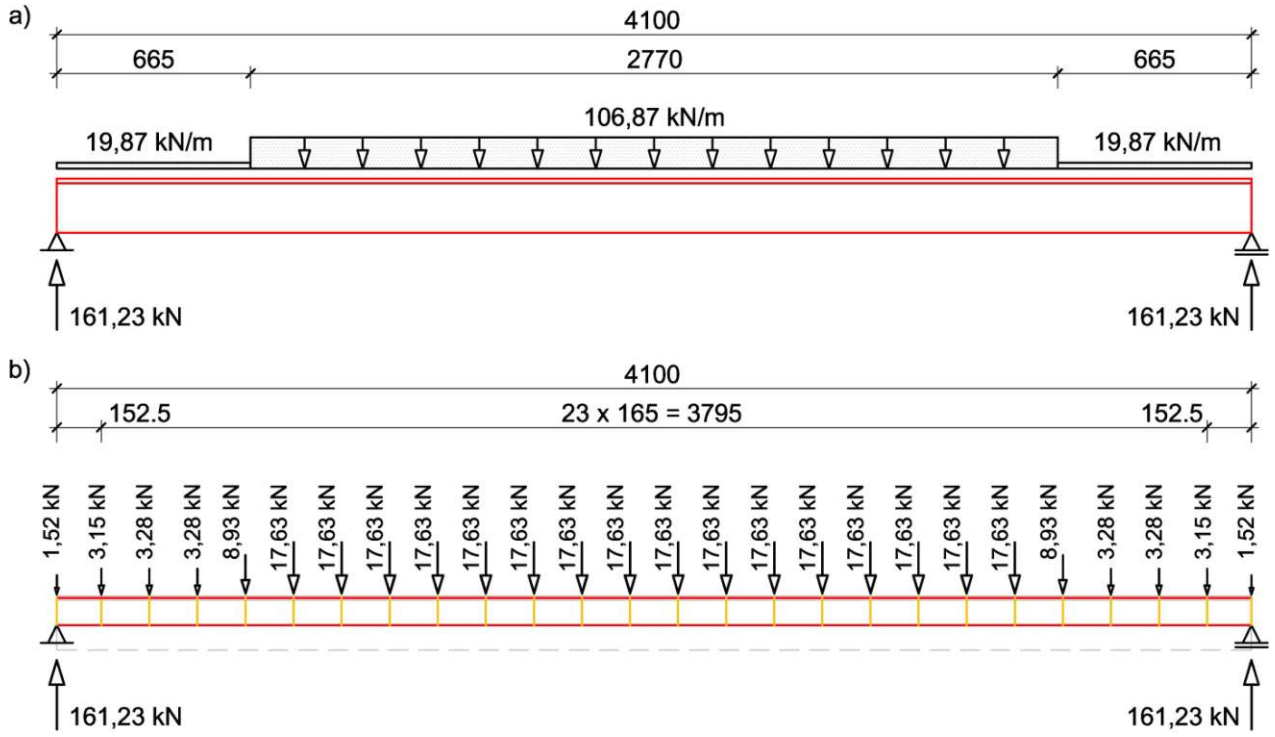

Figure 3.7: The top steel section of the SCSC plate as a structure with a span length of 4.1m: a) beam with distributed loads for the calculation of the real displacement and internal forces; b) framework model with nodal loads for the Direct Stiffness Method. Dimensions in [mm]

3.4.1.2 The displacement and internal forces according to the analytical solution

Several formulas are available to calculate the precise values of displacement and internal forces of a single beam. These precise values are also called as real values in this dissertation. However, these results are just approximations of the reality. This is due to the fact that the formulas are based on the Euler-Bernoulli Beam Theory, which itself consists of approximations. For instance, the shear stiffness of the beam is not used in the deformation analysis. Even so, the results demonstrated below will be used as basis values for the validation of the framework model in the chapter 3.4.1.3. The calculations through the formulas will also be named as analytical calculations. Formulas from Rubin [20] are used and the calculations are presented in appendix D.1. The cross section of the beam is illustrated in figure 3.8. The steel plate and the steel shear connector are welded together. However, the welding is not shown in the figure. The position of the centre of mass calculated from the upper edge is also illustrated.

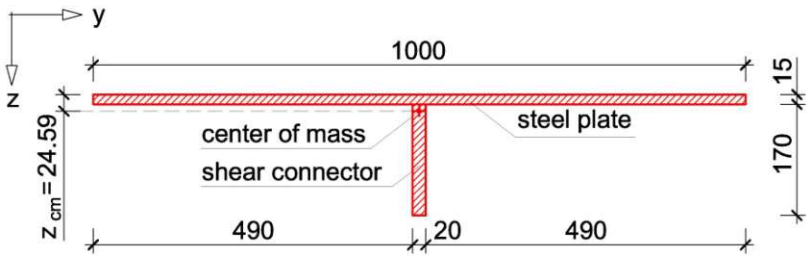

Figure 3.8: The cross section of the top steel section of the SCSC plate. Dimensions in [mm]

The area moment of inertia of the cross section around the axis "y" is given in equation 3.4 without a detailed calculation.

$$I_y = 32\,185\,276\,mm^4 \tag{3.4}$$

The modulus of elasticity (Young's modulus) of the steel (S355) is:

$$E = 210\,000\ N/mm^2 \tag{3.5}$$

The bending stiffness with Young's modulus and the area moment of inertia is given in equation 3.6.

$$E \cdot I_y = 210\,000 \cdot 32\,185\,276 \cdot 10^{-9} = 6\,758{,}908\ kNm^2 \tag{3.6}$$

When using Rubin's formulas [20], the baseline data consist of the bending stiffness of the beam (see equation 3.6), the span, and the loading scheme (illustrated in figure 3.7(a)). Without the detailed calculation, the vertical displacements of the beam are illustrated in figure 3.9.

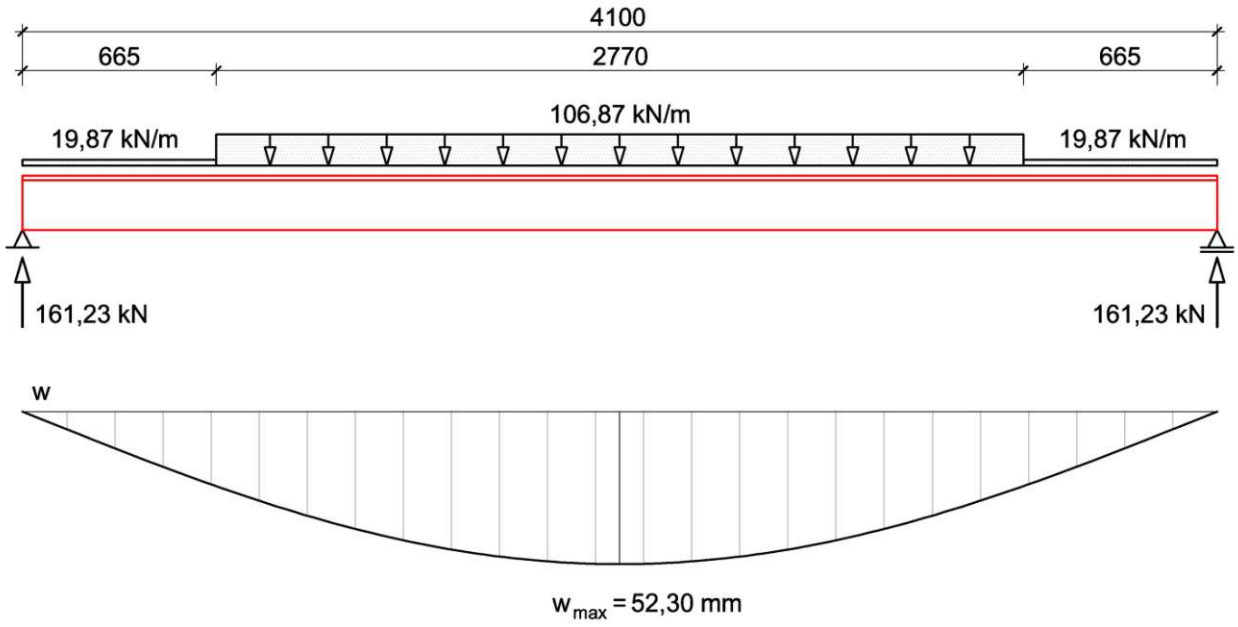

Figure 3.9: The loaded top steel section of the SCSC plate and its vertical displacement. Dimensions in [mm]

Next, the internal forces in the middle of the span are considered. The shear force in the middle of the span that arises from the formulas is zero. This is expected because the loading of the beam is symmetrical. For this reason, the moment in the middle of the span is the maximal moment of the beam. The calculated values are presented in equations 3.7 and 3.8.

$$V_m = 0\ kN \tag{3.7}$$

$$M_m = 205{,}32\ kNm \tag{3.8}$$

By means of the internal forces in the middle of the span (given in equations 3.7 and 3.8), the internal forces of the steel plate and the shear connector are demonstrated separately in figure 3.10. In this way, it is possible to validate the framework model in chapter 3.4.1.3.

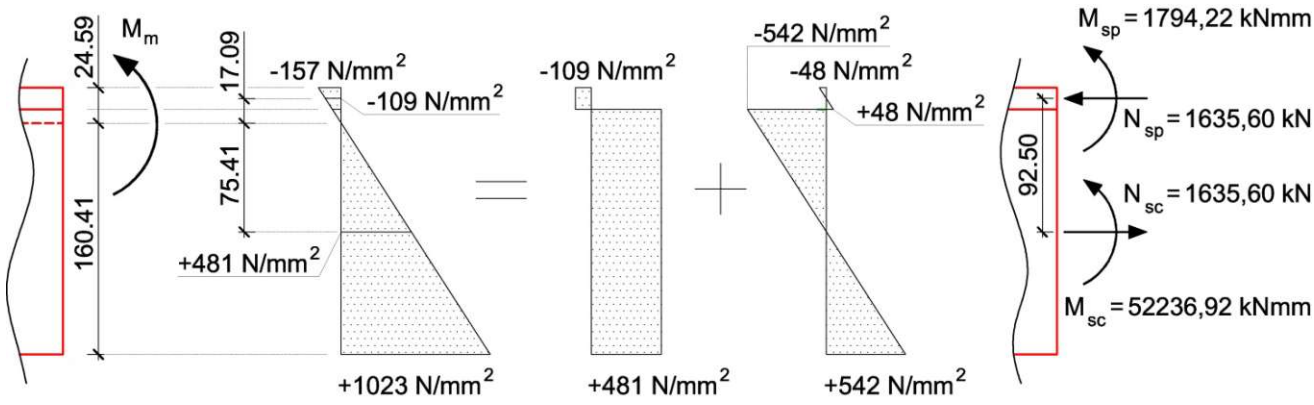

Figure 3.10: The internal forces and the stresses in the steel plate and in the shear connector derived from the resultant internal forces of the beam. Dimensions in [mm]

Finally, the bending moment is illustrated along the entire length of the beam in figure 3.11.

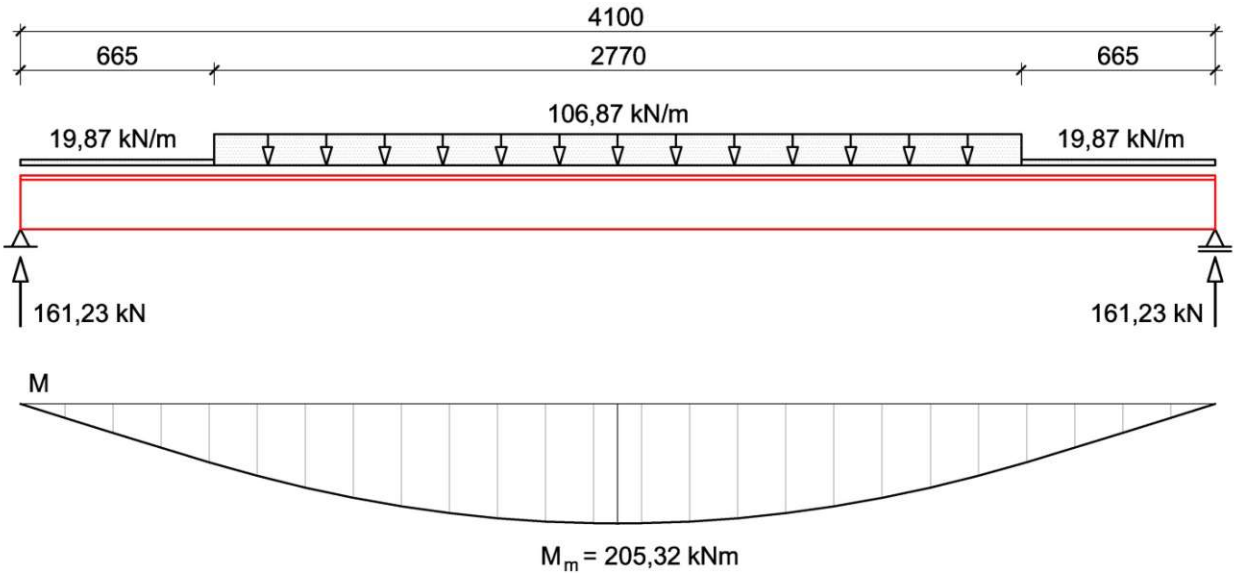

Figure 3.11: The loaded top steel section of the SCSC plate and the bending moment diagram. Dimensions in [mm]

3.4.1.3 Framework model calculation

The framework model calculation is based on the Direct Stiffness Method, which was introduced in chapter 3.3. Even though the model used is relatively simple (see figure 3.12), due to the large number of nodes in the model, the solution is performed using the program MATLAB. According to figure 3.7(b), the framework model is supported at the level of the shear connector's centroid and the loading of the SCSC plate is represented with nodal loads. Figure 3.12(a) demonstrates

the cross section of the beam, which is modelled through the framework model. Figure 3.12(b) illustrates the design of the framework model. The model consists of two separate horizontal beam elements (red lines in figure 3.12(b)) which represent both the steel plate and the shear connector. Also in the model, the vertical rigid members between the nodes of the steel plate and the shear connector are shown (orange-coloured lines in figure 3.12(b)). The vertical rigid members are designed to have a 165 mm distance between them.

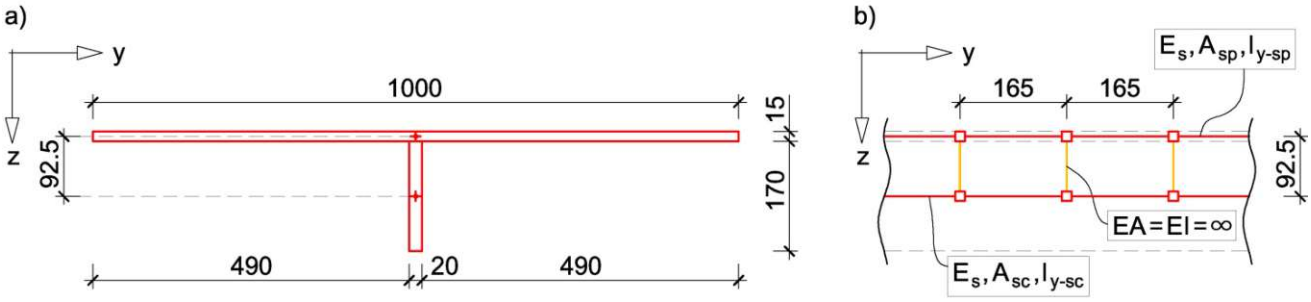

Figure 3.12: a) The top steel section of the SCSC plate; b) framework model with vertical rigid members at a 165 mm distance. Dimensions in [mm]

The member properties (E, A, I) belong to the given part of the structure which is symbolised. These are presented as:

$E_s = 210\ kN/mm^2$ (Young's modulus of the steel)

$A_{sp} = 15000\ mm^2$ (Area of the steel plate)

$A_{sc} = 3400\ mm^2$ (Area of the shear connector)

$I_{y-sp} = 281250\ mm^4$ (Area moment of inertia of the steel plate around the axis y)

$I_{y-sc} = 8188333\ mm^4$ (Area moment of inertia of the shear connector around the axis y)

In the case of the vertical rigid members, the longitudinal stiffness and the bending stiffness are marked as infinity. However, in the calculation with the Direct Stiffness Method these values are also defined:

$EA = 10^{14}\ kN$ (Longitudinal stiffness of the vertical rigid members)

$EI = 10^{14}\ kNmm^2$ (Bending stiffness of the vertical rigid members)

The vertical displacements of the beam calculated with the Direct Stiffness Method are illustrated in figure 3.13. Logically, the highest vertical displacement occurs in the middle of the span. According to the framework model calculation this displacement is 52,41 mm (see figure 3.13). The displacement calculated through the analytical solution is 52,30 mm (see figure 3.9). Therefore, the difference is only 0,2 percent and the displacement curves demonstrated in figures 3.9 and 3.13 practically overlap each other. The used framework model reproduces the real values with a good approximation. However, a second variation of the framework model is also analysed. In this case, many more sections are used, so that the distance between the vertical rigid members is only 10 mm. Also, more nodal loads are used, so that the loading scheme better approximates the distributed loads. Therefore, the maximal vertical displacement is 52,30 mm, which is equivalent to the real value of the displacement in the middle of the span.

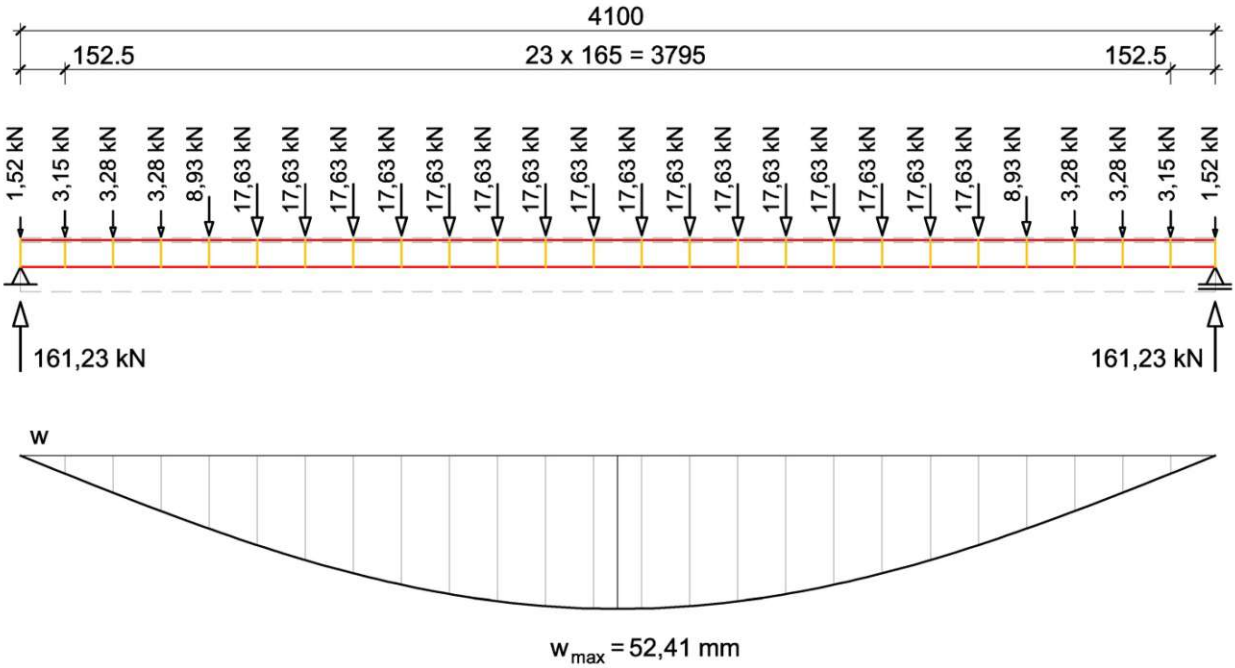

Figure 3.13: The loaded framework model of the steel section and its vertical displacement calculated with the Direct Stiffness Method. Dimensions in [mm]

Next, the internal forces in the middle of the span will be examined. Due to the fact that the framework model represents separate members of the steel plate and the shear connector; the moments and the forces are directly available for these single construction parts. Figure 3.14 demonstrates the moments and forces for both framework models. In comparison with the basis values (see figure 3.10), the framework model with vertical rigid members at a 165 mm distance reproduces the results with only 0,2 percent difference. In the case of the framework model with vertical members at a 10 mm distance, the difference is less than 0,01 percent.

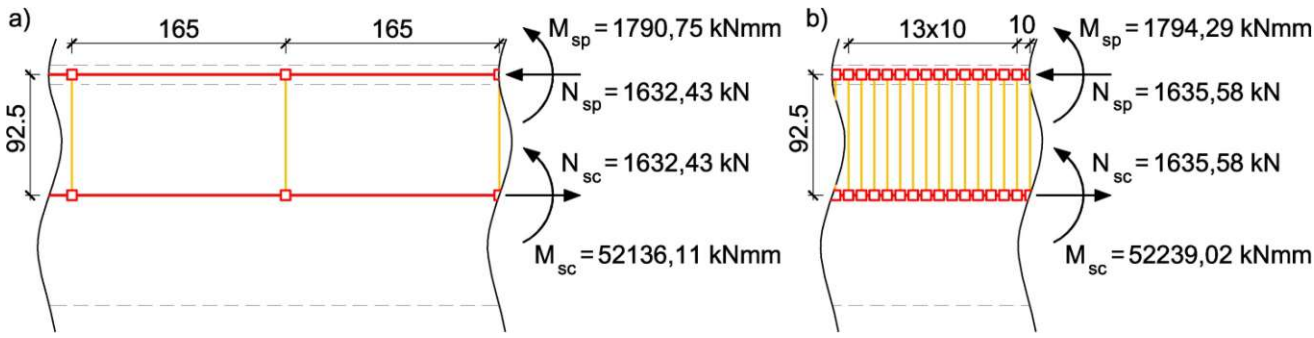

Figure 3.14: a) The framework model with vertical rigid members at a 165 mm distance. The internal forces are illustrated in the middle of the span. b) The framework model with vertical rigid members at a 10 mm distance. The internal forces are illustrated in the middle of the span. Dimensions in [mm]

Finally, the resultant bending moment diagrams will be compared. In the case of the framework model, the resultant bending moment needs to be calculated using the internal forces of the construction parts. For instance, the resultant bending moment in the middle of the span is calculated using the internal forces illustrated in figure 3.14(a). The two bending moments M_{sp} and M_{sc}, and the bending moment from the normal forces are added together. This calculation needs to be done at the position of every single vertical rigid member in order to create the bending moment diagram in figure 3.15. The bending moment diagrams demonstrated in figures 3.11 and 3.15 practically overlap each other. Due to

this, the framework model with vertical rigid members at a 165 mm distance reproduces the real values of moments with a good approximation.

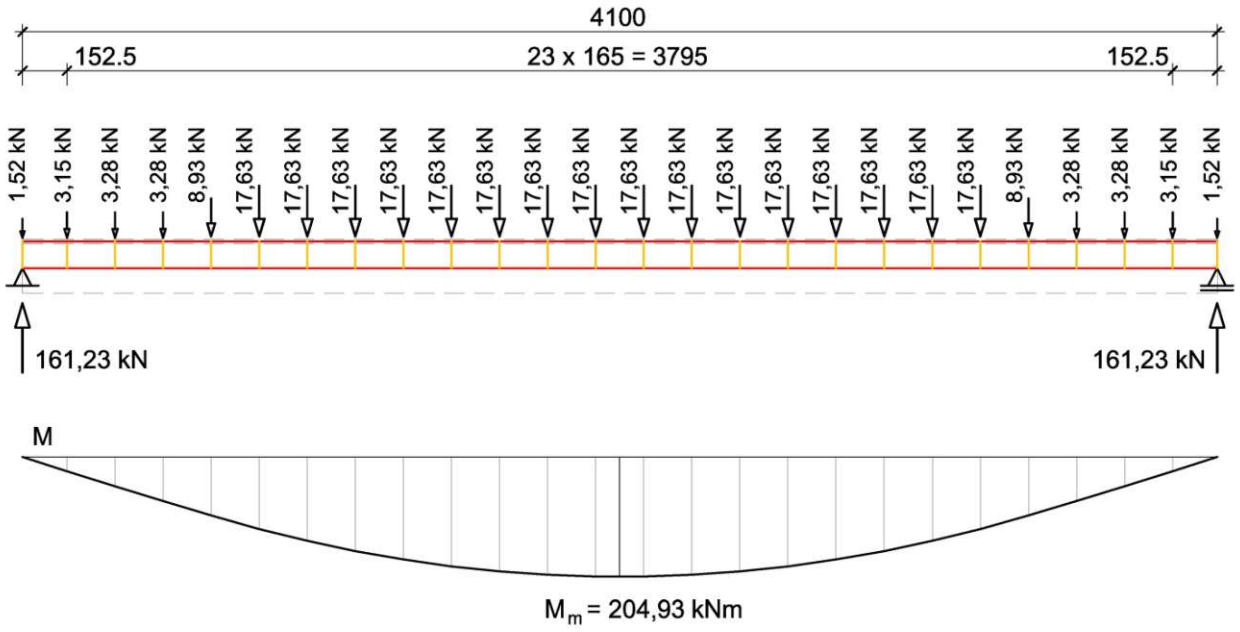

Figure 3.15: The loaded framework model and the bending moment diagram. Dimensions in [mm]

The conclusion of this chapter is that the framework model with vertical rigid members at a 165 mm distance is a good substitution for calculating the displacement and internal forces of a single beam. It is also illustrated, that the accuracy is higher through using a more partitioned model. Moreover, this validation method also legitimates the used MATLAB program, which will be developed further in the chapters 3.5, 3.6 and 4 to examine the complex SCSC plate of the bridge.

3.4.2 Modelling with the top and the bottom steel sections of the SCSC plate

3.4.2.1 Introduction

The objective of this chapter is to validate a framework model which is more complex than the simple steel beam model from the previous chapter. The model of the previous chapter consisted of only the top steel section of the SCSC plate. Here, the framework model and the calculation method will be described through using the whole steel construction of the SCSC plate. However, this simple model does not include end stiffeners and main steel girder webs. So, the slipping of the two steel sections is not prevented. The used cross section of the model is illustrated in figure 3.16.

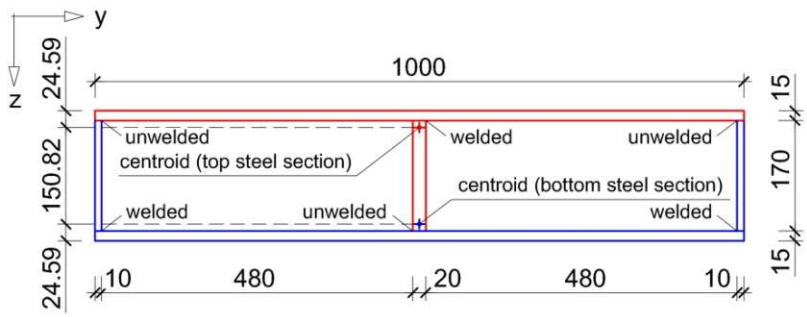

Figure 3.16: The cross section of the steel construction of the SCSC plate. The top steel section is in red and the bottom steel section is in blue. Dimensions in [mm]

As was the case for the shear connector of the model in chapter 3.4.1., here the shear connectors of the top steel section and the bottom steel section do not have any circular holes. The applied span length and loading are also the same as in the previous chapter. It will be demonstrated, that the calculated displacements and internal forces from the framework model reproduce the values according to the analytical solution. Moreover, the relative horizontal displacements between the two shear connectors will also be discussed.

3.4.2.2 The displacement, internal forces and slipping according to the analytical solution

The calculation method is based on the chapter 3.4.1.2. So the real values of displacement and internal forces are reached due to the formulas discussed above. The calculation method to reach the relative horizontal displacements between the two shear connectors is presented hereinafter. The area moment of inertia of the top steel section and the bottom steel section are equal. So the bending stiffness of the two sections is given in equation 3.6. Here, it is presumed that the curves of the vertical displacements are identical in the case of the two beams. This means also that both sections carry 50 percent of the total loading. The results of the analytical solution are available simply through halving the results from chapter 3.4.1.2.

The vertical displacements of the beam with the cross section in the figure 3.16 are illustrated in figure 3.17.

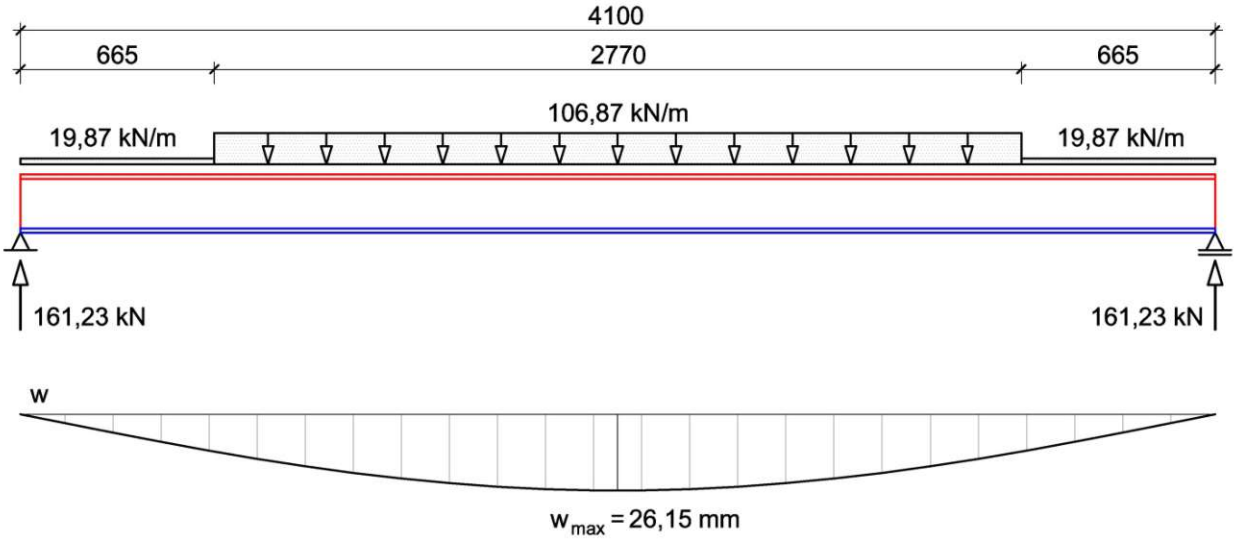

Figure 3.17: The loaded steel construction of the SCSC plate and its vertical displacement. Dimensions in [mm]

The normal forces and the bending moments in the middle of the span are illustrated at both steel sections in figure 3.18.

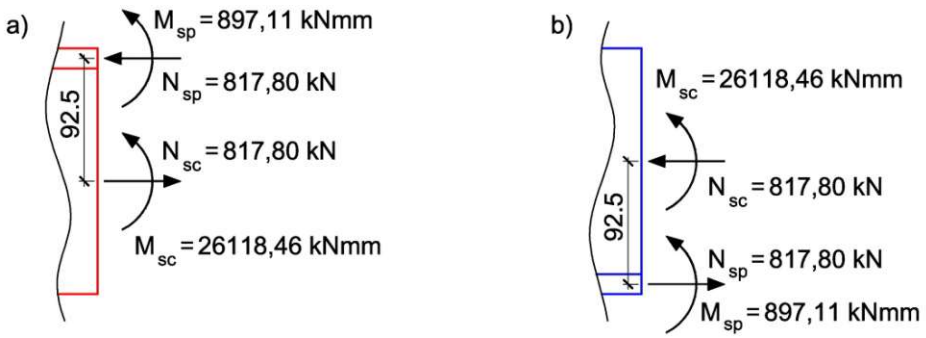

Figure 3.18: The normal forces and the bending moments in the steel plates and in the shear connectors. The illustrated internal forces are calculated in the middle of the span in the case of both steel sections. The two sections are demonstrated separately for ease of view: a) the top steel section of the SCSC plate; b) the bottom steel section of the SCSC plate. Dimensions in [mm]

Finally, the relative horizontal displacements between the two shear connectors will be evaluated. The functions to calculate the deflection at any point are available through Rubin's formulas [20]. The first derivative $w'(x)$ of deflection gives the slope of the deflected beam at any point, which means an angle measured in radians as an approximation in the case for small deflections. Through the assumption of the Euler-Bernoulli Beam Theory it is known, that the plain sections remain plane after the beam deformations. Therefore, the slopes of the plain sections are also given at any point of the beam. At last, the horizontal displacement between the centroid of one of the steel sections and the centroid of the shear connector is calculated by multiplying the first derivative $w'(x)$ of deflection by the vertical distance of these two points. As both of the steel sections have the same bending, the double value of this horizontal displacement provides the relative horizontal displacement between the two shear connectors. The highest slipping occurs at the highest slope, namely at the supports of the beam, which is illustrated in figure 3.19. The detailed calculation is presented in appendix D.2.

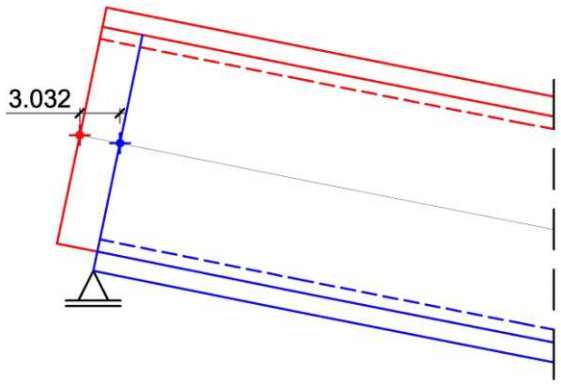

Figure 3.19: Slipping of the steel sections of the SCSC plate (red: the top steel section, blue: the bottom steel section) due to bending in case of a missing concrete core. Just the area at the support is illustrated. The displacements are stretched by a factor of 10 for ease of view. Dimensions in [mm]

3.4.2.3 Framework model calculation

The idea of this chapter is identical to the chapter 3.4.1.3. However, the design of the framework model (see figure 3.20(b)) is more complex. As the framework model is two-dimensional, the two shear connectors at the bottom steel section with the thickness of 10 mm (see figure 3.20(a)) are considered together. Necessarily, the loading of the framework model is represented with nodal loads and the model is supported at the level of the centroid of the bottom steel section's steel plate.

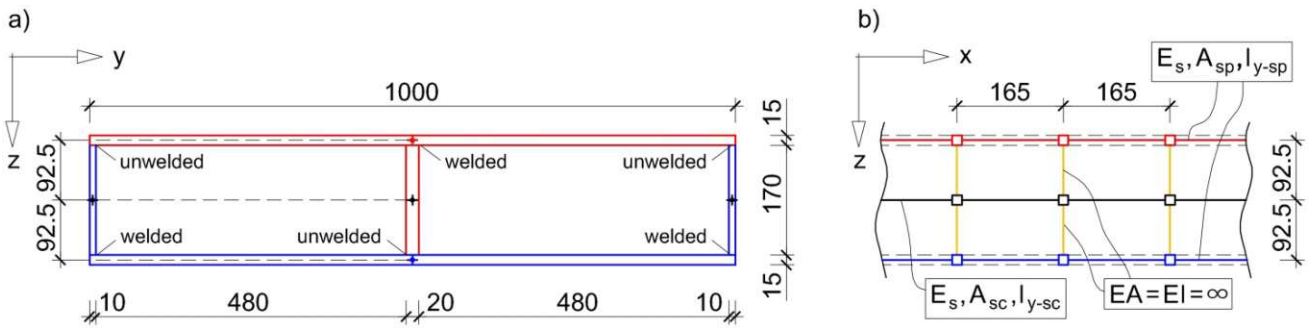

Figure 3.20: a) The steel construction of the SCSC plate; b) framework model with vertical rigid members at a 165 mm distance. Dimensions in [mm]

The model consists of four separate horizontal beam elements (red, blue and black lines in figure 3.20(b)) which represent both the two steel plates and the two shear connectors. As the vertical position of the centroid of the two shear connectors are the same, only one horizontal black line is demonstrated in figure 3.20(b). However, in the framework model necessarily two separate horizontal members are designed here. One is connected to the horizontal members represented the top steel plate, and the other one is connected to the horizontal members represented the bottom steel plate. The connections illustrated with the orange-coloured lines in figure 3.20(b) are vertical rigid members. As the framework model is two-dimensional, the nodes of the shear connectors at the top and the bottom steel section have the same initial position. However, relative displacements of the involved nodes can occur in case of loading. As the unwelded connection between the two steel sections is not able to absorb tensile forces, compression members are used between the nodes of the top steel plate and the bottom steel plate to transfer only compression forces. These compression members are shown just in figure 3.21(c).

To clarify the framework model illustrated in figure 3.20(b), the members are demonstrated more separately in figure 3.21. Through the figure 3.21, it is showed easier that the top steel section (see figure 3.21(a)) and the bottom steel section (see figure 3.21(b)) are connected only by the compression members illustrated in figure 3.21(c).

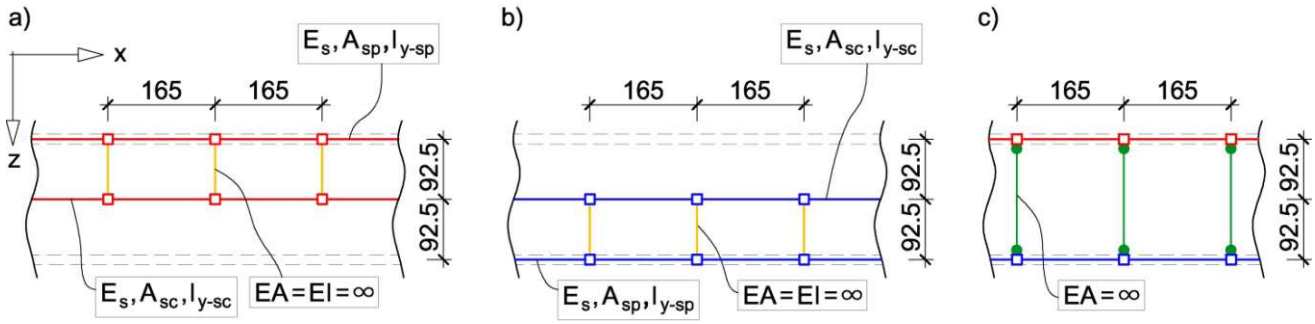

Figure 3.21: a) Framework model of the top steel section; b) framework model of the bottom steel section; c) compression members for the load transfer between the steel sections. Dimensions in [mm]

The member properties (E, A, I) belong to the given part of the structure which is symbolised. The values are given in chapter 3.4.1.3. As the compression member is a special truss element, an iterative calculation becomes necessary. If tension occurred in one of the compression members, this member would be erased in the following iteration step. However, there is not any tension in the compression members due to the calculation results. This means that the iterative calculation is not necessary in the case of this simple model. The longitudinal stiffness of the vertical compression members is marked as infinity. However, in the calculation with the Direct Stiffness Method this value is also defined:

$EA = 10^{14}\ kN$ (Longitudinal stiffness of the vertical compression members)

The enormous value of the longitudinal stiffness of the vertical compression members ensures that the curves of the vertical displacements are identical in the case of the two beams which are connected. The same assumption is used for the analytical calculation above in chapter 3.4.2.2.

The vertical displacements of the beam calculated with the Direct Stiffness Method are illustrated in figure 3.22. The highest vertical displacement in the middle of the span is 26,20 mm according to the framework model calculation (see figure 3.22) and 26,15 mm by the analytical solution (see figure 3.17). The difference is only 0,2 percent and the displacement curves demonstrated in figures 3.17 and 3.22 practically overlap each other.

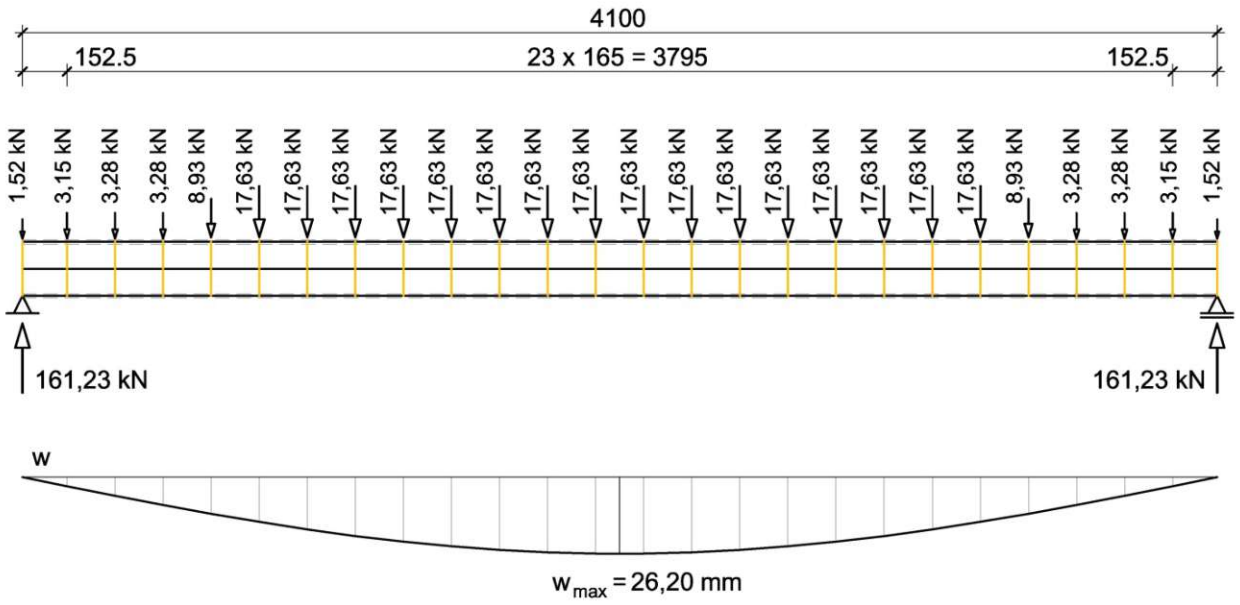

Figure 3.22: The loaded framework model of steel construction of the SCSC plate and its vertical displacement calculated with the Direct Stiffness Method. Dimensions in [mm]

Furthermore, the internal forces in the middle of the span will be examined. Figure 3.23 demonstrates the moments and forces for both steel sections of the framework model. In comparison with the real values (see figure 3.18) the framework model reproduces the results with only 0,2 percent difference.

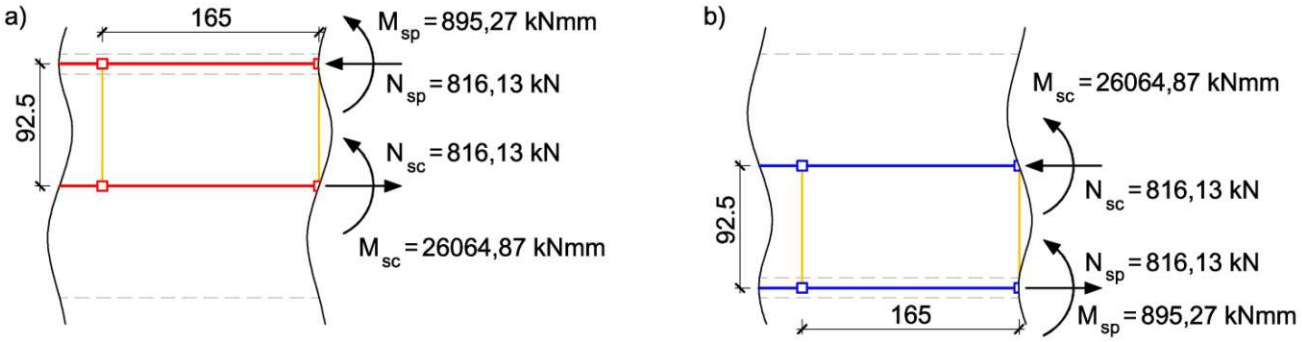

Figure 3.23: The framework model with vertical rigid members at a 165 mm distance. The internal forces are illustrated in the middle of the span: a) the internal forces of the top steel section; b) the internal forces of the bottom steel section.

Finally, the relative horizontal displacements between the two shear connectors will be presented. The displacements of each node can be evaluated with the Direct Stiffness Method. The nodes of the shear connectors at the top and the bottom steel section have the same initial position. Relative displacements of the involved nodes can occur in the case of loading. These relative displacements are calculated easily by the addition of the two displacements of the nodes. The horizontal component is only examined hereinafter. The results of calculation at the area of the beam's support are illustrated in figure 3.24. The relative horizontal displacement at the support is 3,027 mm according to the framework model calculation (see figure 3.24) and 3,032 mm by the analytical solutions (see figure 3.19). The difference is negligible. In comparison with the real values, the framework model reproduces the results of the relative horizontal displacements at each node with less than 0,2 percent difference.

The conclusion of this chapter is that the more complex framework model with vertical rigid members at a 165 mm distance is a good substitution for calculating the displacement and internal forces of the steel construction of the SCSC

plate. It is also illustrated, that the slipping of the steel sections can be calculated properly with the framework model. Moreover, this validation method legitimates the more complex MATLAB program code.

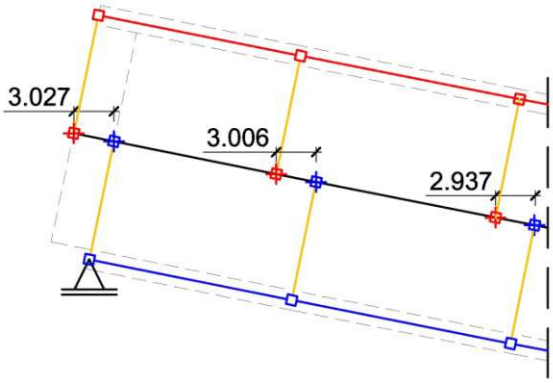

Figure 3.24: Framework model calculation results: horizontal displacements between the nodes of the shear connectors in the case of loading. Just the area at the support is illustrated. The displacements are stretched by a factor of 10 for ease of view. Dimensions in [mm]

3.4.3 The effects due to the circular holes in the shear connector

3.4.3.1 Introduction

Lit.: [7]

Up to this point the shear connectors have not had any circular holes, which is not the case for the shear connector of the SCSC plate. In this chapter, the effects due to the circular holes will be described through the top steel section of the SCSC plate. The model does not include end stiffeners and main steel girder webs. Furthermore, the applied span length and loading are also the same as in the chapter 3.4.1.2. However, the same modified member properties could be calculated with any load level. Instead of an analytical calculation, the structural analysis program RFEM [18] will be used to evaluate the basis values of deformations and internal forces. The area of the shear connector and the area moment of inertia of the shear connector will be modified in the framework model calculation so that the calculated displacements and internal forces reproduce the results of the Finite-Element-Analysis (FEA) software. In this way it will be possible to model the steel construction of the SCSC plate properly through a simple framework model.

3.4.3.2 Results of the Finite-Element-Analysis (FEA) program RFEM

Lit.: [7]

As illustrated in figure 3.25, only half of the top steel section is modelled in cross direction with RFEM. Therefore, the shear connector features 12 circular holes. The left side of the beam is supported with a sliding support and the right side of the beam is fixed with line supports. Through the line supports all of the rotations are prevented and only the vertical displacement is allowed. The mesh refinements are defined as 1 cm in RFEM.

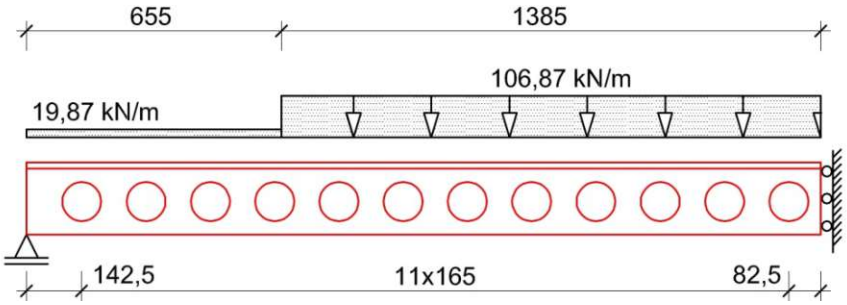

Figure 3.25: The design of the top steel section for the RFEM calculation with the external loading

The maximal vertical deflection in the middle of the span is 86,52 mm. Figure 3.26 demonstrates the internal forces at both parts of the top steel section. These internal forces are calculated indirectly from the normal forces and moments at the line supports.

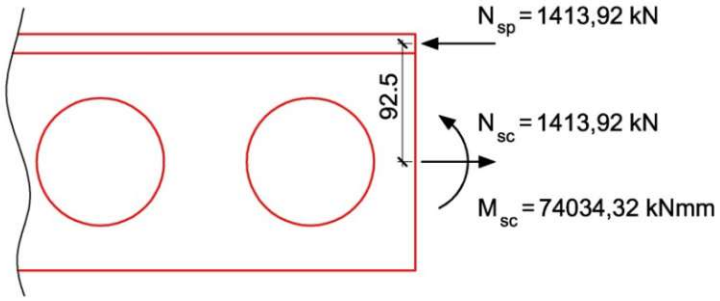

Figure 3.26: The internal forces in the steel plate and in the shear connector through the RFEM calculation. The demonstrated moment and normal forces are calculated in the middle of the span, actually at the right side of the beam illustrated in figure 3.25. Dimensions in [mm]

Due to the holes in the shear connector, the maximal vertical deflection in the middle of the span enlarged with 65.4% compared to the displacement of the top steel section (52,30 mm) introduced in the chapter 3.4.1.2. Through the comparison with the results on figures 3.10 and 3.26, it is showed that the circular holes generate a rearrangement of the internal forces, too. Notable difference is that the RFEM calculation does not deliver moment in the steel plate as an approximation due to the used surface with 2D elements modelling the steel plate.

3.4.3.3 Framework model calculation

Lit.: [7]

The objective of this chapter is to define the modified member properties (A, I) for the shear connector of the framework model so that the calculated displacements and internal forces reproduce the results of the FEA software. In this way, the shear deformation will be also considered in the framework model. However, the beam element stiffness matrix (see chapter 3.3) for the framework model calculation was derived by using the principles of Euler-Bernoulli Beam Theory. The substitutive cross section for the shear connector with circular holes is received through an iterative calculation with the simple framework model. The loading pattern is given in figure 3.15. Firstly, the complete section of the shear connector is used for A_{sc} and $I_{y\text{-}sc}$. In this case the shear connector does not have any circular holes, and the displacement in the middle of the span is logically less than the expected value from RFEM (86,52 mm). Next, the cross section for the calculation of the member properties (A_{sc}, $I_{y\text{-}sc}$) is the shear connector with a small cutting (cut height: 1 mm) in the middle of the section. The size of this opening enlarged in the following iteration steps always with 1 mm until the expected displacement is achieved. Therefore, the substitutive cross section fits the profile of the shear connector with a cutting in the middle with 91 mm. So, the substitutive cross section for the top steel section of the SCSC plate is illustrated in figure 3.27.

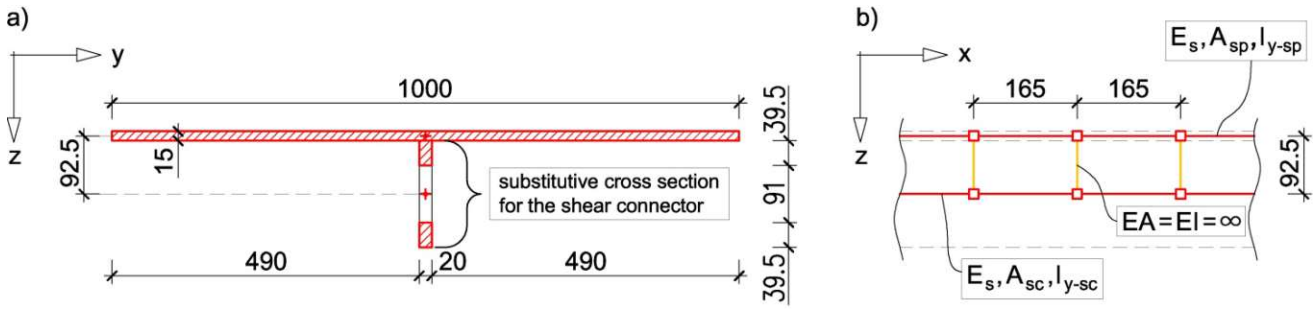

Figure 3.27: a) The substitutive cross section for top steel section of the SCSC plate; b) framework model with vertical rigid members at a 165 mm distance. Dimensions in [mm]

The member properties (E, A, I) belong to the given part of the structure which is symbolised (see figure 3.27). These are presented as:

$E_s = 210\ kN/mm^2$ (Young's modulus of the steel)

$A_{sp} = 15000\ mm^2$ (Area of the steel plate)

$A_{sc} = 1580\ mm^2$ (Area of the substitutive cross section for the shear connector)

$I_{y-sp} = 281250\ mm^4$ (Area moment of inertia of the steel plate around the axis y)

$I_{y-sc} = 6932382\ mm^4$ (Area moment of inertia of the substitutive cross section for the shear connector around y)

The longitudinal stiffness and the bending stiffness of the vertical rigid members are marked as infinity. In the calculation these values are also defined:

$EA = 10^{13}\ kN$ (Longitudinal stiffness of the vertical rigid members)

$EI = 10^{13}\ kNmm^2$ (Bending stiffness of the vertical rigid members)

For the framework models in the chapters 3.4.1.3 and 3.4.2.3 these stiffness values are higher by one order of magnitude. This difference is important because of the mathematical procedure in the MATLAB, to reach a solution without numerical fail (singularity).

The highest vertical displacement of the beam calculated with the framework model is 86,66 mm. Necessarily this deflection is practically equal with the result of the RFEM calculation in the chapter above, because the substitutive cross section was chosen according to the parity of the vertical displacements.

Next, the internal forces in the middle of the span will be compared as the validation of the framework model with the substitutive member properties. Figure 3.28 demonstrates the moments and forces for the framework model. In comparison with the RFEM calculation results (see figure 3.26) the framework model reproduces the results with less than 1,5 percent difference. Furthermore, the framework model calculation delivers moment in the steel plate, too. However, this moment is logically negligible.

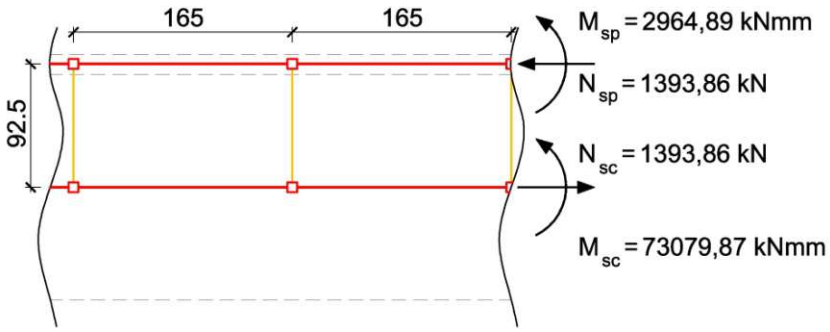

Figure 3.28: The framework model with vertical rigid members at a 165 mm distance. The internal forces are illustrated in the middle of the span. Dimensions in [mm]

As shear deformations of the steel section are also considered with RFEM, the framework model takes into account this effect through the modified member properties of the shear connector.

3.5 The spring framework model with constant spring stiffness values

3.5.1 Model with one horizontal concrete beam

3.5.1.1 Introduction

Lit.: [7], [8]

The 1 m long and 2,06 m wide model for ABAQUS analysis was constructed as a two-dimensional framework model. However, the two shear connectors at the bottom steel section with the thickness of 10 mm are considered together. The displacements, moments and forces were calculated with the Direct Stiffness Method. Because of the complexity of the framework model (large number of nodes), a system of linear equations with 342 unknowns arises. The solution is performed using program MATLAB.

Despite the two-dimensional framework modelling (all nodes are coplanar) a good approximation of reality is achieved, since the results are similar to the ABAQUS calculation results. Figure 3.29 explains the structure of the framework. Basic member types are beam elements transferring all internal forces. Furthermore, the model includes pure compression members. Figures 3.29(a) and 3.29(b) show the beam elements for the top and the bottom steel sections. The vertical connection members between the horizontal members of the steel plate and the horizontal members of the steel shear connector (orange-coloured members in figures 3.29(a) and 3.29(b)) are rigid members in the model with a very high longitudinal and bending stiffness. Figure 3.29(c) illustrates the vertical load transfer between the top and the bottom steel section through the shear connectors. As the unwelded connection is not able to absorb tensile forces, the shear connector members of the steel sections (vertical green lines in figure 3.29(c)) are modelled to transfer only compressive forces between the top and the bottom steel plates. The differences between beam and truss members are considered in the element stiffness matrix. As the compression member is a special truss element, an iterative calculation becomes necessary. If tension occurred in one of the compression members, this member would be erased in the following iteration step. Moreover, to represent the static loading, 100 calculation steps are used, namely the external vertical load of the spring framework model is divided into 100 parts. At each step, the framework model bears 1 % of the total external vertical load. The geometry memorised after one load-step is the start position for the next load-step. Thus, it is important, that in every step just 1 % of the external load acts. Logically, the iterative calculation used for the compression members occurs at each of the 100 calculation steps, if it is necessary. This calculation process requires a computer-based support.

Figure 3.29(d) illustrates the used concrete members. The concrete core is represented here only with one horizontal layer as an approximation. As the vertical compression between the steel plates and the concrete core is possible, the framework model includes vertical compression members too, which are pointed out in green in figure 3.29(d).

Considering that the framework model is two-dimensional, the spring framework model has nodes with different node-numbers in one position. For example, the nodes of the shear connectors at the top and the bottom steel section have the same initial position (see figures 3.29(a) and 3.29(b): i_t and i_b). However, relative displacements of the involved nodes can occur in the case of loading.

The particularity of the framework model is that it includes some springs. In figures 3.29(a), 3.29(b) and 3.29(d) the marked nodes (i_t, i_b, i_c) are start or end nodes of springs. Two springs always join to any node of the concrete beam. The one spring is effective between the shear connector of the top steel section and the concrete, the other one between the shear connector of the bottom steel section and the concrete (see figure 3.29(e)). Obviously, there are no springs between the two steel sections. Thus, a total number of 72 springs is used in the spring framework model.

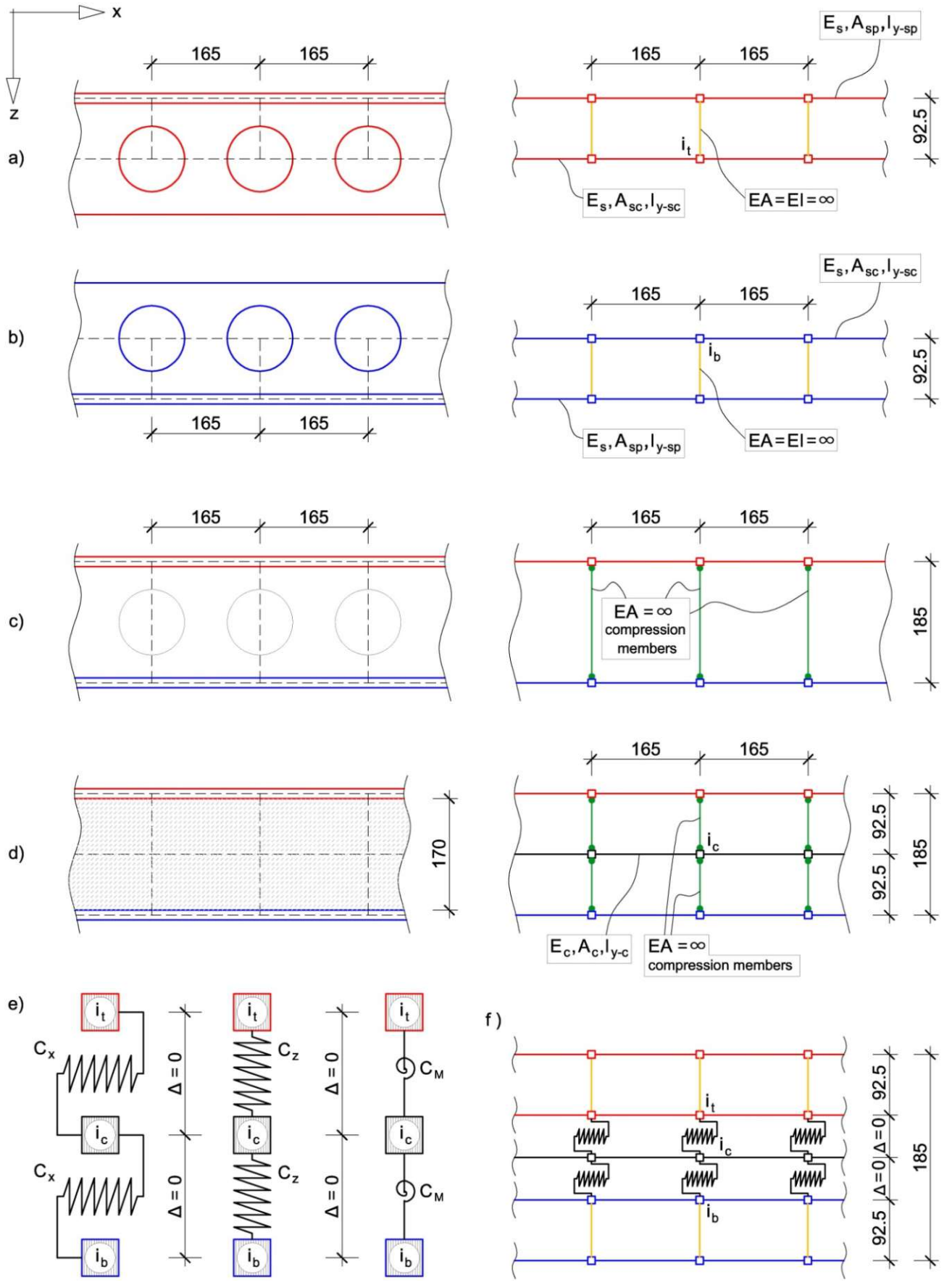

Figure 3.29: The design of the spring framework model: a) members for the top steel section; b) members for the bottom steel section; c) members for the vertical load transfer between the steel sections; d) members for the concrete; e) spring model for horizontal, vertical and rotational stiffness; f) the complex framework model. Dimensions in [mm]

The nodes connected with a spring are defined by the same coordinates x, z at the unloaded phase in the framework model. Anyway, the springs do not need any length because their stiffness matrix consists only of the spring constants. With the same stiffness matrix it is possible to take into account the horizontal, vertical and rotational stiffness. As the holes in the shear connectors are circular, the concrete cannot transfer significant moments to the steel sections there, thus the rotational stiffness (C_M) was set to zero.

Figure 3.29(f) shows the interaction between the steel sections due to the concrete core. For ease of view just the horizontal springs are illustrated in the figure.

3.5.1.2 The loading of the structure

Lit.: [7], [8]

Figure 3.30(a) shows the external vertical load in ABAQUS analysis used for fatigue limit state (see chapter 2.2), calculated with dead load and traffic Load Model 71 which is multiplied with a load factor of 1,48. This factor includes the partial safety factor Υ_{Ff}, the impact factor Φ_2, and the damage equivalent factor λ. As in the Direct Stiffness Method just the nodes can be loaded: figure 3.30(b) illustrates the framework model used loading scheme. This pattern is equivalent with the loading in ABAQUS, and means a total vertical load of 161 kN at the support. Moreover, figure 3.30 demonstrates that both ABAQUS and framework model have supports in the middle of the span as only half of the plate is modelled in cross direction. The left side of both models is supported with a sliding support and the right side of both models is fixed with line supports. Through the line supports all of the rotations are prevented and only the vertical displacement is allowed. However, in the case of the framework model it would be also possible to model the entire construction as in chapter 3.4 (see figures 3.7(b) and 3.22).

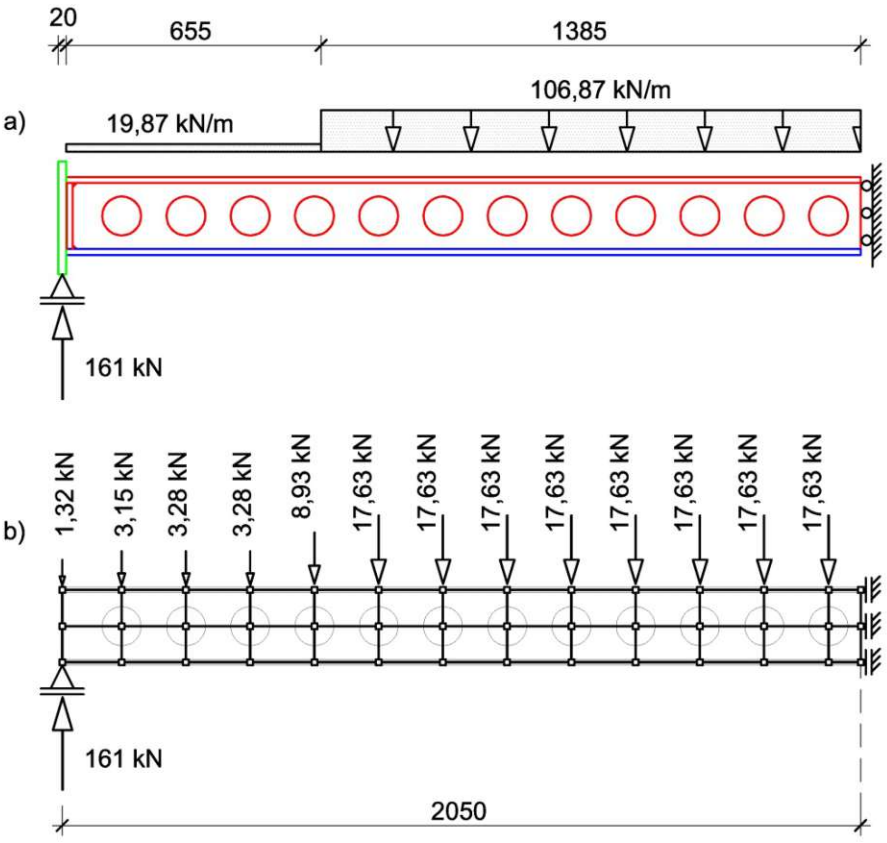

Figure 3.30: The external vertical loading for fatigue limit state: a) ABAQUS model; b) spring framework model. Dimensions in [mm]

3.5.1.3 The member properties of the spring framework model

Lit.: [7], [8]

The member properties (E, A, I, L) belong to the given part of the structure which is symbolised. However, as it was shown in chapter 3.4.3, the area of the shear connectors and the area moment of inertia of the shear connectors (A_{sc}, $I_{y\text{-}sc}$) are modified so that the effects due to the circular holes are considered. The member properties (E, A, I), which belong to the spring framework model (see figure 3.29), are shown in table 3.1. The calculations (A, I) are presented in appendix D.3.

E_s	=	210 000	N/mm^2
A_{sp}	=	15 000	mm^2
$I_{y\text{-}sp}$	=	281 250	mm^4
A_{sc}	=	1580	mm^2
$I_{y\text{-}sc}$	=	6 932 382	mm^4
E_c	=	35 200	N/mm^2
A_c	=	163 200	mm^2
$I_{y\text{-}c}$	=	393 040 000	mm^4

Table 3.1: The member properties (E, A, I) used for the spring framework model

The longitudinal stiffness and the bending stiffness of the vertical rigid members (marked as infinity) are given in chapter 3.4.3.3. The vertical connection members between the horizontal concrete members (in the case of three horizontal concrete layers, see figure 3.33) are rigid members, too. Thus, the shear deformations of the concrete beam are neglected as a good approximation in the case of this thin plate construction. In the model all of the compression members also have a very high longitudinal stiffness ($EA = 10^{13}$ kN) as an approximation.

3.5.1.4 The spring stiffness values

Lit.: [7], [8]

As it was demonstrated in chapter 3.2, to evaluate the spring stiffness values depending on the force, experimental tests were performed in February 2020 at the laboratory of TU Wien, Institute of Structural Engineering. The stiffness of a spring depends on the elasticity of the materials (steel and concrete), on the geometrical feature of the joint and on the forces occurring in the shear connectors. In the case of external vertical loading, all the horizontal and vertical forces in the shear connectors are different. This means that the 24 springs used have individual stiffness both in a horizontal and in a vertical direction. However, in this chapter the horizontal and vertical spring stiffness used for the framework model are constant. Therefore, two different calculations are carried out to get the results from figure 3.5. Firstly, a horizontal spring stiffness ($C_{x,a}$ = 325,0 kN/mm) calculated from the maximal force in the shear connectors is used (see figure 3.5). As at this point results from the framework model were not available, the maximal force for the spring stiffness evaluation (91,0 kN) was chosen from the ABAQUS results as an approximation. With this approach, conservative results will appear for the vertical displacement. Secondly, a horizontal spring stiffness ($C_{x,b}$ = 527,4 kN/mm) belonging to the average force in the shear connectors (54,5 kN) is used. In this case, conservative results will emerge for the horizontal forces in the shear connectors and for the internal forces of the structure elements. The aim of these two calculations is to keep on the safe side while analysing. This means that the higher displacement and the higher internal forces are chosen from the results of the two cases. According to the fact that the vertical forces in the shear connectors are smaller by about one order of magnitude as the highest horizontal force in the shear connector, a uniform vertical spring stiffness C_z = 10 000 kN/mm was assumed of both methods as an approximation.

3.5.1.5 The evaluation of results

Lit.: [7], [8]

The vertical displacement and the internal forces of the structure elements will be compared in this chapter with the ABAQUS calculation results.

In the first step, the results in the middle of the span are compared. In this part of the structure the highest vertical displacement and the highest normal forces in the SCSC plate occur. The maximal vertical displacement is 7,01 mm according to the ABAQUS calculation, and 7,14 mm by the spring framework model with the horizontal spring stiffness $C_{x,a}$ = 325 kN/mm. So, the framework model delivers a higher result, with an increase of 1,9 %.

The normal forces in the steel plates are compared in figure 3.31. The green line shows the ABAQUS results, and the black line represents the results calculated with the spring framework model. ABAQUS gives the maximum bottom steel plate tensile force as 933,6 kN. The spring framework model with the horizontal spring stiffness $C_{x,b}$ = 527,4 kN/mm delivers 767,0 kN which is 82,2 % of the ABAQUS result. The top steel plate has a compressive force of 751,2 kN in ABAQUS, and of 739,1 kN (98,4 %) in the framework model calculation. In the upper horizontal compressed concrete zone we get a compressive force of 442,5 kN in ABAQUS. Moreover, as in the used ABAQUS concrete damaged plasticity-model (CDP), tensile material behaviour for concrete is allowed for, a resultant tensile force (237,1 kN) occurs in the bottom concrete zone. In the framework model, the horizontal concrete beam has a resulting compressive force of 30,1 kN in the middle of span. Notable is that it is not possible to represent the compression in the upper concrete zone and the tension in the lower concrete zone through a single horizontal beam in the framework. In this case, it could not be considered with the framework model, if in the horizontal concrete beam the tensile stress reached the ultimate tensile strength of the concrete. Therefore, the results through the calculation of the spring framework model differ from the ABAQUS results.

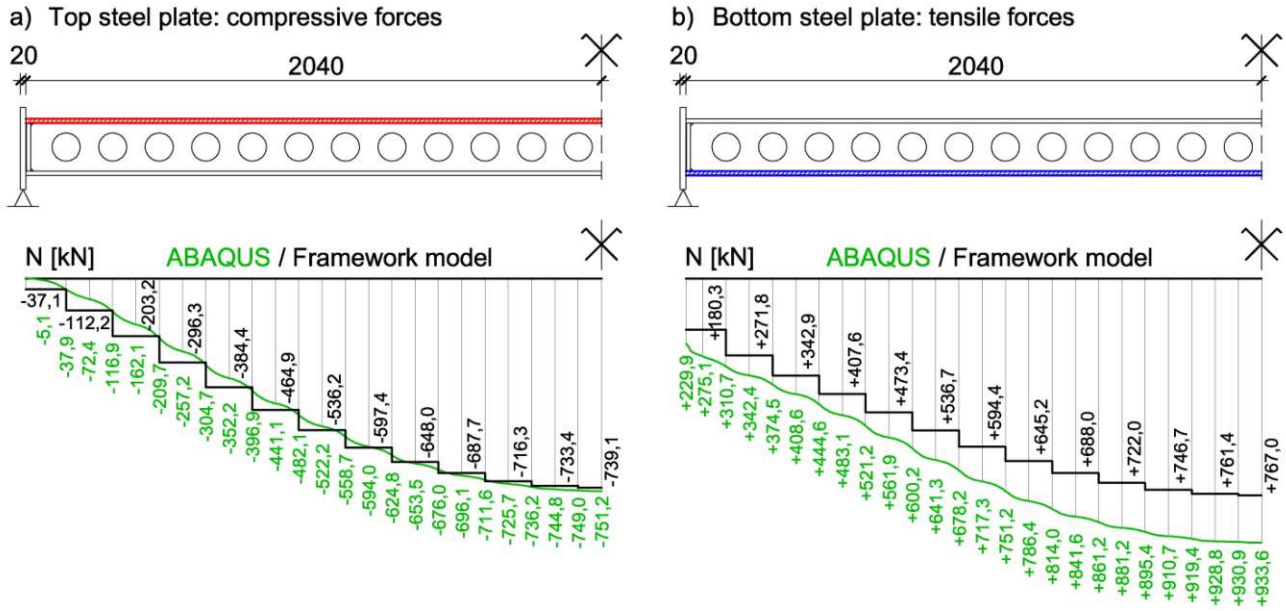

Figure 3.31: Normal forces in the steel plates of the SCSC-plate: a) compressive forces in the top steel plate; b) tensile forces in the bottom steel plate. Dimensions in [mm]

In the second step, the horizontal forces in the shear connectors are compared. The values of the forces in the shear connectors 1 - 12 are shown in figure 3.32 in a graph format for ease of view. The green line shows the ABAQUS results, and the black line represents the horizontal forces in the shear connectors calculated with the spring framework model.

According to the ABAQUS results, the maximum force in the shear connector at the top steel section occurs in the second circular hole from the support. This horizontal force component amounts to 98,5 kN. The framework model with the horizontal spring stiffness $C_{x,b}$ = 527,4 kN/mm shows a maximum force of 88,62 kN (90,0 %) at the first hole. The ABAQUS calculation method indicates that the maximum force (73,6 kN) in the shear connector at the bottom steel section will be at the fifth hole. The framework model delivers a maximum force of 55,60 kN (75,5 %) at the fourth hole.

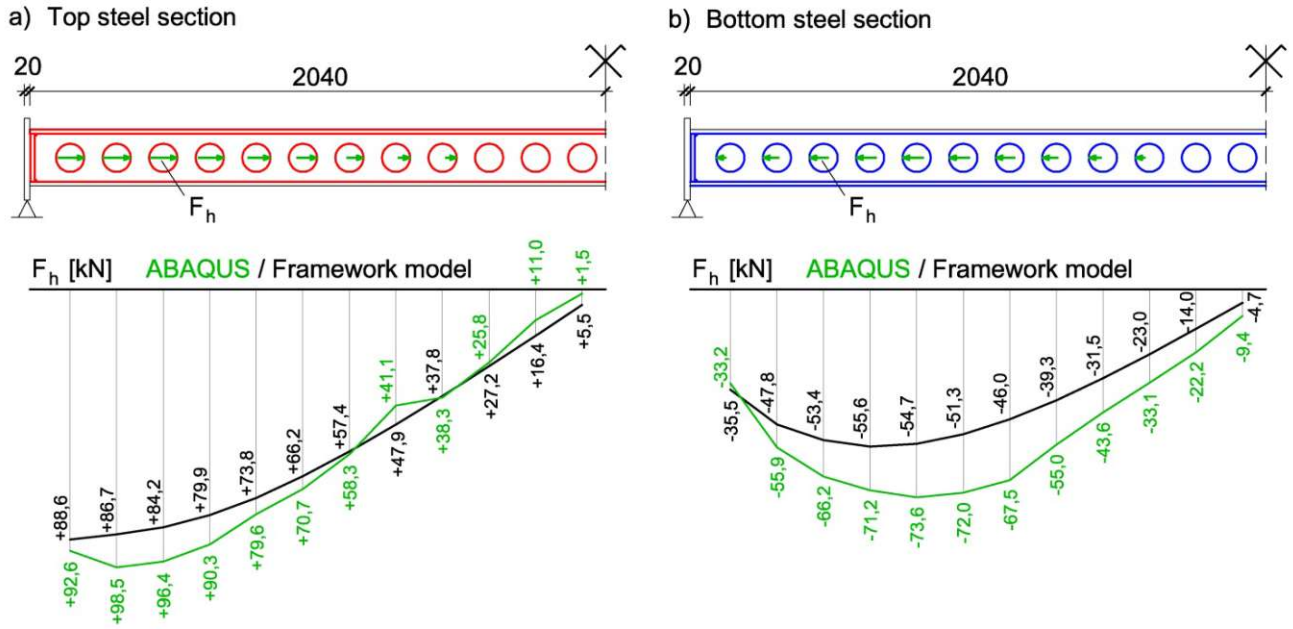

Figure 3.32: Horizontal forces in the shear connectors of the SCSC-plate: a) forces in the top steel section; b) forces in the bottom steel section. Dimensions in [mm]

The reason for the difference in results is partly due to the approximation that the spring stiffness is constant in the framework model. Moreover, the concept to represent the inelastic behaviour of concrete is different in ABAQUS compared to the framework model working with the laboratory test results. The used concrete damaged plasticity model in ABAQUS (see chapter 2.3.3) describes the tensile cracking and the compressive crushing of the concrete material, too. The response of concrete to uniaxial loading in tension and compression was defined in the PROPERY module of ABAQUS. For instance in the case of compression, the response is linear until the given value of initial yield. After this point it is characterized by stress hardening and strain softening. The framework model does not represent the tensile cracking and the softening stress-strain response in the concrete structure. This approach is right at the used load level (see chapter 2.2) because the ABAQUS results do not detect significant irreversible damage that occurs during the failure mechanisms. The inelastic deformations through the stress hardening of the concrete are considered in the framework model by the spring stiffness values of the composite connections. These values, based on the laboratory tests, differ from the spring stiffness values calculated indirectly from the ABAQUS results (see chapter 3.7.1). Consequently, the results in the ABAQUS calculation and the framework model are different because of the various parameters of compressive plasticity of concrete.

Furthermore, the framework model with one horizontal concrete beam cannot perfectly replace the complex ABAQUS model. Therefore, a more detailed spring framework model with three horizontal concrete layers will be presented in the following chapter. As this framework model reproduces better the real construction, the results should converge to the ABAQUS calculation results.

3.5.2 Model with three horizontal concrete layers

3.5.2.1 Introduction

The model is similar to the structure introduced in chapter 3.5.1.1. The only difference is that the concrete core is divided into three horizontal layers for calculation (see figure 3.33). The vertical connection members between the horizontal members of the concrete beams (orange-coloured members in figure 3.33) are rigid members. As the vertical compression between the steel plates and the concrete core is possible, the framework model includes vertical compression members too, which are pointed out in green in figure 3.33.

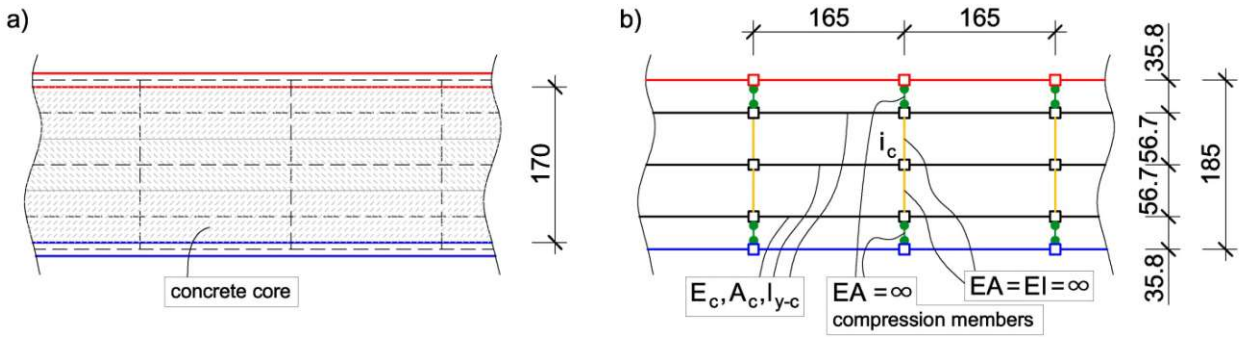

Figure 3.33: The members for the concrete of the spring framework model. Dimensions in [mm]

The loading of the structure, the member properties of the spring framework model and the spring stiffness values have already been represented also in chapter 3.5.1. However, the area of a horizontal concrete beam is here 54 400 mm^2 and the area moment of inertia of a concrete beam is 14 557 037 mm^4. The calculations of these two values are presented in appendix D.4.

3.5.2.2. The evaluation of results

Lit.: [7], [8]

Correspondingly to the chapter 3.5.1.5, the vertical displacement and the internal forces of the structure elements will be compared with the ABAQUS calculation results.

In the first step, the results in the middle of the span are compared. In this part of the structure the highest vertical displacement and the highest normal forces in the SCSC plate occur. The maximal vertical displacement is 7,01 mm according to the ABAQUS calculation, and 7,82 mm by the spring framework model with the horizontal spring stiffness $C_{x,a}$ = 325 kN/mm. So, the framework model delivers a greater deflection, with an increase of 11,5 %. ABAQUS gives the maximum bottom steel plate tensile force as 933,6 kN. The spring framework model with the horizontal spring stiffness $C_{x,b}$ = 527,4 kN/mm delivers 896,9 kN which is 96,1 % of the ABAQUS result. The top steel plate has a compressive force of 751,2 kN in ABAQUS, and of 751,3 kN (100,0 %) in the framework model calculation. In the upper horizontal compressed concrete zone we get a compressive force of 442,5 kN in ABAQUS and of 412,0 kN (93,1 %) from the framework model. As in the used ABAQUS concrete damaged plasticity-model (CDP), tensile material behaviour for concrete is allowed for, a resultant tensile force (237,1 kN) occurs in the bottom concrete zone. In the framework model, the lower and middle horizontal concrete beams have a resulting tensile force of 253,7 kN (107,0 %). Notable is that in the lower horizontal concrete beam the tensile stress reaches the ultimate tensile strength of the concrete. Therefore, in the calculation of the spring framework model it is considered, that the bearable loads of the concrete beams are limited.

The normal forces in the steel plates are compared in figure 3.34. The green line shows the ABAQUS results, and the black line represents the results calculated with the spring framework model.

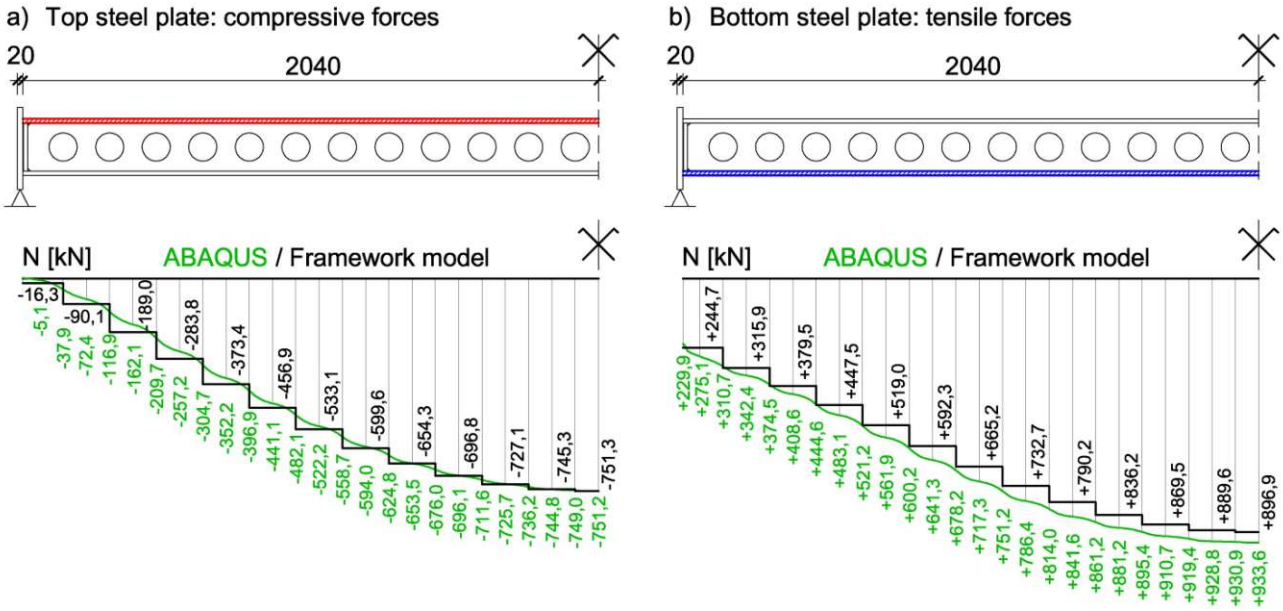

Figure 3.34: Normal forces in the steel plates of the SCSC-plate: a) compressive forces in the top steel plate; b) tensile forces in the bottom steel plate. Dimensions in [mm]

In the second step, the horizontal forces in the shear connectors are compared. According to the ABAQUS results, the maximum force in the shear connector at the top steel section occurs in the second circular hole from the support. This horizontal force component amounts to 98,5 kN. The framework model with the horizontal spring stiffness $C_{x,b}$ = 527,4 kN/mm shows a maximum force of 90,0 kN (91,4 %) at the first hole. Both calculation methods indicate that the maximum force in the shear connector at the bottom steel section will be at the fifth hole. ABAQUS gives 73,6 kN while the framework model delivers 64,4 kN (87,5 %). The values of the forces in the shear connectors 1 - 12 are similar in both calculation methods. These values are shown in figure 3.35 in a graph format for ease of view.

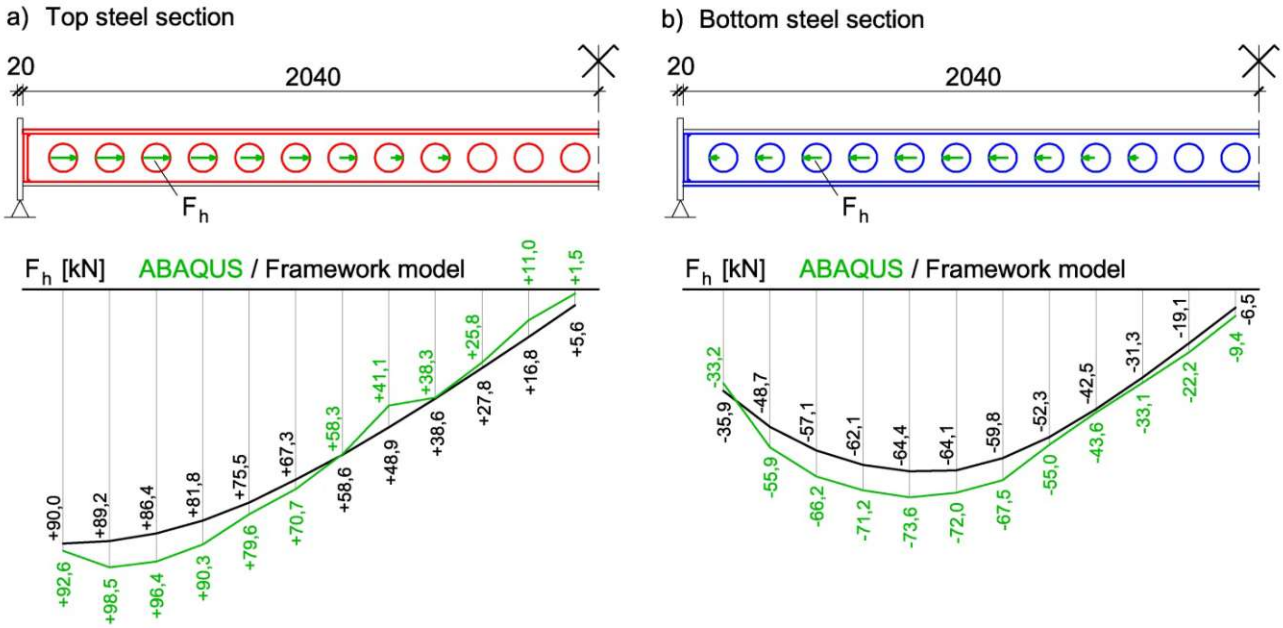

Figure 3.35: Horizontal forces in the shear connectors of the SCSC-plate: a) forces in the top steel section; b) forces in the bottom steel section. Dimensions in [mm]

The green line shows the ABAQUS results, and the black line represents the horizontal forces in the shear connectors calculated with the spring framework model. The reason for the difference in results was explained in chapter 3.5.1.5. Actually, through the comparisons with the ABAQUS results in chapter 3.5, the framework model calculation cannot be validated. However, it is clear through the comparison of the results of chapter 3.5.1.5 and 3.5.2.2, that the more detailed spring framework model with three horizontal concrete layers reproduces better the results of ABAQUS model.

3.6 The spring framework model with different spring stiffness values

3.6.1 Model with one horizontal concrete beam

3.6.1.1 Introduction

In this chapter, the force-slip curve for the first loading is considered for the calculation of the spring stiffness values. The force-slip diagram was introduced in chapter 3.2. Figure 3.36 illustrates the framework model calculation used approximation of the force-slip diagram by line segments. With the calculation method of this chapter can be considered that the spring stiffness value depends on the force in the shear connector. Moreover, it is not necessary to use any results from the ABAQUS calculation as in the case of the model in chapter 3.5. Actually, the forces in the shear connectors were chosen from the ABAQUS results for the spring stiffness evaluation in chapter 3.5.1. Now, the spring stiffness values are calculated according to the force-slip curve (see figure 3.36) at each loading step. Thus, the forces in the shear connectors increase and the spring stiffness values (C_1 – C_7 in figure 36) decrease through the external load increments.

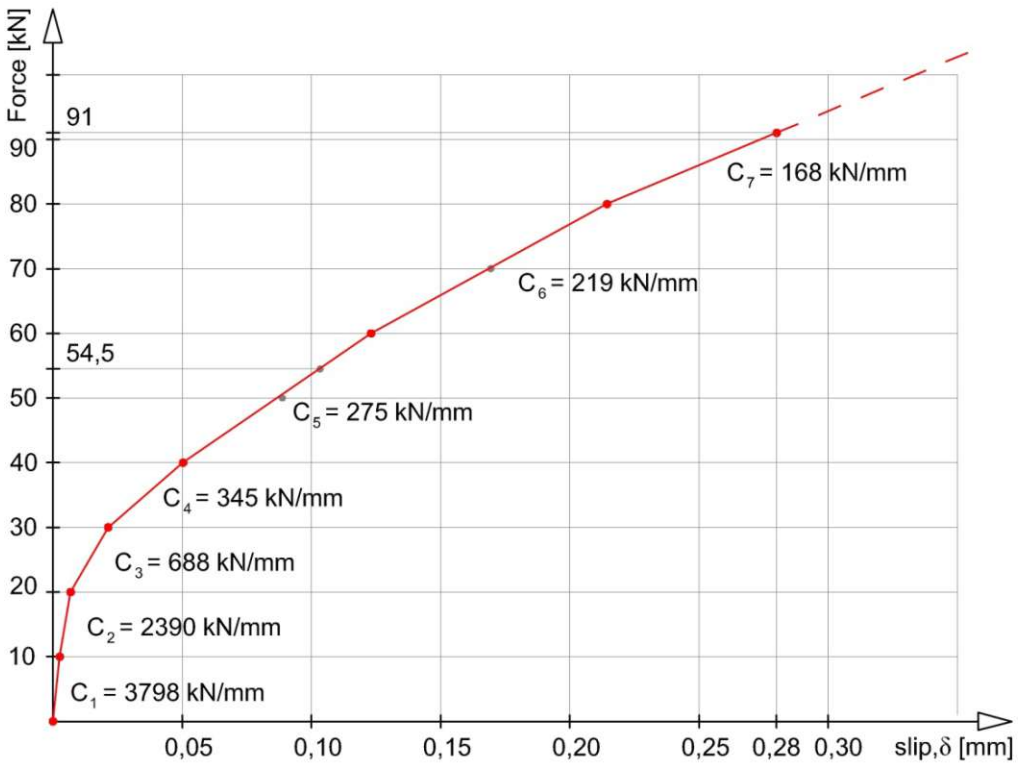

Figure 3.36: The approximation of the force-slip diagram of the shear connector in the case of the first loading

For the framework model calculation, straight line segments were sketched through the 8 points (red points in figure 3.36) from the laboratory tests described in chapter 3.2. It is illustrated with the dashed line in the figure 3.36 that the function created for the calculation in MATLAB continues above the load level of 91 kN. This is needful because the maximal slip

from the framework model calculation is not known at this point. Namely it is not warranted that the slip does not exceed the slip value of 0.28mm illustrated in figure 3.36.

Here, the external vertical load of the spring framework model is divided into 500 parts in the framework model. Thus, 500 calculation steps are used to represent the static loading (first loading). At each calculation step, the used horizontal spring stiffness value (C; the slope of a line segment in figure 3.36) is chosen according to the actual slip in the shear connector through the force-slip function in figure 3.36. The large number (500) of calculation steps ensures that the force-slip characteristic curve is considered precisely in the spring framework model calculation. Moreover, according to the chapter 3.5, a uniform vertical spring stiffness C_z = 10 000 kN/mm is assumed as an approximation.

3.6.1.2 The evaluation of results

Correspondently to the chapter 3.5.1.5., the vertical displacement and the internal forces of the structure elements will be compared in this chapter with the ABAQUS calculation results.

The maximal vertical displacement is 7,01 mm according to the ABAQUS calculation, and 6,64 mm by the spring framework model with the different horizontal spring stiffness values. So, the framework model delivers a smaller result, with a decrease of 5,3 %. ABAQUS gives the maximum bottom steel plate tensile force as 933,6 kN. The spring framework model delivers 802,0 kN which is 85,9 % of the ABAQUS result. The top steel plate has a compressive force of 751,2 kN in ABAQUS, and of 745,6 kN (99,3 %) in the framework model calculation.

The normal forces in the steel plates are compared in figure 3.37. The green line shows the ABAQUS results, and the black line represents the results calculated with the spring framework model.

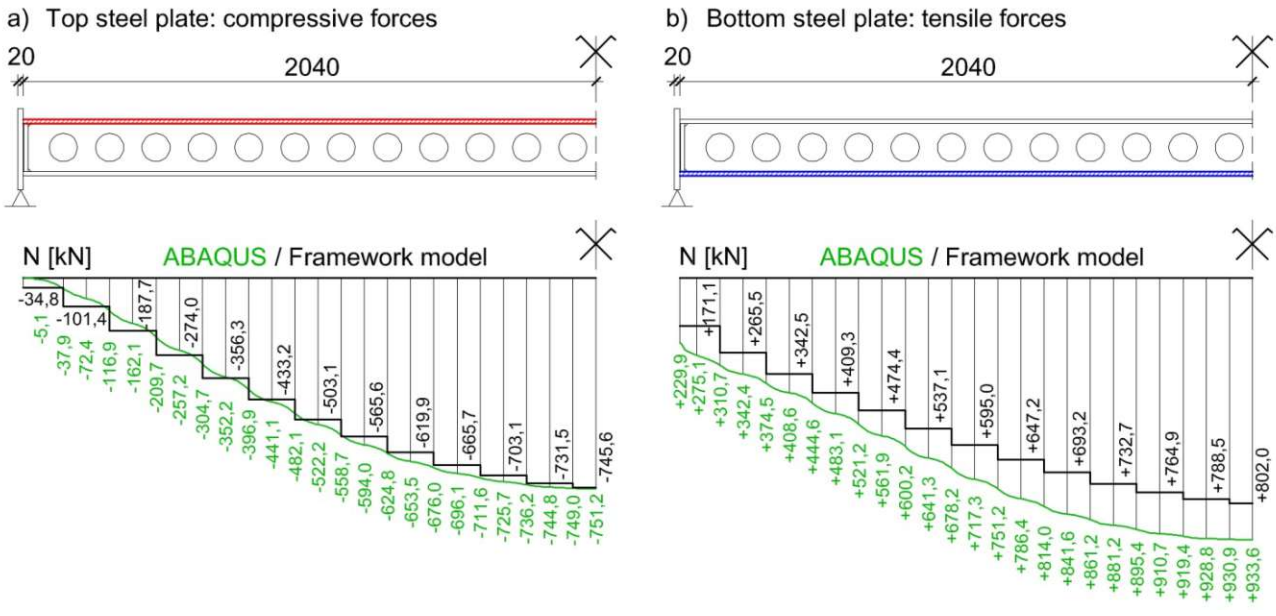

Figure 3.37: Normal forces in the steel plates of the SCSC-plate: a) compressive forces in the top steel plate; b) tensile forces in the bottom steel plate. Dimensions in [mm]

In the second step, the horizontal forces in the shear connectors are compared. According to the ABAQUS results, the maximum force in the shear connector at the top steel section occurs in the second circular hole from the support. This horizontal force component amounts to 98,5 kN. The framework model shows a maximum force of 77,3 kN (78,5 %) at the first hole. The ABAQUS calculation method indicates that the maximum force (73,6 kN) in the shear connector at the

bottom steel section will be at the fifth hole. The framework model delivers a maximum force of 54,2 kN (73,6 %) at the fourth hole. The values of the forces in the shear connectors 1 - 12 are shown in figure 3.38 in a graph format for ease of view. The green line shows the ABAQUS results, and the black line represents the horizontal forces in the shear connectors calculated with the spring framework model.

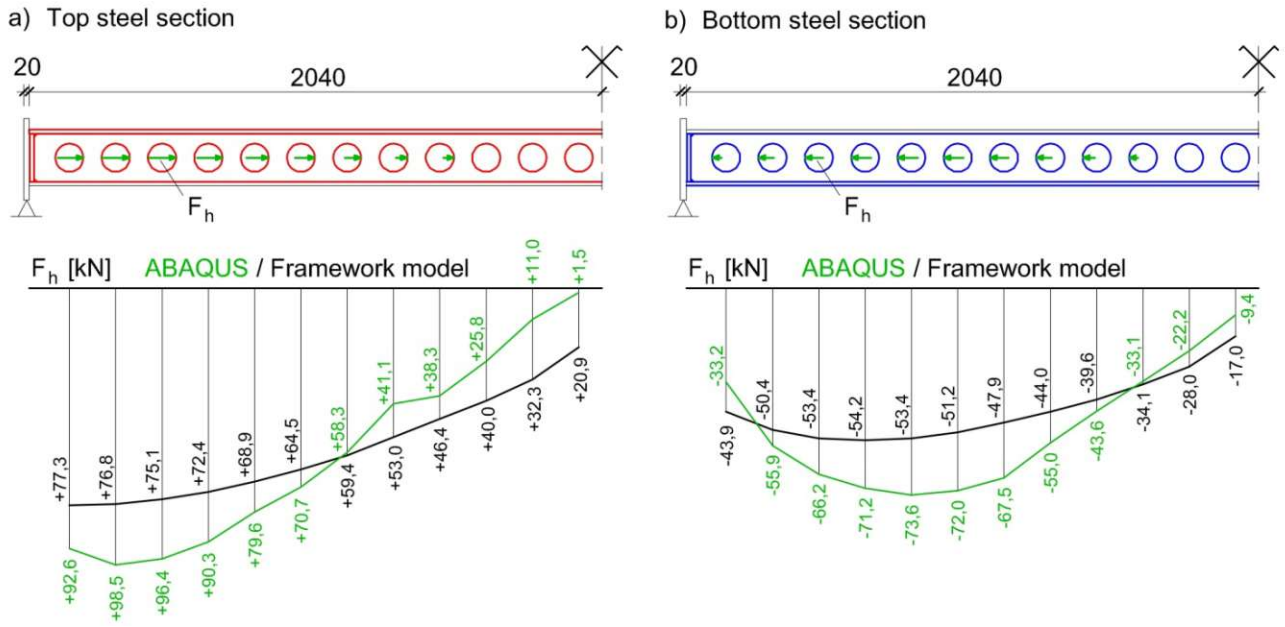

Figure 3.38: Horizontal forces in the shear connectors of the SCSC-plate: a) forces in the top steel section; b) forces in the bottom steel section. Dimensions in [mm]

It is clear through the comparison of the results of figures 3.32 and 3.38 that the spring framework model with constant spring stiffness values reproduces better the results of ABAQUS. This conclusion was not expected, because a more advanced model should describe better the reality. The reason for the higher difference in results is due to the fact that the ABAQUS calculation takes into consideration differently the inelastic behaviour of concrete. In the case of the ABAQUS calculation, the spring stiffness values at the shear connectors can only be calculated from the results (see chapter 3.7.2). Actually, the horizontal forces in the shear connectors and the slips of the shear connectors can be evaluated from the results of ABAQUS. The quotients of forces and slips provide the spring stiffness for the composite connections. This evaluation of results shows that the spring stiffness is approximately constant in the case of the ABAQUS calculation. Namely, similar spring stiffness values arise at the different shear connectors. Thus, according to the ABAQUS calculation, the spring stiffness does not depend on the load level. This is the reason that the framework model with constant spring stiffness values reproduces better the horizontal forces in the shear connectors calculated in ABAQUS.

Actually, the validation of the complex spring framework model through the ABAQUS calculation results is shown in chapter 3.7. There, a spring framework model with three horizontal concrete layers will be examined which considers the same spring stiffness values as ABAQUS. So, the comparison of ABAQUS and framework model calculation results is more meaningful compared to the comparisons in chapters 3.6.1 and 3.6.2.

3.6.2 Model with three horizontal concrete layers

3.6.2.1 Introduction

The model is identical with the structure introduced in chapter 3.5.2.1. Logically, the spring stiffness values are calculated here according to the explanations in chapter 3.6.1.1. Therefore, the different spring stiffness values are used in this chapter through the diagram in figure 3.36. Logically, this more advanced framework model with three concrete layers and different spring stiffness values describes better the real behaviour of a SCSC plate compared to the models examined in the previous chapters.

3.6.2.2 The evaluation of results

The vertical displacement and the internal forces of the structure elements will be compared in this chapter with the ABAQUS calculation results.

The maximal vertical displacement is 7,01 mm according to the ABAQUS calculation, and 7,22 mm by the spring framework model with the different horizontal spring stiffness values. So, the framework model delivers a higher result, with an increase of 3,0 %. ABAQUS gives the maximum bottom steel plate tensile force as 933,6 kN. The spring framework model delivers 914,5 kN which is 98,0 % of the ABAQUS result. The top steel plate has a compressive force of 751,2 kN in ABAQUS, and of 754,2 kN (100,4 %) in the framework model calculation.

The normal forces in the steel plates are compared in figure 3.39. The green line shows the ABAQUS results, and the black line represents the results calculated with the spring framework model.

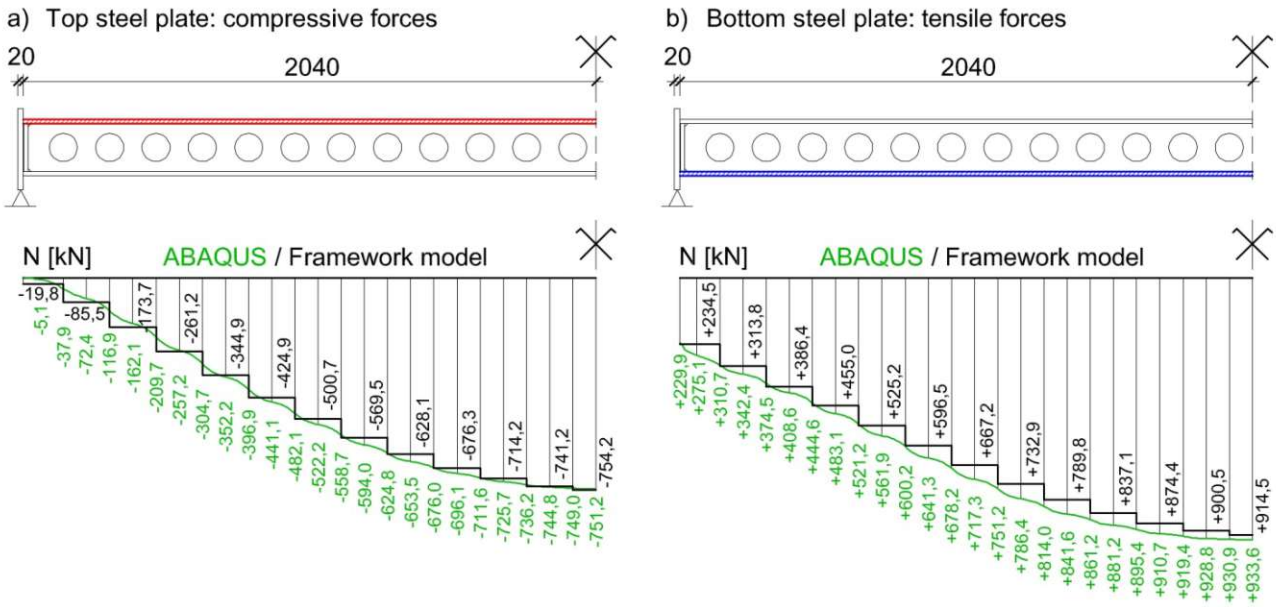

Figure 3.39: Normal forces in the steel plates of the SCSC-plate: a) compressive forces in the top steel plate; b) tensile forces in the bottom steel plate. Dimensions in [mm]

In the upper horizontal compressed concrete zone we get a compressive force of 442,5 kN in ABAQUS and of 404,0 kN (91,3 %) from the framework model. As in the used ABAQUS concrete damaged plasticity-model (CDP), tensile material behaviour for concrete is allowed for, a resultant tensile force (237,1 kN) occurs in the bottom concrete zone. In the framework model, the lower and middle horizontal concrete beams have a resulting tensile force of 228,3 kN (96,3 %).

Next, the horizontal forces in the shear connectors are compared (see figure 3.40). According to the ABAQUS results, the maximum force in the shear connector at the top steel section occurs in the second circular hole from the support. This horizontal force component amounts to 98,5 kN. The framework model shows a maximum force of 78,6 kN (79,8 %) at the first hole. The ABAQUS calculation method indicates that the maximum force (73,6 kN) in the shear connector at the bottom steel section will be at the fifth hole. The framework model delivers a maximum force of 60,5 kN (82,2 %) also at the fifth hole. The values of the forces in the shear connectors 1 - 12 are shown in figure 3.40 in a graph format for ease of view. The green line shows the ABAQUS results, and the black line represents the horizontal forces in the shear connectors calculated with the spring framework model.

As mentioned in the previous section 3.6.1.2., the reason for the difference in results in figure 3.40 is that the ABAQUS calculation takes into consideration differently the inelastic behaviour of concrete. Therefore, the framework model with constant spring stiffness values (see chapter 3.5.2.) reproduces better the values of the forces in the shear connectors calculated in ABAQUS. However, the maximal vertical displacement and the normal forces in the steel plates approximate properly the ABAQUS calculation results. The more developed model with different spring stiffness values will be used to simulate the cyclic loading in chapter 4, because this model does not use ABAQUS results for calculation.

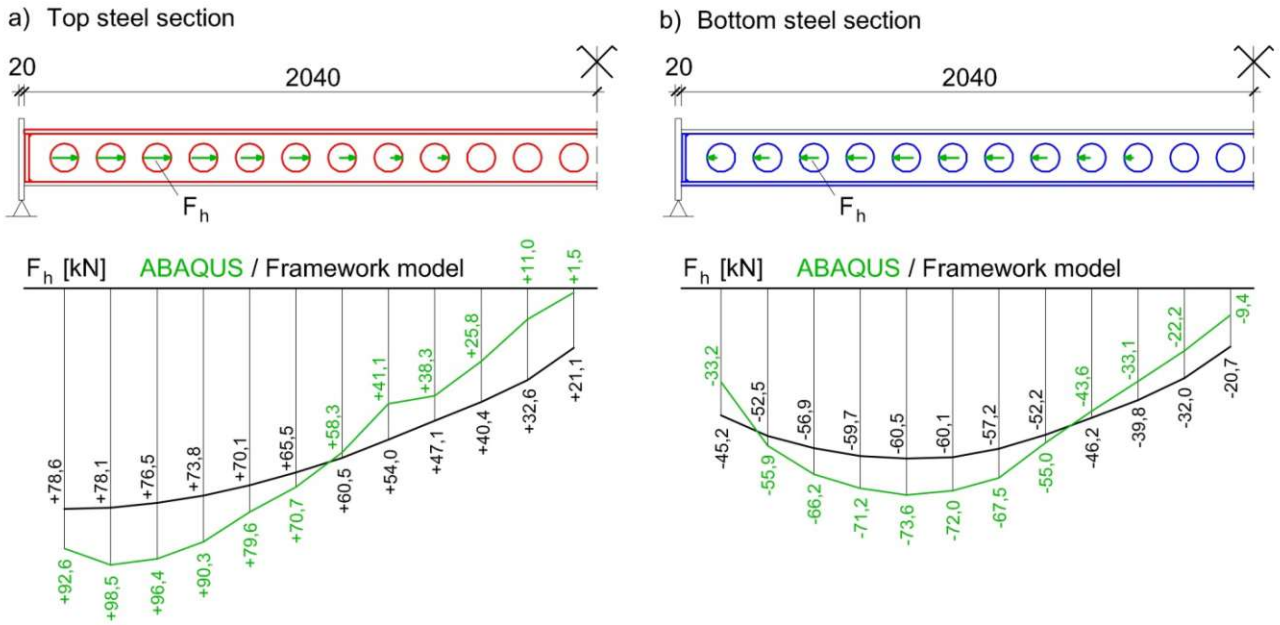

Figure 3.40: Horizontal forces in the shear connectors of the SCSC-plate: a) forces in the top steel section; b) forces in the bottom steel section. Dimensions in [mm]

3.7 On the validation of the complex spring framework model

3.7.1 Introduction

To validate the complex spring framework model through the ABAQUS calculation results, it is necessary to create a spring framework model which considers the spring stiffness values calculated in ABAQUS. In this way, the comparison of results is reasonable as both the ABAQUS and the spring framework model operate with the same basis parameters. Logically, the more complex model with three horizontal concrete layers is used for the framework model. In chapter 3.7.2 the ABAQUS calculation results will be analysed to evaluate the spring stiffness values for the framework model calculation. In chapter 3.7.3 the calculation results will be compared with the ABAQUS results as a validation of the spring framework model.

3.7.2 The stiffness of the composite connection in ABAQUS

The horizontal forces in the shear connectors can be easily evaluated with cylindrical cuts created in the View Cut Manager of ABAQUS. The total horizontal slips (elastic and inelastic slips together) at the shear connectors are derived from the horizontal displacements between the nodes of the shear connectors in case of loading (see figure 3.41). The vertical components of the slips are negligible. The ABAQUS model consists of a 1 m long and 2,06 m wide section of the SCSC plate (see chapter 2.3). Therefore, the two outside shear connectors have a thickness of 10 mm. The central shear connector (thickness of 20 mm) is welded to the upper steel plate, while the outside shear connectors are welded to the bottom steel plate. Figure 3.41 shows the slipping of the central (red coloured part) and one of the outside (blue coloured part) shear connectors due to loading. The horizontal displacements between the marked nodes means the horizontal slips at two shear connectors together. One horizontal displacement marked in figure 3.41 occurs due to the horizontal forces in the two shear connectors. As in the SCSC plate all of the shear connectors are 20 mm thick, the horizontal force in the outside shear connector calculated in ABAQUS need to be doubled. So, the forces in the shear connectors welded to the bottom steel plate are twice as much as the results detected in ABAQUS. However, the slipping needs to be unvarying. The quotients of horizontal forces and horizontal slips provide the spring stiffness value for the composite connections. Notable is that this calculation method delivers an average value of the horizontal spring stiffness referring to two shear connectors. For example the first shear connector welded to the upper steel plate and the first shear connector welded to the bottom steel plate have the same spring stiffness through this evaluation.

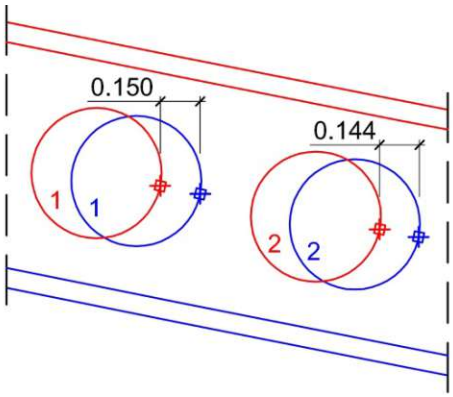

Figure 3.41: ABAQUS calculation results [mm]: horizontal displacements between the nodes of the shear connectors in case of loading. Just the area at the support (shear connectors 1 and 2) is illustrated. The displacements are stretched for ease of view.

This calculation method provides 12 spring stiffness values as 12 circular holes are designed between the support and the plane of symmetry. Figure 3.42 illustrates that the spring stiffness is approximately constant in the case of the ABAQUS calculation with exception of the stiffness values at the first, the eighth and the last (twelfth) shear connectors. Namely, the spring stiffness values are influenced by local damages of the concrete in the case of the first and the eighth shear connectors. To detect these effects, figure 3.43 illustrates the horizontal forces in the shear connectors in the case of different load levels. The load level used for fatigue limit state belongs to the FRAME 15, which is marked with green colour in figure 3.43. Necessarily, at this load level were also compared the results of ABAQUS and framework model in chapters 3.5 and 3.6. The characters of the curves are the same until the FRAME 15 in the case of the bottom steel section (see figure 3.43(b)). Actually, there are not significant inelastic deformations around the shear connectors of the bottom steel section according to the ABAQUS results. However, an increased load induces local damages of the concrete, which lead to the relative reductions of horizontal forces in the composite connection (see figure 3.43(b): frame 20 and 25).

Figure 3.42: Spring stiffness values according to the ABAQUS calculation results

In the case of the top steel section, inelastic deformations occur already due to the loading for fatigue limit state according to the ABAQUS calculation results (see figure 3.43(a): FRAME 15). The FEA software detects local compressive crushing of the concrete material at the first shear connector and tensile cracking of concrete under the eighth shear connector. Through these damages, the stiffness of the given composite connections decreases partly, which shows up also in the graph of the horizontal forces in the shear connectors. Logically, the two destructions are more expressive in the case of higher loads (see figure 3.43(a): FRAME 20 and 25).

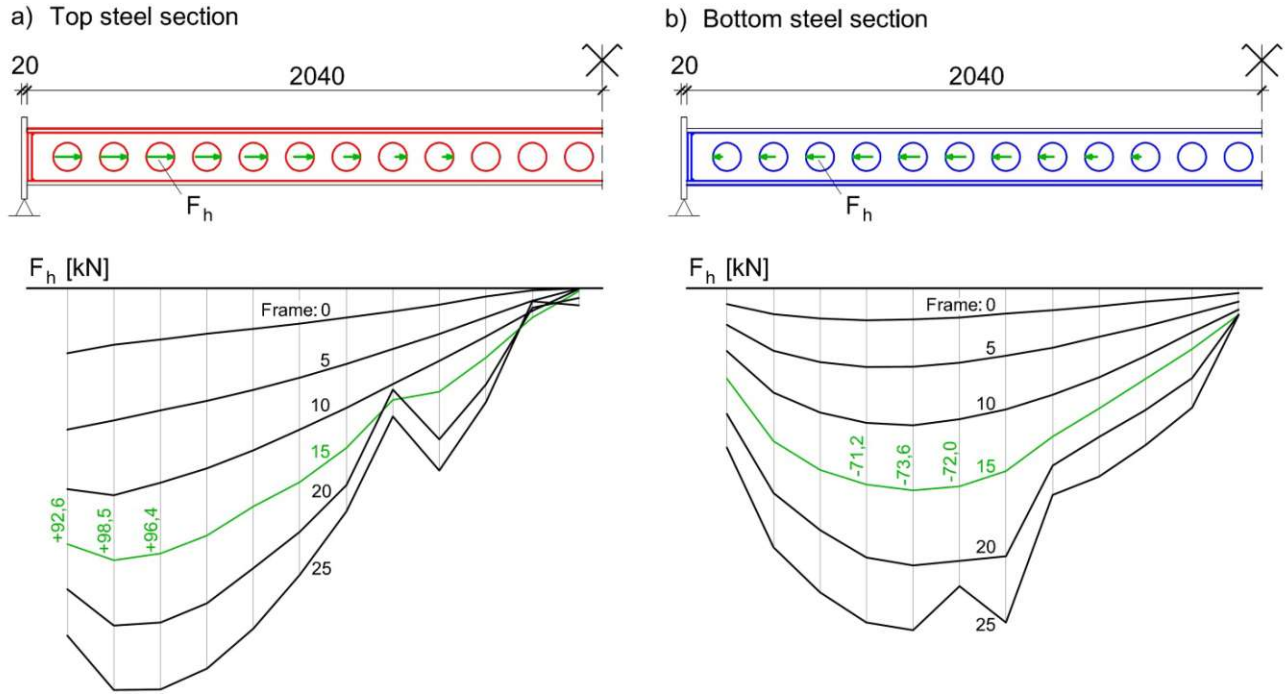

Figure 3.43: Horizontal forces in the shear connectors of the SCSC-plate in the case of different load levels: a) forces in the top steel section; b) forces in the bottom steel section. FRAME 0 means the dead load, while FRAME 15 represents the load used for fatigue limit state. Dimensions in [mm]

It is illustrated in figure 3.42 with red colour that the spring stiffness values at the first, the eighth and the twelfth shear connectors differ markedly from the stiffness values at the remaining shear connectors calculated from the ABAQUS results. Notable is that the horizontal slip between the nodes of the twelfth shear connectors is extremely small, which

gives an excessive spring stiffness value (see figure 3.42). Obviously, the method of the spring stiffness evaluation does not fit at this special location. This means that the spring stiffness in ABAQUS is calculated from the average of nine quotients of horizontal forces and horizontal slips as the results at the first, the eighth and the twelfth shear connectors vary from the other values. This average means a spring stiffness of 1162 kN/mm. Moreover, this value is considered as the constant spring stiffness from ABAQUS, because the nine quotients deflect from 1162 kN/mm with only 4,3 % on average.

The above mentioned ABAQUS results denote that inelastic deformations do not influence significantly the force transfer in the composite connection by the loading used for fatigue limit state. Actually, at ten shear connectors from twelve the spring stiffness can be adopted as 1162 kN/mm. If this stiffness arose merely from the elastic deformations in the shear connectors, the same spring stiffness would be developed from the spring stiffness evaluation by dead load. To control this assumption, the above described method of spring stiffness evaluation from ABAQUS is performed in the case of the dead load of the construction. By reason of the negligible horizontal slip between the nodes of the twelfth shear connectors, the spring stiffness from the eleventh shear connectors is applied at the twelfth shear connectors, too. So, the average of the twelve spring stiffness values is 1163 kN/mm in the case of dead load, which is practically equal the expected stiffness (1162 kN/mm).

3.7.3 Comparison of results

In the first instance, the framework model calculation in MATLAB is performed in the case of dead load with the constant spring stiffness value of 1163 kN/mm. In this case, the comparison between the ABAQUS calculation results and the framework model calculation results is meaningful as both calculation methods include the same spring stiffness representing the composite connection. So, the maximal vertical displacement in the middle of span is 1,24 mm according to the ABAQUS calculation, and 1,17 mm by the spring framework model. Thus, the framework model delivers a smaller result, with a decrease of 5,6 %. However, the difference (0,07 mm) is negligible. The values of the forces in the shear connectors 1 - 12 are shown in figure 3.44 in a graph format. The green line shows the ABAQUS results, and the black line represents the horizontal forces in the shear connectors calculated with the spring framework model.

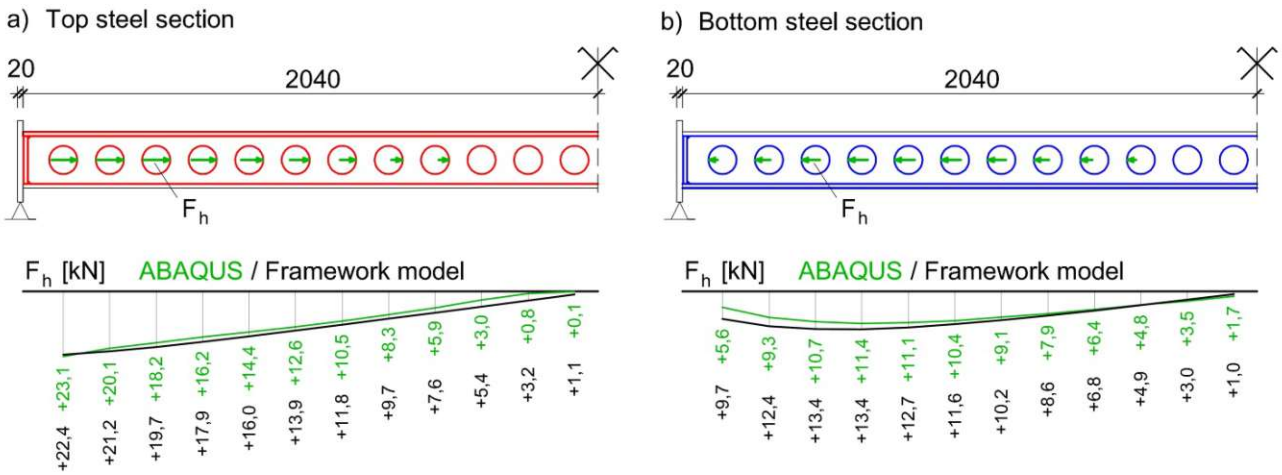

Figure 3.44: Horizontal forces in the shear connectors of the SCSC-plate in the case of dead load of the construction: a) forces in the top steel section; b) forces in the bottom steel section. Dimensions in [mm]

The characters of the curves of the results are the same. However, major differences arise at the first three shear connectors of the bottom steel section (see figure 3.44(b)). The reason is that the concrete is divided into only three

horizontal layers in the framework model. Therefore, the horizontal forces cannot be delivered to the support at the bottom part of the concrete core without bending of the end stiffeners and the main steel girder. However, the ABAQUS calculation detects a high pressure here. In this way, the concrete loads more the shear connectors of the bottom steel section around the support in the framework model calculation. So, the horizontal forces can be transferred to the bottom steel plate close to the support.

Next, the results at the load level used for fatigue limit state are compared. Firstly, the results of the framework model calculation with the constant spring stiffness value from ABAQUS (1162 kN/mm) are presented. Actually, the horizontal forces in the shear connectors are only considered in this case. These values are shown in figure 3.45 in a graph format for ease of view. Through the framework model with constant spring stiffness values, the SCSC-plate is modelled without any damages. In our case, this model is probably an approximation of reality as the ABAQUS calculation signs local damages at the first and the eighth shear connectors of the top steel section.

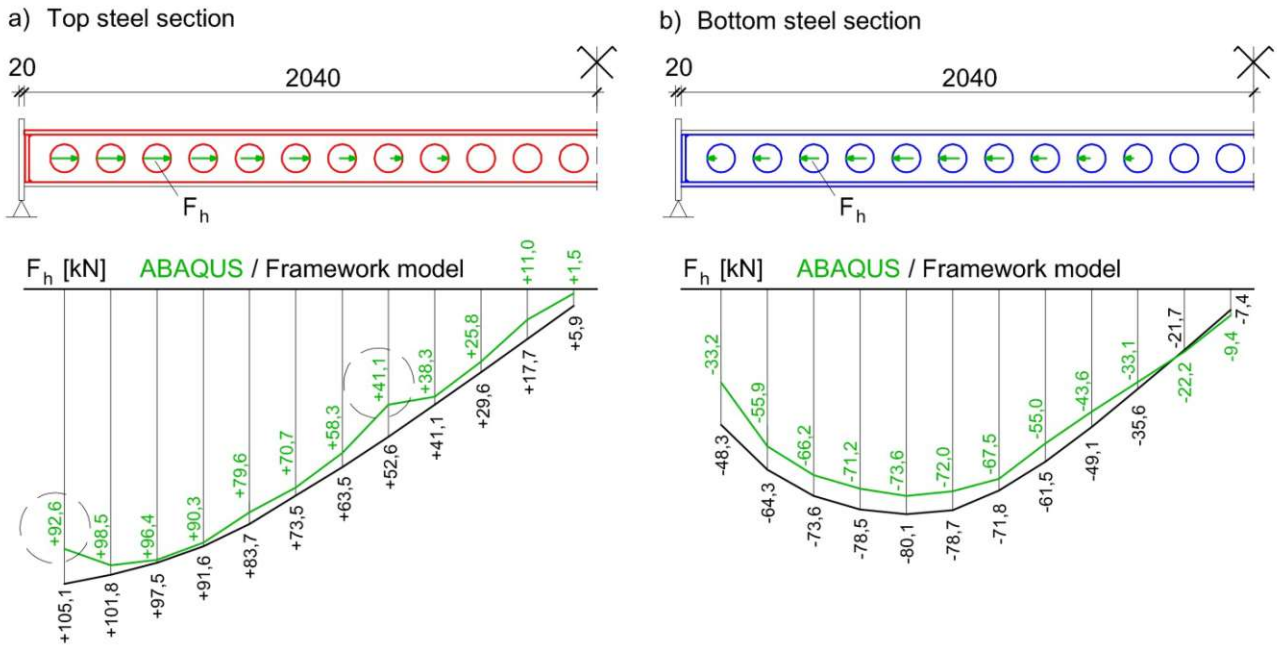

Figure 3.45: Horizontal forces in the shear connectors of the SCSC-plate: a) forces in the top steel section; b) forces in the bottom steel section. The framework model operates with the constant spring stiffness value of 1162 kN/mm.

Logically, the results of the horizontal forces in the shear connectors differ noticeably at these two positions (see figure 3.45(a)). Actually, the characters of the graphs in figure 3.45(a) are different because of the two turning points of the green graph.

Secondly, the results of the framework model with modified spring stiffness values at first and eighth shear connectors of the top steel section are presented at the load level used for fatigue limit state. As ABAQUS detects local compressive crushing of the concrete material at the first shear connector of the top steel section and tensile cracking of concrete under the eighth shear connector of the top steel section, the stiffness of these two composite connections are smaller than the average value (1162 kN/mm) calculated in chapter 3.7.2. To get the spring stiffness value for a single shear connector from ABAQUS, the method of slip evaluation needs to be changed. According to the ABAQUS results, a gap occurs at the circular hole of the shear connector between the edge of the concrete inside the hole and the edge of the steel shear connector in the case of loading. The horizontal component of this gap means now the horizontal slip at the shear

connector as an approximation. The quotient of the horizontal force in the shear connector and the horizontal slip provides the spring stiffness value for the examined composite connection. Due to this method of calculation, the spring stiffness value of the first shear connector of the top steel section is 987,4 kN/mm. Moreover, at the eighth shear connector of the top steel section this stiffness is 1051,2 kN/mm. The detailed calculation is presented in appendix E. Logically, at the remaining 10 shear connectors of the top steel section and at all the 12 shear connectors of the bottom steel sections the spring stiffness are considered with 1162 kN/mm according to the chapter 3.7.2.

In this case, the maximal vertical displacement in the middle of span is 7,01 mm according to the ABAQUS calculation, and 6,27 mm by the spring framework model. Thus, the framework model delivers a smaller result, with a decrease of 10,6 %. The values of the forces in the shear connectors 1 - 12 are shown in figure 3.46 in a graph format. Notable is that the characters of the curves are the same due to the two calculations. However, the framework model delivers higher results than the complex ABAQUS calculation. As it was expected, the framework model calculation reproduces better the results of ABAQUS also at the first and the eighth shear connectors of the top steel section compared with the framework model calculation with constant spring stiffness value (see figures 3.46 and 3.45).

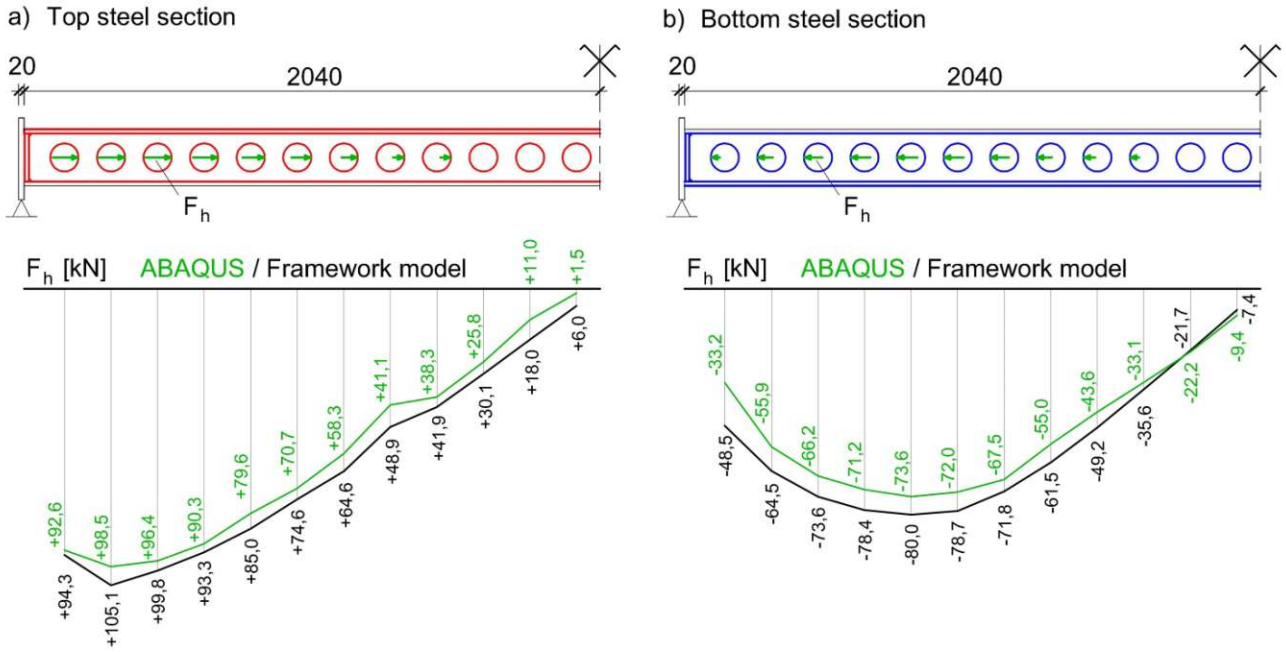

Figure 3.46: Horizontal forces in the shear connectors of the SCSC-plate: a) forces in the top steel section; b) forces in the bottom steel section. The framework model operates with the spring stiffness values from ABAQUS. Dimensions in [mm]

The slip distributions through the two models are shown in figure 3.47. Here, the slips refer to the horizontal displacements between the shear connectors of the top and the bottom steel sections according to figure 3.41. Logically, the results from the framework model converge to the values from the ABAQUS calculation because the spring stiffness values were chosen according to the ABAQUS results. The main reason for the small differences is that the framework model delivers higher horizontal forces in the shear connectors than the ABAQUS calculation (see figure 3.46).

The normal forces in the steel plates are compared in figure 3.48. The green line shows the ABAQUS results, and the black line represents the results calculated with the spring framework model. In the case of the top steel plate, the framework model calculation produces an upper approximation of the ABAQUS results. However, a lower approximation is arisen in the case of the bottom steel plate.

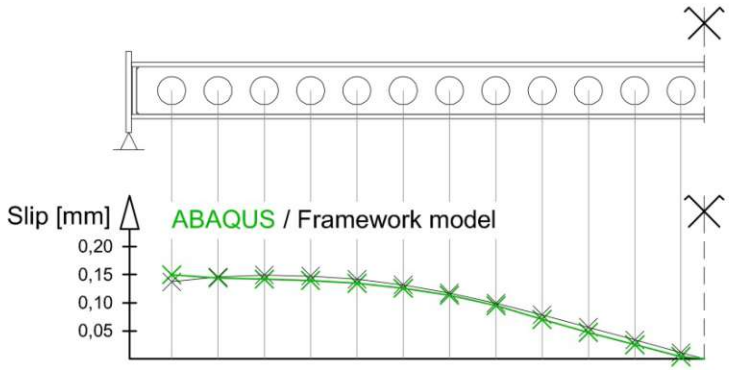

Figure 3.47: Comparison of slip distributions in ABAQUS and in the framework model

ABAQUS gives the maximum bottom steel plate tensile force as 933,6 kN (see figure 3.48(b)). The spring framework model delivers 910,5 kN which is 97,5 % of the ABAQUS result. The top steel plate has a compressive force of 751,2 kN in ABAQUS, and of 799,2 kN (106,4 %) in the framework model calculation (see figure 3.48(a)). Notable is that the framework model with the different spring stiffness values based on the laboratory tests (see chapter 3.6) delivers a better approximation of the ABAQUS results referring to the normal forces in the steel plates (see figure 3.39). However, only the current model is suited to compare with the ABAQUS calculation results for the validation of the spring framework model.

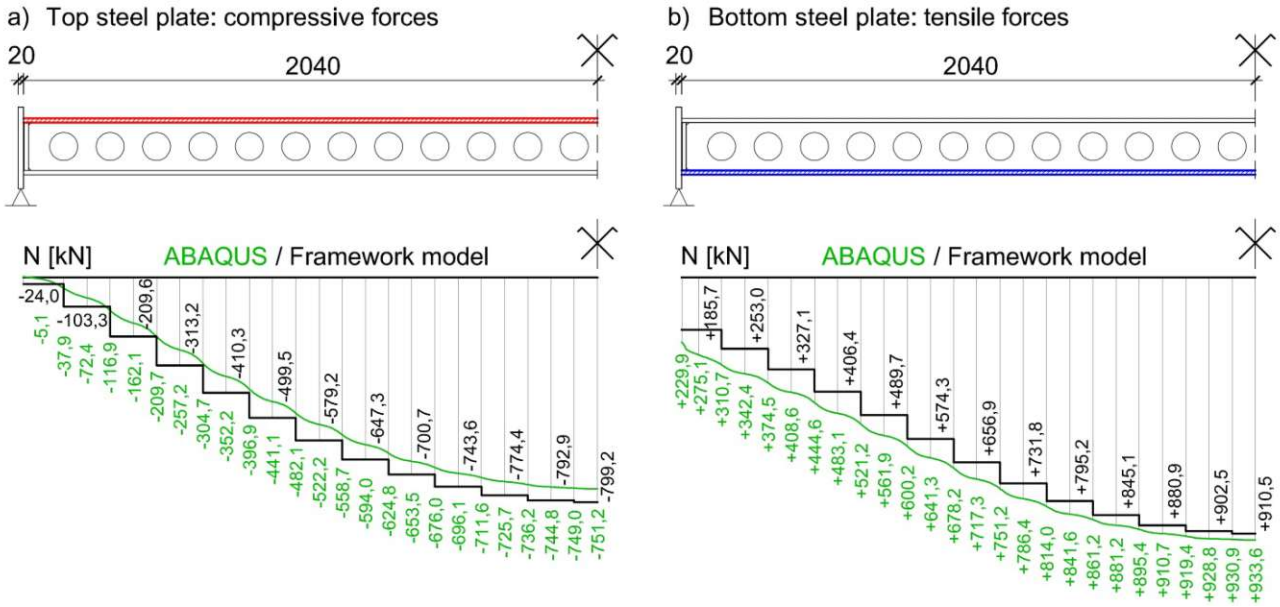

Figure 3.48: Normal forces in the steel plates of the SCSC-plate: a) compressive forces in the top steel plate; b) tensile forces in the bottom steel plate. The framework model operates with the spring stiffness values from ABAQUS. Dimensions in [mm]

Finally, the normal forces in the three concrete layers are compared in figure 3.49. At the concrete zone in the middle, the resultant forces from compressions and tensions are represented in the case of the ABAQUS results for ease of comparison. Moreover, notable is that the tensile cracking of concrete causes a significant reduction in the tensile force at the lower concrete zone (see figure 3.49(c): 130,1 kN) in the case of the ABAQUS calculation. However, the tension in the middle zone is enlarged (see figure 3.49(b): 76,9 kN) as a compensation for the missing tension due to cracking.

The two models show significant differences around the support. The main reason is that the ABAQUS model enables a higher horizontal load transfer (see figure 3.49(c): -284,0 kN) between the concrete core and the main steel girder web at the bottom part of the lower concrete zone. In the framework model the lower concrete zone is represented with beam elements which transfer the forces in a vertical distance of 35,8 mm from the middle of the bottom steel plate (see figure 3.33). Logically, the simple framework model cannot perfectly reproduce the results of the complex ABAQUS model at the support.

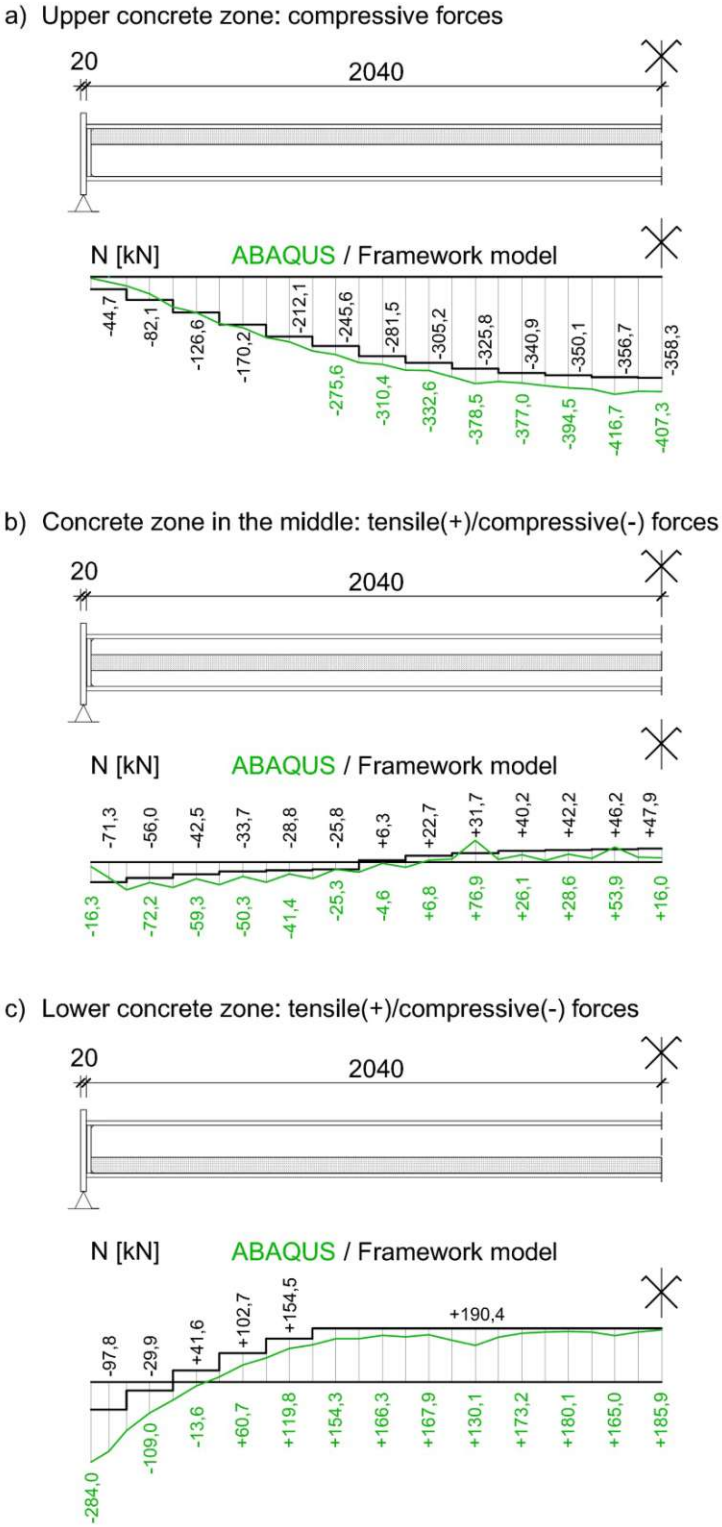

Figure 3.49: Normal forces in the concrete layers of the SCSC-plate: a) upper concrete zone; b) concrete zone in the middle; c) lower concrete zone. Dimensions in [mm]

As shown in this chapter, the ABAQUS results can be reproduced appropriately with a two-dimensional spring framework model. Considering the static deflection, the forces in the composite connection and the maximal internal forces, the differences between the results are fairly small. So, the framework model with three horizontal concrete layers can be validated as a substitute engineering model for the complex three-dimensional model used by the Finite-Element-Analysis software. The structure diagram of the spring framework model calculation is illustrated in the chapter 4.4 (see figure 4.77).

3.8 Conclusion

As shown in chapter 3, the load-bearing behaviour of the SCSC-plate can be illustrated with a two-dimensional spring framework model in the case of static loading. The calculation of the displacements and internal forces of the framework model is performed using the Direct Stiffness Method and the program MATLAB. It was represented that the engineering model is suitable to substitute the complex ABAQUS calculation. Moreover, the spring framework model introduced in chapter 3.6 operates without any results from the ABAQUS calculation because the used spring stiffness values based on laboratory tests (see chapter 3.2). Through this separate model illustrated in chapter 3.6.2, the vertical displacements and the internal forces reflect appropriately the ABAQUS results. For instance, the maximal vertical displacement in the middle of the span is 7,22 mm by the spring framework, and 7,01 mm according to the ABAQUS calculation. The comparisons of the normal forces in the steel plates are shown in figure 3.39. Moreover, the comparisons of the normal forces in the concrete layers are demonstrated below in figure 3.50. However, the horizontal forces in the shear connectors differ through the two calculation methods (see figure 3.40) because the ABAQUS and the framework model calculation take into consideration differently the inelastic behaviour of concrete. Fortunately, this characteristic does not influence significantly the static deflection and the normal forces in the construction parts. Thus, the spring framework model with different spring stiffness values as well as with three concrete layers is adequate to replace the time-consuming calculation of ABAQUS. Namely, calculations with several geometrical shapes or various load levels can be easily done due to the framework model. The parameter study or the geometrical optimization would take a lot of time in ABAQUS because the development of the model is complicated. Furthermore, the computational time is also high in the case of a complex ABAQUS model.

It is important to point out that the framework model does not figure the fracturing process of the materials in the structure. For instance, the tensile cracking of the concrete material is not considered in the simple framework model. Moreover, the softening stress-strain response is not modelled in the developed engineering model. However, it is considered in the framework model that the tensile strength and the compressive strength cannot be exceeded. As shown in figure 3.49(c) and figure 3.50(c), the horizontal forces in the concrete have a constant value of 190,4 kN around the middle of the span. Actually, 190,4 kN is the maximal tensile force of the examined concrete beams calculated from the tensile strength and the area of the members. Thus, logically, the framework model is applicable until the beginning of the fracturing processes. In the case of the load level used for fatigue limit state, ABAQUS detects some tensile cracking and compressive crushing of the concrete material. Fortunately, these failure mechanisms do not influence significantly the main load-bearing behaviour of the steel-concrete-steel composite plate. Thus, the framework model can be applied also at the examined fatigue limit state as an approximation. In the case of higher loads, an expansion of the presented framework model is necessary to evaluate the effects from cracking of concrete.

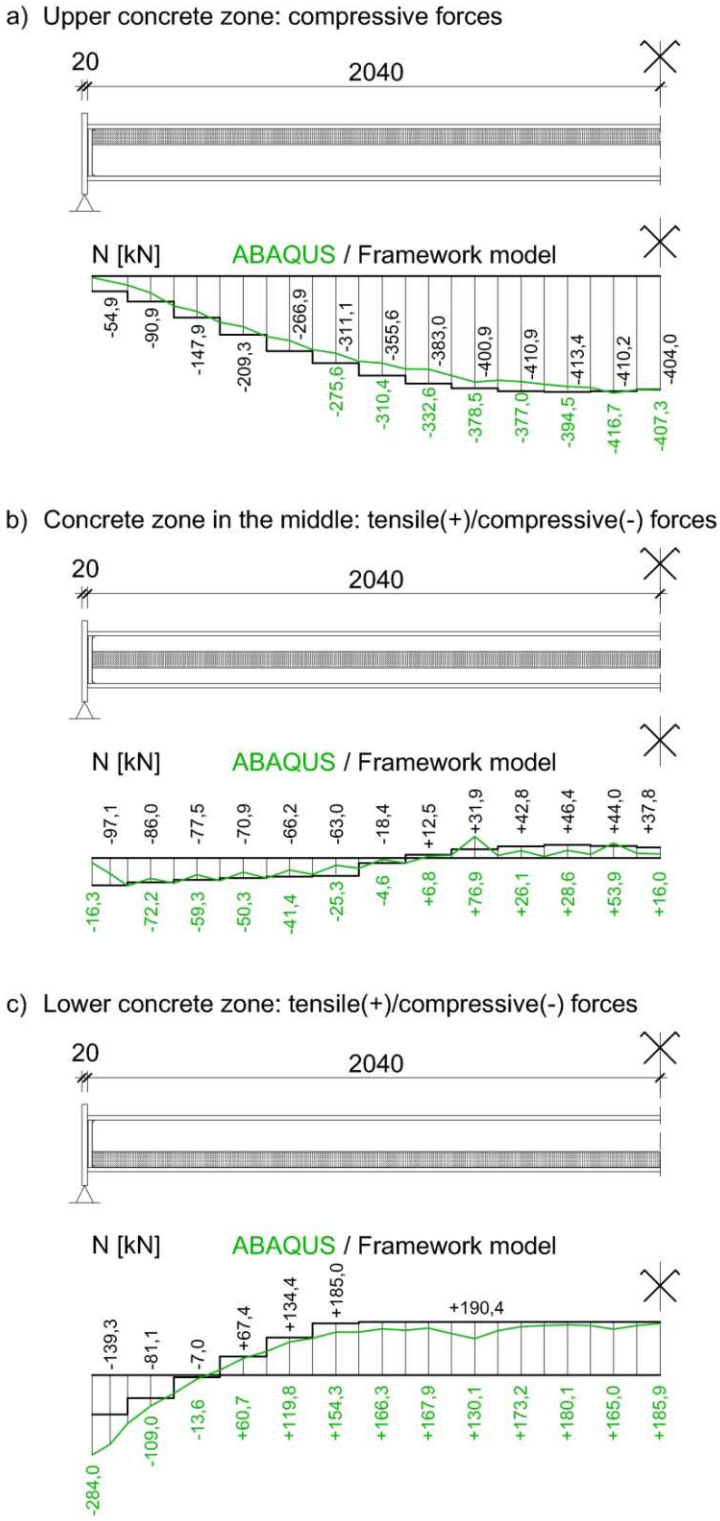

Figure 3.50: Normal forces in the concrete layers of the SCSC-plate: a) upper concrete zone; b) concrete zone in the middle; c) lower concrete zone. The framework model operates with different spring stiffness values according to chapter 3.6. Dimensions in [mm]

4. Simulation of cyclic loading and inelastic slip

4.1 Introduction of the framework model for the cyclic loading

Lit.: [7], [8]

The spring framework model was used for static loads in the previous chapter. However, the SCSC plate will be loaded with a great number of load changes over the lifespan of the bridge. So, the effects of cyclic loading will be analysed with the spring framework model in this chapter. A complex ABAQUS model is not applicable for the calculation of the cyclic loading as the time taken for the calculation is huge. So, the spring framework model presented in this chapter has a relevant advantage over the ABAQUS calculation. Namely, in the case of the framework model calculation, the calculation results can be reached in minutes. So, all the effects of the cyclic loading can be easily evaluated.

Due to the loading of the SCSC plate, permanent displacement appears as a gap between the surfaces of the steel circular hole and the concrete part inside this hole in the case of high forces in the composite connection. This permanent displacement in the composite connection is called inelastic slip, too. Fatigue investigations on composite beams [21] have also shown the fact that this inelastic slip already occurs due to the first loading of the structure (see figure 4.1(a): $\delta_{inel,first}$). First loading means the first traffic load of the bridge. Logically, at the second loading the permanent displacements influence the behaviour of the structure. Namely, before the gap between the surfaces of the steel circular hole and the concrete part inside this hole has closed, there is no load transfer between the steel and concrete elements at the composite connection. This is illustrated in figure 4.1(b). Moreover, according to the laboratory tests (see chapter 3.2), the stiffness of the concrete increases after the first loading, as the concrete at the composite connection becomes more compressed. Therefore, the spring stiffness will be greater at the second loading (C_{hys}, see figure 4.1(a): n=2). From the second loading, this spring stiffness (C_{hys}), which is calculated on the basis of the hysteresis loops, can be assumed constant.

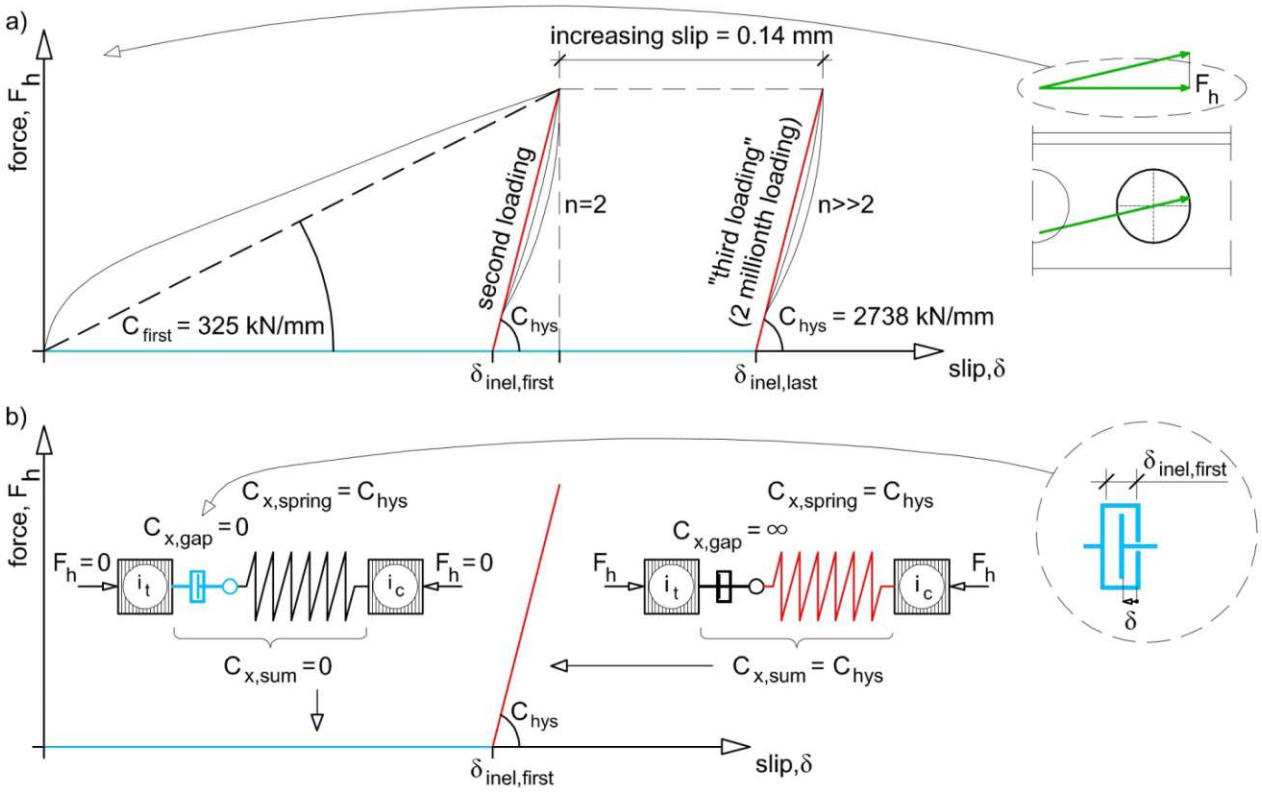

Figure 4.1: Force-slip diagrams for the shear connectors: a) increasing slip due to a high number of cycles; b) spring model to consider inelastic slip in the case of the second loading

The inelastic slips in the case of different load levels (maximal forces: 91 kN, 78 kN, 67 kN) were evaluated by the laboratory tests presented in chapter 3.2. According to these test results, the unloading after the first loading occurs along a curve with a gradient of 2738 kN/mm (C_{hys}, see figure 4.1(a): n=2) on average. The results of the six experimental tests indicate that this gradient is unrelated to the load level. Logically, some dispersion of results can be detected. Moreover, at the framework model inelastic slips are not calculated until a horizontal force of 25 kN in the shear connector. This assumption is based on the force-slip diagram for the first loading in figure 3.5. It is shown there that in the case of small forces (< 25 kN) the stiffness of the composite connection is high and the slips are small. So, in this force range, after an unloading along a curve with a gradient of 2738 kN/mm (C_{hys}) permanent displacements would not remain. In the case of any higher horizontal force (> 25 kN) in the shear connectors, the inelastic slips due to the first loading are calculated in the spring framework model. As mentioned above, at the beginning of the second loading, these inelastic slips are considered as gaps at the composite connections (see figure 4.1(b)). Moreover, the used spring stiffness at the second loading cycle is C_{hys} = 2738 kN/mm (see figure 4.1) in the spring framework model.

Additional loading cycles induce further increase of the inelastic slip (see figure 4.1(a): increasing slip). This slip increment, which represents the effects of the loadings over the lifespan of the bridge, is considered in the third loading cycle of the framework model. Actually, the increasing slip (see figure 4.1(a): 0,14 mm) after the last load cycle (the 2 millionth cycle) of the laboratory tests (see chapter 3.2) is added to the value of inelastic slip used as the gap for the second loading. According to the laboratory tests, there are not significant relationship between the force in the shear connector and the value of increasing slip. So, the increment of 0,14 mm represents the average increasing slip of the six experimental tests. Logically, if the horizontal force in the shear connector did not exceed 25 kN, increasing slip would not consider in the composite connection. So, it is important to divide up the third loading cycle to be able to consider the effects of the changes of horizontal forces on the value of the inelastic slip increment. Thus, in the spring framework model 100 loading cycles represent all of the loading cycles after the second loading. At each cycle only 1% of the increment of 0,14 mm is used at the shear connectors where the horizontal force exceeds 25 kN. Actually, the horizontal forces in the shear connectors typically decrease due to the increase of the inelastic slip. As small forces (< 25 kN) do not induce further increase of the inelastic slip, at some shear connectors the inelastic slip increment is less than 0,14mm after the last (102th) loading cycle of the framework model. To calculate all the 102 loading cycles, the computational time is approximately 10 minutes in MATLAB in the case of the spring framework model with three horizontal concrete layers. The reason of the high time is that the system of linear equations with 342 unknowns needs to be solved 51 000 times (at each of the 102 loading cycles 500 times). To represent an additional loading cycle, 500 calculation steps (loading steps) were used, as in the case of the static loading. The step-by-step loading is here especially important. Namely, at each of the 500 calculation steps it needs to be examined whether the actual slip at the holes in the shear connectors have reached the value of the inelastic slip. Before the inelastic slip is reached, the calculation of the framework model performed in MATLAB runs without the horizontal spring element. After that point, the spring is taken into consideration with the increased stiffness (C_{hys}).

In chapter 4 two models will be examined. As in the chapters 3.5 and 3.6, at the first model the concrete core is represented with one horizontal beam, and at the second model it is divided into three horizontal layers for calculation. Referring to the evaluation of the spring stiffness values, two models were examined in the previous chapters. Firstly, the spring stiffness values were constant as an approximation. Secondly, different spring stiffness values were used according to the force-slip diagram from the laboratory test results (see chapter 3.2). Here, the more precise method with the different spring stiffness values will be used. So, both of the models in chapter 4 operates with spring stiffness values depending on the actual horizontal force in the shear connectors.

4.2 The spring framework model with different spring stiffness values

4.2.1 Model with one horizontal concrete beam

4.2.1.1 Introduction

The model is identical with the structure introduced in chapter 3.5.1.1. Moreover, the spring stiffness values for the first loading are calculated here according to the interpretations in chapter 3.6.1.1. So, different spring stiffness values are used through the diagram in figure 3.36. Figure 4.2 illustrates the total slips and the inelastic slips due to the first loading at each shear connectors. These inelastic slip values will be considered as gaps in the composite connections in the case of the second loading.

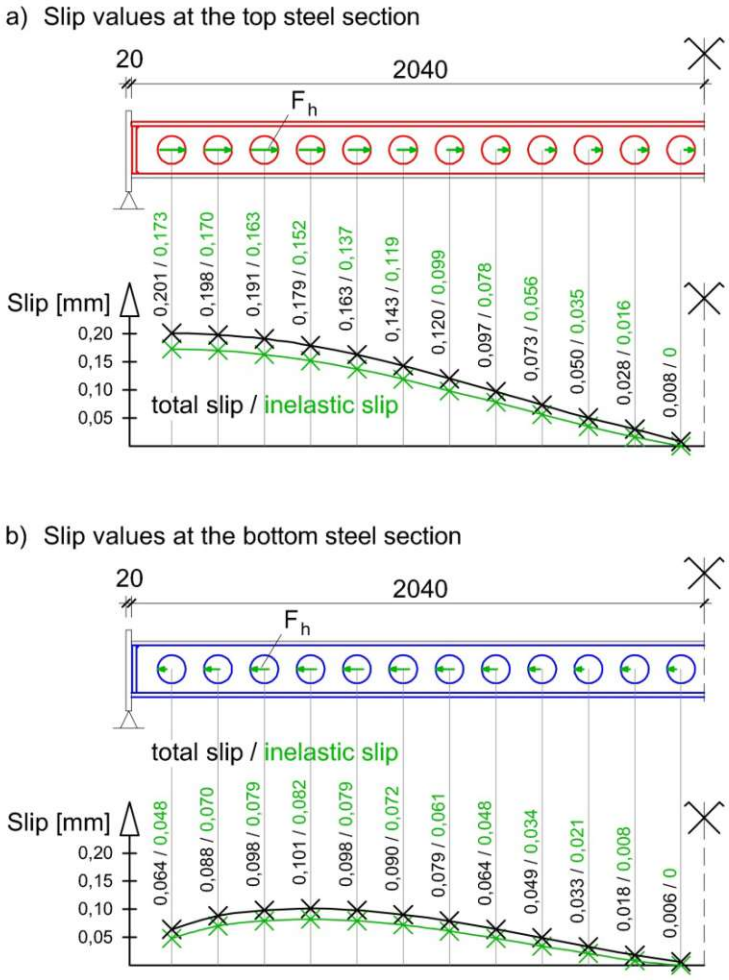

Figure 4.2: Total slips and inelastic slips due to the first loading cycle: a) slips between the concrete and the shear connectors of the top steel section; b) slips between the concrete and the shear connectors of the bottom steel section. Dimensions in [mm]

The inelastic slip values are calculated from the total slip at a composite connection in MATLAB. Actually, at each composite connection the total slip is decreased with the quotient of the horizontal force in the shear connector (see figure 3.38) and the spring stiffness value used for the unloading phase after the first loading (C_{hys} = 2738 kN/mm). However, in the case of the two composite connections, where the horizontal forces are smaller than 25 kN (see figure 3.38), the inelastic slips are defined zero without any calculation. So, gap elements are modelled at only 22 composite connections of the structure.

4.2.1.2 Effects due to the second load cycle

In this chapter, the spring framework model calculation results of the second loading are examined. According to the framework model calculation results, the structure has a vertical displacement of 1,19 mm in the middle of the span when the first gap of 22 gaps at the holes of the shear connectors closes. At this point, the 55th calculation step of the 500 calculation steps is activated, which means that actually 11 % of the external vertical load is acting. Up to this point, the horizontal load transfer is only possible at the two holes of the shear connectors where the inelastic slips were defined zero (see figure 4.2). In the case of the first loading, at the 55th calculation step the deflection in the middle of the span was only 0,59 mm. Logically, the transfer of forces between the steel and the concrete material was better at the first loading. Actually, the gaps at the second loading induce the increment of the vertical displacement of the structure.
All the gaps at the holes of the top steel section close when 29,8 % of the external vertical load is effective (149th calculation step). The vertical deflection is 2,78 mm at this loading step (149/500). Figure 4.4 illustrates that only 5 shear connectors of the bottom steel section are activated at this point. Moreover, the horizontal forces in the shear connectors are compared with the forces in the case of the first loading in figure 4.4.

After this, the gaps at the shear connector of the bottom steel section close by the time that 39,8 % of the load has been reached (199th calculation step). In this case the vertical displacement in the middle of the span is 3,35 mm. The horizontal forces in the shear connectors are also illustrated in figure 4.4 in comparison with the forces at the first loading.

At the total loading (500th calculation step) the total vertical displacement is 6,64 mm which is practically equal to the result from the first loading. The increment is only 0,002 mm. The comparison of the deflections at each loading step is illustrated in figure 4.3. The black line shows the results at the first loading, the green line represents the results calculated at the second loading. The 500th loading step in the figure means the total vertical load of the structure.

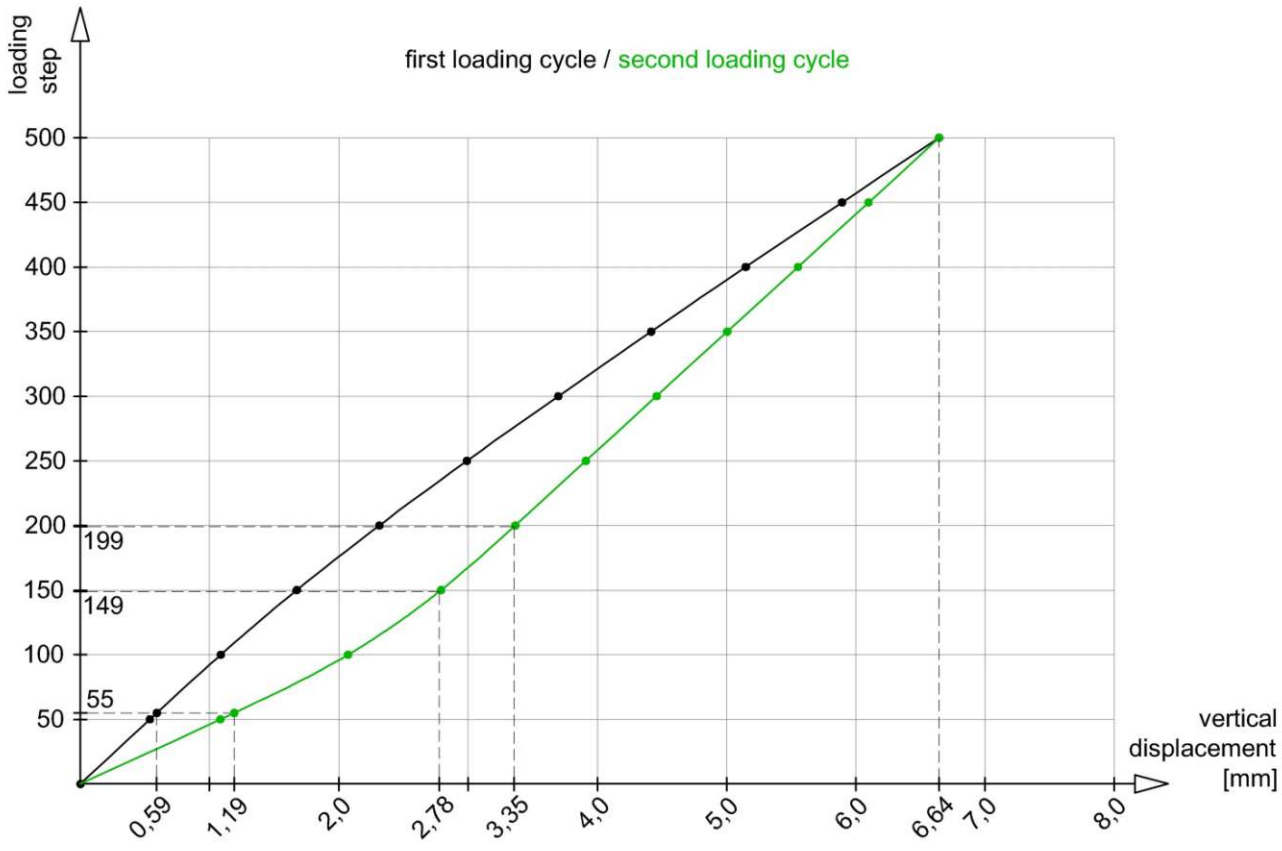

Figure 4.3: Comparison of the vertical displacements at midspan at different loading steps

Figure 4.4: Horizontal forces in the shear connectors of the SCSC-plate in the case of different loading steps at the first and the second load cycles: a) forces in the top steel section; b) forces in the bottom steel section. Dimensions in [mm]

Although vertical displacements occur until the gaps close, after that the greater spring stiffness value (C_{hys}) is used. Therefore, there are no great differences between the total vertical displacements of the first and second loadings. Due to the total second loading, the horizontal forces in the shear connectors do not change significantly compared with the forces in the case of the total first loading (see figure 4.4: loading step 500/500).

The normal forces in the steel plates at the second loading are illustrated in figure 4.5. Correspondingly to the horizontal forces in the shear connectors, the normal forces in the steel plates (see figure 4.5) are also similar to the results at the first loading (see figure 3.37).

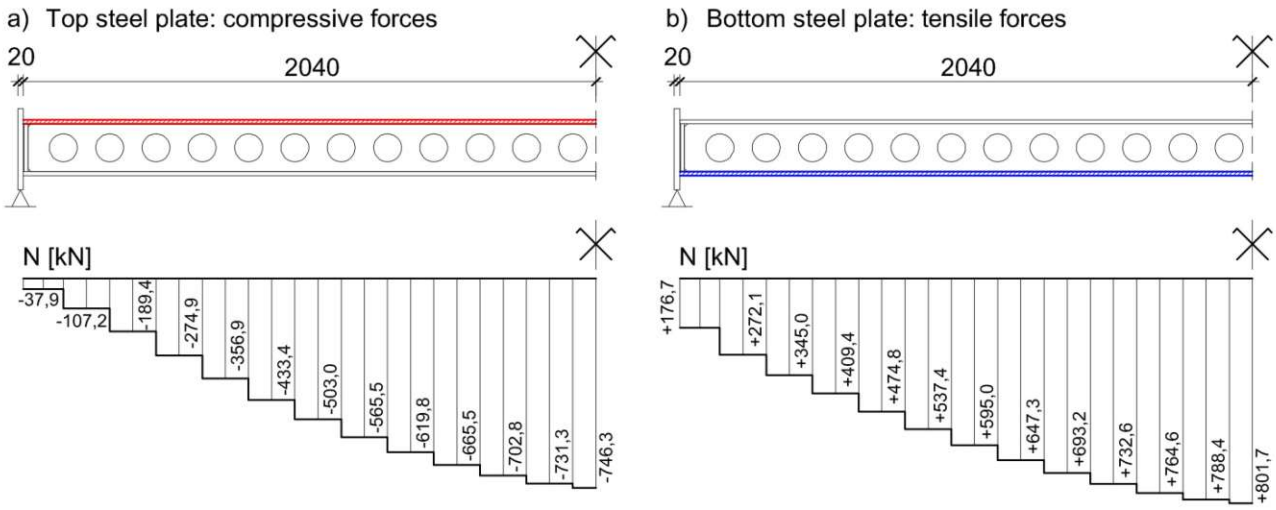

Figure 4.5: Normal forces in the steel plates of the SCSC-plate: a) compressive forces in the top steel plate; b) tensile forces in the bottom steel plate. Dimensions in [mm]

4.2.1.3 Effects from the growth of the inelastic slip after the second load cycle

As mentioned in the chapter 4.1, after the second loading, 100 loading cycles will be modelled additionally with the spring framework model to represent all the 2 million loading cycles. According to the laboratory tests (see chapter 3.2), the total increment of the inelastic slip is 0,139 mm. However, the rounded value (0,14 mm) was illustrated in the previous chapter (see figure 4.1). Logically, at each of the 100 loading cycles in the framework model only 1% of the total increment is used at the shear connectors. However, in the case of small forces in the composite connection (< 25 kN) the inelastic slip is not enlarged with additional increasing slip.

Figure 4.6 illustrates the inelastic slips due to the second and 2 millionth (102th loading in the framework model) loading at each shear connectors. It is noticeable that the inelastic slip values rise significantly through the great number of load changes. However, this effect arises from the results of the laboratory tests which are considered in the framework model calculation. As shown in figure 4.7, the increasing slip is actually the difference between the inelastic slip values illustrated in figure 4.6 at each shear connector. Logically, the maximal value of the increasing slip is 0,139 mm. According to the framework model calculation results, the increasing slip value reaches the maximal value at only six composite connections (see figure 4.7). These maximal values are marked with 100 % in figure 4.7. This indicates that at each of the 100 loading cycles the increment of the increasing slip (0,00139 mm) was added to the current inelastic slip value. Actually, the addition of these increments occurs automatically in MATLAB as the horizontal forces in these six shear connectors exceed 25 kN at each of the 102 loading cycle. As an example, the horizontal forces in the first shear connector of the top steel section are illustrated in figure 4.8(a).

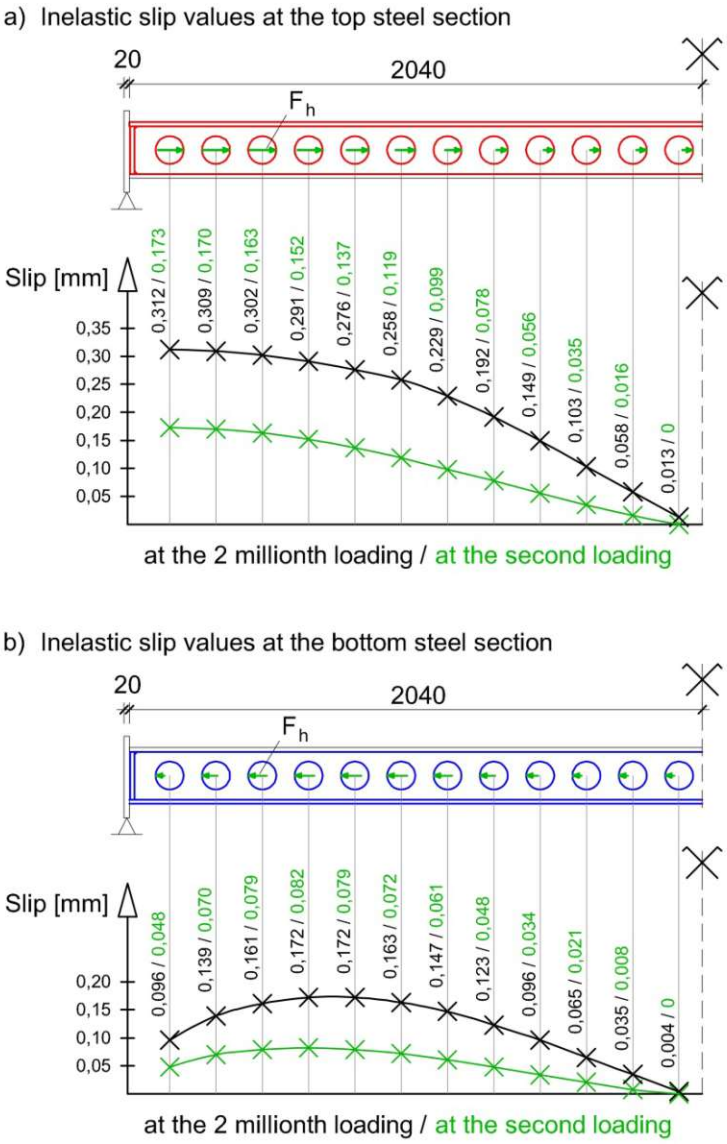

Figure 4.6: Inelastic slips due to the second and 2 millionth loading cycle: a) inelastic slips between the concrete and the shear connectors of the top steel section; b) inelastic slips between the concrete and the shear connectors of the bottom steel section

As an additional example, the ninth shear connector of the top steel section has an increasing slip of 0,093 mm (see figure 4.7(a)). Namely, at 67 loading cycles of the 100 loading cycles the increment of the increasing slip (0,00139 mm) was added to the current inelastic slip value. So, 67 % of the maximal value of the increasing slip is activated after the 2 millionth loading cycle. At each loading cycle it is examined whether the force in the shear connector at the previous loading cycle reached the value of 25 kN. Figure 4.8(b) shows that at the second loading and approximately at the first 29 loading cycles of the 100 loading cycles after the second loading the horizontal force in the composite connection exceeds 25 kN. After the 29th loading cycle, the force fluctuate around 25 kN. This fluctuation is reasonable. If the force failed to reach 25 kN, the inelastic slip would not increase at the next loading cycle. So, this composite connection will be effective earlier which generates a higher force in this shear connector. Earlier means here that the gap at the composite connection closes at a smaller loading step compared to the loading step at the previous loading cycle. If this force exceeded 25 kN again, the inelastic slip would increase at the following loading cycle with the increment of 0,00139 mm. So, at this load cycle the composite connection will be effective later which induces a smaller force in the shear connector. In this way the force will be less than 25 kN again.

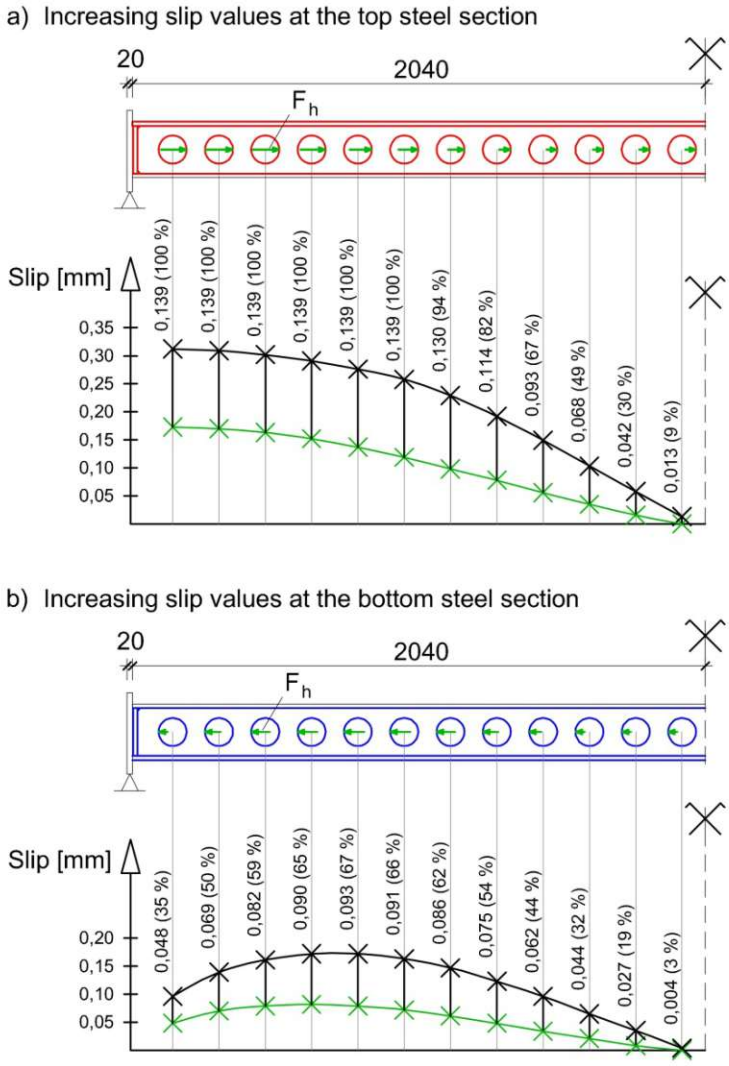

Figure 4.7: Increasing slips due to 2 million load cycle: a) increasing slips between the concrete and the shear connectors of the top steel section; b) increasing slips between the concrete and the shear connectors of the bottom steel section

It is also notable in figures 4.6 and 4.7 that increasing slips occur at each shear connectors. However, in the case of the twelfth shear connectors of the top and bottom steel sections permanent displacements haven't remained after the second loading. Moreover, the forces in these two shear connectors are smaller than 25 kN at the second loading (see figure 4.4). So, at the third loading cycle in the framework model calculation (first loading cycle of the 100 cycles after the second loading) these two composite connections do not include any inelastic slip. However, the horizontal forces in this two shear connectors change due to the additional loading cycles. According to the results, in the case of the top steel section, at the twelfth shear connector the horizontal force is higher than 25 kN at 9 loading cycles. In the case of the bottom steel section, this limit is exceeded at only 3 loading cycles. In this way, small increasing slip values can be emerged at these composite connections, too. So, at the 2 millionth loading cycle the spring framework model consists gaps at each of the 24 shear connectors.

Next, the spring framework model calculation results after the 2 millionth loading are examined. The comparison of the deflections with the results from the first and second loadings is illustrated in figure 4.9 at each loading step. According to the framework model calculation results, the structure has a vertical displacement of 1,70 mm in the middle of the span when the first gap of 24 gaps at the holes of the shear connectors closes. At this point, the 78th calculation step of the 500 calculation steps is activated, which means that actually 15,6 % of the external vertical load is acting. Up to this point, the

horizontal load transfer is not possible at the holes of the shear connectors. In the case of the first loading, at the 78th calculation step the deflection in the middle of the span was only 0,84 mm. Logically, the increased gaps due to 2 million loading cycles induce the increment of the vertical displacement of the structure.

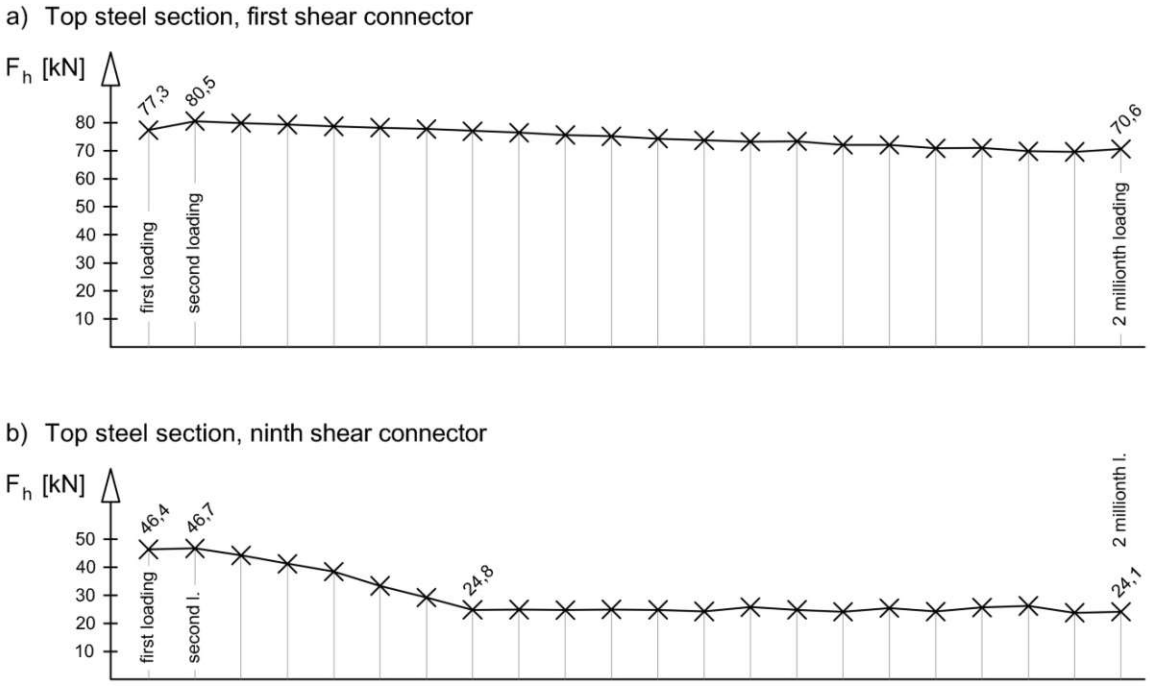

Figure 4.8: Horizontal forces in the shear connectors depending on the loading cycles: a) horizontal forces in the first shear connector of the top steel section; b) horizontal forces in the ninth shear connector of the top steel section

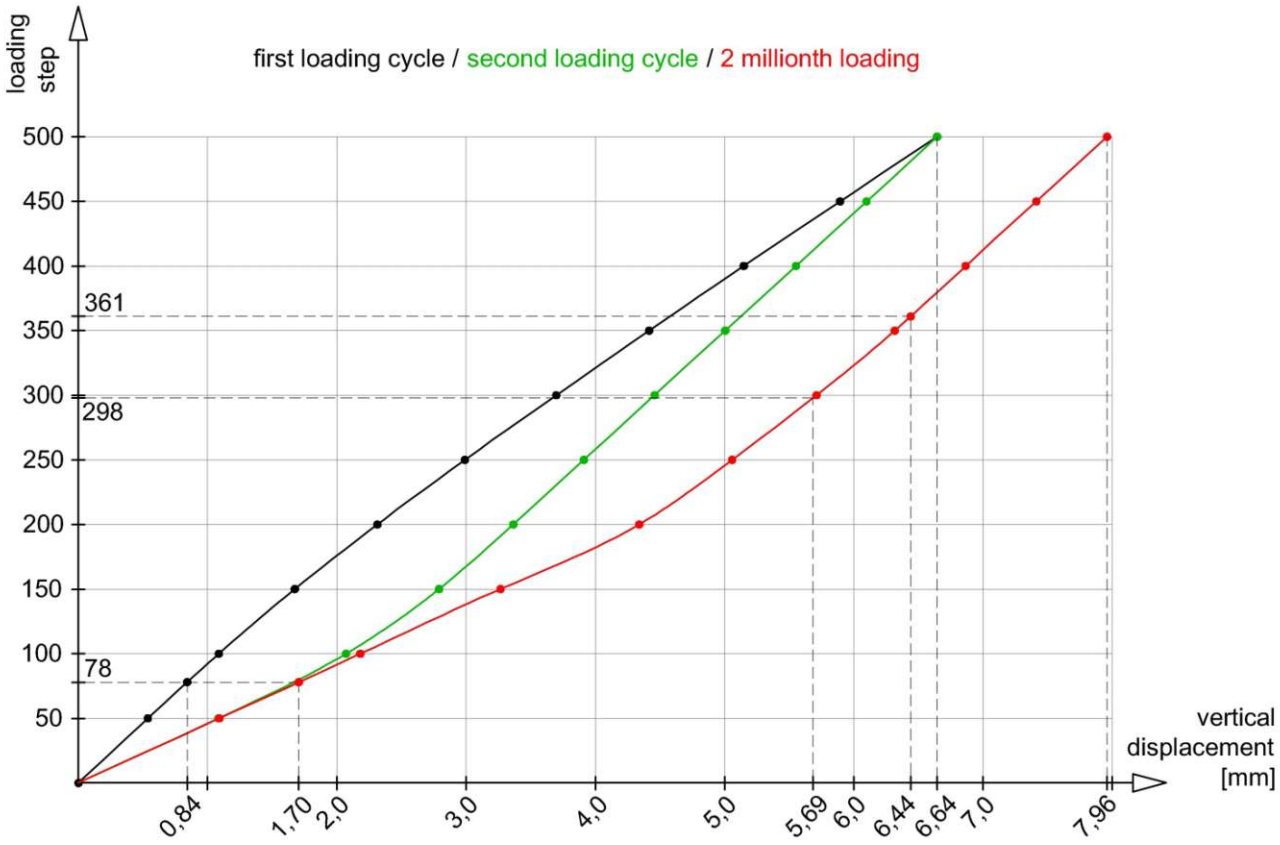

Figure 4.9: Comparison of the vertical displacements at midspan at different loading steps

All the gaps at the holes of the top steel section close when 59,6 % of the external vertical load is effective (298th calculation step). The vertical deflection is 5,69 mm at this loading step (298/500). Figure 4.10 illustrates that only 3 shear connectors of the bottom steel section are activated at this point. Moreover, the horizontal forces in the shear connectors are compared with the forces in the case of the first loading in figure 4.10.

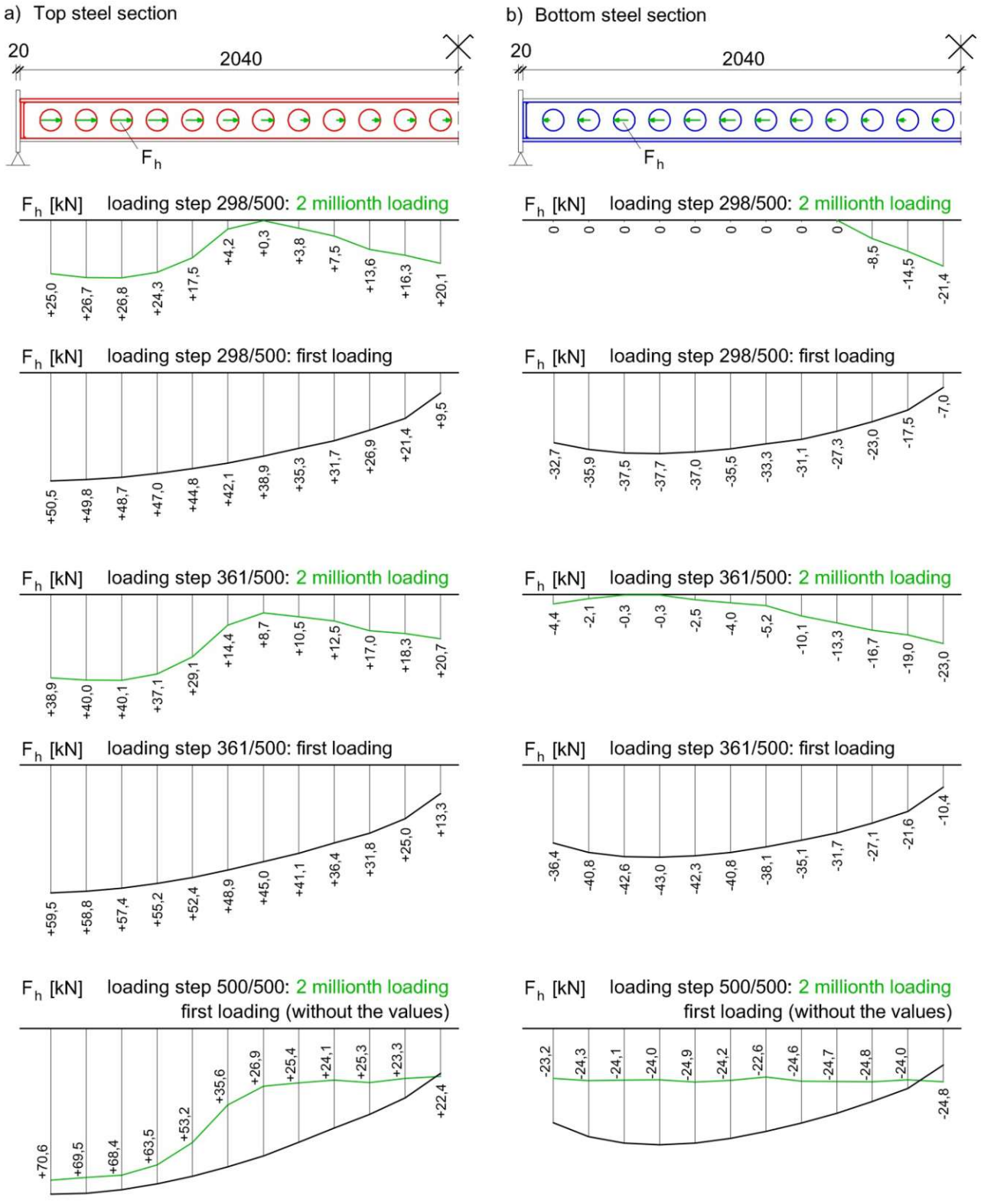

Figure 4.10: Horizontal forces in the shear connectors of the SCSC-plate in the case of different loading steps at the first and the 2 millionth load cycles: a) forces in the top steel section; b) forces in the bottom steel section. Dimensions in [mm]

After this, the gaps at the shear connector of the bottom steel section close by the time that 72,2 % of the load has been reached (361th calculation step). In this case the vertical displacement in the middle of the span is 6,44 mm. The horizontal forces in the shear connectors are also illustrated in figure 4.10 in comparison with the forces at the first loading.

At the total loading (500th calculation step) the total vertical displacement is 7,96 mm. Compared with the deflection due to the first loading, the increment is 1,32 mm, which means a 19,9 % increase (see figure 4.9).

At the 2 millionth loading, the horizontal forces in the shear connectors decrease noticeably compared to the results of the first loading (see figure 4.10: loading step 500/500). The reason of this effect is that the gaps at the holes are enlarged with the value of the increasing slip, so the load transfer between the steel and concrete elements at the shear connectors are effective just for a smaller part of the total external vertical load. Moreover, after the second loading the same spring stiffness value (C_{hys}) is used. So, there is no compensation of the enlarged inelastic slips with greater spring stiffness values, as was the case with the second loading. It is also evident that the top steel section and the bottom steel section do not work together until the first gap closes. These effects of the growth of the inelastic slip after the second loading cycle play a significant role. For instance, in the middle of the span, the normal forces in the steel plates are smaller at the 2 millionth loading (102th loading in the framework model). Figure 4.11 shows the above mentioned decrease of horizontal forces, too. The green line represents the results at the 2 millionth loading, the black line shows the results at the first loading.

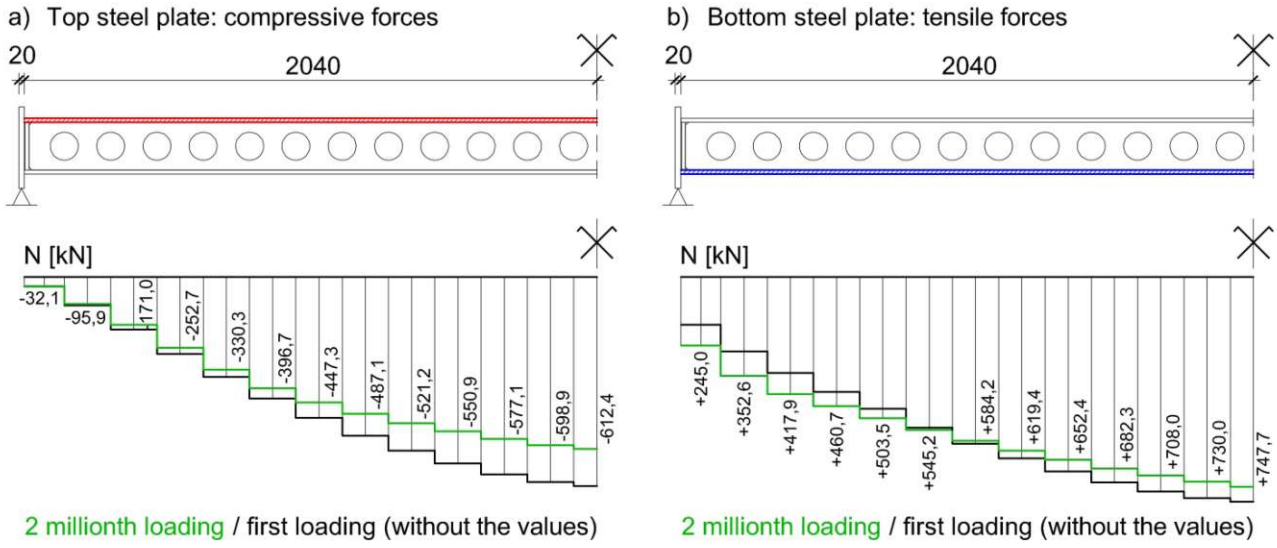

Figure 4.11: Normal forces in the steel plates of the SCSC-plate: a) compressive forces in the top steel plate; b) tensile forces in the bottom steel plate. Dimensions in [mm]

4.2.2 Model with three horizontal concrete layers

4.2.2.1 Introduction

The spring framework model with three horizontal concrete layers is identical with the structure introduced in chapter 3.5.2.1. Moreover, different spring stiffness values are used through the diagram in figure 3.36, as in the case of the previous chapter. The aim of this chapter is to calculate the effects from the cyclic loading with a more precise model compared to the simple model with one concrete beam used in the chapter 4.2.1. Through the model with more concrete layers it will be possible to detect the effects of the increasing slip on the internal forces in the concrete, too.

Figure 4.12 illustrates the total slips and the inelastic slips due to the first loading at each shear connectors. These inelastic slip values will be considered as gaps in the composite connections in the case of the second loading.

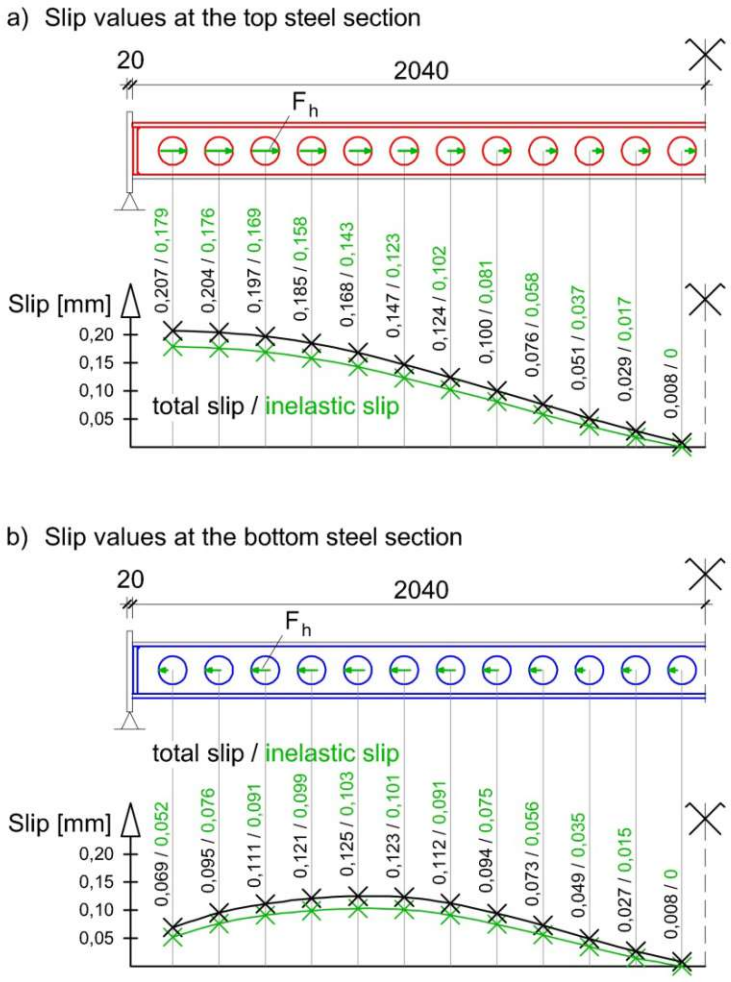

Figure 4.12: Total slips and inelastic slips due to the first loading cycle: a) slips between the concrete and the shear connectors of the top steel section; b) slips between the concrete and the shear connectors of the bottom steel section

The inelastic slip values are calculated from the total slip at each composite connection. However, in the case of the two composite connections, where the horizontal forces are smaller than 25 kN (see figure 3.40), the inelastic slips are defined zero without any calculation. So, as in the case of the model with one horizontal concrete beam (see chapter 4.2.1.1), gap elements are modelled at only 22 composite connections of the structure.

4.2.2.2 Effects due to the second load cycle

In this chapter, the spring framework model calculation results of the second loading are examined. According to the framework model calculation results, the structure has a vertical displacement of 1,23 mm in the middle of the span when the first gap of 22 gaps at the holes of the shear connectors closes. At this point, the 56th calculation step of the 500 calculation steps is activated, which means that actually 11,2 % of the external vertical load is acting. Up to this point, the horizontal load transfer is only possible at the two holes of the shear connectors where the inelastic slips were defined zero (see figure 4.12). In the case of the first loading, at the 56th calculation step the deflection in the middle of the span was only 0,60 mm. Logically, the transfer of forces between the steel and the concrete material was better at the first loading. Actually, the gaps at the second loading induce the increment of the vertical displacement of the structure.

All the gaps at the holes of the top steel section close when 31,8 % of the external vertical load is effective (159th calculation step). The vertical deflection is 2,98 mm at this loading step (159/500). Figure 4.14 illustrates that only 2 shear connectors of the bottom steel section are activated at this point. Moreover, the horizontal forces in the shear connectors are compared with the forces in the case of the first loading in figure 4.14.

After this, the gaps at the shear connector of the bottom steel section close by the time that 48,6 % of the load has been reached (243th calculation step). In this case the vertical displacement in the middle of the span is 4,07 mm. The horizontal forces in the shear connectors are also illustrated in figure 4.14 in comparison with the forces at the first loading.

At the total loading (500th calculation step) the total vertical displacement is 7,22 mm which is practically equal to the result from the first loading. The increment is only 0,003 mm. The comparison of the deflections at each loading step is illustrated in figure 4.13. The black line shows the results at the first loading, the green line represents the results calculated at the second loading. The 500th loading step in the figure means the total vertical load of the structure.

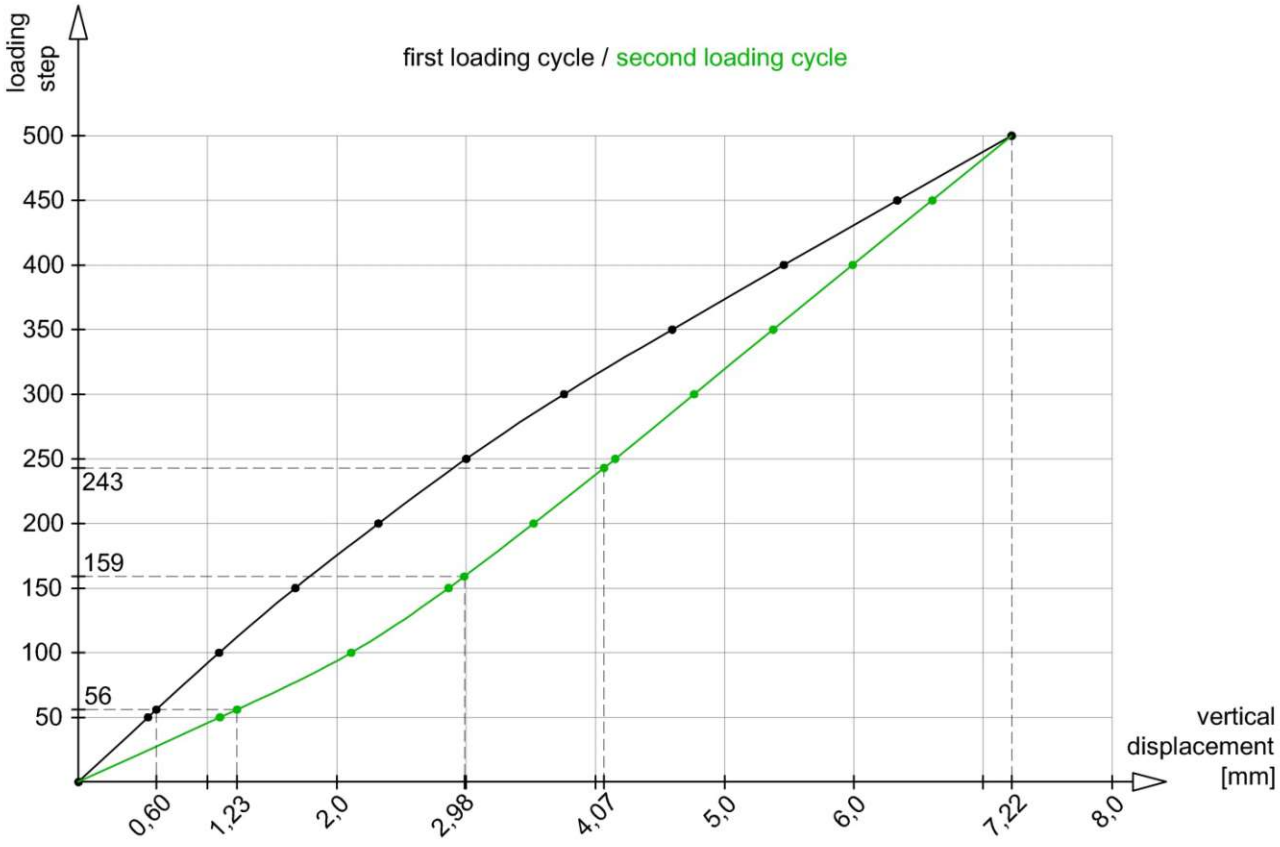

Figure 4.13: Comparison of the vertical displacements at midspan at different loading steps

Although vertical displacements occur until the gaps close, after that the greater spring stiffness value (C_{hys}) is used. Therefore, there are no great differences between the total vertical displacements of the first and second loadings. Due to the total second loading, the horizontal forces in the shear connectors do not change significantly compared with the forces in the case of the total first loading (see figure 4.14: loading step 500/500). So, the model with three horizontal concrete layers has the similar behaviour as the model with only one concrete layer examined in chapter 4.2.1.2.

The normal forces in the concrete layers are illustrated in figure 4.15. Correspondingly to the horizontal forces in the shear connectors, these normal forces in the concrete are also similar to the results at the first loading (see figure 4.15).

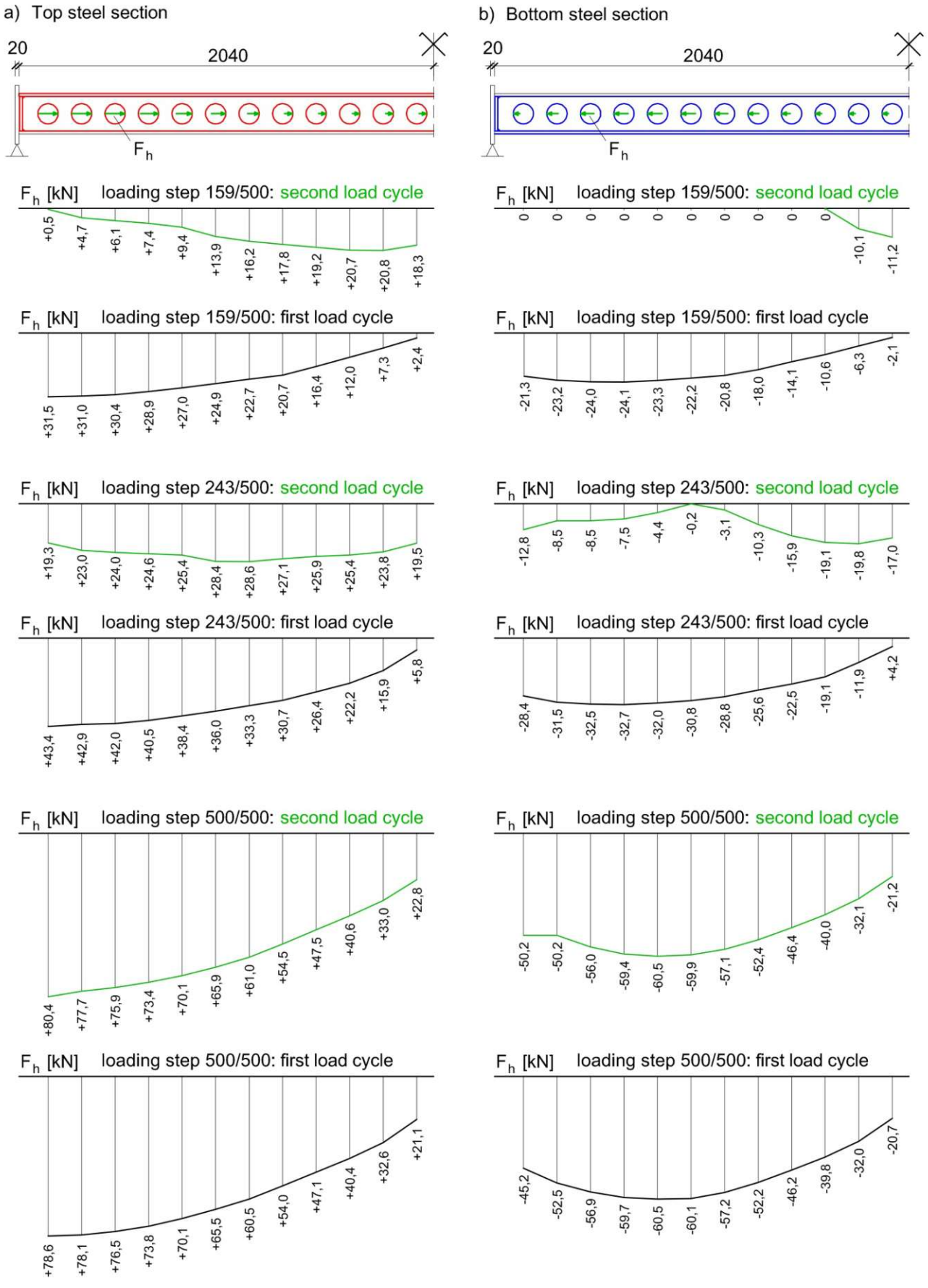

Figure 4.14: Horizontal forces in the shear connectors of the SCSC-plate in the case of different loading steps at the first and the second load cycles: a) forces in the top steel section; b) forces in the bottom steel section. Dimensions in [mm]

As shown in figure 4.15, the horizontal forces have a constant value of 190,4 kN around the area of the middle of the span in the lower horizontal concrete beam. The reason for this fact is that the tensile stress reaches here the ultimate tensile strength of the concrete. Therefore, the bearable loads of the concrete beams are limited in the spring framework model with the maximal tensile force of 190,4 kN.

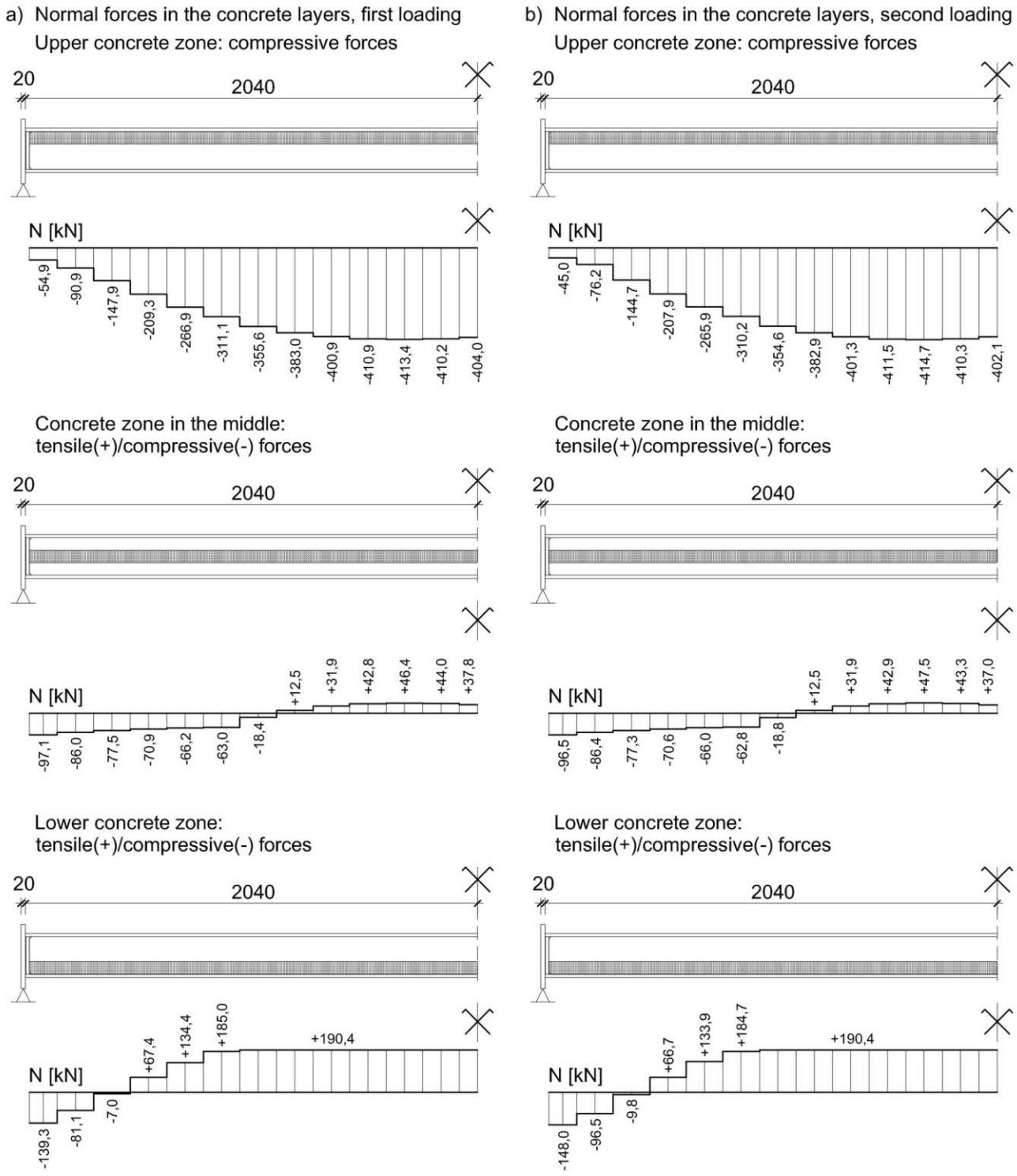

Figure 4.15: Normal forces in the concrete layers of the SCSC-plate: a) first loading; b) second loading. Dimensions in [mm]

The normal forces in the steel plates at the second loading are illustrated in figure 4.16. Logically, these forces are also similar to the results detected at the first loading (see figure 3.39).

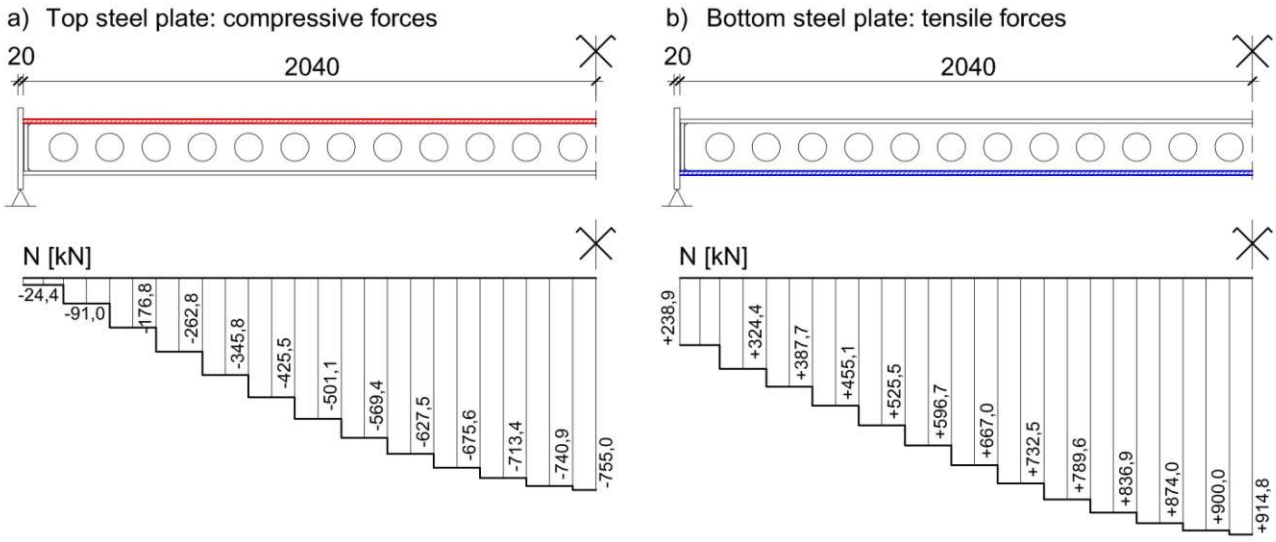

Figure 4.16: Normal forces in the steel plates of the SCSC-plate: a) compressive forces in the top steel plate; b) tensile forces in the bottom steel plate. Dimensions in [mm]

4.2.2.3 Effects from the growth of the inelastic slip after the second load cycle

Accordance with the chapter 4.2.1.3, after the second loading, the loading cycles until 2 millionth loading are represented with 100 loading cycles in the framework model. At each of the 100 loading cycles in the framework model only 1% of the increment of the total increment is used at the shear connectors. However, in the case of small forces in the composite connection (< 25 kN) the inelastic slip is not enlarged with additional increasing slip. Figure 4.17 illustrates the inelastic slips due to the second and 2 millionth (102th loading in the framework model) loading at each shear connectors. It is noticeable that the inelastic slip values rise significantly through the great number of load changes. However, this effect arises from the results of the laboratory tests which are considered in the framework model calculation. The increasing slip (see figure 4.18) is the difference between the inelastic slip values illustrated in figure 4.17 at each shear connector. As in the case of the model with one concrete beam, the maximal value of the increasing slip is 0,139 mm. According to the framework model calculation results, the increasing slip value reaches the maximal value at only eight composite connections (see figure 4.18). These maximal values are marked with 100 % in figure 4.18. This indicates that at each of the 100 loading cycles the increment of the increasing slip (0,00139 mm) was added to the current inelastic slip value.

As an example, the horizontal forces in the first shear connector of the top steel section are illustrated in figure 4.19(a). Here, the horizontal forces exceed 25 kN at each loading cycle. Logically, the increasing slip reaches the maximal value (0,139 mm).

The ninth shear connector of the top steel section has an increasing slip of 0,098 mm (see figure 4.18(a)). Namely, at 70 loading cycles of the 100 loading cycles the increment of the increasing slip (0,00139 mm) was added to the current inelastic slip value. So, 70 % of the maximal value of the increasing slip is activated after 2 millionth loading cycles. At each loading cycle it is examined whether the force in the shear connector at the previous loading cycle reached the value of 25 kN. Figure 4.19(b) shows that at the second loading and approximately at the first 30 loading cycles of the 100 loading cycles after the second loading the horizontal force in the composite connection exceeds 25 kN. After the 30th loading cycle, the force fluctuate around 25 kN. The reason of this fluctuation was described in chapter 4.2.1.3.

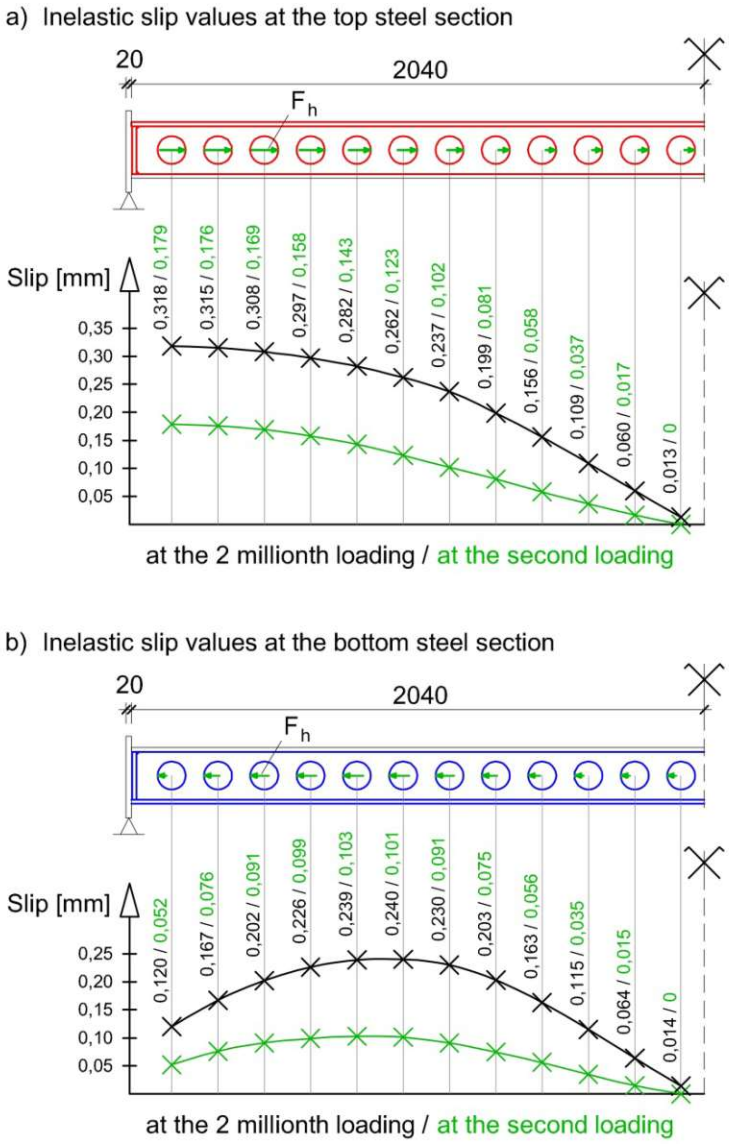

Figure 4.17: Inelastic slips due to the second and 2 millionth loading cycle: a) inelastic slips between the concrete and the shear connectors of the top steel section; b) inelastic slips between the concrete and the shear connectors of the bottom steel section

It is also notable in figures 4.17 and 4.18 that increasing slips occur at each shear connectors. However, in the case of the twelfth shear connectors of the top and bottom steel sections permanent displacements have not remained after the second loading. Moreover, the forces in these two shear connectors are smaller than 25 kN at the second loading (see figure 4.14). So, at the third loading cycle in the framework model calculation (first loading cycle of the 100 cycles after the second loading) these two composite connections do not include any inelastic slip. However, the horizontal forces in this two shear connectors change through the additional loading cycles. According to the results, in the case of the top steel section, at the twelfth shear connector the horizontal force is higher than 25 kN at 9 loading cycles. In the case of the bottom steel section, this limit is exceeded at 10 loading cycles. In this way, small increasing slip values can be emerged at these composite connections, too. So, at the 2 millionth loading cycle the spring framework model consists gaps at each of the 24 shear connectors.

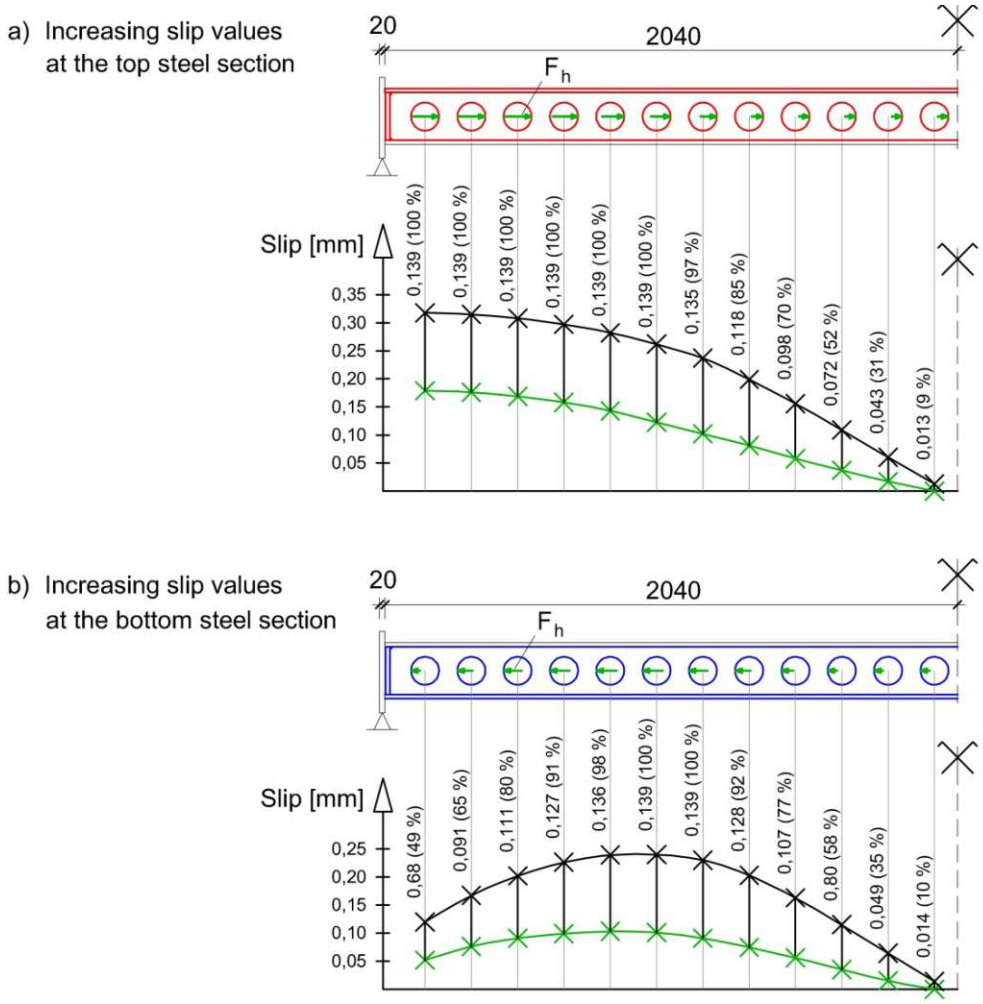

Figure 4.18: Increasing slips due to 2 million load cycle: a) increasing slips between the concrete and the shear connectors of the top steel section; b) increasing slips between the concrete and the shear connectors of the bottom steel section

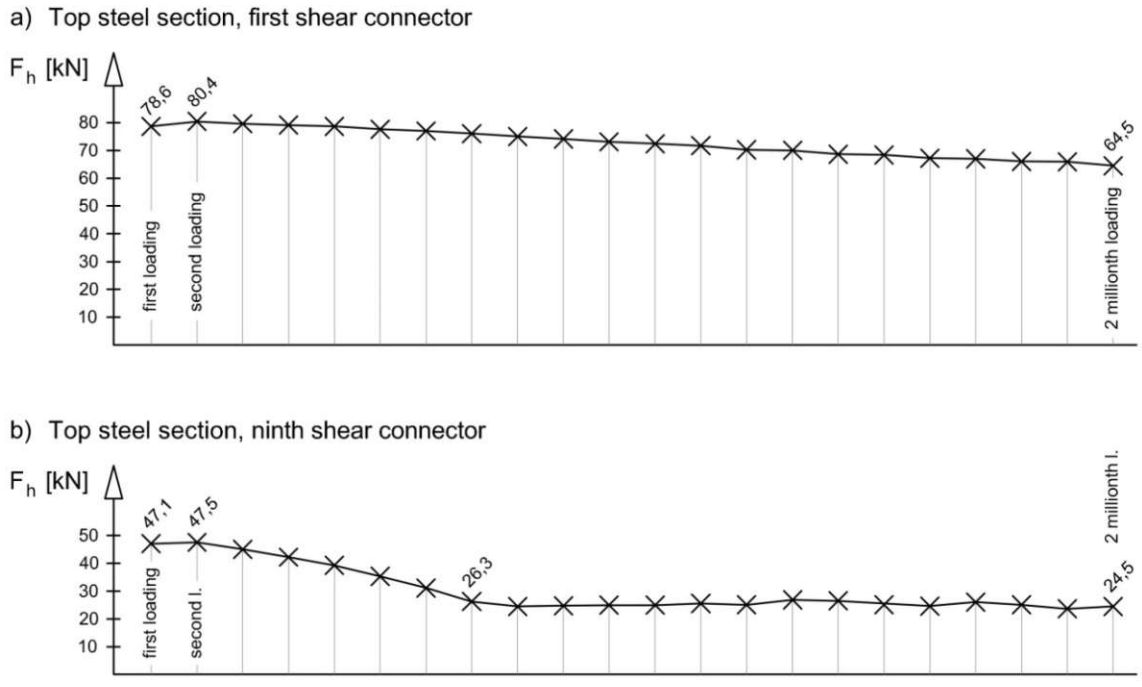

Figure 4.19: Horizontal forces in the shear connectors depending on the loading cycles: a) horizontal forces in the first shear connector of the top steel section; b) horizontal forces in the ninth shear connector of the top steel section

Next, the spring framework model calculation results after the 2 millionth loading are examined. The comparison of the deflections with the results from the first and second loadings is illustrated in figure 4.20 at each loading step. According to the framework model calculation results, the structure has a vertical displacement of 2,60 mm in the middle of the span when the first gap of 24 gaps at the holes of the shear connectors closes. At this point, the 118th calculation step of the 500 calculation steps is activated, which means that actually 23,6 % of the external vertical load is acting. Up to this point, the horizontal load transfer is not possible at the holes of the shear connectors. In the case of the first loading, at the 118th calculation step the deflection in the middle of the span was only 1,30 mm. Logically, the increased gaps due to 2 million loading cycles induce the increment of the vertical displacement of the structure.

All the gaps at the holes of the top steel section close when 61,2 % of the external vertical load is effective (306th calculation step). The vertical deflection is 6,38 mm at this loading step (306/500). Figure 4.21 illustrates that only 2 shear connectors of the bottom steel section are activated at this point. Moreover, the horizontal forces in the shear connectors are compared with the forces in the case of the first loading in figure 4.21.

After this, the gaps at the shear connector of the bottom steel section close by the time that 79,2 % of the load has been reached (396th calculation step). In this case the vertical displacement in the middle of the span is 7,74 mm. The horizontal forces in the shear connectors are also illustrated in figure 4.21 in comparison with the forces at the first loading. At the total loading (500th calculation step) the total vertical displacement is 9,03 mm. Compared with the deflection due to the first loading, the increment is 1,81 mm, which means a 25,1 % increase (see figure 4.20).

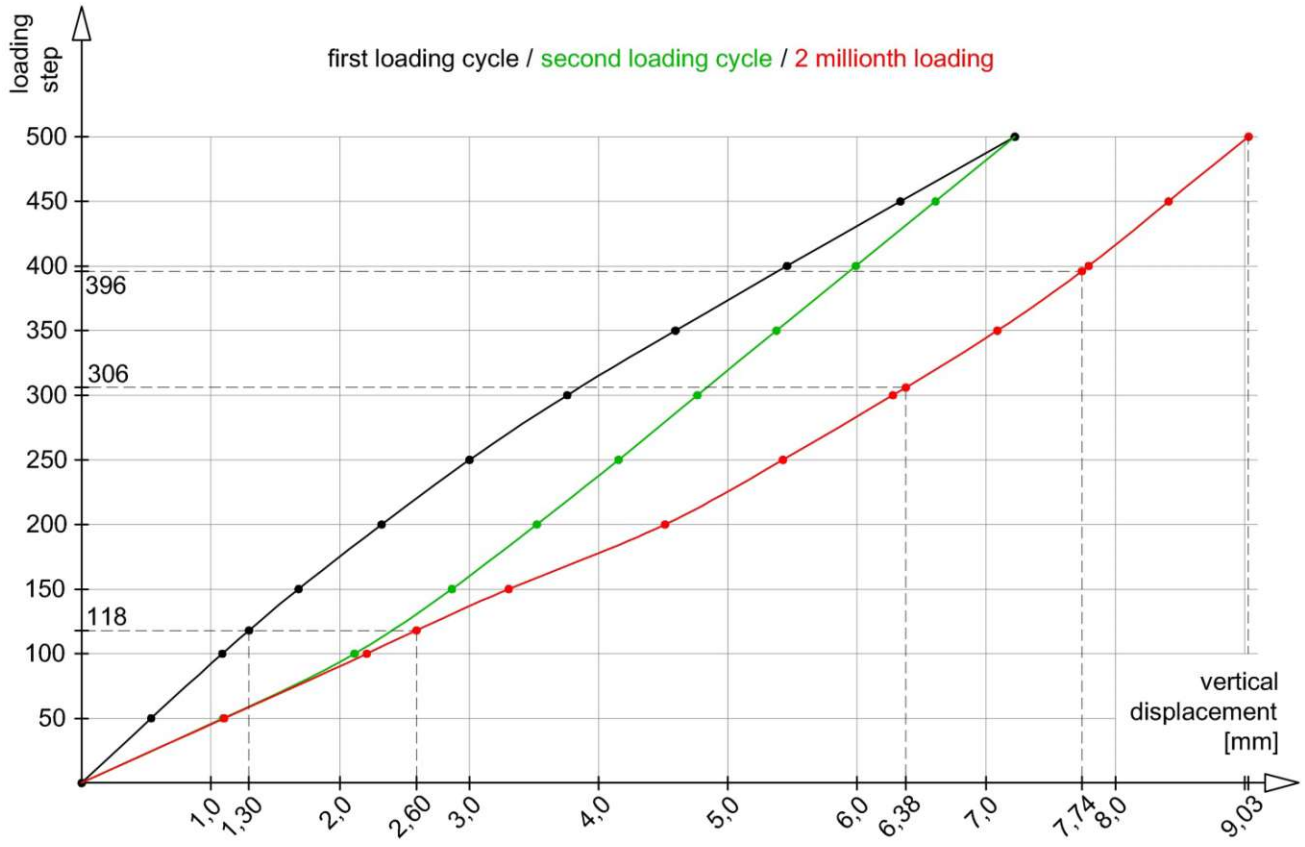

Figure 4.20: Comparison of the vertical displacements at midspan at different loading steps

At the 2 millionth loading, the horizontal forces in the shear connectors decrease noticeably compared to the results of the first loading (see figure 4.21: loading step 500/500). The reason of this effect is that the gaps at the holes are enlarged with the value of the increasing slip, so the load transfer between the steel and concrete elements at the shear connectors

are effective just for a smaller part of the total external vertical load. Moreover, after the second loading the same spring stiffness value (C_{hys}) is used. So, there is no compensation of the enlarged inelastic slips with greater spring stiffness values, as was the case with the second loading.

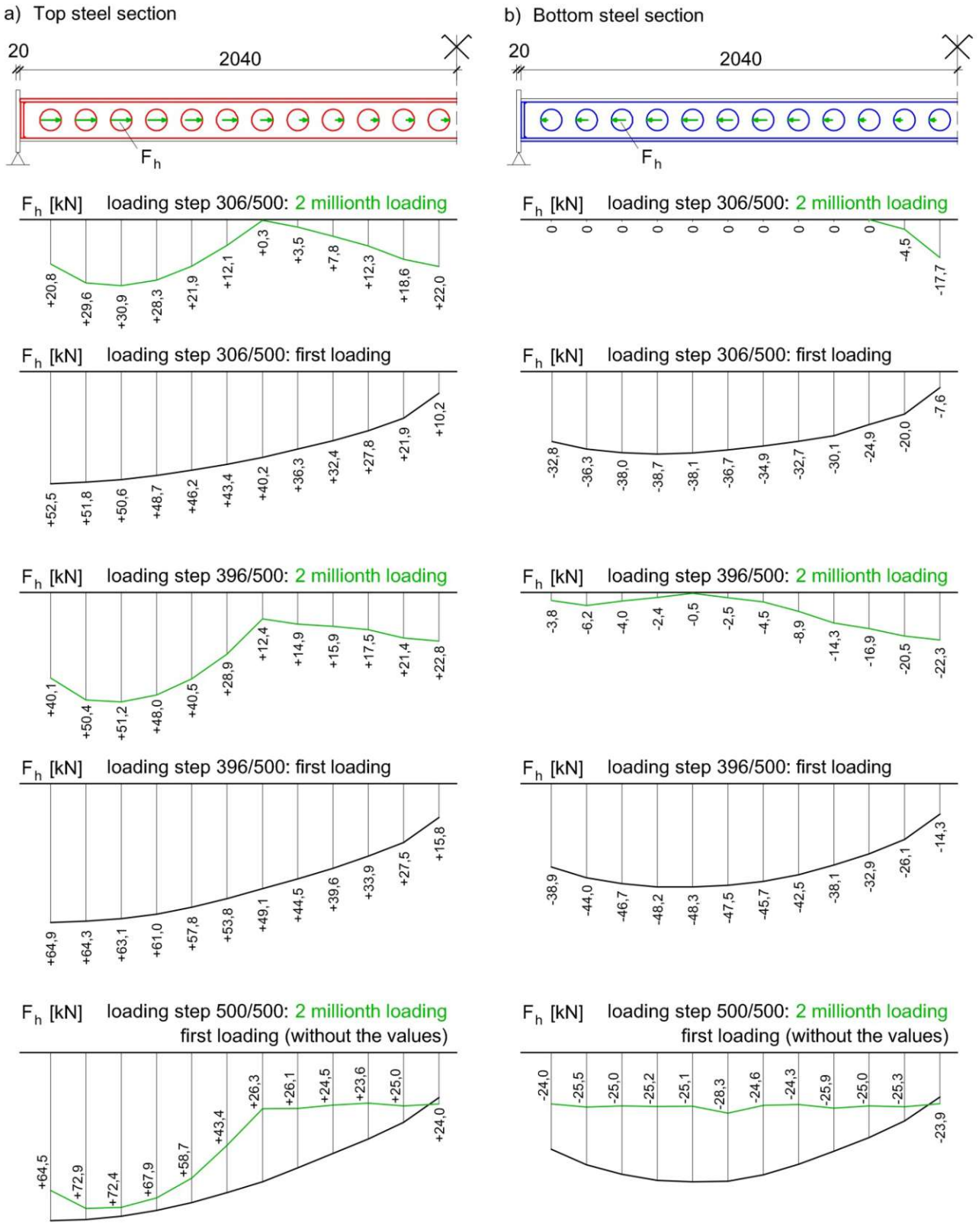

Figure 4.21: Horizontal forces in the shear connectors of the SCSC-plate in the case of different loading steps at the first and the 2 millionth load cycles: a) forces in the top steel section; b) forces in the bottom steel section. Dimensions in [mm]

The top steel section and the bottom steel section do not work together until the first gap closes. This effect of the growth of the inelastic slip after the second loading cycle plays a significant role. For instance, in the middle of the span, the normal forces in the concrete are lager at the 2 millionth loading (102th loading in the framework model). Figure 4.22 illustrates the normal forces in the horizontal concrete layers.

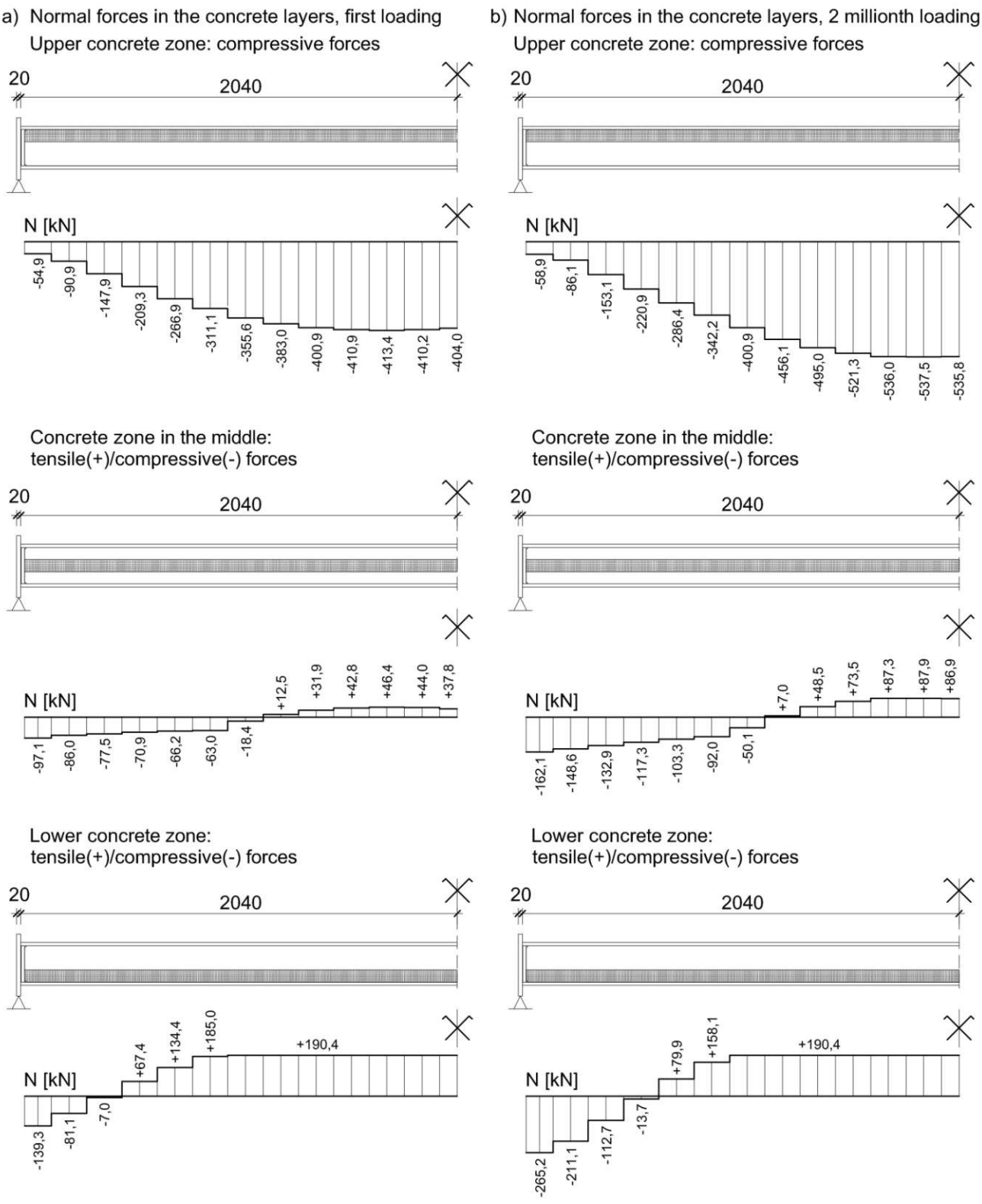

Figure 4.22: Normal forces in the concrete layers of the SCSC-plate: a) first loading; b) 2 millionth loading. Dimensions in [mm]

Compared to the first loading, the framework model delivers a higher result (535,8 kN) in the upper horizontal compressed concrete zone in the middle of the span (see figure 4.22), with an increase of 32,6 %. The lower and middle horizontal concrete beams together have a resulting tensile force of 277,3 kN, which means an increase of 21,5 %.

In the framework model, according to the ABAQUS results in the case of static loads, the tensile strength of concrete is not reduced by concrete cracking. However, as shown above, the horizontal tensile forces in the concrete increase significantly through the increasing slip. Therefore, it would be useful to evaluate the effects from cracking of concrete with an expansion of the presented framework model.

Finally, figure 4.23 shows that the normal forces in the steel plates are smaller at the 2 millionth loading (102th loading in the framework model) in the middle of the span compared to the forces at the first loading.

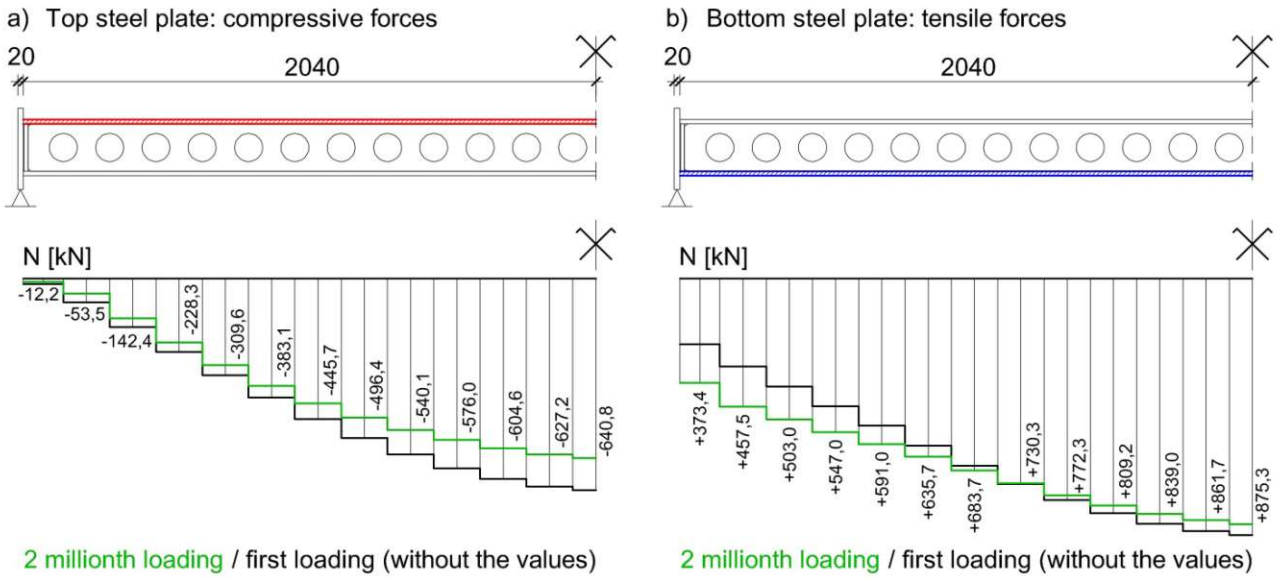

Figure 4.23: Normal forces in the steel plates of the SCSC-plate: a) compressive forces in the top steel plate; b) tensile forces in the bottom steel plate. Dimensions in [mm]

4.3 Comparison of results

In chapter 4.2.1 the model with one horizontal concrete beam was analysed. The results with the more precise model with three horizontal concrete beams were demonstrated in the chapter 4.2.2. Finally, in this chapter, the results of these two different models will be compared.

The comparison of the deflections at each loading step is illustrated in figure 4.24 in the case of the second loading. The black line shows the results from the model with one horizontal concrete beam, the green line represents the results calculated from the model with three horizontal concrete layers. At the 500th loading step the total vertical load of the structure is shown in the figure. At this point, the deflection with the simple model with one concrete beam is 6,64 mm. The more detailed model with three concrete layers indicates a vertical displacement of 7,22 mm. The 0,58 mm difference between the results indicates actually that the model with one concrete beam reflects an increased stiffness compared to the model with three concrete layers. This fact is reasonable as the moment capacity of the concrete beam isn't limited in the framework model. Actually, as an approximation, only the bearable normal forces of the concrete beams are limited with the maximal tensile force calculated from the ultimate tensile strength of the concrete. However, the bending moment in a beam element induces tensile stress additionally, which is not checked in the framework model. In the case of the model with one horizontal concrete beam the tensile force does not exceed the limit value. So the calculation runs

without any limitation of the concrete beams. However, the high moment in the concrete section produce higher tensile stress than the tensile strength of the concrete. In this way, the resistance of the concrete modelled in the framework model is higher than the reality. The model with three horizontal concrete layers gives a better approximation for the real behaviour of concrete. Namely, the tensile forces in the lower concrete zone are limited in several horizontal concrete beams (see figures 4.15 and 4.22). Due to the bending moment transferred in the beams, the tensile stress exceeds the tensile strength of the concrete in the case of the model with three horizontal concrete layers, too. The difference between the tensile stress and strength, which means actually the failure from the approximation used in the framework model, is much less than in the case of the model with one horizontal concrete beam. So, the strength of the concrete core modelled with three concrete layers is logically smaller than the strength in the case of the model with one concrete beam. This induces higher vertical displacements of the structure at the model with three concrete layers. Logically, if the concrete core was divided into more than three horizontal layers, the above mentioned failure would be lower.

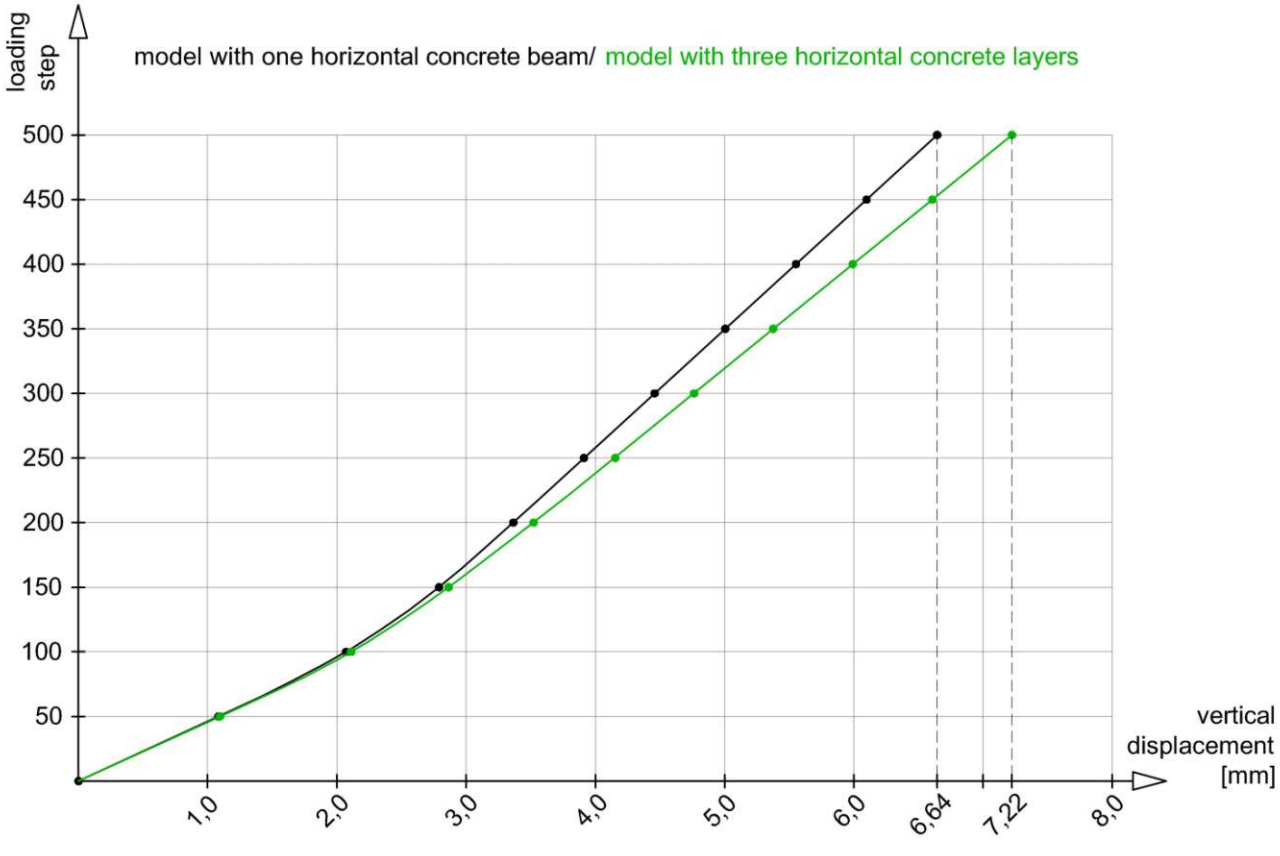

Figure 4.24: Comparison of the vertical displacements of the two models at midspan in the case of the second loading

In the case of the 2 millionth loading the total deflection with the simple model with one concrete beam is 7,96 mm (see figure 4.25). The more detailed model with three concrete layers indicates a vertical displacement of 9,03 mm. The difference of 1,07 mm between the results indicates again that the model with one concrete beam reflects an increased stiffness compared to the model with three concrete layers. The explanation of this fact was described above.

Figure 4.26 illustrates that both of the models delivers similar horizontal forces in the shear connectors in the case of the 2 millionth loading. In the case of the first and the second loading the results are also corresponding. This means that the simple model with one horizontal concrete beam is also appropriate to evaluate the forces in the composite connections. Moreover, it is clear to see that the horizontal forces in the shear connectors do not decrease largely 25 kN. So, in the

framework model used limit value (25 kN) for the consideration of inelastic slips plays a significant role relating to the forces in the composite connections.

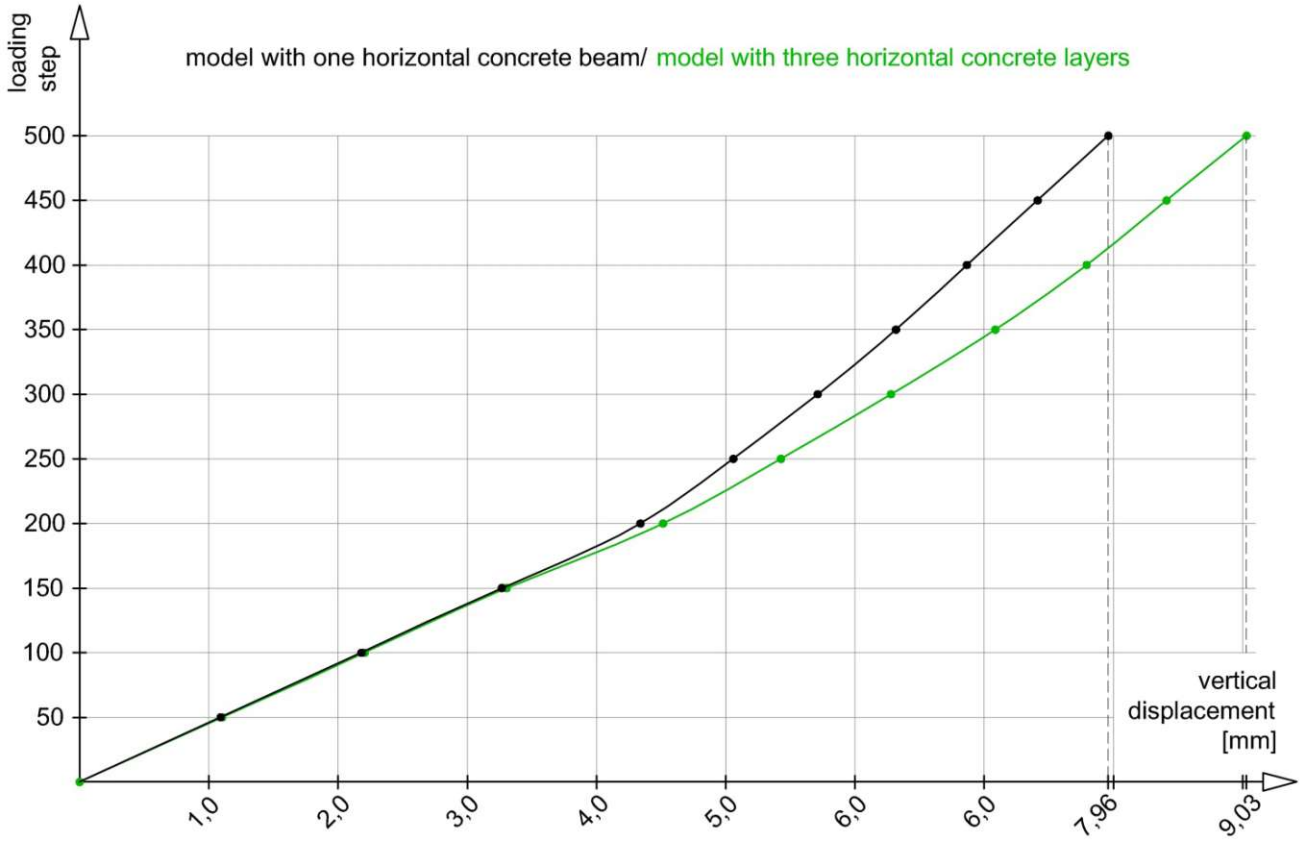

Figure 4.25: Comparison of the vertical displacements of the two models at midspan in the case of the 2 millionth loading

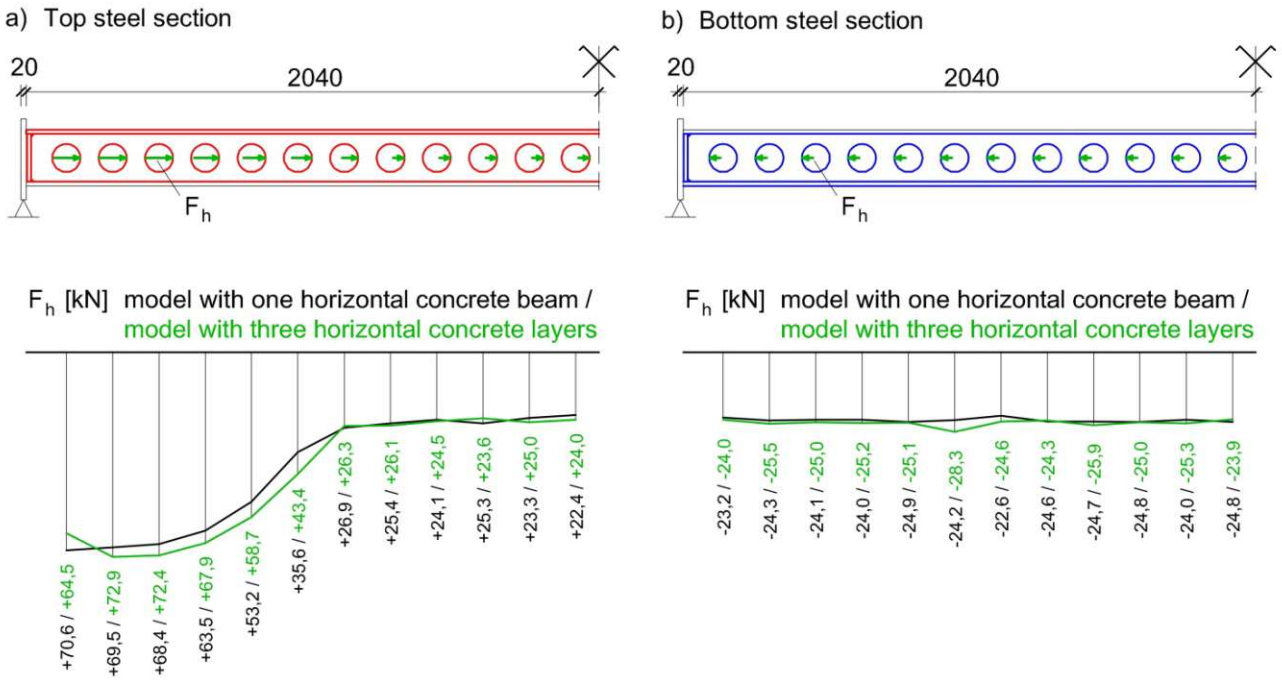

Figure 4.26: Comparison of the horizontal forces in the shear connectors of the two models at the 2 millionth loading: a) forces in the top steel section; b) forces in the bottom steel section. Dimensions in [mm]

4.4 Flowchart of the MATLAB code

Finally, the structure diagram of the spring framework model calculation is shown in this chapter. Actually, the flowchart represents the MATLAB code referring to the framework models in chapter 4. The differences between the model with one horizontal concrete beam (chapter 4.2.1) and the model with three horizontal concrete layers (chapter 4.2.2) cannot be detected in the flowchart because only the data input (geometry) is different. Figure 4.27 illustrates the structure diagram for the first loading. Figure 4.28 shows the diagram for the second loading. At last, figure 4.29 represents the chart in the case of the third loading. The third loading demonstrates 2 million loading cycles after the second loading cycle. Logically, the three charts are connected to each other as the results of the first loading are required for the additional calculations.

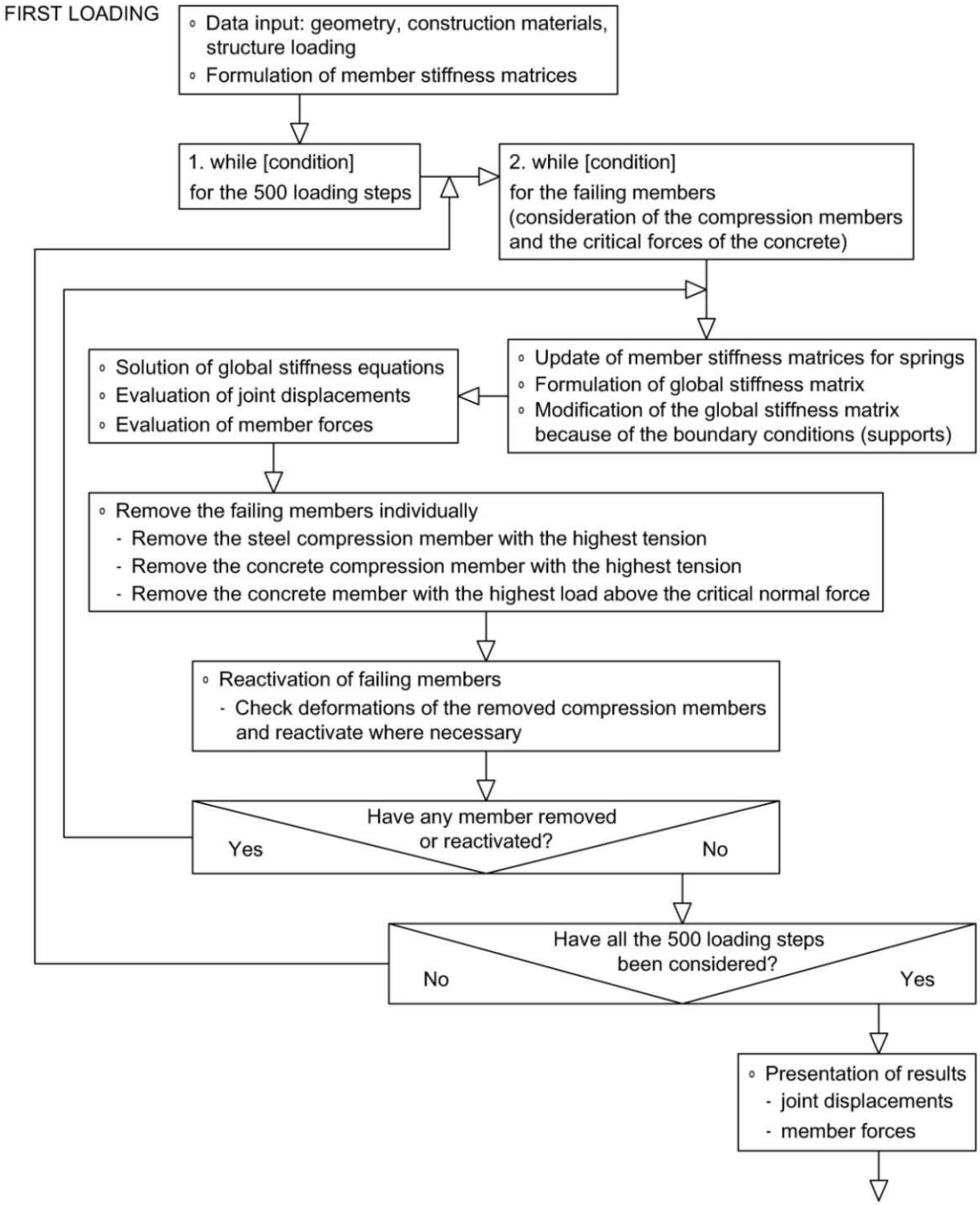

Figure 4.27: Flowchart of the MATLAB code: part 1/3 (first loading)

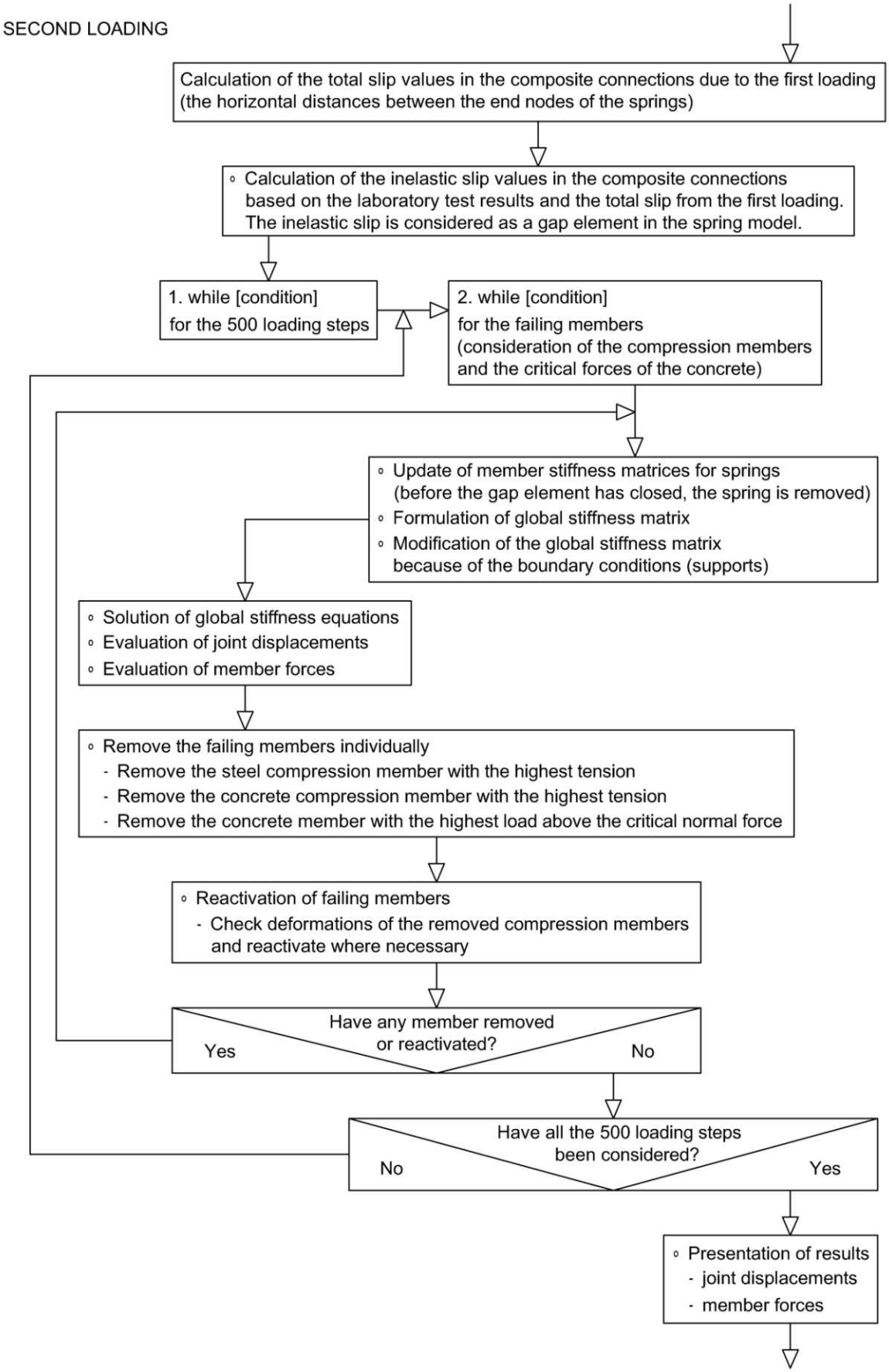

Figure 4.28: Flowchart of the MATLAB code: part 2/3 (second loading)

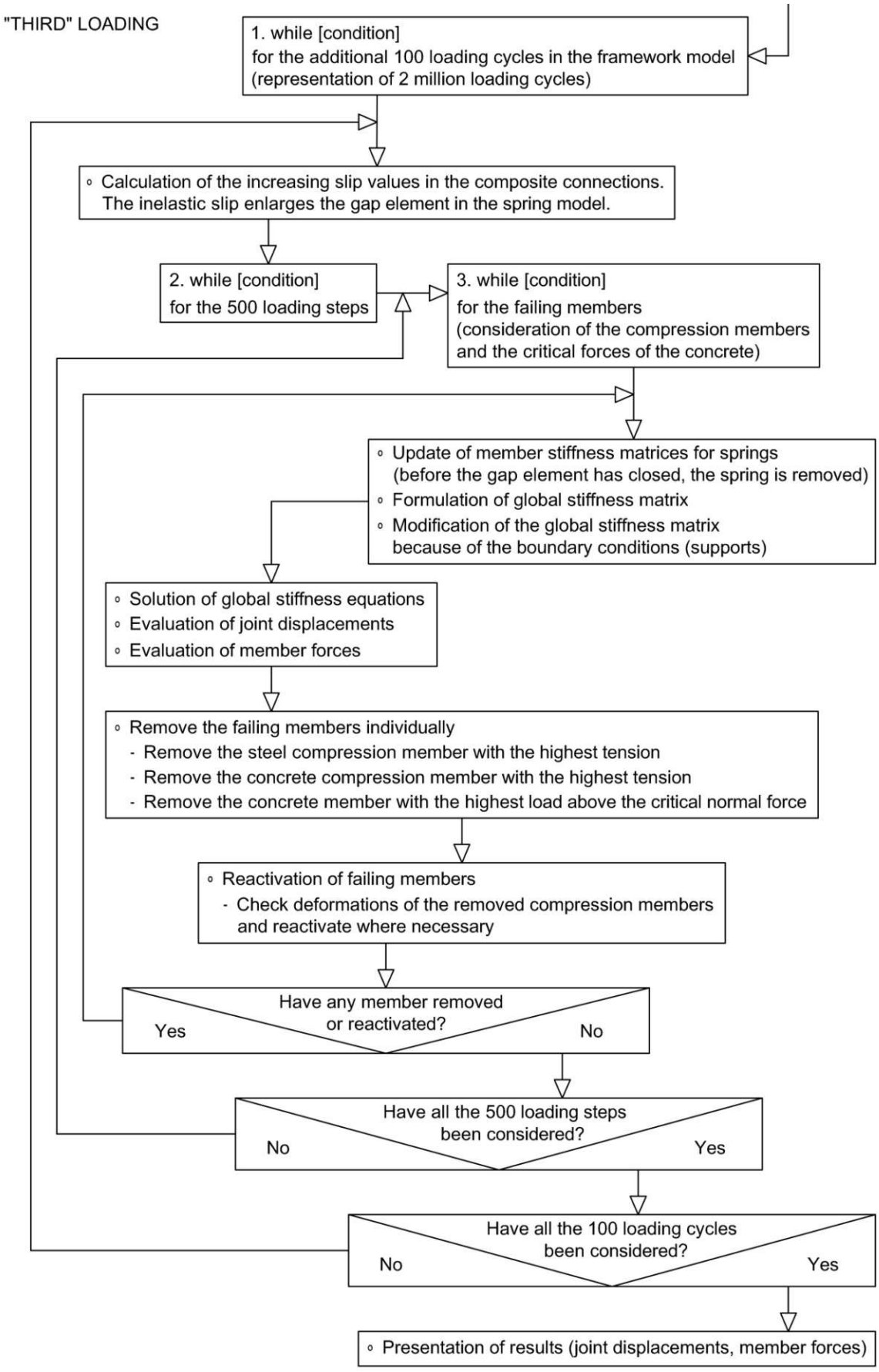

Figure 4.29: Flowchart of the MATLAB code: part 3/3 (“third” loading)

4.5 Conclusion

As shown in chapter 4, cyclic loading can be considered with the two-dimensional spring framework model. As a complex ABAQUS model is not applicable for the fatigue analysis, the framework model calculation is the only solution to get important information about the load-bearing behaviour of the SCSC-plate in the case of the high number of cycles. Thus, the presented spring framework model is appropriate for the engineering practice to analyse composite structures.

Based on the laboratory tests described in chapter 3.2, increasing inelastic slips arise in the composite connections due to the cyclic loading. This effect, which means actually the cyclic creep of the concrete, is modelled with the gap elements in the spring framework model. Fatigue investigations on composite beams [21] have demonstrated that the consideration of fatigue damage in the shear connectors has positive consequences, too. Namely, the forces in the composite connections are redistributed towards the less stressed connections. Figure 4.21 illustrates that this advantage exists also in the case of the SCSC plate: the maximal horizontal force in the shear connectors decrease by 7,3 % due to the 2 million loading cycles in the case of the spring framework model with three horizontal concrete layers.

In contrast to composite beams, negative consequences arise also from the inelastic slip increments in the case of the SCSC plate. The maximal vertical displacement in the middle of the span increase significantly by 25,1 %. However, the increment is only 1,81 mm. Moreover, the stresses of the concrete are lager at the 2 millionth loading (102th loading in the framework model) compared to the first loading (see figure 4.22). This conclusion is reasonable. According to the results of the framework model with three concrete layers at the 2 millionth loading, 23,6 % of the external vertical load is acting when the first gap of 24 gaps at the holes of the shear connectors closes. Until this point, the top steel section and the bottom steel section do not work together, so the concrete beam has to carry most of the external load.

It was shown in chapter 3 that ABAQUS detects some tensile cracking and compressive crushing of the concrete material in the case of the static loading (first loading). Moreover, these failure mechanisms do not influence significantly the main load-bearing behaviour of the steel-concrete-steel composite plate. As the load of the concrete core is enlarged due to the additional loading cycles, tensile cracking and compressive crushing are not negligible anymore. It is important to point out that the presented spring framework model needs to be developed to consider the fracturing process of the concrete core in the structure. Logically, the tensile cracking in the concrete plays a significant role. As a rough estimate to illustrate the effects of tensile cracking, the spring framework model with three horizontal concrete layers can be analysed after the second loading cycle with a modified concrete material which does not have any tensile strength. In that case, the deflection in the middle of the span is 9,65 mm at the 2 millionth loading. Compared to the result at the first loading (7,22 mm), the increment is 33,7 %. Moreover, the tensile forces in the bottom steel plate increase obviously (1055,0 kN in the middle of the span). Logically, the horizontal forces in the shear connectors of the bottom steel section are also larger.

The results of this chapter demonstrated also that the forces in the composite connections are sensitive to the initial conditions (inelastic slip values) of the model. So, at the 2 millionth loading most of the forces are approximately 25 kN, which is equal the limit value for the increasing slip calculation in the framework model. Thus, it is important to perform additional experimental tests to evaluate more precise the spring stiffness values and the inelastic slips referring to the composite connection.

The most important conclusion is that the cyclic behaviour of concrete cannot be neglected in the case of the examined composite plate. The presented calculations have shown that the effects of cyclic creep of the concrete can be considered through a spring framework model. This simple model can be a proper solution for the practical applications, too.

5. Conclusion and perspective

This chapter contains conclusions for the different calculations performed, and summarizes the suggestions for further research.

As shown in chapter 2, the extremely slender SCSC plate developed for a trough bridge system for the Austrian Federal Rail Company (ÖBB) is appropriate to transfer the loads in the transverse direction. The ABAQUS calculation results were analysed in fatigue limit state (FLS) in this thesis. Additionally, four different simple engineering models were introduced which can describe approximately the main mechanisms of the complex composite construction. However, these simple models cannot substitute the ABAQUS calculation, because they operate partly with the results from the Finite-Element-Analysis software.

Obviously, it would be useful to perform the presented analyses of the ABAQUS results in ultimate limit state (ULS), too. Moreover, further studies are required in order to take into account the tensile stresses in the longitudinal direction of the trough bridge. As mentioned also in the introduction, the normal stresses in the SCSC plate from bending of the whole bridge are not considered through the construction part modelled with ABAQUS in this thesis. For this purpose, numerical analyses with ABAQUS and experimental tests are currently performed at TU Wien, Research Unit Steel Structures.

As it was illustrated in chapter 3, a two-dimensional spring framework model is suitable to substitute the complex ABAQUS calculation referring to the SCSC-plate. However, ABAQUS and the spring framework model calculation take into consideration differently the inelastic behaviour of concrete. As the spring stiffness values of the framework model are based on six laboratory tests, it is relevant to perform additional experiments to evaluate more precise the input data of the calculation.

The developed spring framework model does not figure the fracturing process of the materials (for example the tensile cracking and compressive crushing of the concrete) in the structure. Thus, the used model is applicable until the beginning of these failure mechanisms. According to the ABAQUS results, at the examined fatigue limit state the effects from material damage can be neglected as an approximation. However, an expansion of the presented framework model is necessary in the case of higher external loads to evaluate the effects from cracking and crushing of concrete.

As shown in chapter 4, increasing inelastic slip in the composite connection due to the cyclic loading (cyclic creep of the concrete) needs to be considered. This effect can be modelled with the spring framework model. Actually, a system of linear equations with 342 unknowns is solved 51000 times in MATLAB to get results. Both the positive and the negative consequences of fatigue damage in the shear connectors were presented. It is meaningful that the maximal vertical displacement in the middle of the span increase by 25,1 %. Another important result is that the stresses of the concrete are enlarged due to the cyclic loading. Thus, in contrast with the approximation at static loading, tensile cracking and compressive crushing of the concrete material are not negligible anymore. Therefore, the spring framework model needs further development to consider the failure mechanisms, too.

Furthermore, it is necessary to perform additional experiments to evaluate reliably the increasing inelastic slip values in the composite connection of the SCSC plate.

Another benefit of the presented spring framework model is that slab railway bridges constructed with the SCSC plate can be also easily analysed. Here, railway bridges with short spans (up to 8 m) are designed so that the shear connectors of the SCSC plate lie parallel to the length of the slab bridge. In this case the SCSC plate is the solo load-bearing element

in the longitudinal direction. Logically, the presented framework model needs to be modified according to the actual length of the slab bridge. Moreover, the loading of the spring framework model is also a bit different.

The presented dissertation is a preliminary step to derive the design models for the SCSC plate in the fatigue limit state (FLS). Logically, based on the presented result analyses and engineering models, final design methods need to be developed for the verifications of the fatigue limit state (FLS) and the ultimate limit state (ULS).

Appendix A – *The dead load of the SCSC plate applied in chapter 2.2*

The volume (V) and weight (W) of the steel structures of the ABAQUS model:

$V_{bottom\ steel\ plate} = 15 \cdot 1000 \cdot 2040 = 30600000\ mm^3$

$W_{bottom\ steel\ plate} = 30600000\ [mm^3] \cdot 7{,}85 \cdot 10^{-6}\ [kg/mm^3] \cdot 10\ [m/s^2] = 2402\ N = 2{,}402\ kN$

$V_{top\ steel\ plate} = 15 \cdot 1000 \cdot 2040 = 30600000\ mm^3$

$W_{top\ steel\ plate} = 30600000\ [mm^3] \cdot 7{,}85 \cdot 10^{-6}\ [kg/mm^3] \cdot 10\ [m/s^2] = 2402\ N = 2{,}402\ kN$

$V_{shear\ connector\ 1} = 10 \cdot 170 \cdot 2023 - 12 \cdot 10 \cdot 50^2 \cdot \pi = 2496622\ mm^3$

$W_{shear\ connector\ 1} = 2496622\ [mm^3] \cdot 7{,}85 \cdot 10^{-6}\ [kg/mm^3] \cdot 10\ [m/s^2] = 196\ N = 0{,}196\ kN$

$V_{shear\ connector\ 2} = 20 \cdot 170 \cdot 2023 - 12 \cdot 20 \cdot 50^2 \cdot \pi = 4993244\ mm^3$

$W_{shear\ connector\ 2} = 4993244\ [mm^3] \cdot 7{,}85 \cdot 10^{-6}\ [kg/mm^3] \cdot 10\ [m/s^2] = 392\ N = 0{,}392\ kN$

$V_{shear\ connector\ 3} = 10 \cdot 170 \cdot 2023 - 12 \cdot 10 \cdot 50^2 \cdot \pi = 2496622\ mm^3$

$W_{shear\ connector\ 3} = 2496622\ [mm^3] \cdot 7{,}85 \cdot 10^{-6}\ [kg/mm^3] \cdot 10\ [m/s^2] = 196\ N = 0{,}196\ kN$

$V_{end\ stiffener\ 1} = 15 \cdot 55 \cdot 170 = 140250\ mm^3$

$W_{end\ stiffener\ 1} = 140250\ [mm^3] \cdot 7{,}85 \cdot 10^{-6}\ [kg/mm^3] \cdot 10\ [m/s^2] = 11\ N = 0{,}011\ kN$

$V_{end\ stiffener\ 2} = 15 \cdot 110 \cdot 170 = 280500\ mm^3$

$W_{end\ stiffener\ 2} = 280500\ [mm^3] \cdot 7{,}85 \cdot 10^{-6}\ [kg/mm^3] \cdot 10\ [m/s^2] = 22\ N = 0{,}022\ kN$

$V_{end\ stiffener\ 3} = 15 \cdot 55 \cdot 170 = 140250\ mm^3$

$W_{end\ stiffener\ 3} = 140250\ [mm^3] \cdot 7{,}85 \cdot 10^{-6}\ [kg/mm^3] \cdot 10\ [m/s^2] = 11\ N = 0{,}011\ kN$

Total sum of the weights of the steel structures of the ABAQUS model without the end plate:

$W_{steel\ structures} = 2{,}402 + 2{,}402 + 0{,}196 + 0{,}392 + 0{,}196 + 0{,}011 + 0{,}022 + 0{,}011 = 5{,}632\ kN$

The volume (V) and weight (W) of the concrete structures of the ABAQUS model:

$V_{concrete\ dowel\ 1} = 20 \cdot 170 \cdot 2023 + 12 \cdot 10 \cdot 50^2 \cdot \pi = 7820678\ mm^3$

$W_{concrete\ dowel\ 1} = 7820678\ [mm^3] \cdot 2{,}40 \cdot 10^{-6}\ [kg/mm^3] \cdot 10\ [m/s^2] = 188\ N = 0{,}188\ kN$

$V_{concrete\ dowel\ 2} = 2 \cdot 20 \cdot 170 \cdot 2023 + 12 \cdot 20 \cdot 50^2 \cdot \pi = 15641356\ mm^3$

$W_{concrete\ dowel\ 2} = 15641356\ [mm^3] \cdot 2{,}40 \cdot 10^{-6}\ [kg/mm^3] \cdot 10\ [m/s^2] = 375\ N = 0{,}375\ kN$

$V_{concrete\ dowel\ 3} = 20 \cdot 170 \cdot 2023 + 12 \cdot 10 \cdot 50^2 \cdot \pi = 7820678\ mm^3$

$W_{concrete\ dowel\ 3} = 7820678\ [mm^3] \cdot 2{,}40 \cdot 10^{-6}\ [kg/mm^3] \cdot 10\ [m/s^2] = 188\ N = 0{,}188\ kN$

$V_{concrete\ core\ 1} = 390 \cdot 170 \cdot 17 + 440 \cdot 170 \cdot 2023 = 152447500\ mm^3$

$W_{concrete\ dowel\ 1} = 152447500\ [mm^3] \cdot 2{,}40 \cdot 10^{-6}\ [kg/mm^3] \cdot 10\ [m/s^2] = 3659\ N = 3{,}659\ kN$

$V_{concrete\ core\ 2} = 390 \cdot 170 \cdot 17 + 440 \cdot 170 \cdot 2023 = 152447500\ mm^3$

$W_{concrete\ dowel\ 2} = 152447500\ [mm^3] \cdot 2{,}40 \cdot 10^{-6}\ [kg/mm^3] \cdot 10\ [m/s^2] = 3659\ N = 3{,}659\ kN$

Total sum of the weights of the concrete structures of the ABAQUS model:

$W_{concrete\ structures} = 0{,}188 + 0{,}375 + 0{,}188 + 3{,}659 + 3{,}659 = 8{,}069\ kN$

Total sum of the weights of the steel and concrete structures of the ABAQUS model without the end plate:

$W_{steel\ and\ concrete\ structures} = 5{,}632 + 8{,}069 = 13{,}701\ kN$

The distributed load on the ABAQUS model from the dead weight of the steel and concrete structures:

$g_{k,steel\ and\ concrete\ structures} = 13{,}701/2{,}04 = 6{,}716\ kN/m^2$

The weights of the superstructures (ballast bed with a height of 550 mm, the insulation, the reinforced concrete sleepers, the rails (2 x UIC 60) and the rail fastening system) of the trough bridge (1 m length of the bridge is examined in accordance with the ABAQUS model):

$W_{ballast\ bed} = V \cdot \rho \cdot g = 2495545000\ [mm^3] \cdot 2{,}00 \cdot 10^{-6}\ [kg/mm^3] \cdot 10\ [m/s^2] = 49911\ N = 49{,}911\ kN$

where:

The volume (V) is based on the area of the ballast bed (A = 2 495 545 mm^2) measured in the digital drawing (see figure 2.4(a))

$W_{insulation} = (10 \cdot 4200 \cdot 1000)\ [mm^3] \cdot 2{,}50 \cdot 10^{-6}\ [kg/mm^3] \cdot 10\ [m/s^2] = 1050\ N = 1{,}05\ kN$

Comment: the insulation with 10 mm thickness is installed on the surface of the top steel plate of the SCSC plate illustrated in figure 2.4(a).

$W_{sleepers} = (2600 \cdot 260 \cdot 210)\ [mm^3] \cdot (2{,}50 - 2{,}00) \cdot 10^{-6}\ [kg/mm^3] \cdot 10\ [m/s^2] \cdot \frac{1000}{600} = 1183N = 1{,}183\ kN$

$\rightarrow W_{sleepers} = 1{,}00\ kN$ (According to the approximation in [4])

Comment: the density difference between the reinforced concrete and the ballast bed is considered because the volume of the sleeper was counted in the area of the ballast bed.

$W_{rails\ and\ rail\ fastening\ system} = 1{,}70\ kN$ (According to ÖNORM EN 1991-1-1, table A.6)

Total sum of the weights of the superstructures:

$W_{steel\ and\ concrete\ structures} = 49{,}911 + 1{,}05 + 1{,}00 + 1{,}70 = 53{,}661\ kN$

The distributed load on the ABAQUS model from the dead weight of the superstructures:

$g_{k,superstructures} = 53{,}661/4{,}08 = 13{,}152\ kN/m^2$

The total dead load for the ABAQUS model:

$g_k = 6{,}716 + 13{,}152 = 19{,}868\ kN/m^2 \cong 19{,}87\ kN/m^2$

Appendix B – *The total sum of the normal forces and bending moments in figure 2.64*

Figure	**Compression [kN]**	Force arm [mm]	**Moment [kNmm]**
a	202.38	57.6	11 657
b	202.41	56.8	11 497
c	10.81	55.6	601
d	16.24	60.4	981
e	10.63	55.3	588
f	751.2	92.5	69 486
g	25.24	62.8	1 585
h	23.29	66.3	1 544
i	25.24	62.8	1 585
Σ	**1267.44**		**99 524**

Figure	**Tension [kN]**	Force arm [mm]	**Moment [kNmm]**
a	109.57	46.3	5 073
b	106.43	47	5 002
c	4.8	49.4	237
d	11.61	42.4	492
e	4.64	50.6	235
f	933.6	92.5	86 358
g	16.02	63.8	1 022
h	66.77	61.5	4 106
i	16.09	63.6	1 023
Σ	**1269.53**		**103 549**

ΣM = 203 073 kNmm

Appendix C – *The average slip values based on the six laboratory test results used for figure 3.5*

Force [kN]	Slip - Test 1 [mm]	Slip - Test 2 [mm]	Slip - Test 3 [mm]	Slip - Test 4 [mm]	Slip - Test 5 [mm]	Slip - Test 6 [mm]	**Avarage slip [mm]**
91	0.2578	0.3033	-	-	-	-	**0.2806**
80	0.2383	0.2454	-	0.1594	-	-	**0.2144**
70	0.2079	0.1931	0.1422	0.1342	-	-	**0.1694**
60	0.1708	0.1407	0.1127	0.1075	0.0390	0.1676	**0.1231**
54.5	0.1450	0.1150	0.0950	0.0850	0.0300	0.1500	**0.1033**
50	0.1244	0.0914	0.0826	0.0717	0.0285	0.1338	**0.0887**
40	0.0670	0.0467	0.0515	0.0231	0.0188	0.0949	**0.0503**
30	0.0309	0.0162	0.0231	0.0091	0.0115	0.0373	**0.0214**
20	0.0069	0.0039	0.0090	0.0056	0.0070	0.0085	**0.0068**
10	0.0021	0.0011	0.0034	0.0024	0.0035	0.0033	**0.0026**

Appendix D – *Calculations and member properties for the validation of the framework model*

D.1 The calculation with the formulas from Rubin referring to chapter 3.4.1.2

Firstly, the detailed calculation of the bending stiffness of the beam (see the cross section in figure 3.8) is presented, because this stiffness is the baseline data when using Rubin's formulas.

The distance of the centre of mass from the upper edge (see figure 3.8):

$$z_{cm} = \frac{A_{sp} \cdot z_{sp} + A_{sc} \cdot z_{sc}}{A_{sp} + A_{sc}} = \frac{15000 \cdot 7{,}5 + 3400 \cdot 100}{15000 + 3400} = \frac{452500}{18400} = 24{,}592\ mm$$

where:

$A_{sp} = 15000\ mm^2$ (Area of the steel plate)

$A_{sc} = 3400\ mm^2$ (Area of the shear connector)

$z_{sp} = 7{,}5\ mm$ (Distance between the centre of mass of the steel plate and the upper edge of the steel plate)

$z_{sc} = 100\ mm$ (Distance between the centre of mass of the shear connector and the upper edge of the steel plate)

The area moment of inertia of the cross section around the axis "y":

$$I_y = I_{y-sp} + A_{sp} \cdot \left(z_{cm} - z_{sp}\right)^2 + I_{y-sc} + A_{sc} \cdot (z_{sc} - z_{cm})^2 =$$

$$= \frac{1000 \cdot 15^3}{12} + 1000 \cdot 15 \cdot (24{,}592 - 7{,}5)^2 + \frac{20 \cdot 170^3}{12} + 20 \cdot 170 \cdot (100 - 24{,}592)^2 = 32\,185\,276\ mm^4$$

where:

I_{y-sp}: Area moment of inertia of the steel plate around the axis "y"

I_{y-sc}: Area moment of inertia of the shear connector around the axis "y"

The modulus of elasticity (Young's modulus) of the steel (S355) is:

$E = 210\,000\ N/mm^2$

Thus, the bending stiffness which was also given in equation 3.6 (see chapter 3.4.1.2):

$E \cdot I_y = 210\,000 \cdot 32\,185\,276 \cdot 10^{-9} = 6\,758{,}91\ kNm^2$

Next, the deflection in the middle of the span is calculated with the linear static analysis through Rubin's formulas (see the tables below). In the case of a linear static analysis the coefficient K is zero and the solution function b_j is simple:

$$b_1(l) = l = 4{,}1\ m$$

$$b_2(l) = \frac{l^2}{2} = 8{,}405\ m^2$$

$$b_3(l) = \frac{l^3}{6} = 11{,}48683333\ m^3$$

$$b_4(l) = \frac{l^4}{24} = 11{,}77400417\ m^4$$

Two separate distributed loads are used for the following calculation according to figure 3.7(a).

$q_1 = 19{,}87\ kN/m$ (The load part on the whole beam)

$q_2 = 106{,}87 - 19{,}87 = 87\ kN/m$ (The load part in the middle of the beam)

The shear forces at the support from the distributed loads calculated with Rubin's table below:

$$Q_{i,q_1} = \frac{b_2(l)}{b_1(l)} \cdot q_1 = \frac{8{,}405}{4{,}1} \cdot 19{,}87 = 40{,}7335\ kN$$

$$Q_{i,q_2} = \frac{b_2(3{,}435) - b_2(0{,}665)}{b_1(l)} \cdot q_2 = \frac{\frac{3{,}435^2}{2} - \frac{0{,}665^2}{2}}{4{,}1} \cdot 87 = 120{,}495\ kN$$

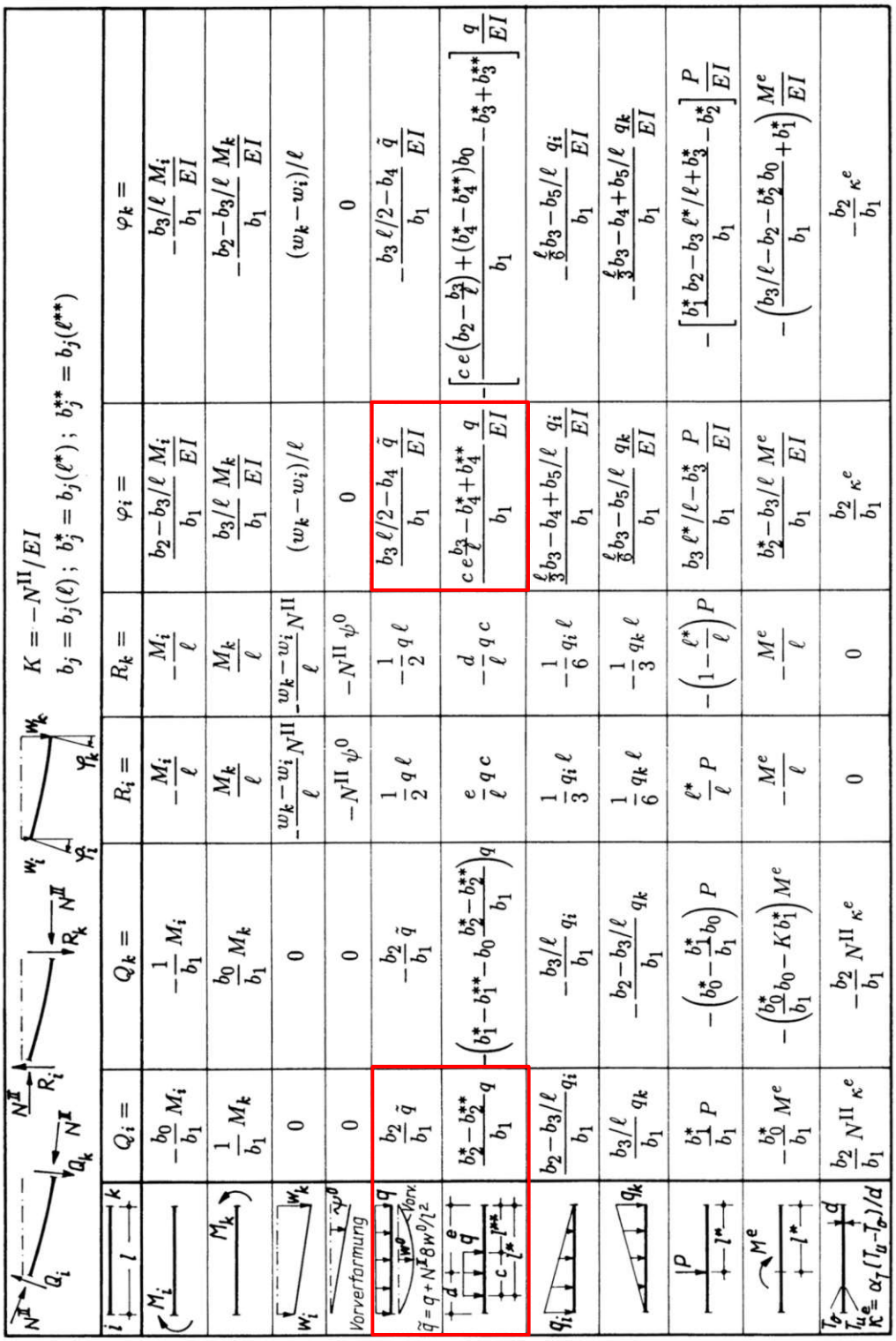

Shear forces Q_i, Q_k, transversal forces R_i, R_k, rotation angle of the cross section φ_i, φ_k depending on M_i, M_k, w_i, w_k and the actions on the member in the case of the support condition

The total sum of the shear forces at the support:

$$Q_i = Q_{i,q_1} + Q_{i,q_2} = 40{,}7335 + 120{,}495 = 161{,}2285\ kN$$

The rotation angles of the cross section at the support from the distributed loads calculated with Rubin's table above:

$$\varphi_{i,q_1} = \frac{b_3(l) \cdot \frac{l}{2} - b_4(l)}{b_1(l)} \cdot \frac{q_1}{EI} = \frac{11{,}48683333 \cdot \frac{4{,}1}{2} - 11{,}77400417}{4{,}1} \cdot \frac{19{,}87}{6\,758{,}91} = 0{,}008442315$$

$$\varphi_{i,q_2} = \frac{c \cdot e \cdot \frac{b_3}{l} - b_4(3{,}435) + b_4(0{,}665)}{b_1(l)} \cdot \frac{q_2}{EI} = \frac{2{,}77 \cdot 2{,}05 \cdot \frac{11{,}48683333}{4{,}1} - \frac{3{,}435^4}{24} + \frac{0{,}665^4}{24}}{4{,}1} \cdot \frac{87}{6\,758{,}91} =$$

$$= 0{,}031760649$$

The total sum of the rotation angles at the support:

$$\varphi_i = \varphi_{i,q_1} + \varphi_{i,q_2} = 0{,}008442315 + 0{,}031760649 = 0{,}040202964$$

The following table from Rubin is used to calculate the deflection in the middle of the span depending on the shear force and the rotation at the support as well as the distributed loads on the beam.

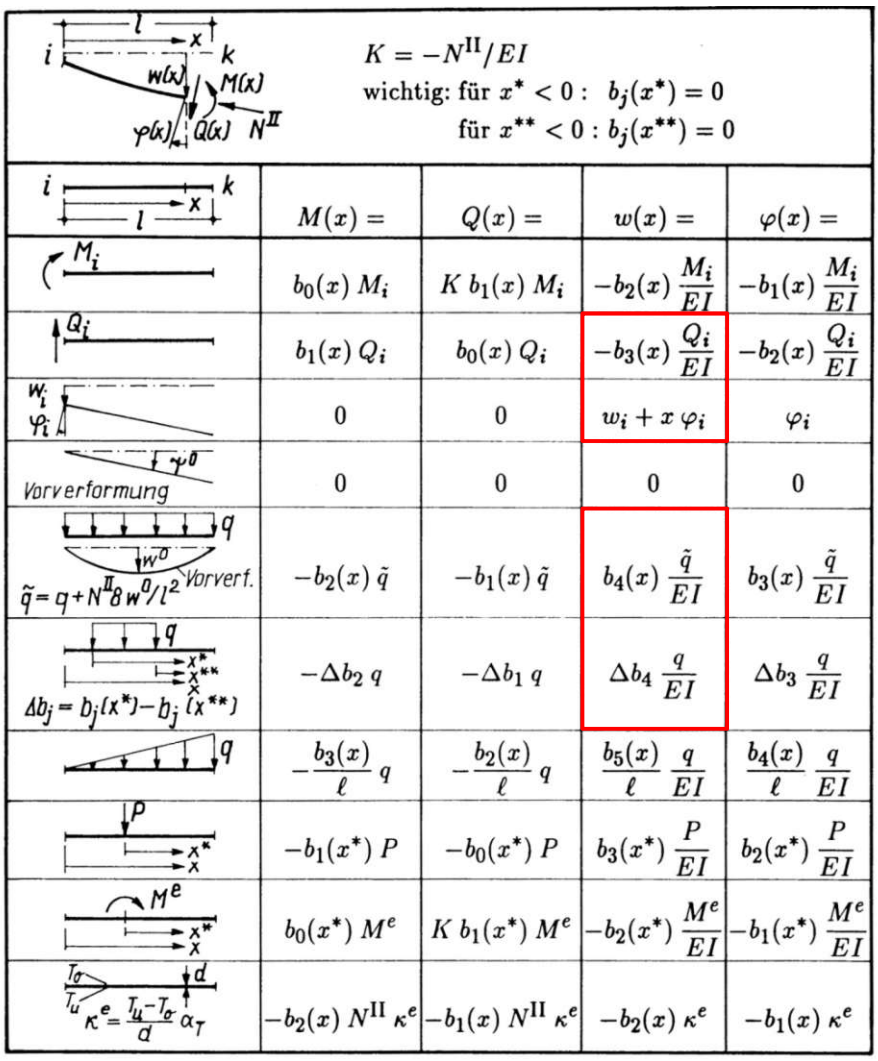

	$M(x) =$	$Q(x) =$	$w(x) =$	$\varphi(x) =$
M_i	$b_0(x)\, M_i$	$K\, b_1(x)\, M_i$	$-b_2(x)\, \frac{M_i}{EI}$	$-b_1(x)\, \frac{M_i}{EI}$
Q_i	$b_1(x)\, Q_i$	$b_0(x)\, Q_i$	$-b_3(x)\, \frac{Q_i}{EI}$	$-b_2(x)\, \frac{Q_i}{EI}$
w_i, φ_i	0	0	$w_i + x\, \varphi_i$	φ_i
Vorverformung	0	0	0	0
q, $\tilde{q} = q + N^{II} 8 w^0 / l^2$, Vorverf.	$-b_2(x)\, \tilde{q}$	$-b_1(x)\, \tilde{q}$	$b_4(x)\, \frac{\tilde{q}}{EI}$	$b_3(x)\, \frac{\tilde{q}}{EI}$
q, $\Delta b_j = b_j(x^*) - b_j(x^{**})$	$-\Delta b_2\, q$	$-\Delta b_1\, q$	$\Delta b_4\, \frac{q}{EI}$	$\Delta b_3\, \frac{q}{EI}$
q	$-\frac{b_3(x)}{\ell}\, q$	$-\frac{b_2(x)}{\ell}\, q$	$\frac{b_5(x)}{\ell}\, \frac{q}{EI}$	$\frac{b_4(x)}{\ell}\, \frac{q}{EI}$
P	$-b_1(x^*)\, P$	$-b_0(x^*)\, P$	$b_3(x^*)\, \frac{P}{EI}$	$b_2(x^*)\, \frac{P}{EI}$
M^e	$b_0(x^*)\, M^e$	$K\, b_1(x^*)\, M^e$	$-b_2(x^*)\, \frac{M^e}{EI}$	$-b_1(x^*)\, \frac{M^e}{EI}$
$\kappa^e = \frac{T_u - T_o}{d}\, \alpha_T$	$-b_2(x)\, N^{II}\, \kappa^e$	$-b_1(x)\, N^{II}\, \kappa^e$	$-b_2(x)\, \kappa^e$	$-b_1(x)\, \kappa^e$

Moment M(x), shear force Q(x), deflection w(x), rotation angle of the cross section φ(x) depending on M_i, Q_i, w_i, φ_i and the actions on the member

$$w(l/2)_{Q_i} = -b_3(l/2) \cdot \frac{Q_i}{EI} = -\frac{2{,}05^3}{6} \cdot \frac{161{,}2285}{6\,758{,}91} = -0{,}034251176\ m$$

$$w(l/2)_{\varphi_i} = \frac{l}{2} \cdot \varphi_i = 2{,}05 \cdot 0{,}040202964 = 0{,}082416076\ m$$

$$w(l/2)_{q_1} = b_4\left(\frac{l}{2}\right) \cdot \frac{q_1}{EI} = \frac{2{,}05^4}{24} \cdot \frac{19{,}87}{6\,758{,}91} = 0{,}002163343\ m$$

$$w(l/2)_{q_2} = b_4(1{,}385) \cdot \frac{q_2}{EI} = \frac{1{,}385^4}{24} \cdot \frac{87}{6\,758{,}91} = 0{,}00197347\ m$$

The total sum of the deflection in the middle of the span:

$$w(l/2) = w(l/2)_{Q_i} + w(l/2)_{\varphi_i} + w(l/2)_{q_1} + w(l/2)_{q_2} =$$

$$= -0{,}034251176 + 0{,}082416076 + 0{,}002163343 + 0{,}00197347 = 0{,}052301713\ m = 52{,}302\ mm$$

D.2 The calculation of the slipping of the steel sections illustrated in chapter 3.4.2

It is presumed that the curves of the vertical displacements are identical in the case of the two beams modelled in chapter 3.4.2. This means also that both sections carry 50 percent of the total loading. Therefore, the results of the analytical solution are available simply through halving the results from appendix D.1.

The rotation angles of the cross section at the support calculated with Rubin's table above:

$$w'(0)_{Q_i} = \varphi(0)_{Q_i} = -b_1(0) \cdot \frac{Q_i}{EI} = -0 \cdot \frac{161{,}2285/2}{6\,758{,}91} = 0$$

$$w'(0)_{\varphi_i} = \varphi(0)_{\varphi_i} = \varphi_i = \frac{0{,}040202964}{2} = 0{,}020101482$$

$$w'(0)_{q_1} = \varphi(0)_{q_1} = b_3(0) \cdot \frac{q_1}{EI} = 0 \cdot \frac{19{,}87/2}{6\,758{,}91} = 0$$

$$w'(0)_{q_2} = \varphi(0)_{q_2} = \Delta b_3(0) \cdot \frac{q_2}{EI} = 0 \cdot \frac{87/2}{6\,758{,}91} = 0$$

Obviously:

$$\varphi(0) = \varphi_i = 0{,}020101482$$

The horizontal displacement between the centroid of one of the steel sections and the centroid of the shear connector:

$$x = z \cdot \varphi(0) = 75{,}41 \cdot 0{,}020101482 = 1{,}516\ mm$$

where:

z is the vertical displacement between the centroid of one of the steel sections and the centroid of the shear connector

As both of the steel sections have the same bending, the double value of this horizontal displacement provides the relative horizontal displacement between the two shear connectors (see figure 3.19):

$$2 \cdot x = 2 \cdot 1{,}516 = 3{,}032\ mm$$

D.3 The member properties (A, I) of the spring framework model with one horizontal concrete beam

Area of the steel plate:

$$A_{sp} = 15 \cdot 1000 = 15000\ mm^2$$

Area moment of inertia of the steel plate around the axis "y":

$$I_{y-sp} = \frac{1000 \cdot 15^3}{12} = 281250\ mm^4$$

Area of the shear connector (substitutive cross section for the shear connector according to chapter 3.4.3.3):

$$A_{sc} = 20 \cdot (170 - 91) = 1580\ mm^2$$

Area moment of inertia of the shear connector (substitutive cross section) around the axis "y":

$$I_{y-sc} = \frac{20 \cdot 170^3}{12} - \frac{20 \cdot 91^3}{12} = 6932382\ mm^4$$

Area of the concrete beam:

$$A_c = (1000 - 20 - 20) \cdot 170 = 163200\ mm^2$$

Area moment of inertia of the concrete beam around the axis "y":

$$I_{y-c} = \frac{960 \cdot 170^3}{12} = 393040000\ mm^4$$

D.4 The member properties (Ac, Iy-c) of the spring framework model with three horizontal concrete layers

Area of one horizontal concrete layer:

$$A_c = (1000 - 20 - 20) \cdot (170/3) = 54400\ mm^2$$

Area moment of inertia of one horizontal concrete layer around the axis "y":

$$I_{y-c} = \frac{960 \cdot (170/3)^3}{12} = 14557037 mm^4$$

Appendix E – *Spring stiffness calculation based on the ABAQUS results*

At the first shear connector of the top steel section:

The horizontal force in the shear connector: $F_{h,1,top\ steel\ section} = 92{,}58\ kN$

The horizontal gap inside the hole: $\delta_{h,1,top\ steel\ section} = 0{,}093761\ mm$

The horizontal spring stiffness value: $C_{h,1,top\ steel\ section} = 92{,}58/0{,}093761 = 987{,}4\ kN/mm$

At the eighth shear connector of the top steel section:

The horizontal force in the shear connector: $F_{h,8,top\ steel\ section} = 41{,}12\ kN$

The horizontal gap inside the hole: $\delta_{h,8,top\ steel\ section} = 0{,}039117\ mm$

The horizontal spring stiffness value: $C_{h,8,top\ steel\ section} = 41{,}12/0{,}039117 = 1051{,}2\ kN/mm$

References

[1] SIMULIA: ABAQUS/CAE 2019 [Software]. https//www.3ds.com/products-services/simulia/products/abaqus/abaquscae/

[2] Hermann, P. (2013) *Tragfunktionsanalyse und rechnerische Modellbildung einer neuartigen Sandwich-Verbundplatte (SCSC-Platte) als Fahrbahndeck für Eisenbahnbrücken.* Doctoral Thesis, TU Wien, Vienna, Austria.

[3] Steurer, M.; Petraschek, T.; Fink, J. (2016) *Development of an innovative sandwich plate for trough-type railway bridges.* Steel Construction, Volume 9, Issue 3, ISBN 1867-0520.

[4] Takács, P. (2018) *Analyse der Ermüdungsverhaltens der SCSC-Platte.* Doctoral Thesis, TU Wien, Vienna, Austria.

[5] Lorenz, S. (2021) *Ausgewählte Detailanalysen zur Anwendung der SCSC-Platte als Plattenbrücke.* Diploma Thesis, TU Wien, Vienna, Austria.

[6] MathWorks: MATLAB R2018b [Software]. https//uk.mathworks.com/products/matlab.html

[7] Palotás, B.; Takács, P.; Fink, J. (2021) *Simulation of the SCSC plate with a spring framework model including the effects of inelastic slip.* Steel Construction, Volume 14, Issue 2, Pages 83-94. https://doi.org/10.1002/stco.202000055

[8] Palotás, B.; Takács, P.; Fink, J. (2021) *On the Load-Bearing Behaviour of the Steel-Concrete-Steel Composite (SCSC) Plate.* ce/papers, Volume 4, Issue 2-4 (Special Issue: EUROSTEEL 2021 Sheffield – Steel's coming home), Pages 648-656. https://doi.org/10.1002/cepa.1344

[9] ÖNORM EN 1991-2: *Eurocode 1: Actions on structures – Part 2: Traffic loads on bridges*, Austrian Standards, 01.03.2012.

[10] ÖNORM B 1991-2: *Eurocode 1: Actions on structures – Part 2: Traffic loads on bridges – National specifications concerning ÖNORM EN 1991-2 and national supplements*, Austrian Standards, 01.08.2018.

[11] ÖNORM EN 1993-1-9: *Eurocode 3: Design of steel structures – Part 1-9: Fatigue*, Austrian Standards, 01.04.2013.

[12] ÖNORM EN 1993-2: *Eurocode 3: Design of steel structures – Part 2: Steel Bridges*, Austrian Standards, 15.08.2010.

[13] ÖNORM B 1993-2: *Eurocode 3: Design of steel structures – Part 2: Steel Bridges – National specifications concerning ÖNORM EN 1993-2, national comments and national supplements*, Austrian Standards, 01.03.2008.

[14] ÖNORM EN 1990: *Eurocode: Basis of structural design*, Austrian Standards, 15.03.2013.

[15] Ramberg, W.; Osgood, W. R.; *Description of stress-strain curves by three parameters,* NACA, Technical Notes, No. 902, Washington, July 1943.

[16] Steurer, M.; Fink, J. (2017) *Weiterführende Forschung zur neuartigen Sandwich Verbundplatte als Fahrbahnplatte für Eisenbahnbrücken; SCSC-Platte (Ein Projekt finanziert im Rahmen der Verkehrsinfrastrukturforschung 2012 (VIF2012))*, Final Report, May 2017.

[17] Pavlović, M.; Markovic, Z.; Veljkovic, M.; Budevac, D. (2013) *Bolted shear connectors vs. headed studs in push-out tests.* Journal of Constructional Steel Research, Volume 88, S. 134-149.: Elsevier, September 2013.

[18] DLUBAL: RFEM 5.20 [Software].
https://www.dlubal.com/en/products/rfem-fea-software/

[19] DLUBAL: RSTAB 8.11 [Software].
https://www.dlubal.com/en/products/rstab-beam-structures/

[20] Rubin, H.; Schneider K.-J.: *Bautabellen für Ingenieure - Kapitel 4A Baustatik.* Werner Verlag, 2012.

[21] Wolters, K.; Feldmann, M. (2018) *Ermüdungsuntersuchungen an Verbundträgern mit Verbunddübelleisten und nachgiebiger Verbundfuge mittels Stabwerkmodellen.* Bauingenieur 93, H. 11, S. 429-437.